Author:
Chapman, Geoffrey John Douglas

Title:
A weakly singular integral equation approach for water wave problems

A WEAKLY SINGULAR INTEGRAL EQUATION APPROACH FOR WATER WAVE PROBLEMS

Geoffrey John Douglas Chapman
School of Mathematics
University of Bristol

September 2005

A thesis submitted to the University of Bristol
in accordance with the requirements of the degree
of Doctor of Philosophy in the Faculty of Science

ALL MISSING
PAGES ARE
BLANK
IN
ORIGINAL

Abstract

In this thesis we consider a range of problems concerned with the interaction of small-amplitude waves with topography of arbitrary profile. The work was motivated by the success of two-dimensional techniques which switch from normal to tangential derivatives and the lack of any obvious means of extension to three dimensions. We introduce a novel approach which generalises these earlier techniques and applies the full linear theory to three-dimensional problems.

Chapter 1 provides a brief introduction to the thesis and is followed in Chapter 2 by a summary of the basic theory of water waves together with an overview of the main techniques either used, or discussed, in this thesis. Throughout this thesis, the main approach is to formulate an integral equation and convert it to weakly singular form by switching from normal to tangential derivatives. With this novel technique in mind, we typically present two distinct approaches, each with their own advantages and each dealing with the most singular part of the equation analytically.

In Chapter 3 we investigate two-dimensional sloshing over an arbitrary bed, demonstrating the approach we extend in this thesis. We then move to three-dimensional problems and in Chapter 4 we employ multipole techniques to address problems involving semicircular and hemispherical geometries. In Chapter 5 we introduce our main techniques by investigating the interaction of waves with a uniform infinite underwater ridge and in Chapter 6 we extend these ideas to deal with an infinite step of arbitrary profile. In Chapter 7 we investigate the scattering of plane waves by an axisymmetric seamount. Finally, in Chapter 8 we introduce a fully linear general theory for applying these techniques to arbitrary patches of topography.

In memory of my parents

John and Jenny Chapman

and for

Ghislaine, Samuel and Faye.

Acknowledgements

I would like to thank Dr Richard Porter for his supervision, guidance and many hours of enlightening discussions throughout the course of this study. I would also like to thank Professor David Porter for his very useful discussions and insights into integral equation techniques. Thanks are also due to Dr Pete Chamberlain for producing experimental data for me to compare my results against. The financial support of the Natural Environment Research Council under grant no. NER/S/A/2002/10333, is also gratefully acknowledged.

I would like to acknowledge the support and guidance given to me by my parents throughout my life - I will always be grateful to them. I would also like to thank everyone who has supported me, made my life easier and generally shown an interest in my work over the last three years, particularly Paul and Joan, Andy, and Marshall and Jennifer.

I would like to thank Samuel and Faye for helping to keep a sense of normality in my life and for all the pleasure and happiness they have brought to my life. Above all I would like to thank Ghislaine for her patience, emotional and practical support and her unfailing confidence in me.

Author's Declaration

I declare that the work in this thesis was carried out in accordance with the regulations of the University of Bristol. The work is original except where indicated by special reference in the text and no part of this thesis has been submitted for any other degree. Any views expressed in this thesis are those of the author and do not necessarily represent those of the University of Bristol. This thesis has not been presented to any other university for examination either in the United Kingdom or overseas.

G.J.D. Chapman

Date: 24th September 2005

Contents

List of Figures

List of Tables

Chapter 1

Introduction

The problem of the effect of submerged bodies or topographic features on the propagation of surface gravity waves is one of considerable interest to engineers designing coastal or offshore structures. With the rapid recent growth in offshore exploration and engineering projects this continues to be the case, with increasingly accurate methods being sought as well as extending our knowledge about the environment for which the engineers must design.

In this thesis we develop techniques for applying fully linear wave theory to problems involving the interaction of water waves with topography of arbitrary profile. We develop our techniques illustrating the key points in their application by solving three-dimensional problems involving classes of geometry having some degree of symmetry. The thesis concludes by presenting a fully linear theory for genuinely three-dimensional problems involving arbitrary patches of topography. Our approach is to form an integral equation which is at most weakly singular. We then make significant analytical progress in the formulation, deriving a new form of integro-differential equation and associated integro-differential operator which is perfectly constructed for solution by extremely efficient and accurate techniques.

The three-dimensional problem of wave/body or wave/topography interactions is extremely complicated primarily due to the Neumann boundary condition on an arbitrary curve. To date, only one explicit solution has been found for a specific varying topography by Roseau [84]. Inevitably the complicated nature of the boundary

condition over an arbitrary bed has demanded approximations of some sort to be made in order to progress. Perhaps the most obvious approach is to perform a direct numerical assault on the equations of motion, an approach reviewed extensively by Mei [60] to whom the reader is referred. Typical examples of the issues involved are highlighted in Davis [18] who investigated two-dimensional oscillations in a canal of arbitrary cross section, and Fenton [34] who considered the forces on axisymmetric bodies of revolution. Both of these papers illustrate the type of numerical issues arising in a direct approach. We shall not consider this style of approach any further and will instead consider approaches which are analytic in character.

In order to extract some of the key features of the problem numerous papers investigated the scattering of waves by a step, or sill of constant depth. Lamb [49] first dealt with scattering by a vertical step using the shallow water equations, an approach repeated in Mei [61]. Miles [62] used a variational approach in conjunction with an eigenfunction matching technique to deal with this same problem and in the course of doing so, introduced the scattering matrix formulation that we employ in our problems. Mei & Black [59] extended these ideas to deal with scattering by rectangular obstacles whereas Kirby & Dalrymple [46] solved the similar problem of oblique diffraction by a rectangular trench. Devillard, Dunlop & Souillard [22] approximated the arbitrary step problem by using a step discretisation, approximating the bed profile by a series of piecewise constant steps; following an identical approach, Bender and Dean [5] investigated the scattering of waves by axisymmetric topographies. Fitz-Gerald, [35] looking at the two-dimensional step problem, used complex-variable techniques to convert the problem into one defined on an infinite strip, albeit with a more complicated free-surface boundary condition. As a by product of this approach he was also able to prove uniqueness for the problem. Evans & Linton [27] combined the approaches of Devillard, Dunlop & Souillard,[22] and Fitz-Gerald, [35] to derive an alternative step approximation; however, this approach remains limited to two dimensions due to the use of complex-variable techniques, and furthermore the mapping function must be known.

Porter [73] revisited Miles' [62] problem for oblique scattering by a step, developing Miles' eigenfunction expansion matching approach and solving the resulting integral equations by a Galerkin method. More recently Rhee [82] and [83] has looked at the scattering of oblique waves over a step to second-order.

Prior to the 1960's, typical methods of dealing with more complicated problems involving wave/topography interaction were the shallow water equations and also geometrical optics or ray theory which had been deduced from the shallow water equations. For a literature survey up to this date the reader is referred to Wehausen & Laitone [101]. Keller [45] gave the geometrical optics approach a more rigourous footing by demonstrating that it could be deduced from the full linear theory. Shen, Meyer and Keller [85] employed these techniques to investigate the scattering and trapping of waves around conical islands and submerged sills. Shen *et al* found that their theory predicted finely tuned near-resonances over a sill. Interestingly Provis [80] conducted experiments to verify the existence of these near-resonances but was unable to excite them experimentally. Longuet-Higgins [52] also considered the trapping of wave energy round islands but using shallow water theory, and similarly to Shen *et al* they found that their theory predicted near-resonances over the sill. This time Barnard, Pritchard and Provis [4] tried to verify the results experimentally, but again these near-resonances could not be excited. Renardy [81] considered the sill problem using full linear theory and although near-resonances were still predicted, he found that their locations and the associated amplitudes differed markedly from Longuet-Higgins' [52] results.

The obvious practical implications of near-resonance water wave motions in certain geometric configurations, briefly reviewed above, has led many researchers to consider an associated, but more theoretical situation in which waves are completely trapped by topography/structures. Such waves are often referred to in the literature as trapped waves or edge waves. Stokes [90] established the existence of edge waves for a plane beach and Ursell [98] found that the Stokes' edge wave was the first in a sequence of such modes that increased as the beach slope became shallower. These

edge waves travel along the shoreline, whilst their amplitude decays exponentially away from the shoreline. Some years later, Ursell [97] also proved the existence of edge waves over a submerged cylinder; there also, waves are able to travel along the direction of the cylinder supported above, but decaying exponentially away from, the cylinder. Lavrentiev & Chabat [50] proved that edge waves were supported by any ridge protruding from a bed of otherwise constant depth, a result also considered by Jones [44]. Many papers, deal with such edge waves using a variety of techniques such as the multipole technique presented by Thorne [92]. These multipole techniques, which are extensively reviewed in Linton & McIver [51] are naturally suited to circular boundaries as we shall see in Chapter 4. These papers tend to look for trapped modes around various configurations of either horizontal or vertical cylinders. One example of the full linear theory being applied to edge waves is Evans & McIver [28] who investigated edge waves over a shelf, a problem with an obvious connection to the problem considered in Chapter 6 .

Smith & Sprinks [86] introduced the mild slope equations (MSE) (also independently derived by Berkhoff [6]) which performed a depth averaging and allowed complicated topographies to be handled albeit in an approximate way. Many papers followed from this and it still remains a very popular approach to water wave problems because of its relative simplicity and its practical ease of use. Booij [8] produced a significant paper benchmarking the accuracy of the MSE which, despite its name, can be accurate for slopes of $O(1)$. Various improvements to the MSE have subsequently been proposed, for example Chamberlain & Porter [11] who termed their improvement the modified mild slope equations (MMSE), Porter & Staziker [71] who develop more accurate matching conditions at the joins of different topographies and Chamberlain [13] who investigates the inclusion of evanescent modes in the MMSE approach. Yet more sophisticated modifications were proposed by Athanassoulis & Belibassakis [3] who include extra terms in the approximation to handle the bottom slope better, also by Miles & Chamberlain [64] who proposed a systematic hierarchy of approximations of which the first terms include the MSE and the third term is,

in essence, the MMSE. Porter & Chamberlain [70] used the MMSE to consider the scattering and near-trapping of water waves by axisymmetric topography, a problem which we consider in Chapter 7.

Staziker, Porter and Stirling [89] presented a different approach for the two-dimensional (normal incidence) problem of waves incident on a submerged ridge that we generalise to three dimensions in Chapter 5. They formulated it as an integral equation and converted from normal to tangential derivatives. Subsequently this technique has been used to good effect for example by Porter [74] investigating scattering by an arbitrary submerged cylinder and again by Porter [75] in looking at two-dimensional wave trapping by pairs of cylinders. It was also used in a polar coordinate system by McIver & Porter [58], who investigated axisymmetric wave trapping by a submerged torus (a three-dimensional problem, but on account of the assumed modes of motion, quasi two-dimensional). These techniques for two-dimensional water wave problems are capable of producing extremely accurate results. They accomplish the high degree of accuracy in part by retaining an exact formulation of certain integral equations which incorporate the complicated Neumann boundary condition on some arbitrary curve with no approximation, but also by using a formulation which is amenable to solving by the Rayleigh-Ritz method. However, in these two-dimensional problems mentioned above, the derivation of the integral equations relies essentially on the existence of the Cauchy-Riemann equations which have no analogue in three dimensions.

The key point to note from the literature is that almost all of the work either solves a two-dimensional problem, and/or solves a three-dimensional problem having made some simplifying assumptions. In contrast, in this thesis we seek to generalise exact two-dimensional "derivative-switching" approaches to deal with fully three-dimensional problems. We achieve this by applying an idea introduced by Noblesse [67] and Noblesse & Yang [68]. However, in a radical departure from their approach, which they apply to floating bodies, we shall show how these techniques may be applied, to three-dimensional problems retaining an exact formulation. We develop

a complete theory and a new form of integro-differential equation which is amenable to extremely powerful solution techniques. As a by product of this analysis we also introduce a deceptively simple boundary element scheme, which due to the way the kernel of the associated operator is constructed is also capable of impressive results.

The content of Chapter 3 forms the basis of the publications Chapman & Porter [14] and [15]. Aspects of the material in Chapters 5 and 7 form the basis of Chapman & Porter [16].

Chapter 2

Background theory

2.1 Equations of motion

We consider wave motions of an ideal fluid (i.e. one which is inviscid and incompressible) within a domain bounded by a fixed bottom and having a free surface with the atmosphere. Coordinate systems may be chosen to suit the geometry, however, without loss of generality we may proceed using a Cartesian co-ordinate system with the x and y axes in the undisturbed free surface of the fluid and the z axis oriented vertically downwards. The fluid motion is assumed to be irrotational; therefore the fluid velocity may be written as the gradient of a scalar potential Φ. Furthermore if we assume the fluid is incompressible then the fluid velocity, given by $\mathbf{u} = \nabla\Phi$, must have zero divergence and hence the potential Φ must satisfy Laplace's equation

$$\nabla^2\Phi \equiv \frac{\partial^2\Phi}{\partial x^2} + \frac{\partial^2\Phi}{\partial y^2} + \frac{\partial^2\Phi}{\partial z^2} = 0. \tag{2.1.1}$$

As the fluid is inviscid we may also apply Bernoulli's theorem to the fluid motion which in its most general form gives

$$\frac{\partial\Phi}{\partial t} + \frac{1}{2}(\nabla\Phi.\nabla\Phi) + \frac{P}{\rho} - gz = C(t), \tag{2.1.2}$$

where g is the acceleration due to gravity and P the pressure such that in the absence of external forcing the rest position of the free surface is at $z = 0$. Further analysis will proceed on the assumption that there is no excess external pressure or forcing at the fluid surface and therefore we may set $C(t) = P_a/\rho$ where P_a is the

atmospheric pressure and ρ is the fluid density, both of which are assumed to be constant.

In order to formulate the boundary conditions we note that the free surface may be defined by the equation $\xi = 0$ where ξ is given by

$$\xi = z - \zeta(x, y, t), \tag{2.1.3}$$

and where ζ gives the surface depression. For this fluid motion, one boundary condition is that fluid does not cross the free surface. Hence

$$\frac{D\xi}{Dt} = 0, \qquad \text{on } \xi = 0, \quad \text{or} \quad \frac{\partial\Phi}{\partial x}\frac{\partial\zeta}{\partial x} + \frac{\partial\Phi}{\partial y}\frac{\partial\zeta}{\partial y} - \frac{\partial\Phi}{\partial z} + \frac{\partial\zeta}{\partial t} = 0 \qquad \text{on } \xi = 0. \tag{2.1.4}$$

Also fluid does not penetrate fixed boundaries, therefore the component of fluid velocity normal to the boundary is zero or,

$$\frac{\partial\Phi}{\partial n} = 0, \tag{2.1.5}$$

where n is the normal to the boundary, oriented so that it points out of the fluid domain. The fluid motion is therefore defined by the following set of equations

$$\nabla^2\Phi = 0 \qquad \text{throughout } D, \tag{2.1.6}$$

subject to the kinematic and dynamic boundary conditions given by

$$\frac{\partial\Phi}{\partial x}\frac{\partial\zeta}{\partial x} + \frac{\partial\Phi}{\partial y}\frac{\partial\zeta}{\partial y} - \frac{\partial\Phi}{\partial z} + \frac{\partial\zeta}{\partial t} = 0, \qquad \text{on } z = \zeta(x, y, t), \tag{2.1.7}$$

and

$$-g\zeta + \frac{\partial\Phi}{\partial t} + \frac{1}{2}(\nabla\Phi)^2 = 0, \qquad \text{on } z = \zeta(x, y, t) \tag{2.1.8}$$

respectively and

$$\frac{\partial\Phi}{\partial n} = 0 \qquad \text{on solid boundaries.} \tag{2.1.9}$$

Given the complicated form of the free surface boundary conditions, the usual approach is to form a perturbation expansion in a small parameter and proceed using either a linearised theory, or sometimes also continue to second-order to solve a so-called weakly non-linear formulation of the problem. For a detailed discussion of the

equations of motion and their linearisation see, for example, Weihausen & Laitone [101] or Mei [61]. We will see that higher terms in a perturbation expansion become increasingly complex, therefore in domains where linear theory is no longer valid, it becomes more common to solve the above equations using a fully non-linear solution technique. This latter approach often becomes an exercise in numerical analysis, which although undeniably useful, arguably does not give the same physical insight as a more analytical approach to a linearised problem. Therefore, for most of this thesis we will use classical linear water waves theory, however, as in Chapter 3 we solve a specific problem to second-order, we shall proceed to derive the equations of motions to second-order.

The choice of small parameter should arise naturally from a scaling analysis of the equations of motion although often this approach is not presented and the small parameter is simply given. We will adapt the approach of Mei [61] who used a scaling analysis to deduce the linearised equations, and apply the same analysis to deduce the first 2 terms in the small parameter expansion. We now seek to transform $(x, y, z, \zeta, \Phi, g) \longrightarrow (x', y', z', \zeta', \Phi', g')$ where the primed variables are dimensionless. We suppose that the dimensions (x, y, z, h) are characterized by comparison with a typical surface wave's wavelength λ which is related to the wavenumber k by $\lambda/2\pi = 1/k$. Time is characterised by $1/\omega$ where ω is the angular frequency, the surface elevation by a and the potential by $ka\omega$ where this latter scaling is chosen to ensure that the surface velocities are $a\omega$ as expected. Therefore

$$(x, y, z) = \frac{1}{k}(x', y', z'), \tag{2.1.10}$$

$$\zeta = a\zeta', \tag{2.1.11}$$

$$\Phi = \frac{a\omega}{k}\Phi', \tag{2.1.12}$$

$$t = \frac{1}{\omega}t', \tag{2.1.13}$$

$$g = \frac{\omega^2}{k}g', \tag{2.1.14}$$

where g has also been scaled according to the appropriate scalings for length and

time. We now transform the general equations and find that in terms of the new variables, equations (2.1.6) and (2.1.9) remain unchanged so that

$$\nabla^2\Phi' = 0 \qquad \text{throughout } D \tag{2.1.15}$$

and

$$\frac{\partial\Phi'}{\partial n'} = 0 \qquad \text{on solid boundaries.} \tag{2.1.16}$$

The remaining free surface conditions require more careful treatment. Firstly consider the kinematic boundary condition (2.1.7) which transforms into

$$ka\left(\frac{\partial\Phi'}{\partial x'}\frac{\partial\zeta'}{\partial x'} + \frac{\partial\Phi'}{\partial y'}\frac{\partial\zeta'}{\partial y'}\right) - \frac{\partial\Phi'}{\partial z'} + \frac{\partial\zeta'}{\partial t'} = 0 \qquad \text{on } z' = ka\,\zeta'. \tag{2.1.17}$$

We define the parameter ε by

$$\varepsilon = ka \tag{2.1.18}$$

in which case the kinematic boundary condition becomes

$$\frac{\partial\zeta'}{\partial t'} + \varepsilon\left(\frac{\partial\Phi'}{\partial x'}\frac{\partial\zeta'}{\partial x'} + \frac{\partial\Phi'}{\partial y'}\frac{\partial\zeta'}{\partial y'}\right) = \frac{\partial\Phi'}{\partial z'} \qquad \text{on } z' = \varepsilon\zeta'. \tag{2.1.19}$$

Likewise the dynamic boundary condition transforms into

$$\frac{\partial\Phi'}{\partial t'} - g'\zeta' + \frac{\varepsilon}{2}(\nabla\Phi)^2 = 0 \qquad \text{on } z' = \varepsilon\,\zeta'. \tag{2.1.20}$$

We shall now assume ε to be a small parameter thus obtaining the condition for linearised water wave theory that wave height is small in comparison to wavelength. For the time being we shall balance terms assuming that $g' = O(1)$ although we will return to this point later. We proceed by making a perturbation expansion in the small parameter to $O(\varepsilon)$ which will yield the linearised and second-order equations. Therefore substituting

$$\Phi' = \Phi'_1 + \varepsilon\,\Phi'_2 + O(\varepsilon^2) \tag{2.1.21}$$

$$\zeta' = \zeta'_1 + \varepsilon\,\zeta'_2 + O(\varepsilon^2) \tag{2.1.22}$$

into the scaled free surface equations and expanding terms in Φ' as a Taylor series about the undisturbed free surface $z' = 0$. We obtain to $O(\varepsilon)$

$$\frac{\partial\zeta'_1}{\partial t'} + \varepsilon\,\frac{\partial\zeta'_2}{\partial t'} + \varepsilon\left(\frac{\partial\Phi'_1}{\partial x'}\frac{\partial\zeta'_1}{\partial x'} + \frac{\partial\Phi'_1}{\partial y'}\frac{\partial\zeta'_1}{\partial y'}\right) = \frac{\partial\Phi'_1}{\partial z'} + \varepsilon\,\zeta'_1\frac{\partial^2\Phi'_1}{\partial z'^2} + \varepsilon\,\frac{\partial\Phi'_2}{\partial z'} \tag{2.1.23}$$

and

$$\frac{\partial \Phi_1'}{\partial t'} + \varepsilon \frac{\partial \Phi_2'}{\partial t'} + \varepsilon \zeta_1' \frac{\partial^2 \Phi_1'}{\partial z' \partial t'} - g'(\zeta_1' + \varepsilon \zeta_2') + \frac{\varepsilon}{2}(\nabla \Phi_1')^2 = 0 \qquad (2.1.24)$$

where both equations are evaluated on $z' = 0$. Therefore the linearised (first-order) equations are

$$\frac{\partial \zeta_1'}{\partial t'} = \frac{\partial \Phi_1'}{\partial z'}, \qquad (2.1.25)$$

$$\zeta_1' = \frac{1}{g'} \frac{\partial \Phi_1'}{\partial t'}, \qquad (2.1.26)$$

both of which may be combined to give

$$\frac{\partial^2 \Phi_1'}{\partial t'^2} - g' \frac{\partial \Phi_1'}{\partial z'} = 0 \qquad \text{on } z' = 0. \qquad (2.1.27)$$

At second order we have

$$\frac{\partial \zeta_2'}{\partial t'} + \frac{\partial \Phi_1'}{\partial x'} \frac{\partial \zeta_1'}{\partial x'} + \frac{\partial \Phi_1'}{\partial y'} \frac{\partial \zeta_1'}{\partial y'} = \frac{\partial \Phi_2'}{\partial z'} + \zeta_1 \frac{\partial^2 \Phi_1'}{\partial z'^2} \qquad (2.1.28)$$

$$\frac{\partial \Phi_2'}{\partial t'} - g' \zeta_2' = -\tfrac{1}{2}(\nabla \Phi_1')^2 - \zeta_1' \frac{\partial^2 \Phi_1'}{\partial z' \partial t'} \qquad (2.1.29)$$

which combine similarly to give

$$\frac{\partial^2 \Phi_2'}{\partial t'^2} - g' \frac{\partial \Phi_2'}{\partial z'} = \frac{1}{g'} \frac{\partial \Phi_1'}{\partial t'} \frac{\partial}{\partial z'} \left(\frac{\partial^2 \Phi_1'}{\partial t'^2} - g' \frac{\partial \Phi_1'}{\partial z'} \right) - \frac{\partial}{\partial t'} (\nabla \Phi_1)^2 \qquad \text{on } z' = 0. \quad (2.1.30)$$

We now return to physical variables by simply dropping the prime on the variables and summarise as below

$$\nabla^2 \Phi_i = 0 \qquad i = 1, 2 \qquad \text{throughout the fluid,} \qquad (2.1.31)$$

$$\frac{\partial \Phi_i}{\partial n} = 0 \qquad \text{on solid boundaries.} \qquad (2.1.32)$$

With linear free surface boundary condition and surface elevation given by

$$\frac{\partial^2 \Phi_1}{\partial t^2} - g \frac{\partial \Phi_1}{\partial z} = 0 \qquad (2.1.33)$$

$$\zeta_1 = \frac{1}{g} \left. \frac{\partial \Phi_1}{\partial t} \right|_{z=0} \qquad (2.1.34)$$

respectively and the second-order free surface boundary condition and surface elevation given by

$$\frac{\partial^2 \Phi_2}{\partial t^2} - g \frac{\partial \Phi_2}{\partial z} = \frac{1}{g} \frac{\partial \Phi_1}{\partial t} \frac{\partial}{\partial z} \left(\frac{\partial^2 \Phi_1}{\partial t^2} + g \frac{\partial \Phi_1}{\partial z} \right) - \frac{\partial}{\partial t} (\nabla \Phi_1)^2 \qquad (2.1.35)$$

$$\zeta_2 = \frac{1}{g} \left(\frac{\partial \Phi_2}{\partial t} + \zeta_1 \frac{\partial^2 \Phi_1}{\partial z \partial t} + \frac{1}{2} (\nabla \Phi_1)^2 \right) \qquad (2.1.36)$$

respectively.

Throughout this thesis we will work in the frequency domain. Therefore assuming time-harmonic motion of angular frequency ω, we may introduce complex valued functions ϕ_1 , η_1 such that

$$\Phi_1(x,y,z,t;K) = \mathrm{Re}\left\{\phi_1(x,y,z;K)\mathrm{e}^{-\mathrm{i}\omega t}\right\} \tag{2.1.37}$$

$$\zeta_1(x,y,z,t;K) = \mathrm{Re}\left\{\eta_1(x,y;K)\mathrm{e}^{-\mathrm{i}\omega t}\right\} \tag{2.1.38}$$

where the frequency parameter is

$$K = \frac{\omega^2}{g}. \tag{2.1.39}$$

The time-independent first-order potential now satisfies

$$\left.\begin{aligned} \nabla^2\phi_1 &= 0, && \text{throughout the fluid,} \\ \frac{\partial\phi_1}{\partial z} + K\phi_1 &= 0, && \text{on } z = 0, \\ \frac{\partial\phi_1}{\partial n} &= 0, && \text{on solid boundaries,} \end{aligned}\right\} \tag{2.1.40}$$

with the surface elevation recovered from

$$\eta_1 = \mathrm{Re}\left\{\frac{-\mathrm{i}\omega}{g}\phi_1\right\}, \qquad \text{on } z = 0. \tag{2.1.41}$$

We shall use the solution of the linearised problem in a domain of constant depth h as the basic building block of the solution method for more complicated geometries. In such a domain it is routine to separate variables to find that the solution to equations (2.1.40) corresponding to surface waves propagating at an angle θ to the x axis is given by

$$\phi(x,y,z) = \frac{\mathrm{i}ga}{\omega}.\frac{\cosh k(h-z)}{\cosh kh}\,\mathrm{e}^{\mathrm{i}k(x\cos\theta + y\sin\theta)} \tag{2.1.42}$$

in which case the free surface boundary condition yields the dispersion relation

$$K = k\tanh kh \tag{2.1.43}$$

relating the wavenumber k to the frequency. As an aside our scaling assumptions required that $g' = O(1)$, which we see from (2.1.43) is equivalent to requiring

$\tanh kh = O(1)$ as well as $ka \ll 1$. In practical terms this tells us that the equations of motion are valid in intermediate to deep water, a constraint which was clear in Stokes' [91] original exposition. Alternatively, if the amplitude of the wave motion is comparable to the fluid depth then one would re-expand and in fact recover the shallow water equations; see for example Wehausen & Laitone [101] who give a very clear exposition of this approximation.

It can be seen graphically that for a fixed K, (2.1.43) has only one positive real root (see for example Mei [61] §7.4). However, by allowing the wavenumber to be complex there is an infinite number of eigenvalues $\mathrm{i}k_n$, $n \geq 1$ which lie on the imaginary axis and satisfy the dispersion relation

$$K + k_n \tan k_n h = 0. \tag{2.1.44}$$

It is customary to order the k_n in ascending order so that

$$\left(n - \tfrac{1}{2}\right)\pi < k_n h < n\pi \tag{2.1.45}$$

and, in fact as $n \to \infty$

$$k_n h = n\pi + O\left(\frac{1}{n}\right). \tag{2.1.46}$$

If we also define $k_0 = -\mathrm{i}k$, then the separation of variables approach gives a set of depth modes

$$\psi_n(z) = N_n^{-1/2} \cos k_n(h - z) \qquad n \geq 0 \tag{2.1.47}$$

with normalisation

$$N_n = \frac{1}{2}\left(1 + \frac{\sin 2k_n h}{2k_n h}\right) \qquad n \geq 0 \tag{2.1.48}$$

such that the orthogonality relation

$$\int_0^h \psi_n(z)\psi_m(z) = h\delta_{mn} \tag{2.1.49}$$

holds, and which Kreisel [47] has proven is complete. For convenience we note that our definition of k_0 gives

$$\psi_0(z) = N_0^{-1/2} \cosh k(h - z) \tag{2.1.50}$$

and

$$N_0 = \frac{1}{2}\left(1 + \frac{\sinh 2kh}{2kh}\right) \tag{2.1.51}$$

which by comparison with (2.1.42) we see corresponds to depth dependence of a propagating mode.

2.2 The Mild Slope Equation

For wave problems involving variable depth domains, the bed condition usually calls for some kind of approximation. In many physical problems it is appropriate to assume that the bed slope does not vary significantly within a wavelength; this is the basis of the mild slope approximation. The mild-slope equation (MSE), often attributed to Berkhoff [6], and later refinements by Chamberlain & Porter [11] (modified mild-slope equations - MMSE) introduce approximate analytical techniques essentially involving depth-averaging under the assumption of small variations in the bed shape. Chamberlain & Porter [11] derived the MMSE via a variational formulation, whereas Berkhoff [6] derived the MSE by a depth-averaging formulation. We shall follow the derivation in Mei [61] which in turn follows Berkhoff's original exposition; however, we shall recover Chamberlain and Porter's MMSE by retaining some terms which Mei/Berkhoff neglected.

We consider time harmonic waves in a fluid domain having a fixed arbitrary bed defined by $z = h(x, y)$ in which case the exact equations of motion are given by (2.1.40) as

$$\frac{\partial^2 \Phi}{\partial z^2} + \nabla^2 \Phi = 0, \qquad 0 \le z \le h, \qquad \nabla = \left(\frac{\partial}{\partial x}, \frac{\partial}{\partial y}\right) \tag{2.2.1}$$

$$\Phi_z + K\Phi = 0, \qquad \text{on } z = 0, \tag{2.2.2}$$

$$\frac{\partial \Phi}{\partial z} = -\nabla h . \nabla \Phi \qquad z = -h(x, y). \tag{2.2.3}$$

We observe that, for any two sufficiently smooth functions f and Φ

$$\frac{\partial}{\partial z}\left(f\frac{\partial \Phi}{\partial z} - \Phi\frac{\partial f}{\partial z}\right) = f\frac{\partial^2 \Phi}{\partial z^2} - \Phi\frac{\partial^2 f}{\partial z^2} \tag{2.2.4}$$

and we note that in the case of constant depth the potential separates to the form $\Phi = f(z)\phi(x,y)$ where f takes the form

$$f = \operatorname{sech}(kh)\cosh(k(h-z)). \tag{2.2.5}$$

We now suppose that, in the case of slowly varying h (i.e. $\nabla h/kh \ll 1$) we may seek a solution of the form

$$\Phi(x,z) = f(z,h(x,y))\phi(x,y) \tag{2.2.6}$$

where f is given by equation (2.2.5) but we now allow h to vary with the horizontal coordinates. We then remove the depth dependence by integrating equation (2.2.4) over the depth, and using equations (2.2.2), (2.2.3) and the dispersion relation (2.1.43) to give

$$f\frac{\partial\Phi}{\partial z} - \Phi\frac{\partial f}{\partial z}\bigg|_h = -\int_0^h f\nabla^2\Phi + k^2 f\Phi \,\mathrm{d}z. \tag{2.2.7}$$

We note that the bed condition (2.2.3) together with the anticipated form of Φ from (2.2.6) gives

$$f\frac{\partial\Phi}{\partial z}\bigg|_h = -f^2\nabla h.\nabla\phi|_h - f(\nabla h)^2\frac{\partial f}{\partial h}\phi\bigg|_h. \tag{2.2.8}$$

and also

$$\nabla\Phi = f\nabla\phi + \phi\frac{\partial f}{\partial h}\nabla h, \qquad \text{and} \tag{2.2.9}$$

$$\nabla^2\Phi = f\nabla^2\phi + 2\frac{\partial f}{\partial h}\nabla\phi.\nabla h + \phi\frac{\partial^2 f}{\partial h^2}(\nabla h)^2 + \phi\frac{\partial f}{\partial h}\nabla^2 h. \tag{2.2.10}$$

Finally, Leibniz's rule gives

$$\nabla.\int_0^h f^2\nabla\phi \,\mathrm{d}z = \int_0^h \left(f^2\nabla^2\phi + 2f\frac{\partial f}{\partial h}\nabla h.\nabla\phi\right) \mathrm{d}z + f^2\nabla h.\nabla\phi|_h \tag{2.2.11}$$

which allows us to rewrite equation (2.2.7) as

$$\nabla.\int_0^h f^2\nabla\phi \,\mathrm{d}z + (\nabla h)^2\left(\int_0^h f\phi\frac{\partial^2 f}{\partial h^2}\,\mathrm{d}z + f\phi\frac{\partial f}{\partial h}\bigg|_h\right) + \nabla^2 h\int_0^h f\phi\frac{\partial f}{\partial h}\,\mathrm{d}z + \int_0^h k^2 f^2\phi\,\mathrm{d}z = 0 \tag{2.2.12}$$

We note that ϕ is independent of z so (2.2.12) may be rewritten as

$$\nabla.(U_0\nabla\phi) + V_0\phi = 0 \tag{2.2.13}$$

where

$$V_0 = k^2U_0 + U_1\nabla^2 h + U_2(\nabla h)^2, \tag{2.2.14}$$

$$U_0 = \int_0^h f^2\,\mathrm{d}z, \tag{2.2.15}$$

$$U_1 = \int_0^h f\frac{\partial f}{\partial h}\,\mathrm{d}z, \tag{2.2.16}$$

$$U_2 = \int_0^h f\frac{\partial^2 f}{\partial h^2}\,\mathrm{d}z + f\frac{\partial f}{\partial h}\bigg|_{-h}. \tag{2.2.17}$$

We now proceed to calculate the U_i explicitly. U_0 is easily calculated from (2.2.5) as

$$U_0(h) = \frac{1}{2k}\tanh kh\left(1 + \frac{2kh}{\sinh 2kh}\right) \tag{2.2.18}$$

and we note from the dispersion relationship that $k = k(h)$ and therefore we deduce that

$$k'(h) = -2k^2(\mathcal{K} + \sinh\mathcal{K})^{-1} \qquad \text{where } \mathcal{K} = 2kh \tag{2.2.19}$$

which enables us to write

$$\frac{\partial f}{\partial h} = k'(h)\,\mathrm{sech}kh(z\sinh(k(z+h)) - k^{-1}\sinh(kh)\sinh(kz)). \tag{2.2.20}$$

U_1 may now be easily evaluated to give

$$U_1(h) = \frac{k\,\mathrm{sech}^2(kh)}{4(\mathcal{K} + \sinh\mathcal{K})}\{\sinh\mathcal{K} - \mathcal{K}\cosh\mathcal{K}\}. \tag{2.2.21}$$

In principle U_2 can also be calculated in the same manner although the algebra is somewhat simplified if we note that Leibniz's rule combined with (2.2.15) and (2.2.16) gives

$$U_2 = U_1'(h) - \int_0^h \left(\frac{\partial f}{\partial h}\right)^2 \mathrm{d}z \tag{2.2.22}$$

from which we deduce that

$$\begin{aligned} U_2(h) = {} & \frac{k\,\mathrm{sech}^2(kh)}{12(\mathcal{K} + \sinh\mathcal{K})^3}\{\mathcal{K}^4 + 4\mathcal{K}^3\sinh\mathcal{K} - 9\sinh\mathcal{K}\sinh 2\mathcal{K} \\ & +3\mathcal{K}(\mathcal{K} + 2\sinh\mathcal{K})(\cosh^2\mathcal{K} - 2\cosh\mathcal{K} + 3)\}. \end{aligned} \tag{2.2.23}$$

Finally, following Porter and Porter [78] we transform equation (2.2.13) into its canonical form by writing

$$\phi(x) = (U_0(h(x,y)))^{-1/2}\psi(x). \tag{2.2.24}$$

Then ψ satisfies

$$\left.\begin{aligned} \psi'' + \kappa(x,y)\psi &= 0 \\ \kappa(x) &= k^2 + A\nabla^2 h + B(\nabla h)^2, \end{aligned}\right\} \tag{2.2.25}$$

where $A(x)$ and $B(x)$ are found using equations (2.2.12) and (2.2.23) to be

$$A = -2k/(\mathcal{K} + \sinh\mathcal{K}) \tag{2.2.26}$$

$$\begin{aligned} B = {} & k^2\{\mathcal{K}^4 + 4\mathcal{K}^3\sinh\mathcal{K} + 3\mathcal{K}^2(2\cosh^2\mathcal{K} + 1) + 18\mathcal{K}\sinh\mathcal{K} \\ & + 3\sinh^2\mathcal{K}(2\cosh\mathcal{K} + 5)\}/\{3(\mathcal{K} + \sinh\mathcal{K})^4\}. \end{aligned} \tag{2.2.27}$$

Berkhoff/Mei obtain the MSE by discarding the terms including U_1 and U_2 in 2.2.14 on the basis that $\nabla^2 h$ and ∇h are small, although curiously when they introduce the transformation (2.2.24) terms of the same order reappear. In contrast, when we retain terms of this order we obtain Chamberlain & Porter's MMSE [11]. It is not surprising that we obtain the same result as Chamberlain and Porter as the two approaches yield the same forms of modified equations with identical definitions of the U_i.

2.3 Green's identity and integral equations

Throughout this thesis our main method of solution will be to formulate problems as integral equations and then to solve them using techniques appropriate to the structure of the particular form of the integral equation. There is a vast literature dealing with the solution of integral equations and the numerical difficulties therein. For an introduction to solution techniques from a practical perspective see for example Porter & Stirling [72], in which they observe that integral equations

> "offer a powerful (sometimes the only) technique for solving a variety of practical problems. One reason for this utility is that all of the conditions

specifying an initial or boundary value problem for a differential equation can often be condensed into a single integral equation. In the case of partial differential equations the dimension of the problem is reduced in this process so that, for example, a boundary value problem for a partial differential in two independent variables transforms into an integral equation involving an unknown function of only one variable."

This highlights a significant benefit of the integral equation approach, but is by no means the only benefit, as the "smoothing" process inherent in integration proves to have advantages when seeking approximate solutions.

The integral equation is constructed by applying Green's identity to the potential ϕ and a Green's function G so that

$$\iiint_D G\nabla^2\phi - \phi\nabla^2 G \,\mathrm{d}V = \iint G_S \frac{\partial\phi}{\partial n} - \phi\frac{\partial G}{\partial n}\,\mathrm{d}S \tag{2.3.1}$$

where S is the bounding surface of the fluid domain D and n is the outward facing normal. The Green's function represents an oscillating source placed in the fluid at a field point $\mathbf{r_0}$ and as such satisfies

$$\nabla^2 G = -\delta(\mathbf{r} - \mathbf{r_0}). \tag{2.3.2}$$

Typically the structure of the problem and choice of Green's function is such that we end up with an integral equation of the form

$$\phi(\mathbf{r_0}) = \phi_{inc}(\mathbf{r_0}) - \iint_{S_B} \phi\frac{\partial G}{\partial n}\,\mathrm{d}S \tag{2.3.3}$$

where ϕ_{inc} is given, but as yet unspecified function and $S_B \subset S$. For clarity of exposition we now consider a one-dimensional prototype integral equation which is the direct equivalent of (2.3.3)

$$\phi(x) = \int_a^b k(x,t)\phi(t)\,\mathrm{d}t + f(x) \qquad a \le x \le b, \tag{2.3.4}$$

where $k(x,t)$ is called the kernel of the integral equation and the function $f(x)$, which is assumed to be known, is called the free term. Integral equations are also

classified according to their structure, so that

$$f(x) = \int_a^b k(x,t)\phi(t)\,\mathrm{d}t \qquad a \leq x \leq b \tag{2.3.5}$$

is called a Fredholm equation of the first kind whereas (2.3.3) is called a Fredholm equation of the second kind. For completeness, the Fredholm equation of the third kind is

$$\psi(x)\phi(x) = \int_a^b k(x,t)\phi(t)\,\mathrm{d}t + f(x) \qquad a \leq x \leq b, \tag{2.3.6}$$

where $\psi(x)$ is a given function. We do not consider this form of integral equation further, and in any case if $\psi(x)$ does not vanish in $[a,b]$ then it reduces trivially to a second kind integral equation anyway. Finally, an integral equation is defined as singular if:

1. at least one of the integration limits, or the interval in which the equation holds, is infinite; or
2. the kernel is unbounded in the given interval.

Singular integral equations arise naturally in Green's function formulations where the nature of the singularity is a crucial factor in the complexity of the solution technique. If we define r as $|\mathbf{r}-\mathbf{r_0}|$, the distance between the source point and field point then the singularity is classified according to the following behaviour of the kernel as $r \to 0$

Dimension	Weakly singular	Strongly singular	Hypersingular
2D	$O(r^{-\alpha}), \quad \alpha \in (0,1)$	$O(r^{-1})$	$O(r^{-2})$
3D	$O(r^{-1})$	$O(r^{-2})$	$O(r^{-3})$

Thus, in our example (2.3.4) which may be viewed as the integral equation resulting from a two-dimensional problem, then a kernel of the form

$$k(x,t) = \frac{\hat{k}(x,t)}{|x-t|^{\alpha}}, \qquad \alpha \in (0,1) \tag{2.3.7}$$

where $\hat{k}$ is a bounded function is a weakly singular kernel. It should be noted that a logarithmically singular kernel

$$k(x,t) = \hat{k}(x,t)\log|x-t| \tag{2.3.8}$$

if rewritten as

$$k(x,t) = \frac{\hat{k}(x,t)|x-t|^{\varepsilon}\log|x-t|}{|x-t|^{\varepsilon}}, \qquad \varepsilon \in (0,1) \tag{2.3.9}$$

is also seen to be weakly singular. A kernel of the form

$$k(x,t) = \frac{k(x,t)}{x-t} \tag{2.3.10}$$

is called strongly singular, or alternatively Cauchy singular, finally a kernel of the form

$$k(x,t) = \frac{\hat{k}(x,t)}{(x-t)^2} \tag{2.3.11}$$

is called hypersingular. A large body of literature concentrates on techniques for dealing with Cauchy singular or hypersingular problems as these kernels, which require special treatment occur frequently in physical problems, but often as a consequence of the solution technique chosen. Also, for Cauchy and hypersingular kernels the integrals have to be interpreted in a specific way, see, for example Appendix C to Linton & McIver [51]. Weakly singular kernels, in contrast, are much more straightforward to deal with. The main goal of this thesis is, rather than to develop new techniques for dealing with Cauchy singular kernels, to formulate the integral equation so that it has a kernel which is, at worst, only weakly singular.

Once we have formulated the equation as a weakly singular integral equation there is a range of straightforward and powerful methods of solution which require no further special treatment. Typically we define an integral operator

$$(\mathcal{K}\phi)(x) = \phi(x) - \int_a^b k(x,t)\phi(t)\,\mathrm{d}t \tag{2.3.12}$$

where $\mathcal{K} \in L_2(a,b)$ which is equipped with an inner product

$$\langle u, v\rangle = \int_a^b u(x)\overline{v(x)}\,\mathrm{d}x \tag{2.3.13}$$

in which case the integral equation (2.3.4) becomes

$$(\mathcal{K}\phi)(x) = f(x). \tag{2.3.14}$$

Perhaps the most straightforward means of finding an approximate solution to (2.3.14) is collocation, which at its simplest requires the equation to hold exactly at a fixed number N of points. Therefore if x_i is the $i'th$ collocation point, ϕ_i the potential at that point and f_i the value of the forcing term, then the collocation scheme is

$$\phi_i - \frac{b-a}{N}\sum_{j=1}^{N} k(x_i, x_j)\phi_j = f_i, \qquad i = 1, \ldots, N. \tag{2.3.15}$$

The point $i = j$ typically requires careful treatment but can be calculated, see for example Linton & McIver [51]. This has converted the integral equation into a matrix equation of the form

$$(I - A)p = f \tag{2.3.16}$$

where I is the identity matrix and p, f are vectors whose entries are the potential and forcing terms respectively at the collocation points. Solution of the matrix equation is straightforward by standard methods such as LU decomposition. Leaving aside questions of convergence, intuitively one would expect that, as the number of collocation points increases we would get a closer approximation to the potential by interpolating from the values at the collocation points.

A more sophisticated approach is the so called boundary integral element approach where the interval over which ϕ is to be approximated is split into N equal elements of length $2h$ so that $2hN = b - a$. We then collocate at the mid points x_i of the panel to obtain the set of equations

$$\phi(x_i) - \sum_{j=1}^{N}\int_{E_j} k(x_i, t)\phi(t)\,\mathrm{d}t = f(x_i) \qquad i = 1, \ldots, N \tag{2.3.17}$$

where E_j is the $j'th$ element $(t_j - h, t_j + h)$. The potential is then chosen to take a particular form $\phi_j(t)$ in each element such that

$$\int_{E_j} k(x_i, t)\phi_j(t)\,\mathrm{d}t = A_{ij}\phi(x_j) \tag{2.3.18}$$

in which case we again arrive at a matrix equation

$$\phi(x_i) - \sum_{j=1}^{N} A_{ij}\phi(x_j) = f(x_i) \qquad i = 1, \ldots, N. \tag{2.3.19}$$

What now distinguishes various boundary integral element approaches is the choice of the form of the potential on an element. Typically one might choose a polynomial approximation to ϕ on the element with the form (2.3.18) recovered by requiring continuity of ϕ, and as many of its higher derivatives as necessary to determine the polynomial coefficients, at the end points of the elements. Again, intuitively it is expected that increasingly sophisticated choices for the representation of ϕ will give increasingly accurate representations of the solution. For our purposes the simplest possible representation of $\phi_j(t) = \phi(t_j)$ i.e. ϕ is a constant on each panel equal to its value at the midpoint, is ideal as it shows trivially how (2.3.18) is arrived at. In this case

$$A_{ij} = \int_{E_j} k(x_i, t)\,\mathrm{d}t \tag{2.3.20}$$

and the accuracy of the method is also anticipated to be improved by increasing the accuracy of the integration over the boundary element. In contrast if we choose the simplest possible quadrature, namely the midpoint rule, in (2.3.20) we see that we recover the simple collocation scheme (2.3.15).

The final method of solution we will use is the so-called Rayleigh-Ritz method which depends upon a variational approach to equation (2.3.14). To illustrate this method we will assume that $\mathcal{K}$ is a self adjoint operator on a Hilbert space $\mathcal{H} = L_2[a,b]$ i.e.

$$\langle \mathcal{K}u, v\rangle = \langle u, \mathcal{K}v\rangle. \tag{2.3.21}$$

This restriction that $\mathcal{K}$ is self-adjoint is not critical as the theory that follows can be extended to deal with non-self-adjoint operators provided the adjoint problem is given.

We now consider a functional $J : \mathcal{H} \to \mathbb{C}$ defined by

$$J(p) = \langle p, f\rangle + \langle f, p\rangle - \langle \mathcal{K}p, p\rangle, \qquad p \in \mathcal{H} \tag{2.3.22}$$

which is designed to be stationary at $p = \phi$ where its value is

$$J(\phi) = P = \langle \phi, f\rangle \tag{2.3.23}$$

which is typically a quantity of interest in the physical problem. Any approximation to ϕ, say $\tilde{\phi}$ gives rise to an approximate value $\tilde{P}$ of P. Then the variational principle above gives the estimate

$$|P - \tilde{P}| = O(||\phi - \tilde{\phi}||^2) \tag{2.3.24}$$

which implies that approximations to the quantities of interest are second-order accurate with respect to first-order approximations to the exact solutions of the integral equation. Adopting this approach we approximate ϕ by $\tilde{\phi} \in \mathcal{H}_{N+1}$, an $N+1$ dimensional subspace of $\mathcal{H}$ spanned by a set of test functions $p_n(x) \in \mathcal{H}_{N+1}$ by writing

$$\phi \approx \tilde{\phi} = \sum_{n=0}^{N} a_n p_n(x). \tag{2.3.25}$$

This approximation is substituted in place of p in (2.3.22) to give

$$J(\tilde{p}) = \sum_{n=0}^{N} a_n \langle p_n, f \rangle + \sum_{n=0}^{N} \overline{a_n} \langle f, p_n \rangle - \sum_{n=0}^{N} \sum_{m=0}^{N} a_n \overline{a_m} \langle \mathcal{K} p_n, p_m \rangle. \tag{2.3.26}$$

We now make this expression stationary with respect to the coefficients a_n by requiring

$$\frac{\partial J(\tilde{p})}{\partial a_n} = 0 \qquad n = 0, \ldots, N, \tag{2.3.27}$$

which implies the system of equations

$$\langle p_n, f \rangle - \sum_{m=0}^{N} \overline{a_m} \langle \mathcal{K} p_n, p_m \rangle = 0 \qquad , n = 0, \ldots, N. \tag{2.3.28}$$

Finally, taking the complex conjugate of (2.3.28) and using the self-adjointness of $\mathcal{K}$ we arrive at

$$\sum_{m=0}^{N} a_m \langle \mathcal{K} p_m, p_n \rangle = \langle f, p_n \rangle \qquad n = 0, \ldots, N, \tag{2.3.29}$$

which has, once again, reduced the integral equation into a matrix equation.

This method is equivalent to Galerkin's method, a so-called projection method, which is arrived at in a different manner. In this approach we again seek to approximate the solution ϕ to $\mathcal{K}\phi = f$ in E_N, a N dimensional subspace of $\mathcal{H}$. We

assume E_N is spanned by a set of functions p_n so that we may approximate

$$\phi \approx \widetilde{\phi} = \sum_{n=0}^{N} a_n p_n(x). \tag{2.3.30}$$

Galerkin's method then requires that the residual $(\mathcal{K}\widetilde{\phi} - f)$ is orthogonal to each of the functions p_m, $m = 0, \ldots, N$ which ensures that $\mathcal{K}\widetilde{\phi} = f$ is within E_N. This requirement gives equation (2.3.29) exactly, thus establishing the equivalence of the two approaches. We now expect that, by choosing larger dimension subspaces, we will converge to the true solution as $N \rightarrow \infty$ thus enabling us to obtain whatever degree of accuracy we wish by choosing N sufficiently large. One final point is that a judicious choice of the subspace, which incorporates some of the physics of the solution, will give more accurate approximations for fixed N than an injudicious choice. For further discussion of these matters the reader is referred to Porter & Stirling [72].

One interesting consequence of (2.3.29) is that if we choose

$$p_n(x) = \begin{cases} 0 & x \in [a,b] \setminus [(n-1)2h, n2h] \\ 1 & x \in [(n-1)2h, n2h] \end{cases} \tag{2.3.31}$$

where $h = (b-a)/2N$ the set of equations we obtain from the Rayleigh-Ritz/Galerkin method is identical to that obtained from the boundary integral/collocation method. Thus we may infer that the collocation approach is second-order accurate in an L_2 norm sense, although this choice of spanning function is not necessarily the most judicious choice.

Chapter 3

Two-dimensional sloshing over an arbitrary bed

3.1 Introduction

The sloshing problem is a classical eigenvalue problem of fluid mechanics, a standard reference for which is Lamb [49]. The references in Lamb show the problem's long history and the illustrious names involved with it; however, he notes that despite such long standing attention, the number of cases of motion with a variable depth for which the solution has been obtained is very small. Lamb presents the analysis for a triangular canal whose section consists of two straight lines inclined at $\pi/4$ to the vertical and which, to date remains one of the few cases for which an analytical solution is known. During the mid-twentieth century there was an upsurge of interest in the sloshing problem driven by the need to develop a theory of the motion of fluid within partially filled containers. The main applications of the era as highlighted by Moiseev [65] were all aspects of fuel tank problems, ranging from aircraft fuel within wings to liquid-fuelled rockets, as well as, for example, seismic oscillations of structures under water pressure. Moiseev [65] and subsequently Moiseev & Petrov [66] provided extensive reviews of the linear theory and main references of the period. Although Moiseev states that most of the applications occur in circumstances where perturbation theory proves extremely effective, he reiterates that even the linearised case calls for numerical calculation. Moiseev does not deal with non-linear oscillations

where he states that many of the algorithms of the time were clumsy and convergence was unproved.

The advent of high-power computational facilities has enabled researchers to make progress, albeit numerically, in the sloshing problem. The motivation is still driven by the technological problems arising from the often violent motion of the fluid within partially-filled fluid containers. Efficient and accurate calculation of sloshing frequencies remains an important goal as it is desirable to avoid the resonance which is known to occur in a system externally forced at, or near, a sloshing frequency. It is also known that violent motions can induce large pressures so accurate modelling of the motion is also required to estimate the pressures and to engineer safe containers. Research has continued actively in two complementary directions, namely identifying the sloshing frequencies, and modelling the non-linear fluid motion.

There has been much work on non-linear sloshing motions based on improving modal approaches or using computational fluid dynamics code. Some papers are discussed below and the references therein provide a fair coverage of the field. Faltinsen [29] found analytic results for the motion of a two-dimensional rectangular tank forced to oscillate harmonically at frequencies close to the lowest natural mode of oscillation and with small amplitudes of roll or sway. Faltinsen *et al.* [30], Faltinsen & Timokha [31], Faltinsen & Timokha [32] and Faltinsen Rognebakke & Timokha [33] develop a multi-dimensional modal approach using generalized domain and surface modes rather than natural modes. This basic approach, and its refinements in the later papers as they develop are shown to model sloshing in intermediate to small depths and in tanks where the length to breadth ratio is $O(1)$ and therefore a two-dimensional approach is questionable. However, they note the difficulties inherent in a modal approach of dealing with run-up, overturning and dissipation due to local breaking. The sloshing problem is also amenable to non-linear solvers, for example see Wu & Eatock-Taylor [103] who apply their finite-element method code to consider the sloshing problem in a rectangular tank. Their approach is to perform a finite-element analysis, obtaining the solution through a variational principle and

obtaining the fluid motion by a Galerkin approach. They extend this work in Wu & Eatock-Taylor [104] where they consider three-dimensional translational motion in a rectangular tank and observe travelling waves and bores in addition to standing waves. Their work is calibrated by checking that their three-dimensional code applied to two-dimensional motion gives consistent results with two-dimensional solvers. In the course of this paper they clearly demonstrate that there remain many interesting problems associated with the sloshing problem.

The other main direction of research has focussed on the calculation of linear sloshing frequencies. Davis [18] established important results regarding uniqueness of solution and provided asymptotics of the eigenvalues for two-dimensional oscillations in canals of arbitrary cross section. In Davis [19] significant progress was made in asymptotics for the semicircular cross section which at the time remained unsolved. Packham [69] solved the case for a triangular canal with sides inclined at $\pi/6$ to the horizontal. Craggs & Duck [17] show how techniques from complex-variable theory may be applied to two-dimensional problems and proceed to solve the segmental and arbitrary triangular cross section. Fox & Kuttler [36] provide an extensive review of the two-dimensional sloshing problem and appropriate references. In their paper they provide upper and lower bounds for numerous cross sections by using conformal mappings from the specific geometry to one whose explicit solution is known. They also refer to a series of papers by Henrici, Troesch & Wuytack [41], Troesch & Troesch [93], Miles [63], Troesch [94] and Troesch [95] on the 'ice-fishing' problem, or sloshing in a strip aperture in an infinite half-space. This is important in providing bounds on sloshing frequencies through domain monoticity, meaning that if two domains have the same free-surface but one domain contains the other then the containing region has the larger sloshing frequency. This theoretical result is also confirmed in the numerical results we produce in this chapter. Later work by McIver [56] has looked at cylindrical and spherical containers filled to arbitrary depths. Evans & Linton [26] also considered both an infinite and finite cylinder with semicircular cross section as well as a hemisphere, and presented an extremely efficient technique of calculating

the lowest sloshing frequencies.

Despite the long history of the sloshing problem, there is relatively little work on the case of arbitrary bed shapes. Booij [8] has used the MSE (see Chapter 2) to compute oblique sloshing in a tank with a flat sloping bottom and appeared to obtain quite good agreement with a numerical solution based on a finite-element method. The focus of this chapter is on solving the sloshing problem to second-order providing a weakly non-linear solution. Essentially this introduces the much more complicated free-surface problem whereby the first-order potential forces the second-order potential, in essence having the effect of a pressure distribution on the free-surface in the second-order problem. Wehausen & Laitone [101] §21 discuss this problem in general, whereas later papers on second-order scattering such as Vada [99], McIver & McIver [55] and McIver [54] make use of the specific form of this forcing to solve scattering problems. One specific use of the MSE is in McIver & Smith [?] where they investigate sloshing problems in closed basins.

We base our approach on the Green's Identity method of Porter & Porter [77] and, through careful formulation and manipulation, we are able to extend it to the much more complicated second-order problem. Fundamental to this is the use of the Cauchy-Riemann equations to convert normal to tangential derivatives simplifying the integral equations to be solved. It should be emphasized that our formulation is exact at each order, satisfying the no-flow condition at the bed and the complicated free-surface boundary conditions. We show how to apply the approach twice, non-trivially dealing with the problem of defining the first-order potential on the free-surface, which is required to feed into the second-order problem. This key step to our problem did not need to be calculated in Porter & Porter [77] to determine the scattering coefficients and was therefore not considered. The second-order problem requires more careful manipulation as, in this case, the integral equation to be solved is inhomogeneous. However, we find it is possible to solve it and find a solution expressed in terms of the coefficients of the first-order solution. We formulate the problem and then proceed to solve at first-order showing how to calculate the sloshing frequencies and how to obtain

an expression for the first-order potential. We then show how to solve the second-order problem, again yielding solutions for the second-order potential on the free-surface which is required to calculate the free-surface elevation. We present calculations of the sloshing frequencies confirming that our method gives correct results for known bed shapes. We also compare our results for sloshing frequencies with those predicted by the MSE and MMSE and present results showing that, for the sloshing problem at least, the MSE/MMSE's effectiveness not only depends upon the maximum slope but on the specific geometry under consideration. Although our formulation is exact, the Galerkin approximation used to solve the integral equations provides an approximate solution at first-order, so we present data indicating the rapid convergence of the approximation. Finally we show the second-order corrections to the first-order surface elevations.

3.2 Formulation and preliminaries

The problem is to solve the free sloshing problem to second-order in a tank D whose walls are at $x = 0,\ x = l$ and whose bed is given by the curve C defined as $z = h(x)$. The fluid motion, which is taken to be two-dimensional, may therefore be described in terms of a velocity potential $\Phi(x, z, t)$ where x is the horizontal axis and z is the vertical axis. Furthermore, as usual we assume time harmonic motion of angular frequency ω for the first-order potential. The linear boundary value problem from (2.1.31) to (2.1.33) now becomes

$$\nabla^2\phi_1 = 0, \quad (x,y) \in D, \qquad \nabla = \left(\frac{\partial}{\partial x}, \frac{\partial}{\partial z}\right), \tag{3.2.1}$$

$$\frac{\partial\phi_1}{\partial z} + K\phi_1 = 0, \quad \text{on } z = 0,\ 0 < x < l, \tag{3.2.2}$$

$$\frac{\partial\phi_1}{\partial x} = 0, \quad \text{on } \{x = 0, z \in (0, h(0))\} \cup \{x = l, z \in (0 < h(l))\}, \tag{3.2.3}$$

$$\frac{\partial\phi_1}{\partial n} = 0, \quad \text{on } z = h(x),\ 0 < x < l. \tag{3.2.4}$$

In the case of constant depth $h(x) = h_0$ this problem is easily solved by separation of variables to give modal solutions

$$\phi_1^{(n)} = C_n \cos \mu_n x \cosh \mu_n (h_0 - z) \tag{3.2.5}$$

for arbitrary coefficients C_n where

$$\mu_n = \frac{n\pi}{l}, \qquad n = 1, 2, \ldots. \tag{3.2.6}$$

with frequencies $\omega = \omega_n$ determined by the dispersion relation

$$K = \mu_n \tanh(\mu_n h_0). \tag{3.2.7}$$

So for the first mode, for example, the dimensionless wavenumber $\mu_n l$ is given by π which, for a tank where $l/h_0 = 1$ gives a dimensionless frequency $Kl = 3.1299$, and for a tank where $l/h_0 = 2$, gives $Kl = 2.8813$.

We also follow Vada [99] and McIver & McIver [55] to express the second-order free-surface boundary condition (2.1.35) as

$$\frac{\partial^2 \Phi_2}{\partial t^2} - g\frac{\partial \Phi_2}{\partial z} = \mathrm{Re}[F(x)\mathrm{e}^{-2\mathrm{i}\omega t}] + F_s(x), \qquad \text{on } y = 0 \tag{3.2.8}$$

where

$$F(x) = \left[\mathrm{i}\omega(\nabla\phi_1)^2 - \tfrac{1}{2}\mathrm{i}\omega\phi_1\frac{\partial}{\partial z}\left(K\phi_1 + \frac{\partial \phi_1}{\partial z}\right)\right]_{z=0} \tag{3.2.9}$$

and

$$F_s(x) = \frac{\mathrm{i}\omega}{4}\left[\phi_1\overline{\frac{\partial^2\phi_1}{\partial x^2}} - \overline{\phi_1}\frac{\partial^2\phi_1}{\partial x^2}\right]_{z=0} \tag{3.2.10}$$

and $\overline{\phi}$ denotes the complex conjugate of ϕ.

In the solution to both the first and second-order problem we will make use of the Green's function for a two-dimensional infinite domain with a constant depth d which we will denote $G_1(x, z|x_0, z_0)$, and which satisfies

$$\nabla^2 G_1 = -\delta(x - x_0)\delta(z - z_0), \qquad -\infty < x < \infty,\ 0 < z < d, \tag{3.2.11}$$

$$\frac{\partial G_1}{\partial z} + KG_1 = 0 \qquad \text{on } z = 0, \tag{3.2.12}$$

$$\frac{\partial G_1}{\partial z} = 0 \qquad \text{on } z = h_0,\ -\infty < x < \infty\,. \tag{3.2.13}$$

It has the form

$$G_1(x,z|x_0,z_0)=\sum_{n=0}^{\infty}\frac{\psi_n(z)\psi_n(z_0)}{2k_nh_0}\mathrm{e}^{-k_n|x-x_0|}, \tag{3.2.14}$$

and a derivation is presented at Appendix A. An alternative derivation of this Green's function is presented in Mei [61] however, it should be noted that the final expression therein contains a sign error.

We now construct, using the method of images, a Green's function $G(x,z|x_0,z_0;K)$ for the tank satisfying (3.2.11) - (3.2.13) for $0<x<l$ with $G_x=0$ on $x=0,l$ for $0<z<h_0$. Hence

$$G(x,z|x_0,z_0)=\sum_{m=-\infty}^{\infty}\{G_1(2ml+x,z|x_0,z_0)+G_1(2ml-x,z|x_0,z_0)\} \tag{3.2.15}$$

or by using (3.2.14)

$$G(x,z|x_0,z_0)=\sum_{m=-\infty}^{\infty}\sum_{n=0}^{\infty}\frac{\psi_n(z)\psi_n(z_0)}{2k_nh_0}\{\mathrm{e}^{-k_n|2ml+x-x_0|}+\mathrm{e}^{-k_n|2ml-x-x_0|}\}. \tag{3.2.16}$$

from which we deduce that

$$G(x,z|x_0,z_0)=\sum_{n=0}^{\infty}\frac{\psi_n(z)\psi_n(z_0)}{2k_nh_0}\frac{\{\cosh k_n(l-|x-x_0|)+\cosh k_n(l-x-x_0)\}}{\sinh k_nl}. \tag{3.2.17}$$

We note that G converges everywhere in the domain apart from $(x,z)=(x_0,z_0)$ where it possesses a log singularity.

3.3 First-order solution

We proceed to find the first-order potential using the method of Porter & Porter [77].

We apply Green's Identity

$$\int\int_D(\phi_1\nabla^2G-G\nabla^2\phi_1)\,\mathrm{d}D=\int_S\left(\phi_1\frac{\partial G}{\partial n}-G\frac{\partial\phi_1}{\partial n}\right)\,\mathrm{d}s \tag{3.3.1}$$

where s measures the arc length on S, the boundary of D, which gives

$$-\phi_1(x_0,z_0)=\int_S\left(\phi_1\frac{\partial G}{\partial n}-G\frac{\partial\phi_1}{\partial n}\right)\,\mathrm{d}s. \tag{3.3.2}$$

Now the boundary conditions on G and ϕ_1 mean that the only contribution is from C and therefore

$$\phi_1(x_0, z_0) = -\int_C \phi_1 \frac{\partial G}{\partial n}\,\mathrm{d}s. \tag{3.3.3}$$

In this form equation (3.3.3) represents a homogeneous second-kind integral equation for ϕ_1 and hence could be used to determine the sloshing frequencies at first order.

We choose to proceed further following Porter & Porter's [77] technique of converting normal derivatives to tangential derivatives by using the Cauchy-Riemann equations in the form

$$\left.\begin{aligned} \frac{\partial}{\partial s}\psi_n(z)\mathrm{e}^{\pm k_n x} &= \mp\frac{\partial}{\partial n}\chi_n(z)\mathrm{e}^{\pm k_n x}, \\ \frac{\partial}{\partial n}\psi_n(z)\mathrm{e}^{\pm k_n x} &= \pm\frac{\partial}{\partial s}\chi_n(z)\mathrm{e}^{\pm k_n x}, \end{aligned}\right\} \tag{3.3.4}$$

where

$$\left.\begin{aligned} \frac{\partial}{\partial n} &= \frac{1}{\sigma}\left(-h'(x)\frac{\partial}{\partial x} + \frac{\partial}{\partial z}\right), \\ \frac{\partial}{\partial s} &= \frac{1}{\sigma}\left(\frac{\partial}{\partial x} + h'(x)\frac{\partial}{\partial z}\right), \\ \sigma &= \sqrt{(1 + (h'(x))^2)}, \\ \chi_n(z) &= N_n^{-1/2}\sin k_n(h_0 - z). \end{aligned}\right\} \tag{3.3.5}$$

Now using these equations we deduce that

$$\frac{\partial^2 G}{\partial n \partial n_0} = -\frac{\partial^2 H}{\partial s \partial s_0} \tag{3.3.6}$$

where

$$H(x, z|x_0, z_0; K) = \sum_{n=0}^{\infty} \frac{\chi_n(z)\chi_n(z_0)}{2k_n h_0} \frac{\{\cosh k_n(l - |x - x_0|) - \cosh k_n(l - x - x_0)\}}{\sinh k_n l}. \tag{3.3.7}$$

We can now derive an integral equation by differentiating equation (3.3.3) with respect to n_0. To do this we extend the definition of n_0, the normal derivative with respect to field coordinates, into the fluid domain where we perform the differentiation. Then, noting that this derivative must vanish as we approach the curve $z_0 = h(x_0)$ we find that

$$\begin{aligned} 0 = \frac{\partial}{\partial n_0}\phi_1(x_0, y_0) &= -\int_C \phi_1(x, y)\frac{\partial^2}{\partial n_0 \partial n}G(x, z|x_0, z_0)\,\mathrm{d}s \\ &= \int_C \phi_1(x, z)\frac{\partial^2}{\partial s_0 \partial s}H(x, z|x_0, z_0)\,\mathrm{d}s \end{aligned}$$

which on integrating with respect to s_0, becomes

$$C_0 = \int_C \phi_1(x,z)\frac{\partial}{\partial s}H(x,z|x_0,z_0)\,\mathrm{d}s.$$

We take the limit $x_0 \to l$ where it may be shown from the definition of H that the integrand vanishes and hence C_0, the constant of integration, is zero. We may now integrate by parts to obtain,

$$0 = [\phi_1 H(x,z|x_0,h(x_0))]_C - \int_C H\frac{\partial\phi_1}{\partial s}\,\mathrm{d}s.$$

Now it may be easily seen from the definition of $H(x,z|x_0,z_0)$ that the first term above vanishes to give

$$\int_C H\frac{\partial\phi_1}{\partial s}\,\mathrm{d}s = 0. \tag{3.3.8}$$

If we now define

$$q_1(x) = \left[\frac{\partial\phi_1}{\partial x} + h'(x)\frac{\partial\phi_1}{\partial z}\right]_{z=h(x)} \tag{3.3.9}$$

and

$$m(x_0,x;K) = \sum_{n=0}^{\infty}\frac{\chi_n(h(x))\chi_n(h(x_0))}{2k_nh_0}\frac{\{\cosh k_n(l-|x-x_0|)-\cosh k_n(l-x-x_0)\}}{\sinh k_nl} \tag{3.3.10}$$

the integral equation may be rewritten as

$$\int_0^l m(x_0,x;K)q_1(x)\,\mathrm{d}x = 0, \qquad 0 < x_0 < l. \tag{3.3.11}$$

Non-trivial solutions of this homogeneous first kind integral equation furnish the sloshing frequencies for the tank containing the particular bed shape $z = h(x)$ and the corresponding function $q_1(x)$ which is related to the tangential flux along the bed. In order to solve the second-order problem, however, we must find ϕ_1 in a suitable form to feed into the second-order problem. Specifically this requires the value of ϕ_1 on $z = 0$ so we proceed to find the general form of ϕ_1 everywhere in D and, in particular, its value on the free-surface, $z = 0$.

We now use equations (3.3.4) to deduce the relation

$$\frac{\partial G}{\partial n} = \frac{\partial L}{\partial s} \tag{3.3.12}$$

where $L(x, z|x_0, z_0; K)$ is given by

$$L = \begin{cases} \displaystyle\sum_{n=0}^{\infty} \frac{\chi_n(z)\psi_n(z_0)}{2k_n h_0} \left\{ \frac{\sinh k_n(l - |x - x_0| - \sinh k_n(l - x - x_0)}{\sinh k_n l} \right\}, & x < x_0, \\ \displaystyle -\sum_{n=0}^{\infty} \frac{\chi_n(z)\psi_n(z_0)}{2k_n h_0} \left\{ \frac{\sinh k_n(l - |x - x_0|) + \sinh k_n(l - x - x_0)}{\sinh k_n l} \right\}, & x > x_0. \end{cases} \tag{3.3.13}$$

Therefore performing integration by parts in equation (3.3.3) we deduce that

$$\phi_1(x_0, z_0) = -[\phi_1(x, z)L(x, z|x_0, z_0; K)]_C + \int_C L(x, z|x_0, z_0; K)\frac{\partial \phi_1(x, z)}{\partial s}\,\mathrm{d}s. \tag{3.3.14}$$

A careful treatment of the term $[\phi_1 L]_C$ noting that L is discontinuous at $x = x_0$ yields

$$[\phi L]_C = \phi_1(x_0, h(x_0)) \sum_{n=0}^{\infty} \frac{\chi_n(h(x_0))\psi_n(z_0)}{k_n h_0}. \tag{3.3.15}$$

This may be simplified using the result

$$\sum_{n=0}^{\infty} \frac{\chi_n(h(x_0))\psi_n(z_0)}{k_n h_0} = f(z_0) \equiv \begin{cases} 0, & 0 < z_0 < h(x_0), \\ 1, & h(x_0) < z_0 < h_0 \end{cases} \tag{3.3.16}$$

which is found by expanding the function of z_0 on the right hand side in the complete set $\{\psi_n\}$ to give

$$[\phi_1 L]_C = \phi_1(x_0, h(x_0))f(z_0). \tag{3.3.17}$$

Finally, upon substituting in equation (3.3.14) we obtain the equation

$$\phi_1(x_0, z_0) = \int_0^l L(x, h(x)|x_0, z_0; K)q_1(x)\,\mathrm{d}x, \qquad (x_0, z_0) \in D. \tag{3.3.18}$$

This may be used to find ϕ_1 everywhere in D. However, for our purposes we note that we simply require the expression for ϕ_1 on the undisturbed free-surface $z = 0$. Hence

$$\phi_1(x_0, 0) = \int_0^l L(x, h(x)|x_0, 0; K)q_1(x)\,\mathrm{d}x. \tag{3.3.19}$$

This result is in terms of the bed-flux function $q_1(x)$ already computed and gives us all the information we require, both to compute the time-independent first-order wave elevation given by

$$\eta_1(x) = \mathrm{Re}\left\{ -\frac{\mathrm{i}\omega}{g}\phi_1(x, 0) \right\}, \tag{3.3.20}$$

and to feed the first-order results into the second-order problem.

3.4 Second-order solution

Recall the second-order potential Φ_2 must satisfy Laplace's equation together with zero normal derivative on fixed boundaries. Furthermore it must satisfy the complicated free-surface boundary condition (FSBC)

$$\frac{\partial^2 \Phi_2}{\partial t^2} - g\frac{\partial \Phi_2}{\partial z} = \mathrm{Re}[F(x)\mathrm{e}^{-2\mathrm{i}\omega t}] + F_s(x), \qquad \text{on } z = 0 \tag{3.4.1}$$

as stated in (3.2.8) and where the terms on the right hand side are defined in equations (3.2.9) and (3.2.10). Now, following McIver & McIver [55], we observe that the right hand side of the FSBC suggests that Φ_2 has the form

$$\Phi_2(x, z, t) = \Phi_s(x, z) - \Gamma t + \mathrm{Re}[\phi_2(x, z)\mathrm{e}^{-2\mathrm{i}\omega t}] \tag{3.4.2}$$

where the steady and double frequency components of the potential, Φ_s and ϕ_2, both satisfy Laplace's equation and have zero normal derivatives on the fixed boundaries. The FSBC implies the two conditions

$$\frac{\partial \Phi_s}{\partial z} = -\frac{F_s(x)}{g}, \qquad \text{on } z = 0,\ 0 < x < l \tag{3.4.3}$$

and

$$4K\phi_2 + \frac{\partial \phi_2}{\partial z} = g(x), \qquad \text{on } z = 0,\ 0 < x < l \tag{3.4.4}$$

where

$$g(x) = -\frac{\mathrm{i}\omega}{g}\left\{\left(\frac{\partial \phi_1}{\partial x}\right)^2 + \frac{3}{2}K^2\phi_1^2 + \frac{1}{2}\phi_1\frac{\partial^2 \phi_1}{\partial x^2}\right\}_{z=0}. \tag{3.4.5}$$

The choice of Γ simply affects the position of the mean free-surface and is set to a value which guarantees mass conservation, i.e. by requiring no net flux across the undisturbed free-surface. Furthermore, noting that since ϕ_1 satisfies a homogeneous problem, it may be taken to be real without loss of generality, therefore it is evident that $F_s(x) = 0$ in equation (3.4.3) and consequently Φ_s has zero normal derivative on the boundary $z = 0$. Then (see, for example, Dettman [21])

$$\iint_D \nabla\Phi_s.\nabla\Phi_s \,\mathrm{d}D = -\iint_D \Phi_s\nabla^2\Phi_s \,\mathrm{d}D + \int_S \Phi_s\nabla\Phi_s.\mathbf{n} \,\mathrm{d}s = 0. \tag{3.4.6}$$

Therefore $\nabla\Phi_s \equiv 0$ in D and so we deduce that Φ_s is a constant which we may set equal to zero without loss of generality.

We now turn to solving for the double frequency component ϕ_2 and we note that $g(x)$ may be calculated in terms of (3.3.19). The full boundary value problem for ϕ_2 is

$$\left.\begin{aligned} \nabla^2\phi_2 &= 0, && (x,z)\in D,\\ \frac{\partial\phi_2}{\partial x} &= 0, && \text{on } \{x=0,\ z\in(0,h(0))\}\cup\{x=l,\ z\in(0,h(l))\},\\ 4K\phi_2+\frac{\partial\phi_2}{\partial z} &= g(x), && \text{on } z=0,\ 0<x<l,\\ \frac{\partial\phi_2}{\partial n} &= 0, && \text{on } z=h(x),\ 0<x<l. \end{aligned}\right\} \tag{3.4.7}$$

We proceed to solve for ϕ_2 using the same techniques applied at first-order, but now use the Green's function G given by (3.2.17) for a frequency of $4K$. So, applying Green's identity, but this time to $\phi_2(x,z)$ and $G(x,z|x_0,z_0;4K)$, gives contributions from the free surface and the bed only. Thus

$$-\phi_2(x_0,z_0)=\int_{z=0}-\phi_2\frac{\partial}{\partial z}G(4K)+G(4K)\frac{\partial\phi_2}{\partial z}\,\mathrm{d}x+\int_C\phi_2(x,z)\frac{\partial}{\partial n}G(4K)\,\mathrm{d}s. \tag{3.4.8}$$

We now apply the FSBC to obtain

$$-\phi_2(x_0,z_0)=\int_0^l G(x,0|x_0,z_0;4K)g(x)\,\mathrm{d}x+\int_C\phi_2(x,z)\frac{\partial}{\partial n}G(4K)\,\mathrm{d}s. \tag{3.4.9}$$

In order to proceed as before we need the result

$$\frac{\partial}{\partial n_0}G(x,z|x_0,z_0;K)=\frac{\partial}{\partial s_0}L(x_0,z_0|x,z;K) \tag{3.4.10}$$

which is deduced from equations (3.3.4) and where $L(K)$ is defined by (3.3.13). We now differentiate with respect to n_0 to give

$$-\frac{\partial}{\partial n_0}\phi_2(x_0,z_0)=\int_0^l\frac{\partial}{\partial n_0}G(x,0|x_0,z_0;4K)g(x)\,\mathrm{d}x-\int_C\frac{\partial^2}{\partial s\partial s_0}H(4K)\phi_2\,\mathrm{d}s. \tag{3.4.11}$$

Then applying the bed condition and converting from normal to tangential derivatives we find

$$0=\int_0^l\frac{\partial}{\partial s_0}L(x_0,h(x_0)|x,0;4K)g(x)\,\mathrm{d}x-\int_C\phi_2\frac{\partial^2}{\partial s\partial s_0}H(4K)\,\mathrm{d}s \qquad \text{on } z_0=h(x_0). \tag{3.4.12}$$

We may now integrate with respect to s_0. So

$$C_0 = \int_0^l L(x_0, h(x_0)|x, 0; 4K)g(x)\mathrm{d}x - \int_C \phi_2 \frac{\partial}{\partial s} H(4K)\mathrm{d}s \qquad \text{on } z_0 = h(x_0) \quad (3.4.13)$$

and using the limit $x_0 \longrightarrow 0$ we deduce that $C_0 = 0$. Integrating the second integral by parts we find that

$$-\int_0^l L(x_0, h(x_0)|x, 0; 4K)g(x)\mathrm{d}x = -[\phi_2 H(4K)]_C + \int_C H(4K)\frac{\partial \phi_2}{\partial s}\mathrm{d}s \qquad \text{on } z_0 = h(x_0), \quad (3.4.14)$$

where, since $H(4K) = 0$ at $x_0 = 0, l$ the first term on the right hand side of the equation vanishes, giving

$$-\int_0^l L(x_0, h(x_0)|x, 0; 4K)g(x)\,\mathrm{d}x = \int_C H(4K)\frac{\partial \phi_2}{\partial s}\,\mathrm{d}s \qquad \text{on } z_0 = h(x_0). \quad (3.4.15)$$

Now, defining

$$q_2(x) = \left[\frac{\partial \phi_2}{\partial x} + h'(x)\frac{\partial \phi_2}{\partial z}\right]_{z=h(x)} \quad (3.4.16)$$

and using equation (3.3.10) we may rewrite the integral equation (3.4.15) as

$$f(x_0) \equiv -\int_0^l L(x_0, h(x_0)|x, 0; 4K)g(x)\,\mathrm{d}x = \int_0^l m(x, x_0; 4K)q_2(x)\,\mathrm{d}x. \quad (3.4.17)$$

Once we have solved for $q_2(x)$ we find that the solution for ϕ_2 on the free-surface follows using a similar procedure as used previously in equations (3.3.13) to (3.3.19). Thus omitting the details we find

$$\phi_2(x_0, 0) = p(x_0) - \int_0^l L(x, h(x)|x_0, 0; 4K)q_2(x)\,\mathrm{d}x, \quad (3.4.18)$$

where

$$p(x_0) \equiv -\int_0^l G(x, 0|x_0, 0; 4K)g(x)\,\mathrm{d}x. \quad (3.4.19)$$

Once again, ϕ_2 is given in terms of a bed flux function $q_2(x)$ which we have already computed. Now it may be shown from (2.1.36) and (2.1.38) that η_2 may be decomposed as

$$\eta_2 = \eta_{20} + \mathrm{Re}\left\{\eta_{22}\mathrm{e}^{-2\mathrm{i}\omega t}\right\} \quad (3.4.20)$$

with the time independent expressions η_{20} and η_{22} given by

$$\eta_{20} = -\frac{\Gamma}{g} + \frac{1}{4g}\left\{\left(\frac{\partial\phi_1(x,0)}{\partial x}\right)^2 - K^2(\phi_1(x,0))^2\right\} \tag{3.4.21}$$

and

$$\eta_{22} = -\frac{2\mathrm{i}\omega}{g}\phi_2(x,0) + \frac{1}{4g}\left\{\left(\frac{\partial\phi_1(x,0)}{\partial x}\right)^2 + 3K^2(\phi_1(x,0))^2\right\} \tag{3.4.22}$$

respectively. We set Γ by requiring

$$\int_0^l \eta_{20}(x)\,\mathrm{d}x = 0 \tag{3.4.23}$$

therefore obtaining

$$\Gamma = \frac{1}{4}\int_0^l \left(\frac{\partial\phi_1(x,0)}{\partial x}\right)^2 - K^2(\phi_1(x,0))^2\,\mathrm{d}x. \tag{3.4.24}$$

Mass conservation is now equivalent to requiring that

$$\int_0^l \eta_{22}(x)\,\mathrm{d}x = 0, \tag{3.4.25}$$

however, we have no free parameters so it remains to confirm that this identity does indeed hold. To do this we apply the divergence theorem to the boundary value problem for ϕ_2 we find

$$\begin{aligned} 0 = \iint_D \nabla.\nabla\phi_2\,\mathrm{d}x\,\mathrm{d}z &= \int_S \mathbf{n}.\nabla\phi_2\,\mathrm{d}s \\ &= \int_0^l \left.\frac{\partial\phi_2}{\partial z}\right|_{z=0}\mathrm{d}x \\ &= \int_0^l g(x)\,\mathrm{d}x - 4K\int_0^l \phi_2(x,0)\,\mathrm{d}x. \end{aligned} \tag{3.4.26}$$

In which case, on using (3.4.5) and (3.4.26) we find that

$$\frac{2\mathrm{i}\omega}{g}\int_0^l \phi_2(x,0)\,\mathrm{d}x = \frac{1}{4g}\int_0^l 2\left(\frac{\partial\phi_1}{\partial x}\right)^2 + 3K^2\phi_1^2 + \phi_1\frac{\partial^2\phi_1}{\partial x^2}\,\mathrm{d}x, \tag{3.4.27}$$

furthermore we observe that

$$\begin{aligned} \int_0^l \left(\frac{\partial\phi_1}{\partial x}\right)^2 + \phi_1\frac{\partial^2\phi_1}{\partial x^2}\,\mathrm{d}x &= \int_0^l \frac{\partial}{\partial x}\left(\phi_1\frac{\partial\phi_1}{\partial x}\right)\,\mathrm{d}x \\ &= \left[\phi_1\frac{\partial\phi_1}{\partial x}\right]_0^l \\ &= 0. \end{aligned}$$

In which case we deduce that

$$\frac{2\mathrm{i}\omega}{g}\int_0^l \phi_2(x,0)\,\mathrm{d}x = \frac{1}{4g}\int_0^l \left(\frac{\partial\phi_1}{\partial x}\right)^2 + 3K^2\phi_1^2\,\mathrm{d}x, \tag{3.4.28}$$

which when used with (3.4.22) establishes conservation of mass and provides a useful check for our numerical results. We note that we have all the information to calculate the second-order potential throughout D, and specifically to calculate the second-order surface elevation. Therefore we have effectively formulated the solution of the sloshing problem for arbitrary bed topographies exactly to second-order.

3.5 Approximation and numerical method

Although our formulation of the problem so far is exact we must resort to numerical techniques to generate results. A discussion of the key steps involved is presented below.

3.5.1 Calculation of the bed flux $q_1(x)$

We solve the integral equation (3.3.11) numerically by using a Galerkin method where we approximate $q_1(x)$ by

$$q_1 \simeq \widetilde{q_1} \equiv \sum_{n=1}^{N} a_n v_n(x). \tag{3.5.1}$$

We introduce an operator $\mathcal{M}$ where

$$(\mathcal{M}q_1)(x_0) = \int_0^l m(x,x_0;K)q_1(x)\,\mathrm{d}x \tag{3.5.2}$$

and define an associated inner product

$$(q_1,p) = \int_0^l q_1(x)\overline{p(x)}\,\mathrm{d}x. \tag{3.5.3}$$

A variational principle equivalent to Galerkin's method is used to approximate the solution of the integral equation and takes the form

$$(\mathcal{M}\widetilde{q_1}, v_m(x)) = 0, \qquad m = 1,\ldots,N. \tag{3.5.4}$$

This results in the matrix equation

$$\sum_{n=1}^{N} a_n M_{mn} \equiv \sum_{n=1}^{N} a_n (\mathcal{M} v_n, v_m) = 0, \quad m = 1, \ldots, N. \tag{3.5.5}$$

We now choose appropriate trial functions to model $q_1(x)$ the fluid flow along the bed particularly at $x = 0, l$. A local analysis of the fluid flow shows that $q_1(x) \to 0$ as $x \to 0, l$ to give zero normal flux. Therefore we choose

$$v_n(x) = \frac{1}{l} \sin\left(\frac{n\pi x}{l}\right), \tag{3.5.6}$$

and we construct the matrix M with elements M_{mn} defined by

$$\int_0^l v_m(x) \int_0^l \sum_{r=0}^{\infty} \frac{\chi_r(h(x))\chi_r(h(z))}{2k_r d} \frac{\{\cosh k_r(l - |x - z|) - \cosh k_r(l - x - z)\}}{\sinh k_r l} v_n(z) \mathrm{d}z \mathrm{d}x. \tag{3.5.7}$$

We note that the terms in $\cosh k_r(l - x - z)$ are separable, so we define

$$\begin{aligned}
gs_{0n} &= \int_0^l \chi_0(h(x)) \frac{\sin k(l/2 - x)}{\sin kl/2} v_n(x)\, \mathrm{d}x, \\
gc_{0n} &= \int_0^l \chi_0(h(x)) \frac{\cos k(l/2 - x)}{\cos kl/2} v_n(x)\, \mathrm{d}x, \\
G^{(0)}_{mn} &= \frac{1}{4kd} \left\{ gs_{0n} gs_{0m} \tan(kl/2) - \frac{gs_{0n} gs_{0m}}{\tan(kl/2)} \right\}, \\
gs_{rn} &= \int_0^l \chi_r(h(x)) \frac{\sinh k_r(l/2 - x)}{\sinh k_r l/2} v_n(x)\, \mathrm{d}x, \qquad r = 1, 2, \ldots \\
gc_{rn} &= \int_0^l \chi_r(h(x)) \frac{\cosh k_r(l/2 - x)}{\cosh k_r l/2} v_n(x)\, \mathrm{d}x, \qquad r = 1, 2, \ldots \\
G^{(r)}_{mn} &= \frac{1}{4k_r d} \left\{ gs_{rn} gs_{rm} \tanh(k_r l/2) - \frac{gs_{rn} gs_{rm}}{\tanh(k_r l/2)} \right\}.
\end{aligned}$$

We also break the terms in $\cosh k_r(l - |x - z|)$ into

$$w_{mn} = \frac{1}{2kd} \int_0^l \chi_0(h(x)) v_m(x) \int_0^l \chi_0(h(z)) \frac{\cos k(l - |x - z|)}{\sin kl} v_n(z)\, \mathrm{d}z\, \mathrm{d}x \tag{3.5.8}$$

and

$$e_{mn} = \sum_{r=1}^{\infty} \frac{1}{2k_r d} \int_0^l v_m(x) \chi_r(h(x)) \int_0^l \chi_r(h(z)) v_n(z) \frac{\cosh k_r(l - |x - z|)}{\sinh k_r l}\, \mathrm{d}z\, \mathrm{d}x \tag{3.5.9}$$

to give

$$M_{mn} = G^{(0)}_{mn} - \sum_{r=1}^{\infty} G^{(r)}_{mn} + w_{mn} + e_{mn}. \qquad (3.5.10)$$

The only term which presents any computational difficulties is $e_{m,n}$ which contains a logarithmic singularity. Porter & Porter [77] explain how to deal with this term by subtracting the asymptotic leading order contribution and then identifying it as a log function which may be integrated out explicitly. The sloshing frequency and associated bed-flux were found using a standard bisection approach typically involving 12 bisections and hence calculations of the matrix coefficients, to achieve six significant figure accuracy.

3.5.2 Calculation of the first-order potential on $z = 0$

To calculate the first-order wave elevation and to solve the second-order problem we need an easily calculated expression for $\phi_1(x, 0)$. We obtain this by expanding $\phi_1(x, 0)$ as a Fourier cosine series to remain consistent with (3.5.6) thus obtaining the expression for the first-order potential on the free-surface in a readily computable form

$$\phi_1(x, 0) = \sum_{s=0}^{\infty} b_s \cos(s\pi x/l) \qquad (3.5.11)$$

where

$$b_s = \frac{\varepsilon_s}{l} \int_0^l \int_0^l L(x, h(x)|x_0, 0; K) q_1(x) \cos(s\pi x_0/l)\, \mathrm{d}x\, \mathrm{d}x_0. \qquad (3.5.12)$$

Of course, b_0 must be equal to zero to guarantee mass conservation, however, anticipating a more compact means of presenting further results, we leave the summation from $s = 0$ but noting that $b_0 = 0$. Now, using our expression for $q_1(x)$ as calculated above we may insert into equation (3.5.12) to give

$$b_s = \frac{2}{l^2} \sum_{n=1}^{N} a_n \int_0^l \int_0^l L(x, h(x)|x_0, 0; K) \sin(n\pi x/l) \cos(s\pi x_0/l)\, \mathrm{d}x\, \mathrm{d}x_0. \qquad (3.5.13)$$

In practice we truncate the cosine series for $\phi_1(x, 0)$ taking no more terms than N, the truncation size for the Galerkin approximation. Now, the Fourier coefficient b_s in

the form presented at (3.5.13) is computationally expensive in that, for each s, there is a sum of double integrals of the discontinuous function L which itself involves a sum. If we define

$$L_{ns}(K) = \int_0^l \int_0^l L(x, h(x)|x_0, 0; K) \sin\left(\frac{n\pi x}{l}\right) \cos\left(\frac{s\pi x_0}{l}\right) \, \mathrm{d}x \, \mathrm{d}x_0 \qquad (3.5.14)$$

then the b_s may be constructed from sums of the $L_{n,s}(K)$. We note that within the double integral the discontinuous function $L(x, h(x)|x_0, 0; K)$ is evaluated on the free-surface thereby removing the dependence on the arbitrary function $h(x_0)$ and therefore allowing us to separate in the form

$$L_{ns}(K) = -\int_0^l \sum_{r=0}^{\infty} \frac{\chi_r(h(x))\psi_r(0)}{2k_r h_0} \sin\left(\frac{n\pi x}{l}\right) (I_1(x) + I_2(x)) \, \mathrm{d}x \qquad (3.5.15)$$

where

$$I_1(x) = \int_0^l \frac{\mathrm{sgn}(x - x_0) \sinh k_r(l - |x - x_0|)}{\sinh k_r l} \cos\left(\frac{s\pi x_0}{l}\right) \, \mathrm{d}x_0, \qquad (3.5.16)$$

$$I_2(x) = \int_0^l \frac{\sinh k_r(l - x - x_0)}{\sinh k_r l} \cos\left(\frac{s\pi x_0}{l}\right) \, \mathrm{d}x_0. \qquad (3.5.17)$$

Using Gradshteyn & Ryzhik [37] (§2.671:2) we may integrate these directly to give

$$\begin{aligned} I_1(x) &= \frac{k_r l^2}{k_r^2 l^2 + s^2\pi^2} \frac{(-1)^s \cosh k_r x - \cosh k_r(l - x)}{\sinh(k_r l)} + 2\frac{s\pi l}{k_r^2 l^2 + s^2\pi^2} \sin\left(\frac{s\pi x}{l}\right), \\ I_2(x) &= \frac{k_r l^2}{k_r^2 l^2 + s^2\pi^2} \frac{\cosh k_r(l - x) - (-1)^s \cosh k_r x}{\sinh(k_r l)}. \end{aligned} \qquad (3.5.18)$$

Finally, simplifying we obtain

$$I_1(x) + I_2(x) = \frac{2s\pi l}{(k_r^2 l^2 + s^2\pi^2)} \sin\left(\frac{s\pi x}{l}\right) \qquad (3.5.19)$$

which may be used in equation (3.5.15) to compute $L_{n,s}(K)$. In practice no further progress may be made analytically with equation (3.5.15) due to the presence of the $h(x)$ term so it must be computed numerically. This however presents no difficulties for a Gaussian quadrature as the procedure above has reduced the problem to a single integral with smooth integrand. We note from our numerical results that the decrease

of b_s is much more rapid than the worst case of $O(s^{-4})$ predicted by Fourier theory and therefore our evaluation of $\phi_1(x,0)$ is not limited by taking modest truncation sizes in the Galerkin approximation.

3.5.3 Calculation of $g(x)$

We note that $g(x)$ depends on products of the first-order potential on the free surface and its derivatives which we have found as a finite Fourier series as below

$$\phi_1(x,0) = \sum_{n=1}^{N} b_n \cos(n\pi x/l).$$

Therefore treating each component of $g(x)$ separately we have

$$\begin{aligned}
\phi_1^2 &= \sum_{n=1}^{N}\sum_{m=1}^{N} b_n b_m \cos\mu_n x \cos\mu_m x \\
&= \frac{1}{2}\sum_{n=1}^{N}\sum_{m=1}^{N} b_n b_m (\cos\mu_{n+m}x + \cos\mu_{n-m}x).
\end{aligned}$$

Also

$$\begin{aligned}
\left(\frac{\partial\phi_1}{\partial x}\right)^2 &= \sum_{n=1}^{N}\sum_{m=1}^{N} \mu_n\mu_m b_n b_m \sin\mu_n x \sin\mu_m x \\
&= \frac{1}{2}\sum_{n=1}^{N}\sum_{m=1}^{N} \mu_n\mu_m b_n b_m (\cos\mu_{n-m}x - \cos\mu_{n+m}x),
\end{aligned}$$

and

$$\begin{aligned}
\phi_1\frac{\partial^2\phi_1}{\partial x^2} &= -\left(\sum_{n=1}^{N} b_n\cos\mu_n x\right)\left(\sum_{m=1}^{N}\mu_m^2 b_m\cos\mu_m x\right) \\
&= -\frac{1}{2}\left(\sum_{n=1}^{N}\sum_{m=1}^{N} b_n b_m\mu_m^2(\cos\mu_{m+n}x + \cos\mu_{n-m}x)\right).
\end{aligned}$$

Combining the above three results and simplifying we find that

$$\begin{aligned}
\frac{g(x)}{-\mathrm{i}\omega/g} &= \frac{1}{4}\sum_{n=1}^{N}\sum_{m=1}^{N} b_n b_m(3K^2 + 2\mu_n\mu_m - \mu_m^2)\cos\mu_{n-m}x \\
&\quad + \frac{1}{4}\sum_{n=1}^{N}\sum_{m=1}^{N} b_n b_m(3K^2 - 2\mu_n\mu_m - \mu_m^2)\cos\mu_{n+m}x
\end{aligned}$$

Now we seek to write

$$g(x) = \sum_{s=0}^{2N} g_s \cos(s\pi x/l) \tag{3.5.20}$$

where the limits reflect that terms in μ_{n-m} contribute for $s = 0 \ldots N-1$ and the terms in μ_{n+m} contribute for $s = 2 \ldots 2N$. After some algebra it may be seen that the four distinct contributions to the Fourier series for $g(x)$ simplify to give

$$\begin{aligned}
\frac{g(x)}{-\mathrm{i}\omega/g} &= \frac{1}{4}\sum_{n=1}^{N} b_n^2(3K^2+\mu_n^2), \\
&+ \frac{1}{4}\sum_{s=1}^{N-1}\sum_{n=s+1}^{N} b_{n-s}b_n(6K^2+2\mu_n\mu_{n-s}-\mu_s^2)\cos\mu_s x \\
&+ \frac{1}{4}\sum_{s=2}^{N+1}\sum_{n=1}^{s-1} b_{s-n}b_n(3K^2-\mu_{s-n}(2\mu_n+\mu_{s-n}))\cos\mu_s x \\
&+ \frac{1}{4}\sum_{s=N+2}^{2N}\sum_{n=s-N}^{N} b_{s-n}b_n(3K^2-\mu_{s-n}(2\mu_n+\mu_{s-n}))\cos\mu_s x
\end{aligned}$$

This expansion has been extensively verified using Mathematica for a wide range of values of b_n. The coefficients of this series are extremely easy to calculate and give us a much easier form of $g(x)$ to deal with.

3.5.4 Calculation of the integrals $f(x_0)$ and $p(x_0)$

The integrals $f(x_0)$ in equation (3.4.17) and $p(x_0)$ in equation (3.4.19) as they are currently defined are rather complicated. However, the fact that they are defined on $y = 0$ enables us perform the integration analytically. We are able to do this by simplifying the expression for $g(x)$ using the approach presented in section (3.5.3) to calculate $g(x)$ as a Fourier cosine series (3.5.20) in terms of the Fourier coefficients b_s introduced in equation (3.5.12). Thus we write

$$g(x) = \sum_{n=0}^{2N} g_n \cos(n\pi x/l). \tag{3.5.21}$$

and then, using Gradshteyn & Ryzhik [37] (§2.671:2-3) it is possible to integrate $f(x_0)$ and $p(x_0)$ to give

$$f(x_0) = \sum_{r=0}^{\infty} \frac{\chi_r(h(x_0))\psi_r(0)}{2k_r h_0}.f_r(x_0), \tag{3.5.22}$$

where

$$f_r(x_0) = \sum_{s=0}^{2N} g_s \frac{2l\pi s}{k_r^2 l^2 + \pi^2 s^2}\sin(s\pi x_0/l) \tag{3.5.23}$$

and

$$p(x_0) = \frac{l^2}{h_0} \sum_{s=0}^{2N} g_s \left(\sum_{r=0}^{\infty} \frac{\psi_r^2(0)}{(k_r^2 l^2 + \pi^2 s^2)} \right) \cos(s\pi x_0/l). \tag{3.5.24}$$

3.5.5 Calculation of the second-order bed flux $q_2(x)$

Once again we solve using the Galerkin method to find

$$q_2 \simeq \tilde{q_2} \equiv \sum_{n=1}^{N} c_n v_n(x) \tag{3.5.25}$$

where the coefficients c_n are found by solving the matrix equation

$$\sum_{n=1}^{N} c_n M_{mn}(4K) = f_m \qquad m = 1 \ldots N. \tag{3.5.26}$$

Where we define f_m by

$$f_m = \int_0^l f(x_0) v_m(x_0) \, \mathrm{d}x_0 \tag{3.5.27}$$

and $M_{mn}(4K)$ is the matrix defined in equation (3.5.10) but operating at $4K$. The integral in (3.5.27) must be integrated numerically to form the integral equation, but this is relatively inexpensive. In particular, it is worth noting that our code used the extremely efficient routine for summing a Fourier series in Acton [2] to both sum quickly, and to avoid oscillatory effects. Solution of this inhomogeneous problem is routine, and typically an order of magnitude quicker than the first-order solution, requiring only one calculation of the matrix coefficients.

3.5.6 Calculation of the second-order potential on $y = 0$

Calculation of the second-order potential on $y = 0$ poses no additional problems to those encountered for the first-order potential. Equation (3.4.18) gives two contributions to ϕ_2

$$\phi_2(x_0, 0) = p(x_0) + d(x_0) \tag{3.5.28}$$

where

$$d(x_0) = -\int_0^l L(x, h(x) | x_0, 0; 4K) q_2(x) \, \mathrm{d}x. \tag{3.5.29}$$

We see from the definition of $p(x_0)$ (3.5.23) that it is already in the form of a Fourier cosine series, and $d(x_0)$ may be evaluated to give a Fourier cosine series exactly as for the $\{b_s\}$ at first-order. Therefore we may add both contributions to give ϕ_2 as a Fourier cosine series with coefficients $\{d_s\}$ for $s = 0, 1, 2 \ldots$.

3.6 Results

The numerical method for the first-order solution has been checked against several analytic results for its accuracy. The first check is made by comparing the computed sloshing frequencies against the known exact solutions (3.2.5) for a flat-bed. It was found that our method converged to six significant figures for modest truncation sizes ($N = 8$) of the bed flux approximations. Another check can be made by comparing our results with those of Porter & Porter [79] who considered scattering by a periodic ripple bed. In their work they showed that the onset of Bragg resonance for the scattering of waves by a smooth periodic bed was governed by frequencies at which sloshing occurs over a single period of the bed contained within solid vertical walls. In our problem, we have considered a more general situation in which the bed shape does not have to belong to a smooth periodic structure. In particular Porter & Porter [79] produced sloshing frequencies for values of $a/h_0 = \frac{1}{2}$ in the two bed shapes given by the functions

$$h(x) = a + \tfrac{1}{2}(h_0 - a)(1 - \cos(2\pi x/l)) \tag{3.6.1}$$

and

$$h(x) = h_0 - \tfrac{1}{2}(h_0 - a)(1 - \cos(2\pi x/l)). \tag{3.6.2}$$

These functions represent cosine curves with minima of $h(x) = a$ at $x = 0$ and $x = l$ in the former case and at $x = \frac{1}{2}l$ in the latter case. Our results using a truncation parameter of $N = 8$ are $Kl = 3.0739$ and $Kl = 2.9508$ respectively and agree with those of [79] to the same accuracy. In figure (3.1) we show, graphically, the variation of sloshing frequencies Kl as a/h_0 is varied between $a/h_0 = \frac{1}{2}$ and unity, which corresponds to the flat-bed solution previously mentioned. In figure (3.1) we also plot,

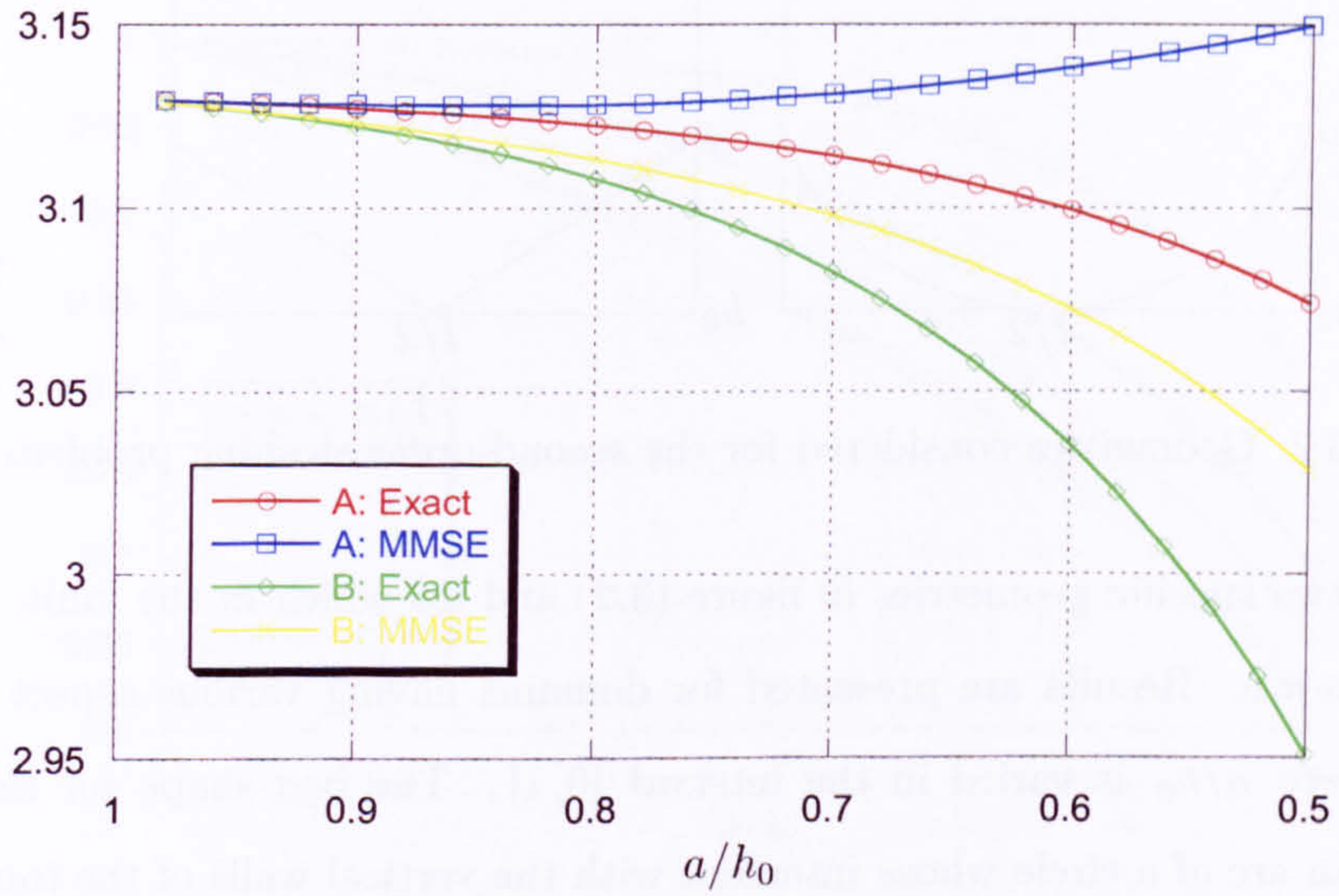

Figure 3.1: Sloshing frequencies for the first mode over periodic beds given by (A: $h(x) = a+0.5(h_0-a)(1-\cos(2\pi x/l))$) & (B: $h(x) = h_0-0.5(h_0-a)(1-\cos(2\pi x/l))$)

for comparison results using the MMSE which were produced via direct integration using an adaptive-stepsize Runge-Kutta-Fehlberg scheme. It can be seen that, as the bed-shape approaches the flat-bed case, all the results approach the analytic solution. Likewise the exact results agree with Porter & Porter [79] as $a/h_0 \to 0.5$ to within four significant figures and with a truncation size of $N = 8$. They also show the correct monotonic decreasing behaviour as $a/h_0 \to 0$ and as predicted by Fox & Kutler [36]. It can be seen that for mild-slopes the MMSE produces reasonable accuracy as expected, whereas for moderate slopes the results appear more geometry-sensitive. In particular, by using the MSE, one of the geometries fails to show the correct monotonic decreasing behaviour of the frequency for even moderate slopes. As a further check, we confirmed the calculations for the MMSE by independently solving via a Green's function formulation giving identical results to those found by direct integration.

We shall adopt the previous notation in what follows by defining a to be the minimum value of $h(x)$ over $0 < x < l$. We proceed for the rest of the paper to

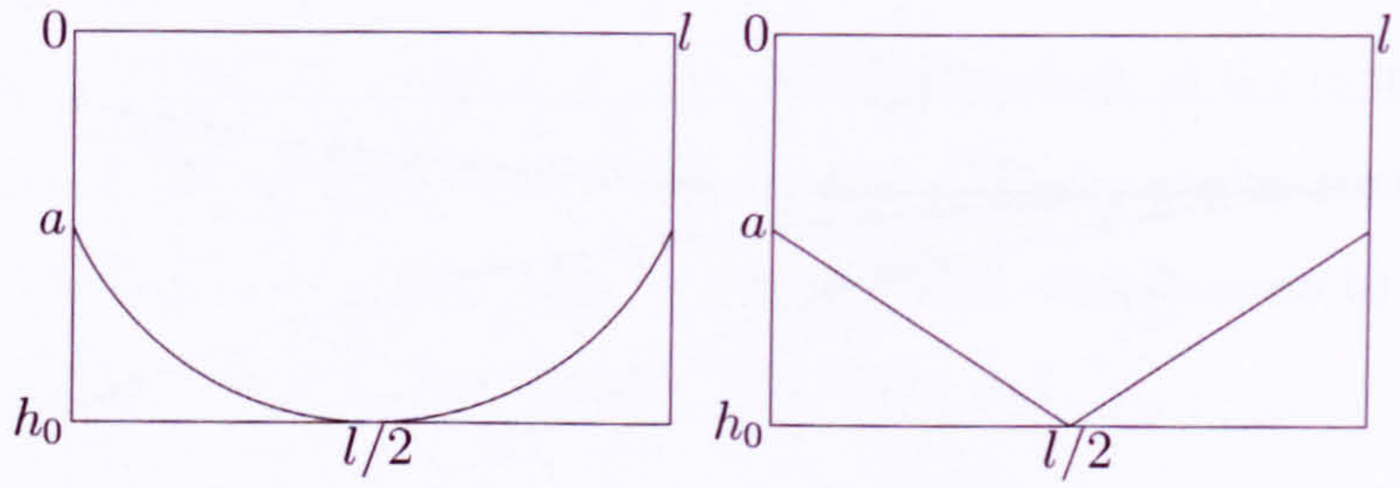

Figure 3.2: Geometries considered for the second-order sloshing problem

consider the two specific geometries in figure (3.2) and for which in the limit $a \to 0$ results are known. Results are presented for domains having various aspect ratios l/h_0 and where a/h_0 is varied in the interval $[0, 1]$. The bed shape for the first geometry is an arc of a circle whose intercept with the vertical walls of the tank at a depth of a defines the radius and in the limit $a \to 0$ (when $l/h_0 = 2$) approaches the semicircular canal for which results have been computed independently by Evans & Linton [26] using a semi-analytical method. The second geometry is a canal with a triangular bed which in the limit $a \to 0$ (when $l/h_0 = 2$) approaches the geometry for which Lamb [49] provides an analytic solution, corresponding to sloshing in a right-angled wedge. Lamb's sloshing frequencies are thus determined by the roots of the equation

$$\tanh kh_0 = \pm \tan kh_0 \tag{3.6.3}$$

where $+(-)$ corresponds to antisymmetric(symmetric) modes.

Figure (3.3) shows a graph of the sloshing frequency normalized by dividing by the flat-bed solution (3.2.7) plotted against a/h_0 for the first sloshing mode over a triangular bed in a tank whose aspect ratio is governed by the relation $l/h_0 = 2\cot(\pi/n)$ for $n = 3, 4, \ldots, 8$. This means that, when $a = 0$, the angle that each section of sloping bottom makes with the horizontal is π/n. Thus, in figure (3.3), the variation of a/h_0 from unity to zero represents the transition from the flat-bed solution to the triangular canal solution. This case was run first with the trial function $\sin(n\pi x/l)$ where we found that in the limits $a/h_0 \to 1$ we obtained the correct results to the required accuracy. In the limit $a/h_0 \to 0$ we obtained the results given

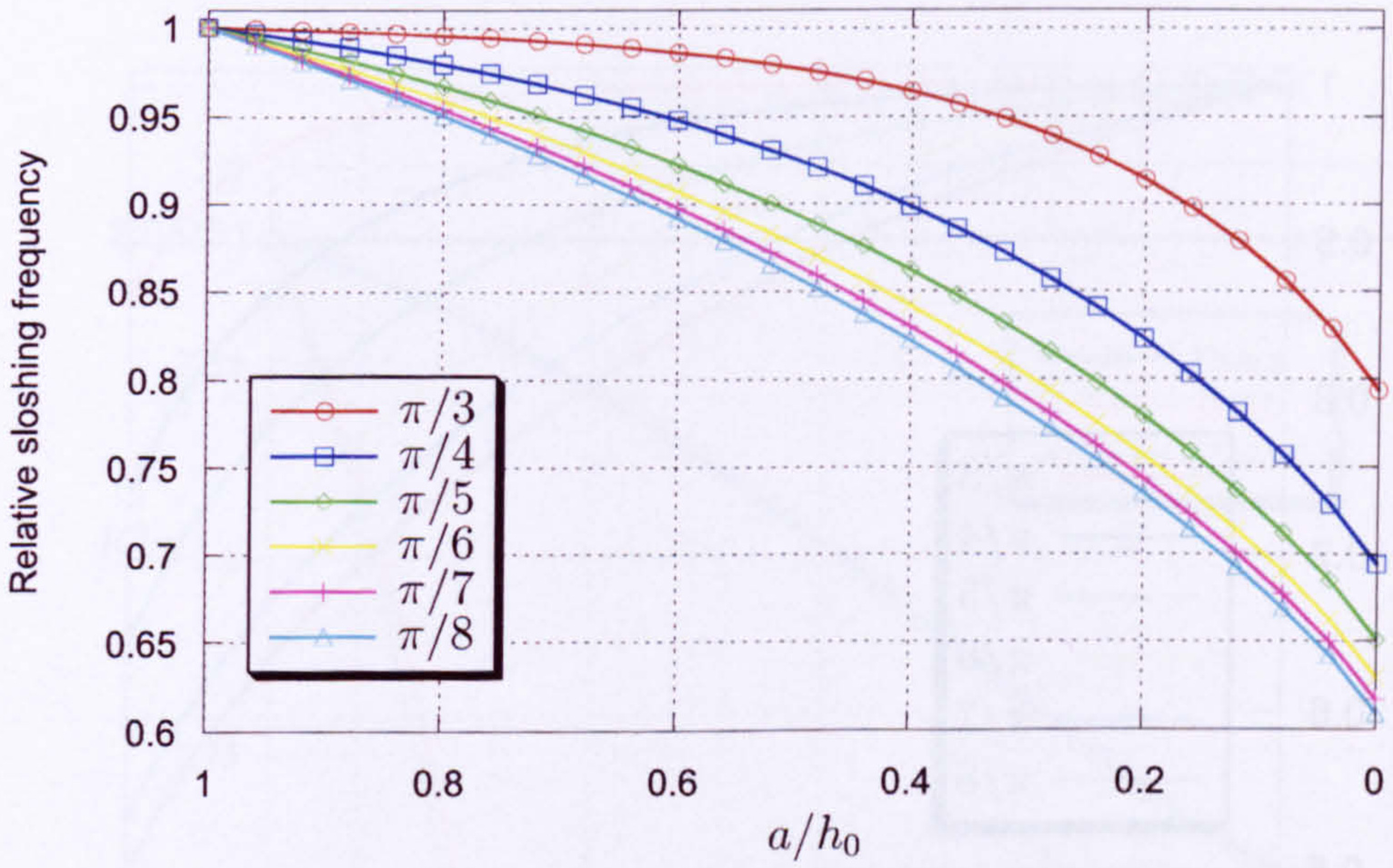

Figure 3.3: Normalized sloshing frequencies for the first mode over a triangular bed making an angle of $\pi/n,\ n = 3, \ldots, 8$ with the horizontal

by Lamb [49] for the bed of slope $\pi/4$ accurate to four significant figures ($Kl = 1.000$). Then, noting that the first mode is antisymmetric, we anticipated a bed-flux symmetric around $l/2$ and therefore ran the code again choosing $\sin((2n-1)\pi x/l)$ as the trial function. The latter results are presented because, as expected, they give slightly better convergence for fixed maximum truncation size. Results over the same bed shapes are also presented at figure (3.4) for the second mode which is symmetric and therefore requires the trial function $\sin(2n\pi x/l)$. In this case we are able to verify that, in the limit $a/h_0 \to 0$, the results for the bed of slope $\pi/6$ agree with analytic results in Lamb [49] and Packham [69] in which $Kl = 3.464$.

Figure 3.5 shows a graph of the non-dimensional frequency Kl against a/h_0 for the first mode over a symmetric bed in the shape of an arc of a circle and where the tank aspect ratio is $l/h_0 = 2$. The results are bounded from above by the rectangular canal solution and from below by the semicircular canal solution which has also been computed by Evans & Linton [26] as $Kl = 2.7114$. This case was run first with the trial function $\sin(n\pi x/l)$ where we found that, in the limits $a/h_0 \to 1$ and $a/h_0 \to 0$ we obtained the correct results. Again we re-ran the code anticipating a bed flux

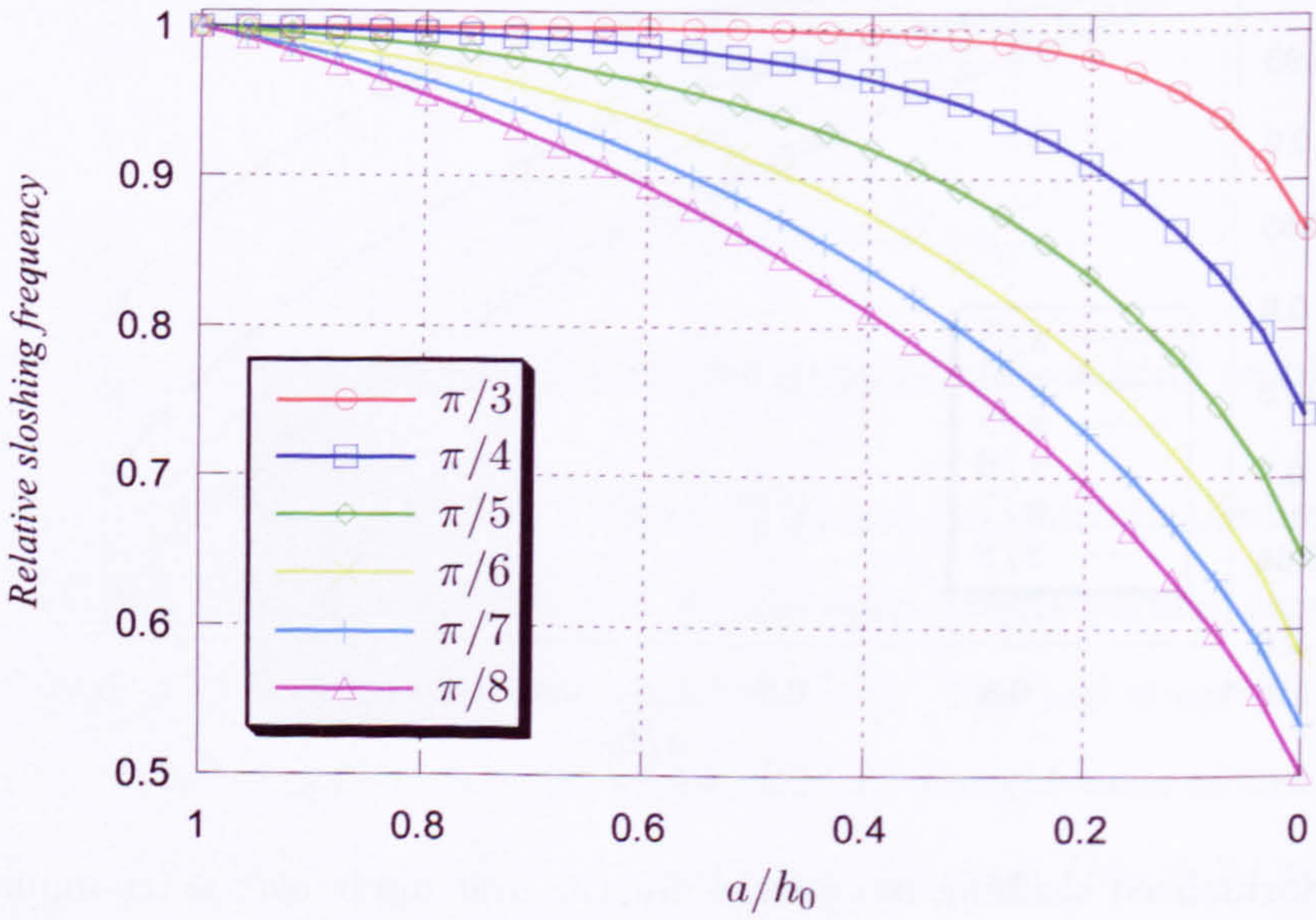

Figure 3.4: Normalized sloshing frequencies for the second mode over a triangular bed making an angle of π/n with the horizontal

symmetric around $l/2$ using $\sin((2n-1)\pi x/l)$ as the trial function and we present the latter results. Alongside we provide, for comparison, equivalent results using the MMSE. Surprisingly in this case the accuracy of the MMSE results is extremely poor even for mild slopes.

For the flat-bed case $a/h_0 = 1$ all of our results were found to agree with the analytical results to six significant figures with modest truncation sizes ($N = 8$). For the limit $a \to 0$ we obtained four significant figure accuracy against known results for the triangular bed shape and three significant figures for the semicircular bed shape using the $\sin(n\pi x/l)$ trial function and using a truncation size of ($N = 48$). Using Legendre functions we were able to obtain six significant figure accuracy for the first symmetric mode in the triangular canal problem where $l/h_0 = 2$. It is to be expected that our approach will cause problems when $a = 0$ as, at this point the bed meets the free-surface. This problem manifests itself in our assumptions about the local behaviour of the fluid flow at the join with the canal walls. In the case of the

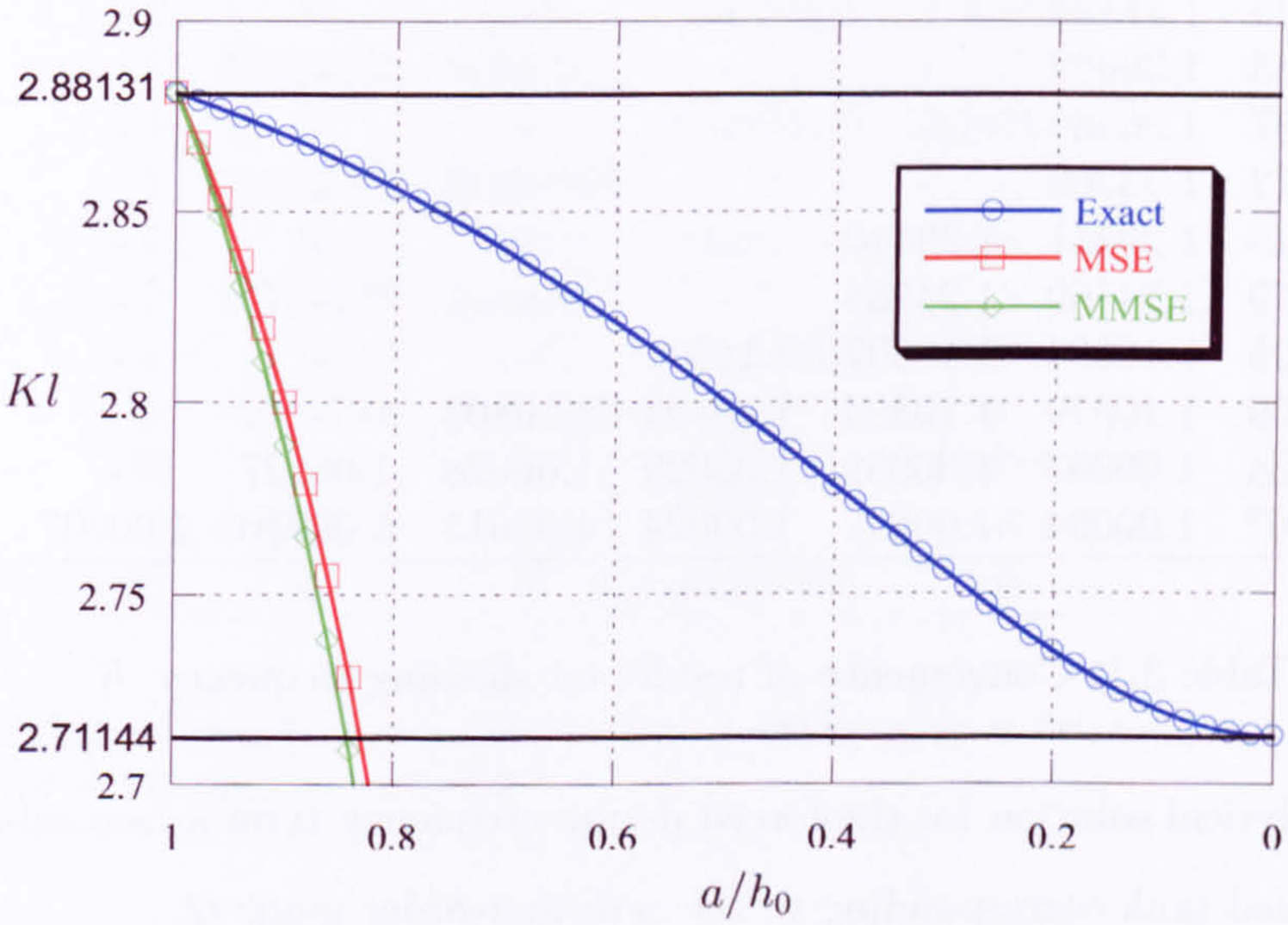

Figure 3.5: Sloshing frequencies for the first mode over an arc shaped bed

semicircular bed the condition at the end of the bed remains zero flux; however, this is inconsistent with the free-surface condition at this point. In the triangular case the Legendre function was chosen to model the high fluxes anticipated in the region thus apparently improving the local modeling and regaining the required accuracy. We found that, in order to improve on these results, we needed to take more terms in the Fourier series expansion and even then found weak convergence as expected with a Fourier series representation in this case.

Table (3.1) shows how convergence for the first mode of the triangular bed depends upon the truncation size. We use a dash to denote no further improvement in results. It is clearly seen that the Galerkin approach provides efficient convergence reaching at least four significant figures for a truncation size of $(N = 12)$. In fact it is only the extreme case where $a/h_0 \approx 0$ that increased truncation size is required to account for the problems we anticipate at that limit in this formulation; nevertheless we see that four significant figures are still obtained for a modest $N = 12$.

We move now to the results for the second-order problem where it can be shown

a/h_0	$N=6$	$N=12$	$N=18$	$N=24$	$N=30$	$N=36$	$N=42$	$N=48$
1.00	1.44066	-	-	-	-	-	-	-
0.90	1.42759	-	-	-	-	-	-	-
0.80	1.41125	1.41124	-	-	-	-	-	-
0.70	1.39083	1.39082	-	-	-	-	-	-
0.60	1.36537	1.36535	-	-	-	-	-	-
0.50	1.33372	1.33369	-	-	-	-	-	-
0.40	1.29445	1.29441	1.29440	-	-	-	-	-
0.30	1.24579	1.24569	1.24568	-	-	-	-	-
0.20	1.18525	1.18504	1.18502	1.18501	-	-	-	-
0.10	1.10859	1.10810	1.10804	1.10803	1.10802	-	-	-
0.05	1.06134	1.06043	1.06032	1.06029	1.06028	1.06027	-	-
0.00	1.00367	1.00094	1.00042	1.00024	1.00015	1.00010	1.00007	1.00006

Table 3.1: Convergence of results for sloshing frequency K

that the analytical solution for the forced double-frequency term at second-order for a flat-bottomed tank corresponding to the nth first-order mode of

$$\phi_1 = \frac{gA\cos\mu_n x\cosh\mu_n(y-d)}{\omega\cosh\mu_n d}$$

where $K=\omega_n^2/g$, is given by

$$\phi_2 = \frac{-\mathrm{i}A^2\sqrt{g}(3K^2+\mu_n^2)}{16\sqrt{K^3}} + \frac{-\mathrm{i}3A^2\sqrt{g}(K^4-\mu_n^4)\cos 2\mu_n x\cosh 2\mu_n(d-z)}{16\sqrt{K^7}\cosh 2\mu_n d}. \quad (3.6.4)$$

The expression for ϕ_2 is easily derived following the formulation of the problem in this paper. For an alternative derivation in the time domain, see Wu & Eatock-Taylor[103] who use this result to calibrate their finite-element analysis code. However, it should be noted that the second term in the expression above differs slightly from that presented in the reference which appears dimensionally incorrect. Our code was run with a Fourier series truncation size of 10 to find the first sloshing frequency to six significant figure accuracy. We found full agreement with the second-order analytic solution in (3.6.4), to five significant figures. In particular we found that in the limit $a\longrightarrow 1$, the contribution to ϕ_2 came from $p(x_0)$, (3.4.19) . However, as we decreased a we found that the contribution from $d(x_0)$ (3.5.29) grew such that we still obtained agreement with (3.6.4) to five significant figures.

n	a_n	b_n	c_n	d_n
0				0.988842i
1	0.925275	2.67999	0	0
2	0	0	0.531020i	-0.493030i
3	0.368583	0.011046	0	0
4	0	0	0.205348i	0.142988i
5	0.012162	0.000303	0	0
6	0	0	0.040089i	0.002149i
7	0.080727	0.000019	0	0
8	0	0	0.039160i	0.000132i
9	0.002728	0.000001	0	0
10	0	0	0.018101i	0.000010i
11	0.036602	0	0	0
12	0	0	0.018440i	0

Table 3.2: Table of results for second-order sloshing over a triangular bed where $a/h_0 = 0.6$, $N = 12$ and $Kl = 2.73073$

We now solve the full second-order problem for second-order sloshing over a triangular bed. Table (3.2) displays the results for the case where $a/h_0 = 0.6$ for a truncation size of $N = 12$. It can be shown from our formulation that mass conservation is guaranteed using the infinite Fourier series representation of the first-order potential on the free-surface. Therefore calculation of the integral of η_{22} over the free-surface provides a valuable measure of the error introduced in truncating the Fourier series. In this case we find that the integral of η_{22} over the surface is 3×10^{-6} which implies that we have retained the 5 significant figure accuracy we obtained for the flat bed with this truncation size.

Figure (3.6) displays as contour plots, the temporal evolution of the free surface elevation over a single period of the first-order wave for (a) linear solution and (b) - (d) to second-order for a range of wave steepness parameters. We normalized the first mode of the free surface potential to give a first-order surface elevation of unit amplitude in order to compare all other contributions with this dominant mode. In order to construct the total surface elevation including both the first and second-order terms we use $\eta = \varepsilon\eta_1 + \varepsilon^2\eta_2$ where ε represents the wave steepness. We observe that the diagrams confirm that the second-order effects tend to increase the crest heights,

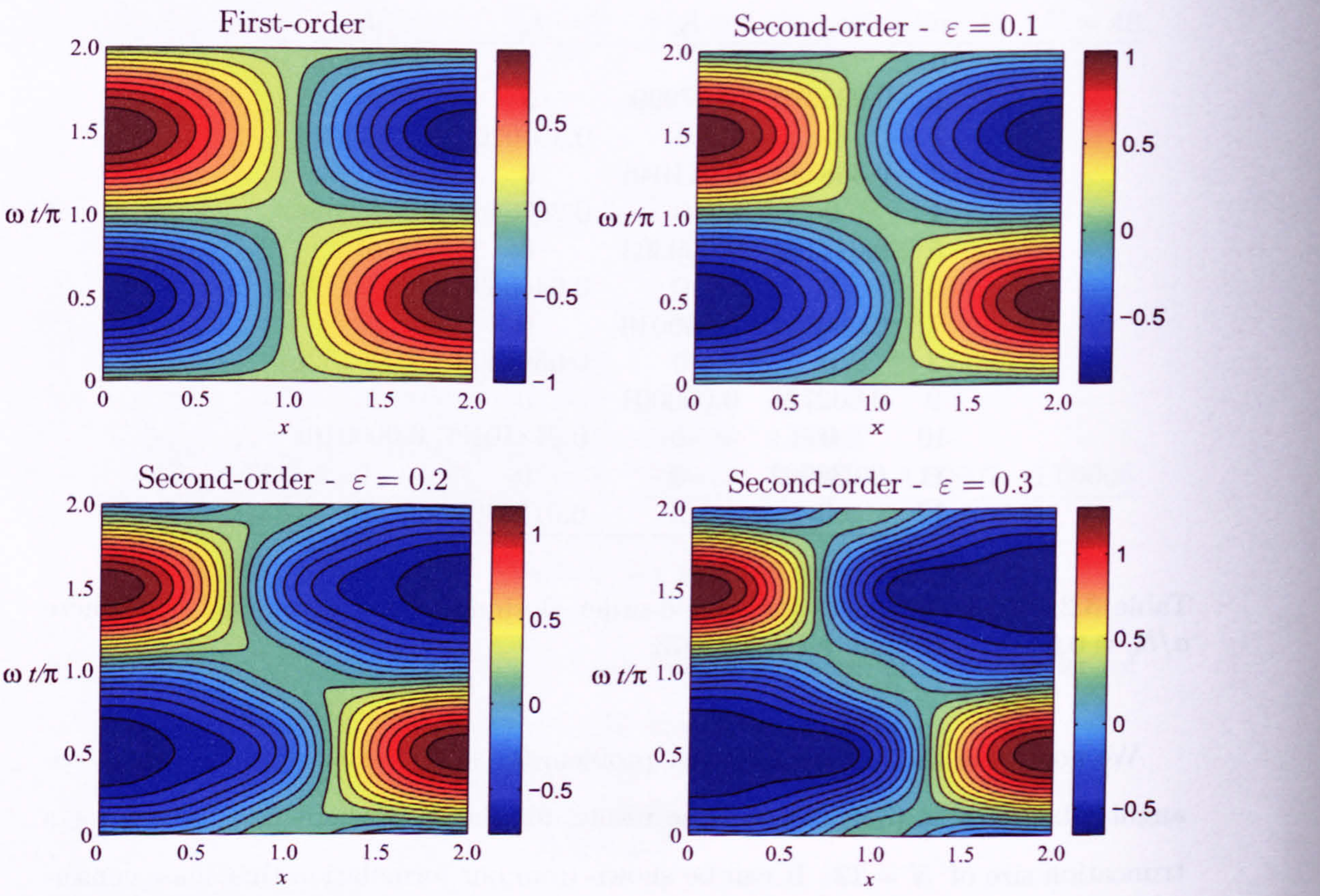

Figure 3.6: Temporal evolution of wave elevations plotted against $x/l \in [0, 2]$ for sloshing over a triangular bed where $(a/h_0) = 0.5$. The vertical axis is $\omega t/\pi \in [0, 2]$

and decrease the troughs as expected. At figure (3.7) we present a three-dimensional representation of the results from (3.6d). To aid interpretation lines of constant time have been marked on the surface so the behaviour of the surface elevation over time is clearer.

The major computational effort is in finding the sloshing frequency via a bisection method where each step involves a calculation of the matrix in (3.5.10). There is significant code reuse provided the matrix equation is coded with frequency as a parameter, in which case to solve the second-order problem we only need calculate the matrix once more using a frequency twice the first-order sloshing frequency. We observe that, once the linear sloshing problem is solved for the bed shape under consideration, the second-order problem may be solved relatively easily with our

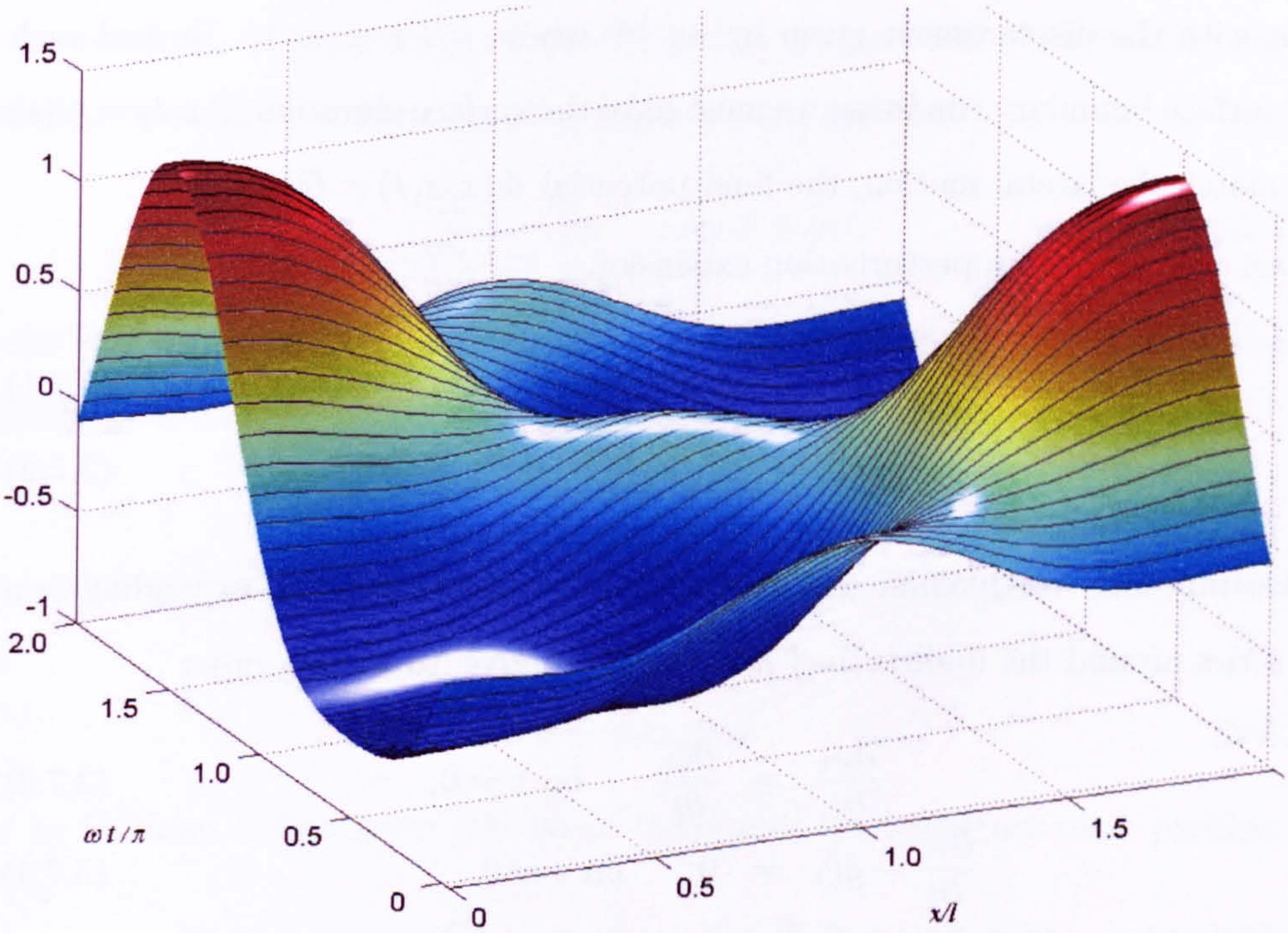

Figure 3.7: Temporal evolution of wave elevation to second-order ($\varepsilon = 0.3$) plotted against $x/l \in [0, 2]$ for sloshing over a triangular bed where $(a/h_0) = 0.5$. The vertical axis is $\omega t/\pi \in [0, 2]$

approach.

3.7 Forced sloshing over an arbitrary bed

We consider the two-dimensional motion of fluid in a tank which is forced laterally at a frequency ω. If the forcing is of small amplitude a in comparison with a typical dimension of the tank l then this suggests the small parameter of the problem as $\varepsilon = a/l$. In this case we could apply the scaling argument of section (2.1) to derive the equations of motion, however, as the small parameter is evident we derive the linearised equations in an unscaled coordinate system.

We consider a 2D tank which if at rest would have vertical walls at $x = 0, l$ and an arbitrary profile bed defined by $z = h(x)$. The tank is forced to move laterally so that positions fixed relative to the tank walls oscillate laterally around their rest

positions with the displacement given by $ae^{-i\omega t}$ where $a/l = \varepsilon \ll 1$. To deal with the free surface boundary condition we must have the surface elevation $\zeta(x,t) = O(\varepsilon)$ and, to match the lateral motion, the fluid potential $\Phi(x,z,t) = O(\varepsilon)$.

In this case we form a perturbation expansion

$$\Phi(x,z,t) = \varepsilon\phi_1(x,z,t) + O(\varepsilon^2) \tag{3.7.1}$$

$$\zeta(x,t) = \varepsilon\zeta_1(x,t) + O(\varepsilon^2) \tag{3.7.2}$$

and substitute into the dynamic and kinematic boundary conditions, expanding as a Taylor series around the undisturbed free surface to give, to leading order

$$\frac{\partial\phi_1}{\partial z} = \frac{\partial\zeta_1}{\partial t} \qquad \text{on } z = 0, \tag{3.7.3}$$

$$\frac{\partial\phi_1}{\partial t} - g\zeta_1 = 0 \qquad \text{on } z = 0. \tag{3.7.4}$$

As there is no other forcing we may write

$$\phi_1(x,z,t) = \phi(x,z)e^{-i\omega t} \tag{3.7.5}$$

$$\zeta_1(x,t) = \eta(x)e^{-i\omega t} \tag{3.7.6}$$

in which case we recover the usual linearised free surface boundary condition

$$\frac{\partial\phi}{\partial z} + K\phi = 0 \qquad \text{on } z = 0, \tag{3.7.7}$$

where, as before $K = \omega^2/g$ and the free surface depression is recovered from

$$\eta = \mathrm{Re}\left\{-\frac{i\omega}{g}\phi(x,0)\right\}. \tag{3.7.8}$$

The solid boundary conditions are now more complicated, and we deal with them in a similar manner to the free surface boundary condition. We assume that the boundary is defined by $\xi(x,z,t) = 0$ in which case the condition that fluid does not penetrate the fixed boundary is compactly written as

$$\frac{D\xi}{Dt} = 0 \qquad \text{on } \xi = 0. \tag{3.7.9}$$

So, for example, on a vertical wall we can define $\xi = x - \varepsilon l e^{-i\omega t}$ in which case the linearised boundary conditions for the vertical walls become

$$\frac{\partial \phi}{\partial x} = -il\omega \qquad \text{on } \xi = 0, l. \tag{3.7.10}$$

On the bed we define ξ by $\xi = z - h(x + \varepsilon l e^{-i\omega t})$ in which the linearised boundary condition becomes

$$\mathbf{n}.\nabla(\phi + ilwx) = 0 \qquad \text{on } z = h(x). \tag{3.7.11}$$

The boundary conditions on the solid boundaries of the tank suggest the transformation

$$\phi + ilwx = \varphi \tag{3.7.12}$$

used by Graham & Rodriguez [38] which transforms the boundary value problem to

$$\nabla^2\varphi = 0 \qquad x \in (0,l), z \in (0,h(x)) \tag{3.7.13}$$

$$\frac{\partial \varphi}{\partial z} + K(\varphi - il\omega x) = 0 \qquad \text{on } z = 0 \tag{3.7.14}$$

$$\frac{\partial \varphi}{\partial x} = 0 \qquad \text{on } x = 0, l \tag{3.7.15}$$

$$\frac{\partial \varphi}{\partial n} = 0 \qquad \text{on } z = h(x) \tag{3.7.16}$$

We proceed in exactly the same manner as section (3.3) by applying Green's Identity to give

$$-\varphi(x_0, z_0) = il\omega \int_0^l x\, G(x, 0; x_0, z_0)\, \mathrm{d}x + \int_C \varphi \frac{\partial G}{\partial n}\, \mathrm{d}s \tag{3.7.17}$$

which when compared with (3.3.3) has an identical form apart from the first integral on the right hand side. Much of the analysis is identical to section (3.3), accordingly we only present key steps below. Therefore, differentiating with respect to n_0 using (3.3.6), (3.3.12) and applying the bed condition we obtain

$$-il\omega \frac{\partial}{\partial s_0} \int_0^l x\, L(x, 0; x_0, z_0)\, \mathrm{d}x = \int_C \varphi \frac{\partial^2 H}{\partial s \partial s_0}\, \mathrm{d}s \tag{3.7.18}$$

Therefore, integrating with respect to s_0, integrating by parts, and then taking the limit $x_0 \to 0$ to determine that the constant of integration is zero, we obtain the

integral equation in the form

$$\mathrm{i}l\omega \int_0^l x\, L(x,0;x_0,z_0)\,\mathrm{d}x = \int_C \frac{\partial\varphi}{\partial s} H\,\mathrm{d}s. \tag{3.7.19}$$

Calculation of the left hand side is routine, and the right hand side is identical to the form in (3.3.8)-(3.3.11). Therefore by comparison with the method of approximation in (3.5.4) we see that, if we define

$$F(x_0) = \mathrm{i}l\omega \int_0^l x\, L(x,0;x_0,z_0)\,\mathrm{d}x \tag{3.7.20}$$

then the solution

$$\hat{q} = \sum_{n=1}^{N} a_n v_n(x) \tag{3.7.21}$$

is given by the solution of

$$(\mathcal{M}\tilde{q}, v_m) = (F, v_m) \qquad m = 1,\ldots,N. \tag{3.7.22}$$

This results in a matrix equation of the form

$$\sum_{n=1}^{N} a_n M_{m,n} = F_m \qquad m = 1,\ldots,N. \tag{3.7.23}$$

where the matrix $M_{m,n}$ is calculated from (3.5.10). Finally, we recall that (3.7.23) solves for φ, therefore to recover the potential ϕ we must use (3.7.12), thus effectively solving the linearised forced sloshing problem.

3.8 Remarks

In a weakly non-linear model of wave problems, in order to produce reliable results at second (and higher) orders, extremely accurate solutions are required at the lower orders. In this chapter we have shown how to provide a lower order(linear) solution for a complicated geometry and feed it into the next higher order of approximation retaining an exact formulation with regards both to the bed condition and the free-surface condition. This approach may be extended to higher orders giving the possibility of highly accurate representations, although it is noted that the calculation of the free-surface coefficients becomes increasingly more complicated as the

order increases. The solutions are shown to converge rapidly requiring quite modest truncations of the series representations of the solutions. We have also shown how the forced sloshing problem may be addressed, presenting the simple linear case away from resonance to illustrate the technique. The more complicated case of forced sloshing near resonance may be tackled by the same approach although this requires solution to third order in an expansion of the parameter $\epsilon^{1/3}$ which is needed to deal with the subharmonic terms arising near resonance.

Although useful in its own rights and offering a practical means of investigating second-order effects, it is envisaged that this method will provide a valuable means of testing fully non-linear solvers. It will enable them to be calibrated against a weakly non-linear model of motion over more realistic geometries.

Chapter 4

Multipole techniques for water wave problems

4.1 Introduction

In this chapter we consider water wave interaction with specific bottom topographies which are amenable to solution by a particular semi-analytical approach, commonly referred to as the "multipole method". The two geometries considered are an infinitely-long semicircular protrusion from an otherwise flat bed and a hemispherical protrusion from an otherwise flat bed. As far as the author is aware, no such work has been done on these three-dimensional problems. It is worth noting that Chakrabarti [10] considered the problem of two-dimensional scattering by a semicircular protrusion, although the author was unaware of this work during the preparation of this thesis. For each problem under consideration the main part of the analysis deals with the scattering of incident wave energy from the topography. We shall also introduce the concept of so-called "edge waves" or trapped waves and establish that the infinite semicircular ridge supports such waves.

Our main reason for solving these specific problems is to produce accurate results for oblique scattering by an infinite ridge and scattering by axisymmetric topography. We use these results to verify the techniques we develop later on in this thesis before applying them to more arbitrary topographies for which no such results exist.

The main idea of multipole techniques is to construct solutions to the boundary

value problem by distributing singularities within a floating body, or in our case patch of topography, so that as many of the boundary conditions as possible are satisfied. We then form a solution by expanding as a series of these multipoles and satisfying any remaining boundary conditions. Although similar techniques had been used in an ad-hoc manner previously (see for example, Havelock [39] and Ursell [96], [97]), Thorne [92] established a framework for the construction and use of multipoles in two and three dimensions in both finite and infinite depth. In fact we follow Thorne's style of approach to construct the multipoles we shall use in this chapter.

Multipole methods have subsequently seen widespread use in similar wave scattering problems involving geometries with a combination of circular and rectangular boundaries. Indeed, so much so that Linton & McIver [51] have compiled a catalogue of multipole potentials in the Appendix of their book which includes complete sets of multipoles potentials for cases in both two and three dimensions and in finite and infinite depth, and for origins that are submerged and in the free-surface. These results are based largely on those presented by Thorne [92], although they do present a greater set of multipoles which are likely to suffice in many problems. They do not, however, explicitly include the case that we are considering here in which the origin coincides with the bottom of the fluid. It is possible to use the appropriate multipole potentials for waves in finite depth, as quoted in Linton & McIver [51] and take the limit as the source point goes to the fluid bottom. However, because they are designed for sources placed arbitrarily within the fluid they are more complicated than they need to be for our case and therefore it is desirable to derive them from first principles. We add that it can be shown that the multipoles derived here do indeed coincide with the definitions of Linton & McIver [51] although some lengthy algebra needs to be done to show this since an image source in the fluid bottom coincides with the source from the fluid domain.

4.2 Scattering of oblique waves by a semicircular ridge

In this section we consider the scattering of oblique waves by an infinite ridge of semicircular cross section protruding from a region of otherwise constant depth h_0.

4.2.1 Statement of the oblique scattering problem

Cartesian coordinates are chosen with z vertically downwards and $z = 0$ coinciding with the mean free surface. A semicircular ridge protrudes within the fluid from otherwise constant depth h_0 so that the axis of the cylinder is on $z = h_0$, $x = 0$ for $-\infty < y < \infty$. Polar coordinates are based on the axis of the cylinder, which is of radius a $(< h_0)$ so that $x = r\sin\theta$ and $h_0 - z = r\cos\theta$. The uniformity in the geometry in y allows the velocity potential to be written $\Phi(x, y, z, t) = \Re\{\phi(x, z)e^{ily}e^{-i\omega t}\}$ where, as in Chapter 2, a time dependence of angular frequency ω has been assumed. It follows that $\phi(x, z)$ satisfies

$$(\nabla^2 - l^2)\phi = 0, \qquad \text{in } D \tag{4.2.1}$$

where $\nabla^2 = \partial_{xx} + \partial_{zz}$ and $D \subset \mathbb{R}^2$ is the cross-section in y of the domain occupied by the fluid. In addition, there are no-flow conditions

$$\frac{\partial\phi}{\partial z} = 0, \qquad \text{on } z = h_0,\ x \notin (-a, a) \tag{4.2.2}$$

and

$$\frac{\partial\phi}{\partial r} = 0, \qquad \text{on } r = a,\ \theta \in (-\pi/2, \pi/2) \tag{4.2.3}$$

on the bottom on the fluid domain and also the linearised free surface condition

$$K\phi + \phi_z = 0, \qquad \text{on } z = 0,\ -\infty < x < \infty \tag{4.2.4}$$

where $K = \omega^2/g$ and g is gravitational acceleration.

We also need to specify radiation conditions at infinity. Thus, a wave is incident from $x = -\infty$, and this may be described by the potential

$$\phi_{inc}(x, z) = N_0^{-1/2}e^{i\alpha x}\cosh k(h_0 - z) \tag{4.2.5}$$

which is found by considering separable solutions, where k is the positive real root of the dispersion relation $K = k\tanh kh_0$ and $\alpha = (k^2 - l^2)^{1/2} = k\cos\theta_{inc}$. Note that l is related to the incident wave angle θ_{inc} (zero for normal incidence) and incident wavenumber k, via $l = k\sin\theta_{inc}$. That is, α and l are the components of k resolved into the x and y directions respectively.

The boundary-value problem is linear and so we may write

$$\phi(x,z) = \phi_{inc}(x,z) + \phi_s(x,z) \tag{4.2.6}$$

where ϕ_s is the scattered part of the potential which has far field behaviour of the form

$$\phi_s \sim \begin{cases} (T-1)N_0^{-1/2}\cosh k(h_0-z)\mathrm{e}^{i\alpha x}, & x \to \infty \\ RN_0^{-1/2}\cosh k(h_0-z)\mathrm{e}^{-i\alpha x}, & x \to -\infty \end{cases} \tag{4.2.7}$$

where R and T represent the reflection and transmission coefficients respectively and are the principle unknowns of the problem.

The scattered part of the potential will be expanded over a sum of multipoles, which are derived below.

4.2.2 Derivation of Multipoles

The functions φ_n we shall derive below are solutions of the modified Helmholtz equation,

$$(\nabla^2 - l^2)\varphi_n = 0, \qquad \text{in } D \tag{4.2.8}$$

satisfying the linearised free surface condition

$$K\varphi_n + \frac{\partial\varphi_n}{\partial z} = 0, \qquad \text{on } z = 0 \tag{4.2.9}$$

and

$$\frac{\partial\varphi_n}{\partial z} = 0, \qquad \text{on } z = h_0 \tag{4.2.10}$$

In addition, it will be required that, for the scattering problem, φ_n represent outgoing waves as $|x| \to \infty$ in accordance with the radiation condition.

The starting point of the multipole method is to consider functions which are singular with respect to polar coordinates, at the centre of the semicircular cylinder,

satisfying the modified Helmholtz equation. These are termed "free space potentials" (because they currently neglect the other conditions that need to be satisfied by φ_n) and involve the modified Bessel function of the second kind, $K_n(lr)$.

We start with an integral representation for K_n, namely

$$K_n(X) = \frac{1}{2}\int_{-\infty}^{\infty} \mathrm{e}^{-X\cosh\mu}\mathrm{e}^{-n\mu}\,\mathrm{d}\mu \tag{4.2.11}$$

which can be found in Watson [100] for example. We let $X = lr$ and make the substitution $\mu = t + \mathrm{i}\theta$ which results in

$$K_n(lr) = \frac{1}{2}\int_{-\infty}^{\infty} \mathrm{e}^{-lr\cosh[t+\mathrm{i}\theta]}\mathrm{e}^{-nt}\mathrm{e}^{-\mathrm{i}n\theta}\,\mathrm{d}t \tag{4.2.12}$$

where the contour of integration is shifted back onto the real axis since there are no poles in the integrand and the contribution from $t = \pm\infty$ is zero. Expanding the hyperbolic function in the exponent in the integrand and using $x = r\sin\theta$ and $h_0 - z = r\cos\theta$ gives

$$K_n(lr)\mathrm{e}^{\mathrm{i}n\theta} = \frac{1}{2}\int_{-\infty}^{\infty} \mathrm{e}^{-l(h_0-z)\cosh t}\mathrm{e}^{-\mathrm{i}lx\sinh t}\mathrm{e}^{-nt}\,\mathrm{d}t \tag{4.2.13}$$

and it is clear that this representation is valid only if $z < h_0$ (in terms of original variables, for $-\frac{1}{2}\pi < \theta < \frac{1}{2}\pi$). Now we can use the relation $K_{-n}(\mu) = K_n(\mu)$ (see Abramowitz & Stegun [1]) to give

$$K_n(lr)\mathrm{e}^{-\mathrm{i}n\theta} = \frac{1}{2}\int_{-\infty}^{\infty} \mathrm{e}^{-l(h_0-z)\cosh t}\mathrm{e}^{-\mathrm{i}lx\sinh t}\mathrm{e}^{nt}\,\mathrm{d}t \tag{4.2.14}$$

and then it follows that

$$K_n(lr)\cos n\theta = \int_0^{\infty} \mathrm{e}^{-l(h_0-z)\cosh t}\cos(lx\sinh t)\cosh nt\,\mathrm{d}t \tag{4.2.15}$$

and

$$K_n(lr)\sin n\theta = \int_0^{\infty} \mathrm{e}^{-l(h_0-z)\cosh t}\sin(lx\sinh t)\sinh nt\,\mathrm{d}t \tag{4.2.16}$$

These can be recognised as functions which are symmetric and antisymmetric (respectively) about $x = 0$. We require only functions which have a Neumann boundary condition on $\theta = \pm\pi/2$, and so this limits us to half the set of multipoles previously derived.

Thus we require

$$K_{2n}(lr)\cos 2n\theta = \int_0^\infty \mathrm{e}^{-l(h_0-z)\cosh t}\cosh 2nt\cos(lx\sinh t)\,\mathrm{d}t \qquad (4.2.17)$$

for $n = 0, 1, 2, \ldots$ and

$$K_{2n-1}(lr)\sin(2n-1)\theta = \int_0^\infty \mathrm{e}^{-l(h_0-z)\cosh t}\sinh(2n-1)t\sin(lx\sinh t)\,\mathrm{d}t \qquad (4.2.18)$$

for $n = 1, 2, \ldots$. These two functions satisfy the modified Helmholtz equation and Neumann boundary conditions on $\theta = \pm\frac{1}{2}\pi$ and the integral representations are valid for $z < h_0$. Before continuing, we briefly mention that a change of variables $\cosh t = v$ seems an appropriate move to make. Some of the resulting terms will become simpler, others more complicated. However, the change of variables introduces a factor of $(v^2-1)^{1/2}$ in the denominator which introduces singular behaviour into the integrand. From a numerical point of view this is not desirable, so we shall stick with the representation already derived.

In the multipole method, we add another function to the 'free-space' potentials introduced, motivated by the integral representations which have already been derived, which also satisfies the field equation and the condition on $z = h_0$ and which can be used to satisfy the free-surface condition. Let us consider first the symmetric multipoles. Then define the multipoles as

$$\varphi_{2n}(lr,\theta) = K_{2n}(lr)\cos 2n\theta + \int_0^\infty A(t)\cosh(l(h_0-z)\cosh t)\cosh 2nt\cos(lx\sinh t)\,\mathrm{d}t \qquad (4.2.19)$$

which satisfies the Neumann condition on $z = h_0$. The function $A(t)$ takes the role of a Fourier transform function, and its definition is now chosen to satisfy the free surface condition, namely

$$\left(K\varphi_n + \frac{\partial\varphi_n}{\partial z}\right)_{z=0} = 0 \qquad (4.2.20)$$

for all $x \in (-\infty, \infty)$. Thus it follows that

$$A(t) = \frac{\mathrm{e}^{-lh_0\cosh t}(l\cosh t + K)}{l\cosh t\sinh(lh_0\cosh t) - K\cosh(lh_0\cosh t)}. \qquad (4.2.21)$$

At this point we need to concern ourselves over possible poles in $A(t)$. These occur if there exists a value of $t_0 \in (0,\infty)$ such that

$$l\cosh t_0 \tanh(lh_0\cosh t_0) = K = k\tanh kh \tag{4.2.22}$$

(on using the dispersion relation (2.1.44)) which implies

$$l\cosh t_0 = k, \qquad \text{or} \qquad t_0 = \cosh^{-1}(k/l). \tag{4.2.23}$$

Clearly, for a scattering problem where $l = k\sin\theta_{inc}$ we have $k > l$ and therefore such a value of t_0 does exist. To proceed we now rewrite (4.2.19) following Thorne [92], in terms of a principal valued integral plus an as yet unspecified function χ_{2n}. Thus

$$\varphi_{2n}(lr,\theta) = K_{2n}(lr)\cos 2n\theta + \int_0^\infty A(t)\cosh(l(h_0-z)\cosh t)\cosh 2nt\cos(lx\sinh t)\mathrm{d}t + \chi_{2n}, \tag{4.2.24}$$

where χ_{2n} satisfies (4.2.8) to (4.2.10). Again, following Thorne [92] we evaluate the principal valued integral by considering a contour integral consisting of the real axis indented at t_0 so that the contour does not enclose the pole, the imaginary axis plus a circular arc of large radius. The contour is closed in the first quadrant for $x > 0$ and in the fourth quadrant for $x < 0$ to ensure that the contribution from the large arc vanishes in the limit $x \to \pm\infty$. Thus in the limit $x \to \pm\infty$ the principal valued integral is equal to $\pm i\pi$ respectively times the residue at the pole.

We now work out the value of the residue at the pole by first concentrating on $A(t)$. We write

$$G(t) = l\cosh t\sinh(lh_0\cosh t) - K\cosh(lh_0\cosh t) \tag{4.2.25}$$

which defines the denominator of $A(t)$. Then, as discussed, $G(t_0) = 0$ whilst

$$G'(t) = l\sinh t[\sinh(lh_0\cosh t) + lh_0\cosh t\,\mathrm{sech}(lh_0\cosh t))] \tag{4.2.26}$$

and using $l\cosh t_0 = k$, $\alpha = (k^2 - l^2)^{1/2} = l\sinh t_0$ we find

$$G'(t_0) = 2\alpha kh_0\,\mathrm{sech}kh_0 N_0, \tag{4.2.27}$$

In which case the residue of $A(t)$ at t_0 is found to be

$$\mathrm{Res}(A(t_0)) = \lim_{t-t_0}(t-t_0)A(t) = \frac{1}{2N_0\alpha h_0} \tag{4.2.28}$$

Then, as $x \to \pm\infty$, the contribution from the principal valued integral is evaluated as

$$\mathrm{Re}\left\{\pm\pi\mathrm{i}\frac{\mathrm{e}^{-kh_0}(1+K/k)\cosh kh_0}{2\alpha h_0 N_0}\cosh k(h_0-z)\cosh[2nt_0]\mathrm{e}^{\mathrm{i}\alpha x}\right\} \tag{4.2.29}$$

which then simplifies to

$$\frac{-\pi}{2\alpha h N_0}\cosh k(h_0-z)\cosh[2nt_0]\sin\alpha|x|. \tag{4.2.30}$$

Then, in order that the multipole is proportional to $\mathrm{e}^{\mathrm{i}\alpha|x|}$ as $|x| \to \infty$, the function χ_{2n} is given by

$$\chi_{2n} = \frac{\mathrm{i}\pi}{2\alpha h_0 N_0}\cosh k(h_0-z)\cosh[2nt_0]\cos\alpha x \tag{4.2.31}$$

It thus follows that as $x \to \pm\infty$,

$$\varphi_{2n} \sim \frac{\mathrm{i}\pi}{2\alpha h_0 N_0}\cosh k(h_0-z)\cosh[2nt_0]\mathrm{e}^{\mathrm{i}\alpha|x|}. \tag{4.2.32}$$

We apply a similar procedure to derive the 'antisymmetric' multipole potentials, φ_{2n-1}. Then we find

$$\begin{aligned}\varphi_{2n-1}(lr,\theta) &= K_{2n-1}(lr)\sin(2n-1)\theta \\ &\quad + \int_0^\infty A(t)\cosh(l(h_0-z)\cosh t)\sinh(2n-1)t\sin(lx\sinh t)\,\mathrm{d}t + \chi_{2n-1}\end{aligned} \tag{4.2.33}$$

and that

$$\chi_{2n-1} = \frac{\pi\mathrm{i}}{2\alpha h_0 N_0}\cosh k(h_0-z)\sinh[(2n-1)t_0]\sin\alpha x \tag{4.2.34}$$

such that as $x \to \pm\infty$,

$$\varphi_{2n-1} \sim \frac{\pm\pi}{2\alpha h_0 N_0}\cosh k(h_0-z)\sinh[(2n-1)t_0]\mathrm{e}^{\mathrm{i}\alpha|x|}. \tag{4.2.35}$$

The final part of the process is to re-expand the integrand in terms of polar coordinates. In the following we will use the formula (see Abramowitz & Stegun [1])

$$\mathrm{e}^{\frac{1}{2}z(v+1/v)} = \sum_{m=-\infty}^{\infty} v^m I_m(z) \tag{4.2.36}$$

where $I_m(z)$ is the first kind modified Bessel function of order m. In addition the identities $I_m(-z) = (-1)^m I_m(z)$, $I_{-m}(z) = I_m(z)$ will be used.

Using $z = \pm lr$ with $v = \exp(t \pm i\theta)$ in the equation above,

$$e^{\pm lr\cosh(t\pm i\theta)} = \sum_{m=-\infty}^{\infty} e^{mt} e^{\pm im\theta} (\pm 1)^m I_m(lr) \tag{4.2.37}$$

Expanding the cosh on the left hand side and reintroducing x and z through their relation to r and θ gives

$$e^{\pm l(h_0-z)\cosh t} e^{ilx\sinh t} = \sum_{m=-\infty}^{\infty} e^{mt} e^{\pm im\theta} (\pm 1)^m I_m(lr) \tag{4.2.38}$$

From this it follows (after substantial algebra) that

$$\cosh(l(h_0 - z)\cosh t) e^{ilx\sinh t} = I_0(lr) + 2\sum_{m=1}^{\infty} I_{2m}(lr)\cosh 2mt \cos 2m\theta + 2i\sum_{m=1}^{\infty} I_{2m-1}(lr)\sinh(2m-1)t \sin(2m-1)\theta \tag{4.2.39}$$

Thus, taking real and imaginary parts gives

$$\cosh(l(h_0 - z)\cosh t)\cos(lx\sinh t) = \sum_{m=0}^{\infty} \epsilon_m I_{2m}(lr)\cosh 2mt \cos 2m\theta \tag{4.2.40}$$

where $\epsilon_m = 2$, $m \geq 1$ and $\epsilon_0 = 1$ whilst

$$\cosh(l(h_0 - z)\cosh t)\sin(lx\sinh t) = 2\sum_{m=1}^{\infty} I_{2m-1}(lr)\sinh(2m-1)t \sin(2m-1)\theta. \tag{4.2.41}$$

These results can now be used to give, for $n = 0, 1, 2, \ldots$,

$$\varphi_{2n}(lr, \theta) = K_{2n}(lr)\cos 2n\theta + \sum_{m=0}^{\infty} A_{mn} I_{2m}(lr)\cos 2m\theta \tag{4.2.42}$$

where

$$A_{mn} = \epsilon_m \int_0^{\infty} A(t)\cosh 2nt \cosh 2mt \, dt + \frac{i\epsilon_m \pi}{2\alpha h_0 N_0}\cosh[2nt_0]\cosh[2mt_0] \tag{4.2.43}$$

and for $n = 1, 2, \ldots$,

$$\varphi_{2n-1}(lr, \theta) = K_{2n-1}(lr)\sin(2n-1)\theta + \sum_{m=1}^{\infty} B_{mn} I_{2m-1}(lr)\sin(2m-1)\theta \tag{4.2.44}$$

where

$$B_{mn} = 2\int_0^\infty A(t)\sinh(2n-1)t\sinh(2m-1)t\,\mathrm{d}t + \frac{\mathrm{i}\pi}{\alpha h_0 N_0}\sinh[(2n-1)t_0]\sinh[(2m-1)t_0]. \qquad (4.2.45)$$

Note that these representations are only valid within the range $0 \le r < 2h_0$ (see, for example, Thorne [92]).

4.2.3 Solution of the scattering problem

The scattered component of the potential is a sum over all possible multipoles,

$$\phi_s(x,z) = N_0^{-1/2}\sum_{n=0}^{\infty}\epsilon_n a_{2n}\varphi_{2n}(lr,\theta) + 2\mathrm{i}N_0^{-1/2}\sum_{n=1}^{\infty}a_{2n-1}\varphi_{2n-1}(lr,\theta) \qquad (4.2.46)$$

where a_n, $n = 0, 1, \ldots$ are undetermined coefficients and other terms provide simplification in the final expressions.

The reflection and transmission coefficients, R and T, are given by the far-field behaviour of the multipole potentials so that, after some algebra we find

$$R = \frac{\pi\mathrm{i}}{2\alpha h_0 N_0}\left(\sum_{n=0}^{\infty}\epsilon_n a_{2n}\cosh[2nt_0] - 2\sum_{n=1}^{\infty}a_{2n-1}\sinh[(2n-1)t_0]\right) \qquad (4.2.47)$$

and

$$T = 1 + \frac{\pi\mathrm{i}}{2\alpha h_0 N_0}\left(\sum_{n=0}^{\infty}\epsilon_n a_{2n}\cosh[2nt_0] + 2\sum_{n=1}^{\infty}a_{2n-1}\sinh[(2n-1)t_0]\right) \qquad (4.2.48)$$

The only part of the solution which needs to be applied is the condition on $r = a$, $-\frac{1}{2}\pi \le \theta \le \frac{1}{2}\pi$, and this will determine the coefficients a_n. In order to do this, we need to expand the incident wave potential in terms of the polar coordinate system used. Thus, referring to equations (4.2.5), (4.2.23), (4.2.40) and (4.2.41)

$$\phi_{inc} = N_0^{-1/2}\mathrm{e}^{\mathrm{i}\alpha x}\cosh k(h_0 - z) = N_0^{-1/2}\sum_{m=0}^{\infty}\epsilon_m\cosh[2mt_0]I_{2m}(lr)\cos 2m\theta + 2\mathrm{i}N_0^{-1/2}\sum_{m=1}^{\infty}\sinh[(2m-1)t_0]I_{2m-1}(lr)\sin(2m-1)\theta \qquad (4.2.49)$$

Now imposing the no-flow condition

$$\frac{\partial\phi_s}{\partial r} = -\frac{\partial\phi_{inc}}{\partial r}, \qquad \text{on } r = a,\ -\tfrac{1}{2}\pi \le \theta \le \tfrac{1}{2}\pi \qquad (4.2.50)$$

implies the decoupled systems of equations (after subsequently equating coefficients of $\cos 2m\theta$, $\sin(2m-1)\theta$),

$$a_{2m} + Z_{2m} \sum_{n=0}^{\infty} a_{2n} \frac{\epsilon_n}{\epsilon_m} A_{mn} = -Z_{2m} \cosh[2mt_0], \qquad m = 0, 1, 2, \ldots \tag{4.2.51}$$

and

$$a_{2m-1} + Z_{2m-1} \sum_{n=1}^{\infty} a_{2n-1} B_{mn} = -Z_{2m-1} \sinh[(2m-1)t_0], \qquad m = 1, 2, \ldots \tag{4.2.52}$$

where we have written

$$Z_m = \frac{I'_m(la)}{K'_m(la)}. \tag{4.2.53}$$

The decoupling is expected, and is as of a consequence of the symmetry of the geometry about $x = 0$. Thus, one could have separated the original problem into symmetric and antisymmetric parts from the outset and, in doing so, the incident wave potential would also have to be decomposed into the sum of a symmetric and antisymmetric part. This explains why the two systems represent equations for the coefficients associated with the symmetric and antisymmetric multipole potentials, and the forcing terms on the right hand side are then simply the effect of the symmetric and antisymmetric components of the incident wave.

4.2.4 Numerical procedure

Numerically, the system is truncated at a finite value, N, say so that coefficients b_n, for $n = 0, 1, \ldots, 2N+1$ are found and then the reflection and transmission coefficients can be found from (4.2.47) and (4.2.48). Some numerical efficiency can be exploited by noting that A_{mn}/ϵ_m and B_{mn} are symmetric with respect to the integer variables m and n.

The core of the numerical procedure is in the computation of the integrals defining A_{mn} and B_{mn} which are of principal value type. A standard method for dealing with these types of integrals is encapsulated in the following prototype example. Consider the following integral,

$$I = \int_0^{\infty} \frac{f(t)}{g(t)} \, \mathrm{d}t \tag{4.2.54}$$

where there is a pole in the integrand at $t = t_0$. That is, $g(t_0) = 0$, $g'(t_0) \neq 0$. Then as $t \to t_0$, $g(t) \approx (t - t_0)g'(t_0)$, so that we may write

$$I = \int_0^{2t_0} \left[\frac{f(t)}{g(t)} - \frac{f(t_0)}{(t - t_0)g'(t_0)} \right] \mathrm{d}t + \int_{2t_0}^{\infty} \frac{f(t)}{g(t)} \, \mathrm{d}t \qquad (4.2.55)$$

since the second term in the first integral evaluates to zero, whilst the integrand is now bounded (in fact zero) at $t = t_0$.

Applying this to A_{mn} we find

$$A_{mn} = \epsilon_m \int_0^{2t_0} \left[A(t) \cosh 2nt \cosh 2mt - \frac{\cosh 2nt_0 \cosh 2mt_0}{(t - t_0)2\alpha h_0 N_0} \right] \mathrm{d}t$$
$$+ \epsilon_m \int_{2t_0}^{\infty} A(t) \cosh 2nt \cosh 2mt \, \mathrm{d}t + \frac{\mathrm{i}\epsilon_m \pi}{2\alpha h_0 N_0} \cosh[2nt_0] \cosh[2mt_0] \qquad (4.2.56)$$

and to B_{mn} gives

$$B_{mn} = 2 \int_0^{2t_0} \left[A(t) \sinh(2n-1)t \sinh(2m-1)t - \frac{\sinh[(2n-1)t_0] \sinh[(2m-1)t_0]}{(t - t_0)2\alpha h_0 N_0} \right] \mathrm{d}t$$
$$+ 2 \int_{2t_0}^{\infty} A(t) \sinh(2n-1)t \sinh(2m-1)t \, \mathrm{d}t$$
$$+ \frac{1\pi}{\alpha h_0 N_0} \sinh[(2n-1)t_0] \sinh[(2m-1)t_0]. \qquad (4.2.57)$$

The analysis leading to the second terms in the integrals $[0, 2t_0]$ is essentially the same as in the determination of the residues in the derivation of the multipoles previously.

We shall use a Gaussian quadrature routine for finite intervals of integration and truncate the integrals at a finite value T based on assuming large-t asymptotics for each of the integrands. Thus, if we wish to ignore any contribution to the integrals from values of the integrand which has absolute value less than ϵ, we find that the appropriate condition is

$$lh_0 \mathrm{e}^T - qT = -\log(\epsilon) \qquad (4.2.58)$$

where $q = 2n + 2m$ and $q = 2m + 2n + 2$ for the symmetric and antisymmetric systems (respectively).

4.2.5 Normal incidence scattering

We note that the systems derived for oblique scattering do not encompass the case of $\theta_{inc} = 0$ (that is when $l = 0$) where the waves are normally-incident upon the

semicircular ridge. In this case the problem is fully two-dimensional.

The multipole method can be used to derive systems of equations for the case of normal incidence, and it is usual in this case to start from scratch, replacing the singular Bessel functions $K_n(lr)$ in combination with trigonometric functions $\cos n\theta$ and $\sin n\theta$, used for the oblique-incidence ($l \neq 0$), with the corresponding singular two-dimensional harmonic functions

$$r^{-n}\cos n\theta, \qquad r^{-n}\sin n\theta, \tag{4.2.59}$$

The process of deriving multipole potentials using the functions above as the starting point is essentially the same as outlined for the oblique case, with integral representations for those functions being used to derive expressions in terms of Cartesian coordinates. See Linton & McIver [51] for more details. Thus, a similar system of equations can be derived as for the obliquely-incident case from which the reflection and transmission coefficients can be determined. However, another route to this formulation comes from taking the asymptotic limit as $l \to 0$ in the expressions already derived for oblique incidence and in some sense provides a more direct route when compared with the approach outlined earlier.

First we note the asymptotic forms for small argument,

$$K_0(x) \sim -\log(x), \qquad K_m(x) \sim \tfrac{1}{2}(m-1)!\left(\frac{2}{x}\right)^m, \qquad I_m(x) \sim \frac{1}{m!}\left(\frac{x}{2}\right)^m. \tag{4.2.60}$$

Also relations for derivatives of Bessel functions exist, namely $I_0'(x) = -I_1(x)$, $K_0'(x) = -K_1(x)$ with

$$I_m'(x) = \tfrac{1}{2}(I_{m-1}(x) + I_{m+1}(x)), \qquad K_m'(x) = -\tfrac{1}{2}(K_{m-1}(x) + K_{m+1}(x)), \tag{4.2.61}$$

Therefore, as $l \to 0$, it can be shown that

$$Z_0 \sim -2\left(\frac{la}{2}\right)^2 \tag{4.2.62}$$

With some further work, it can also be shown that as $l \to 0$,

$$Z_m \sim \frac{-2}{m!(m-1)!}\left(\frac{la}{2}\right)^{2m}, \qquad m = 1, 2, \ldots \tag{4.2.63}$$

where Z_m are defined by (4.2.53). The next point to consider is

$$t_0 = \cosh^{-1}(k/l) \sim \log(2k/l), \qquad \text{as } l \to 0. \tag{4.2.64}$$

It follows that

$$\cosh(2mt_0) \sim \frac{1}{\epsilon_m}\left(\frac{2k}{l}\right)^{2m}, \qquad \sinh(2mt_0) \sim \frac{1}{2}\left(\frac{2k}{l}\right)^{2m}. \tag{4.2.65}$$

The factor of ϵ_m in the denominator accounts for the special case of $m = 0$, where $\cosh 2mt = 1$.

The next part of the process we consider is the integrals defining A_{mn} and B_{mn}. A change of variable is needed to extricate the variable l from those integrals and we use $u = lh_0 \cosh t$. Then

$$t = \cosh^{-1}(u/lh_0) \sim \log(2u/lh_0) \tag{4.2.66}$$

It follows that, for $n = 0, 1, 2, \ldots$,

$$\cosh 2nt \sim \frac{1}{\epsilon_n}\left(\frac{2u}{lh_0}\right)^{2n}, \qquad \sinh(2n-1)t \sim \frac{1}{2}\left(\frac{2u}{lh_0}\right)^{2n-1} \tag{4.2.67}$$

Under this proposed change of variable, it can be readily shown that $\mathrm{d}t \sim \mathrm{d}u/u$ in the limit $l \to 0$ and so

$$A_{mn} \sim \frac{1}{\epsilon_n}\int_{lh_0}^{\infty} \frac{\mathrm{e}^{-u}(u + Kh_0)}{u\sinh u - Kh_0\cosh u}\left(\frac{2u}{lh_0}\right)^{2n+2m}\frac{\mathrm{d}u}{u} + \frac{\mathrm{i}\pi}{2\epsilon_n kh_0 N_0}\left(\frac{2k}{l}\right)^{2n+2m}, \tag{4.2.68}$$

where we have used $\alpha \to k$ as $l \to 0$. This expression holds for all $m, n = 0, 1, 2, \ldots$.

Continuing further still, the matrix elements for normal incidence we need to consider are

$$\hat{A}_{mn} = Z_{2m}\frac{\epsilon_n}{\epsilon_m}A_{mn} \tag{4.2.69}$$

At this point we need to make a clear distinction between the case of $m = 0$ and $m \geq 1$. Using the asymptotic form for Z_{2m} and A_{mn}, for $m \geq 1$ and after some algebra we find

$$\hat{A}_{mn} \sim -\frac{(2/lh_0)^{2n}(a/h_0)^{2m}(la/2)^{2m}}{(2m)!(2m-1)!}\int_0^{\infty}\hat{A}(u)u^{2n+2m-1}\,\mathrm{d}u - \frac{\pi\mathrm{i}}{2kh_0N_0}\frac{(ka)^{2m}(2k/l)^{2n}(la/2)^{2m}}{(2m)!(2m-1)!} \tag{4.2.70}$$

where we have written

$$\hat{A}(u) = \frac{\mathrm{e}^{-u}(u + Kh_0)}{u\sinh u - Kh_0\cosh u}. \tag{4.2.71}$$

In the case where $m = 0$,

$$\hat{A}_{0n} \sim -2(la/2)^2(2/lh_0)^{2n}\int_0^\infty \hat{A}(u)u^{2n-1}\,\mathrm{d}u - \frac{\pi\mathrm{i}}{kh_0N_0}(la/2)^2(2k/l)^{2n}. \tag{4.2.72}$$

A similar procedure for the antisymmetric system yields

$$\hat{B}_{mn} = Z_{2m-1}B_{mn} \tag{4.2.73}$$

so that,

$$\hat{B}_{mn} \sim -\frac{(2/lh_0)^{2n-1}(a/h_0)^{2m-1}(la/2)^{2m-1}}{(2m-1)!(2m-2)!}\int_0^\infty \hat{A}(u)u^{2n+2m-3}\,\mathrm{d}u$$
$$-\frac{\pi i}{2kh_0N_0}\frac{(ka)^{2m-1}(2k/l)^{2n-1}(la/2)^{2m-1}}{(2m-1)!(2m-2)!} \tag{4.2.74}$$

for $m, n = 1, 2, \ldots$.

The right-hand side term can also be approximated in the limit using results already established, so that

$$-Z_{2m}\cosh[2mt_0] \sim \frac{2(la/2)^{4m}}{(2m)!(2m-1)!}\frac{1}{2}\left(\frac{2k}{l}\right)^{2m} = \frac{(la/2)^{2m}}{(2m-1)!}\frac{(ka)^{2m}}{(2m)!} \tag{4.2.75}$$

for $m = 1, 2, \ldots$ and

$$-Z_{2m-1}\sinh[(2m-1)t_0] \sim -\frac{2(la/2)^{4m-2}}{(2m-1)!(2m-2)!}\frac{1}{2}\left(\frac{2k}{l}\right)^{2m-1} = \frac{(la/2)^{2m-1}}{(2m-2)!}\frac{(ka)^{2m-1}}{(2m-1)!} \tag{4.2.76}$$

whilst the case of $m = 0$ simply gives the right-hand side

$$-Z_0 \sim 2(la/2)^2. \tag{4.2.77}$$

We can now substitute in the asymptotic forms for both the symmetric and anti-symmetric systems, and in doing so, find it convenient to re-scale the coefficients with

$$a_n = \frac{b_n}{(n-1)!}\left(\frac{la}{2}\right)^n \tag{4.2.78}$$

for $n = 1, 2, \ldots$ and $a_0 = b_0$ and b_n are the new set of unknowns.

We start first with the system of equations for the even coefficients a_0 given by (4.2.51) with $m = 0$. Then, with all the asymptotic limits in place and with the change of unknown variables we get

$$b_0 + b_0\hat{A}_{00} + \sum_{n=1}^{\infty} \frac{b_{2n}}{(2n-1)!}\left(\frac{la}{2}\right)^{2n} \hat{A}_{0n} = 2(la/2)^2 \tag{4.2.79}$$

Taking the limit as $l \to 0$ in this equation reduces all but the first term on the left-hand side to zero and hence shows that $b_0 = 0$. In fact it shows that $b_0 = O(l^2)$ as $l \to 0$ in the oblique problem. Consideration of the remaining equations for a_{2m} with $m \geq 1$ using all of the terms taken in the limit $l \to 0$ gives, after considerable algebra

$$b_{2m} + \sum_{n=1}^{\infty} b_{2n}\tilde{A}_{mn} = \frac{(ka)^{2m}}{(2m)!}, \qquad m = 1, 2, \ldots \tag{4.2.80}$$

where

$$\tilde{A}_{mn} = -\frac{(a/h_0)^{2n+2m}}{(2n-1)!(2m)!}\int_0^{\infty} \hat{A}(u)u^{2n+2m-1}\,\mathrm{d}u - \frac{\pi \mathrm{i}}{2kh_0N_0}\frac{(ka)^{2n+2m}}{(2n-1)!(2m)!} \tag{4.2.81}$$

The antisymmetric system is transformed, in a similar fashion to give

$$b_{2m-1} + \sum_{n=1}^{\infty} b_{2n-1}\tilde{B}_{mn} = \frac{(ka)^{2m-1}}{(2m-1)!}, \qquad m = 1, 2, \ldots \tag{4.2.82}$$

where

$$\tilde{B}_{mn} = -\frac{(a/h_0)^{2n+2m-2}}{(2n-2)!(2m-1)!}\int_0^{\infty} \hat{A}(u)u^{2n+2m-3}\,\mathrm{d}u - \frac{\pi \mathrm{i}}{2kh_0N_0}\frac{(ka)^{2n+2m-2}}{(2n-2)!(2m-1)!} \tag{4.2.83}$$

These systems are independent of l, as required. It remains to consider expressions for the reflection and transmission coefficients by taking the limit $l \to 0$ in (4.2.47) and (4.2.48) for the oblique scattering coefficients. Using the relationship between the coefficients a_n and b_n (4.2.78) and the asymptotic forms for the other factors we find

$$R = \frac{\mathrm{i}\pi}{2kh_0N_0}\sum_{n=1}^{\infty}\left(b_{2n}\frac{(ka)^{2n}}{(2n-1)!} - b_{2n-1}\frac{(ka)^{2n-1}}{(2n-2)!}\right) \tag{4.2.84}$$

and

$$T = 1 + \frac{\mathrm{i}\pi}{2kh_0N_0}\sum_{n=1}^{\infty}\left(b_{2n}\frac{(ka)^{2n}}{(2n-1)!} + b_{2n-1}\frac{(ka)^{2n-1}}{(2n-2)!}\right) \tag{4.2.85}$$

The systems of equations and expressions for R and T for normal incidence shown here have been independently verified by using the multipole method directly for two-dimensional scattering (as referred to at the beginning of this section).

As a final point, we note that we may write $\hat{A}_{mn} = C_{2m,2n}$ and $\hat{B}_{mn} = C_{2m-1,2n-1}$ where

$$C_{mn} = -\frac{(a/h_0)^{n+m}}{(n-1)!(m)!}\int_0^\infty \hat{A}(u)u^{n+m-1}\,\mathrm{d}u - \frac{\pi \mathrm{i}}{2kh_0N_0}\frac{(ka)^{n+m}}{(n-1)!(m)!} \tag{4.2.86}$$

and by defining

$$F_m = \frac{(ka)^m}{m!} \tag{4.2.87}$$

the systems of equations are simply

$$b_{2m} + \sum_{n=1}^{\infty} b_{2n}C_{2m,2n} = F_{2m}, \qquad m = 1, 2, \ldots \tag{4.2.88}$$

and

$$b_{2m-1} + \sum_{n=1}^{\infty} b_{2n-1}C_{2m-1,2n-1} = F_{2m-1}, \qquad m = 1, 2, \ldots \tag{4.2.89}$$

resulting in

$$R = \frac{\mathrm{i}\pi}{2kh_0N_0}\sum_{n=1}^{\infty}(2nb_{2n}F_{2n} - (2n-1)b_{2n-1}F_{2n-1}) \tag{4.2.90}$$

and

$$T = 1 + \frac{\mathrm{i}\pi}{2kh_0N_0}\sum_{n=1}^{\infty}(2nb_{2n}F_{2n} + (2n-1)b_{2n-1}F_{2n-1}) \tag{4.2.91}$$

4.3 Edge waves

4.3.1 Introduction

In the case where there is an incident wave exciting the system, the problem is prescribed in terms of k and θ_{inc}, the incident wavenumber and wave angle. Edge waves are found by specifying k and l, the "longshore" wavenumber (defined by $l = k\sin\theta_{inc}$ in the scattering problem, as the component of k in the y direction) as independent parameters and seeking solutions in which the wave field decays exponentially away from the ridge. The latter condition, of decay away from the ridge, is

ensured by requiring $l > k$, a condition which is often referred to as being in a regime where the frequency is below a *cut-off* value. Of course, it still remains to satisfy all the remaining conditions of the problem, which has now been rendered homogenous due to the absence of the incident wave term. Basic inspection of the condition $l > k$ with the corresponding relationship between l and k used for a scattering problem, namely $l = k \sin \theta_{inc}$, clearly shows that no real scattering angle θ_{inc} exists.

To illustrate these ideas further, it is useful to consider a prototype problem in which there is a rapid change in depth from h_0 for $x < -a$, to h_1 from $-a < x < a$, and back to h_0 for $x > a$ and consider the water wave problem from the viewpoint of "linearised long wave theory" (see, for example, Mei [61]). Then, a wave of radian frequency ω, satisfies (according to this shallow water theory, in which the depth dependence is integrated out in each of the two constant depths)

$$\left(\frac{\partial^2}{\partial x^2} + \frac{\partial^2}{\partial y^2} + k_0^2\right)\zeta = 0, \qquad x \notin (-a, a) \tag{4.3.1}$$

and

$$\left(\frac{\partial^2}{\partial x^2} + \frac{\partial^2}{\partial y^2} + k_1^2\right)\zeta = 0, \qquad x \in (-a, a) \tag{4.3.2}$$

where

$$\omega^2/gh_i = k_i^2, \qquad i = 0, 1. \tag{4.3.3}$$

It is clear that if $h_0 > h_1$ then $k_0 < k_1$ and vice versa. Note that we have not yet used the fact that $\zeta(x, y) = \eta(x)\mathrm{e}^{ily}$, which is assumed on account of the uniformity of the geometry in the y-direction. This is done so that the equations above can be seen clearly to represent the usual two-dimensional wave equation (occurring in optics, acoustic, electromagnetics etc), with different wavenumbers in the two intervals of x. If c_i, $i = 0, 1$ is the wave speed in the two intervals then $k_i = \omega/c_i$, so that it is seen that the wave speed increases when the depth decreases and vice versa. Now we have

$$\frac{\partial^2 \eta}{\partial x^2} - (l^2 - k_0^2)\eta = 0, \qquad x \notin (-a, a) \tag{4.3.4}$$

and

$$\frac{\partial^2 \eta}{\partial x^2} + (k_1^2 - l^2)\eta = 0, \qquad x \in (-a, a) \tag{4.3.5}$$

after using the complex exponential dependence on y. These two equations have been written in this particular way since it can be seen that if $l > k_0$, then only exponentially decaying solutions can exist for $x < -a$ and $x > a$, whilst if $l < k_1$ wave-like modes will exist in $-a < x < a$. That is, for $k_0 < l < k_1$ a wave would be capable of propagating in the interval $x \in (-a, a)$ but would decay exponentially away from this interval. In order that this condition hold, we must have $h_0 > h_1$. This basic example can be used as a heuristic argument to argue that that edge waves should usually be found in cases where there is a protrusion above some constant depth (where the depth decreases locally). Indeed, there are no known examples of edge waves in the contrasting case of pure submergence below a constant depth. In fact it is believed that Bonnet-Ben Dhia, A.S. & Joly, P. [7] prove that there are no edge waves over a depression, although an important typographical therein introduces and element of uncertainty in this assertion.

Edge waves of this type along one of the Cartesian directions in which the geometry is uniform in a water wave problem have some similarities with optical wave propagation in media of differing refractive index (as already alluded to), and this is a useful analogy to draw on in motivating the physical interpretation of the wave motion in our problem. Thus, when there are two media, one of which possesses a reduced wave speed, there is the possibility of total internal reflection.

Edge waves in the context of water waves have a long history, with Stokes [90] in 1846 demonstrating their existence over a long plane sloping beach. The Stokes edge wave (as it is known) was later classified by Ursell [98] as the first mode in a sequence of possible modes whose number increases as the beach angle decreases. Meanwhile Ursell [97] had proved the existence of symmetric edge waves over a submerged horizontal cylinder in water of infinite depth, provided the radius was sufficiently small. He used the multipole method as the basis of his solution and then used arguments based on the theory of determinants of infinite matrices to prove that an edge wave exists for a cylinder of any radius and submerged to any depth below the free surface. In doing so, an approximate dispersion relation for the edge waves was also derived,

on the basis of the radius of the cylinder being small. Later, McIver & Evans [57] showed by direct numerical computation of the multipole system that this edge wave was the first in a sequence of edge wave modes that increased in number as the cylinder approached the free surface. Thus, the second edge wave mode "cuts in" when $d/a \approx 1.07$ where d is the depth of submergence of the centre of the cylinder below the free surface and a is the radius of the cylinder. Subsequently, Porter & Evans [76] showed that a sequence of antisymmetric edge waves (that is, the wave motion is antisymmetric about the vertical line drawn through the centre of the cylinder as opposed to symmetric in previous work) interlaced those found by McIver [57], the first occurring for $d/a \approx 1.18$. Evans & McIver [28] numerically computed the edge waves over the rectangular protrusion (as used in our basic example above) under the basis of full linear theory (as opposed to shallow water theory) and demonstrated the existence of an interlaced sequence of symmetric and antisymmetric edge wave modes, which increase with increasing shelf width and increasing height of step; a fundamental symmetric edge wave mode exists for all rectangular protrusions of non-zero width. Evans & Kuznetsov [25] discuss trapped modes about submerged bodies in more general situations.

In fact, the existence of trapped modes can be established under quite general conditions although, as we have seen, explicit solutions are rare. It can be proved that when topography protrudes above an otherwise constant depth bed, then that topography supports edge waves. For a detailed proof see Lavrentiev & Chabat [50], Jones [44], or Kuznetsov *et al* [48] who give a thorough review of the theory of edge waves.

4.3.2 Edge waves over a semicircular ridge

Of course, the work on edge waves above circular cylinders in infinite depth, referred to in the introductory paragraphs above, is closely related to our present problem in which we are considering a semicircular bottom protrusion in constant finite depth. The multipole method is used here and we have already identified in the scattering

problem symmetric and antisymmetric components of the solution.

To be specific, let us write down the boundary value problem now being considered. We seek a function $\phi(x,z)$ satisfying

$$(\nabla^2 - l^2)\phi = 0, \qquad \text{in } D \tag{4.3.6}$$

with

$$\phi_z = 0, \qquad \text{on } z = h_0\,,\ x \notin (-a,a) \tag{4.3.7}$$

$$\phi_r = 0, \qquad \text{on } r = a\,,\ \theta \in (0,\pi) \tag{4.3.8}$$

and

$$K\phi + \phi_z = 0, \qquad \text{on } z = 0\,,\ -\infty < x < \infty \tag{4.3.9}$$

with the additional "edge wave" condition

$$\phi \to 0, \qquad \text{as } |x| \to \infty\,,\ 0 < z < h_0 \tag{4.3.10}$$

which can be thought of as replacing the radiation conditions in the scattering problem which defined R and T in terms of a unit amplitude incident wave.

As already mentioned, in the formulation of the scattering problem, when $l > k$, there are no real values of t_0 (defined by $t_0 = \cosh^{-1}(k/l)$) at which poles occur in the function $A(t)$. Consequently, as $|x| \to \infty$, it must be that $\psi_n(lr,\theta) \to 0$ as $|x| \to \infty$ since the function $K_n(lr)$ decays exponentially with lr and the resulting integral modification to this free-space potential defining the multipole also decays to zero by the Riemann-Lebesgue Lemma. In other words the integrand is regular everywhere and modulated by an increasingly oscillatory term in x as $|x|$ increases, so that the in the limit, the integral must vanish. Thus, the integral no longer needs to be indented around any poles, and so (4.2.29) and (4.2.34) are replaced, for $l > k$ by

$$\psi_{2n}(lr,\theta) = K_{2n}(lr)\cos 2n\theta + \int_0^\infty A(t)\cosh(l(h_0 - z)\cosh t)\cosh 2nt\cos(lx\sinh t)\,\mathrm{d}t \tag{4.3.11}$$

and

$$\psi_{2n-1}(lr,\theta) = K_{2n-1}(lr)\cos(2n-1)\theta + \int_0^\infty A(t)\frac{\cosh(l(h_0-z)\cosh t)}{\cosh(lh_0\cosh t)}\sinh(2n-1)t\sin(lx\sinh t)\,\mathrm{d}t \quad (4.3.12)$$

Note that these are now *real* functions. It is a simple matter to follow the procedure used for deriving the solution to the scattering problem with the modified definitions above. In particular, though, we may now consider *separately* symmetric and antisymmetric solutions since there is no longer any asymmetry introduced by the presence of an incident wave and because the problem is linear and homogenous. That is to say, we may write either

$$\phi^s(x,z) = N_0^{-1/2}\sum_{n=0}^{\infty}\epsilon_n a_{2n}\psi_{2n}(lr,\theta) \quad (4.3.13)$$

or

$$\phi^a(x,z) = 2\mathrm{i}N_0^{-1/2}\sum_{n=0}^{\infty}a_{2n-1}\psi_{2n-1}(lr,\theta) \quad (4.3.14)$$

where the superscripts on ϕ are used to denote symmetric and antisymmetric potentials respectively. Such representations are ensured, by the construction of the multipole potentials, to satisfy all but the no-flow condition on the cylinder. There is no incident wave present in this problem, so following through the procedure used for the scattering problem leads to either

$$a_{2m} + Z_{2m}\sum_{n=0}^{\infty}a_{2n}\frac{\epsilon_n}{\epsilon_m}A_{mn} = 0, \qquad m = 0,1,2,\ldots \quad (4.3.15)$$

for the symmetric edge waves or

$$a_{2m-1} + Z_{2m-1}\sum_{n=0}^{\infty}a_{2n-1}B_{mn} = 0 \qquad m = 1,2,\ldots \quad (4.3.16)$$

for the antisymmetric edge waves. These two independent systems of equations are the analogues of those occurring in (4.2.52) and (4.2.53) in the scattering problem, however, note that the definitions of A_{mn} and B_{mn} are now also slightly altered as a consequence of the modified definitions of the multipoles so that

$$A_{mn} = \epsilon_m\int_0^\infty A(t)\cosh 2nt\cosh 2mt\,\mathrm{d}t \quad (4.3.17)$$

and

$$B_{mn} = 2\int_0^\infty A(t)\sinh(2n-1)t\sinh(2m-1)t\,\mathrm{d}t. \tag{4.3.18}$$

Notice that the homogeneous systems of equations (4.3.15) and (4.3.16) for determining the edge waves are *real*, and thus the problem of finding solutions is one in which the real zeros of a real determinant needs to be found. As in the scattering problem, each infinite system of equations is numerically truncated to size $N+1$.

Similar comments made on the numerical procedure for the scattering problem apply here, although the computation of the factors A_{mn} and B_{mn} is somewhat simpler here, since there are no poles in the integrand.

4.4 Scattering by a hemispherical seamount

4.4.1 Statement of the scattering problem

We choose a Cartesian coordinate system with the z axis oriented downwards and with the origin and x and y axes in the undisturbed free surface. A hemispherical seamount of radius a, with center at $(0,0,h_0)$ protrudes into the fluid domain D from a bed of otherwise constant depth h_0. We also define a spherical coordinate system (r,θ,α) with origin at the centre of the hemisphere such that

$$r = (x^2+y^2+(h_0-z)^2)^{1/2}, \tag{4.4.1}$$

$$R = (x^2+y^2)^{1/2} = r\sin\theta, \tag{4.4.2}$$

$$x = R\cos\alpha, \quad y = R\sin\alpha, \quad h_0 - z = r\cos\theta. \tag{4.4.3}$$

We recall the boundary value problem to be solved is

$$\nabla^2\phi = 0, \qquad r\in D, \tag{4.4.4}$$

$$\frac{\partial\phi}{\partial z} + K\phi = 0, \qquad \text{on } z=0, \tag{4.4.5}$$

$$\frac{\partial\phi}{\partial z} = 0, \qquad \text{on } \theta=\pi/2,\ r>a, \tag{4.4.6}$$

$$\frac{\partial\phi}{\partial r} = 0, \qquad \text{on } r=a. \tag{4.4.7}$$

We consider the scattering of an incoming plane wave $\phi_{inc} = \mathrm{e}^{-\mathrm{i}kx}\psi_0(z)$ which may be expanded by the Jacobi-Anger expansion in coordinates (R, α, z) as follows

$$\phi_{inc} = \sum_{m=-\infty}^{\infty} \mathrm{i}^m N_0^{-1/2} J_m(kR)\mathrm{e}^{\mathrm{i}m\alpha} \cosh k(h_0 - z), \tag{4.4.8}$$

or equivalently

$$\phi_{inc} = \sum_{m=0}^{\infty} \phi_{inc}^m \cos m\alpha \equiv \sum_{m=0}^{\infty} \varepsilon_m \mathrm{i}^m N_0^{-1/2} J_m(kR) \cos m\alpha \cosh k(h_0 - z) \tag{4.4.9}$$

where $\varepsilon_0 = 1$ and $\varepsilon_m = 2,\ m \geq 1$. To complete the formulation of the problem, we apply a Sommerfeld radiation condition [88] which may be written as

$$\lim_{R\to\infty} R^{1/2}\left(\frac{\partial}{\partial R} - \mathrm{i}k\right)\phi_s = 0, \tag{4.4.10}$$

where ϕ_s is the scattered wave potential. This radiation condition is equivalent to

$$\phi_s \sim \sum_{m=-\infty}^{\infty} \mathrm{i}^m \psi_0(z) H_m(kR) A_m \mathrm{e}^{\mathrm{i}m\alpha} \tag{4.4.11}$$

in the case of axisymmetric problems, or alternatively

$$\phi_s \sim \sum_{m=0}^{\infty} \varepsilon_m \mathrm{i}^m \psi_0(z) H_m(kR) A_m \cos m\alpha. \tag{4.4.12}$$

This may be written as

$$\phi_s \sim \psi_0(z) H_m(kR) \mathcal{A}(\alpha) \tag{4.4.13}$$

where $\mathcal{A}(\alpha)$, is the angular variation of the scattered wave and is defined by

$$\mathcal{A}(\alpha) = \sum_{m=0}^{\infty} \varepsilon_m \mathrm{i}^m A_m \cos m\alpha. \tag{4.4.14}$$

The total potential ϕ is given by

$$\phi = \phi_{inc} + \phi_s. \tag{4.4.15}$$

and, to remain consistent with (4.4.9), we expand ϕ_s as

$$\phi_s = \sum_{m=0}^{\infty} \phi_m \cos m\alpha. \tag{4.4.16}$$

The solution proceeds by solving the boundary value problem for each α mode in turn. The principal unknown of this problem is now the angular variation of the scattered wave $\mathcal{A}(\alpha)$.

4.4.2 Derivation of the multipoles

We proceed as before by defining multipoles using Thorne's approach [92]. The solution to (4.4.4) in spherical coordinates which is singular at $r = 0,\ z = h_0$ is given as

$$\frac{P_n^m(\cos\theta)}{r^{n+1}} = \frac{(-1)^m}{(n-m)!}\int_0^\infty \mu^n \mathrm{e}^{-\mu(h_0-z)} J_m(\mu R)\,\mathrm{d}\mu, \qquad n \geq m \geq 0, \tag{4.4.17}$$

see, for example, Linton & McIver [51] where $P_n^m(x)$ are the associated Legendre polynomials. Throughout we choose the definition

$$P_n^m(x) = (-1)^m(1-x^2)^{m/2}\frac{\mathrm{d}^m P_n(x)}{\mathrm{d}x^m} \tag{4.4.18}$$

which is consistent with Gradshteyn & Ryzhik [37] and Abramowitz & Stegun [1], but differs by the factor $(-1)^m$ from Thorne [92]. Therefore we define the multipoles as

$$\begin{aligned}\varphi_n^m(r,\theta) = \left(\frac{a}{r}\right)^{n+1} P_n^m(\cos\theta)\\ + \frac{(-1)^n a^{n+1}}{(n-m)!}\int_0^\infty \mu^n A(\mu)\cosh\mu(h_0-z)J_m(\mu R)\,\mathrm{d}\mu.\end{aligned} \tag{4.4.19}$$

Now to satisfy no-flow on the bed (4.4.6) we must have

$$\frac{\mathrm{d}}{\mathrm{d}\theta}P_n^m(\cos\theta) = 0 \qquad \text{for } \theta = \pi/2, \tag{4.4.20}$$

but by Abramawitz & Stegun [1] (8.6.3) we have

$$\left.\frac{\mathrm{d}}{\mathrm{d}t}(P_n^m(t))\right|_{t=0} = \frac{2^{m+1}}{\pi^{1/2}}\sin\tfrac{\pi}{2}(m+n)\frac{\Gamma(\frac{n+m}{2}+1)}{\Gamma(\frac{n-m}{2}+\frac{1}{2})}. \tag{4.4.21}$$

Therefore to satisfy the bed condition we must have $m+n = 2p$. We now choose $A(\mu)$ to satisfy the free surface boundary condition, therefore

$$A(\mu) = \frac{(K+\mu)\mathrm{e}^{-\mu h_0}}{\mu\sinh\mu h_0 - K\cosh\mu h_0}, \tag{4.4.22}$$

which, for a scattering problem, has a pole at $\mu = k$. We recall the radiation condition (4.4.10) which is equivalent to

$$\varphi_n^M \sim H_m(kR) \qquad \text{as } kR \to \infty, \tag{4.4.23}$$

therefore using

$$H_m(z) \sim \sqrt{\frac{2}{\pi z}}\, \mathrm{e}^{\mathrm{i}(z-\frac{m\pi}{2}-\frac{\pi}{4})} \tag{4.4.24}$$

we note that, when we formulate the multipoles using contour integrals, we need to close the contour and go around the pole in the upper half plane to ensure the contribution from the enclosing semicircle goes to zero, in which case the contribution from the pole is $\pi\mathrm{i}$ times the residue at the pole.

We now proceed as before by writing

$$\varphi_n^m(r,\theta) = \left(\frac{a}{r}\right)^{n+1} P_n^m(\cos\theta) + \frac{(-1)^n a^{n+1}}{(n-m)!}\int_0^\infty \mu^n A(\mu)\cosh\mu(h_0-z)J_m(\mu R)\,\mathrm{d}\mu + \chi_n^m \tag{4.4.25}$$

where the imaginary part is included in χ_n^m and is chosen to satisfy the radiation condition. Calculation of the residue proceeds identically as before, therefore after some algebra we find

$$\varphi_n^m \sim \frac{\mathrm{i}\pi}{2N_0}.\left(\frac{a}{h_0}\right)\frac{(-1)^n}{(n-m)!}(ka)^n\cosh k(h_0-z)H_m(kR) \tag{4.4.26}$$

and

$$\chi_n^m = \frac{\mathrm{i}\pi}{2N_0}.\left(\frac{a}{h_0}\right)\frac{(-1)^n}{(n-m)!}(ka)^n\cosh k(h_0-z)J_m(kR), \tag{4.4.27}$$

in which case

$$\varphi_n^m(r,\theta) = \left(\frac{a}{r}\right)^{n+1} P_n^m(\cos\theta) + \frac{(-1)^n a^{n+1}}{(n-m)!}\int_0^\infty \mu^n A(\mu)\cosh\mu(h_0-z)J_m(\mu R)\,\mathrm{d}\mu + \frac{\mathrm{i}\pi}{2N_0}.\left(\frac{a}{h_0}\right)\frac{(-1)^n}{(n-m)!}(ka)^n\cosh k(h_0-z)J_m(kR). \tag{4.4.28}$$

Now, from Cadby & Linton [9] or Thorne [92], we have

$$\mathrm{e}^{\pm\mu(h_0-z)}J_m(\mu R) = (\mp)^m\sum_{s=m}^{\infty}\frac{(\pm\mu r)^s}{(m+s)!}P_s^m(\cos\theta)(\mu r)^s \tag{4.4.29}$$

where the above result takes into account the different definitions of the associated Legendre polynomials. Then, using (4.4.29) we deduce that

$$\cosh\mu(h_0-z)J_m(\mu R) = \frac{1}{2}\sum_{s=m}^{\infty}\frac{((-1)^m+(-1)^s)}{(m+s)!}P_s^m(\cos\theta)(\mu r)^s \tag{4.4.30}$$

in which case we may rewrite (4.4.28) as

$$\varphi_n^m(r,\theta) = \left(\frac{a}{r}\right)^{n+1} P_n^m(\cos\theta) + \sum_{s=m}^{\infty} A_{ns}^m \left(\frac{r}{a}\right)^s P_s^m(\cos\theta) \tag{4.4.31}$$

where, after some simplification,

$$A_{ns}^m = \frac{(1+(-1)^{n+s})}{2(n-m)!(m+s)!}\left\{\frac{\mathrm{i}\pi a}{2N_0 h_0}(ka)^{n+s} + \int_0^{\infty}(a\mu)^{n+s} aA(\mu)\,\mathrm{d}\mu\right\}. \tag{4.4.32}$$

4.4.3 Solution and numerical procedure

We proceed, as before, by expressing the m'th mode of the scattered wave potential ϕ_m as a sum of the multipoles so that

$$\phi_m = \varepsilon_m \mathrm{i}^m N_0^{-1/2} \sum_{n=m}^{\infty} \lambda_n^m \varphi_n^m \tag{4.4.33}$$

where the normalisation of the constant coefficients $\{\lambda_n^m\}$ is chosen to simplify later expressions. We also need to express the incident potential in terms of the associated Legendre polynomials, therefore using (4.4.30) in (4.4.9) we obtain

$$\phi_{inc}^m = \varepsilon_m \mathrm{i}^m N_0^{-1/2} \sum_{s=m}^{\infty} \frac{((-1)^m + (-1)^s)}{2(m+s)!} P_s^m(\cos\theta)(ka)^s \left(\frac{r}{a}\right)^s. \tag{4.4.34}$$

It finally remains to solve the no-flow condition on the sphere (4.4.7) which is equivalent to

$$\left.\frac{\partial \phi_m}{\partial r}\right|_{r=a} = -\left.\frac{\partial \phi_{inc}^m}{\partial r}\right|_{r=a}. \tag{4.4.35}$$

So, using (4.4.33) and (4.4.34) in (4.4.35) we obtain the system of equations

$$\sum_{n=m}^{\infty} \lambda_n^m \left\{-(n+1)P_n^m(\cos\theta) + \sum_{s=m}^{\infty} A_{ns}^m s P_s^m(\cos\theta)\right\} =$$

$$-\sum_{s=m}^{\infty} \frac{((-1)^m + (-1)^s)}{2(m+s)!} s(ka)^s P_s^m(\cos\theta). \tag{4.4.36}$$

This may be simplified if we multiply throughout by $P_s^m(\cos\theta)$ and integrate using the orthogonality condition

$$\int_{-1}^{1} P_n^m(x) P_s^m(x)\,\mathrm{d}x = \frac{2}{2n+1}\frac{(n+m)!}{(n-m)!}\,\delta_{sn}, \tag{4.4.37}$$

(see, for example Gradshteyn & Ryzhik [37]) or alternatively (as $n+s$ is even by the bed condition) using

$$\int_0^1 P_n^m(x)P_s^m(x)\,\mathrm{d}x = \frac{(n+m)!\delta_{sn}}{(2s+1)(s-m)!}, \tag{4.4.38}$$

(Linton & McIver [51]), both of which are equivalent to equating terms containing $P_s^m(\cos\theta)$ and result in the system

$$\lambda_s^m - \sum_{n=m}^{\infty} \lambda_n^m A_{ns}^m \frac{s}{s+1} = (ka)^s \frac{((-1)^m + (-1)^s)s}{2(s+1)}, \qquad s = m, \ldots, . \tag{4.4.39}$$

We recover the Fourier coefficients A_m in the expansion (4.4.14) by substituting the far-field form of the multipoles (4.4.26) into (4.4.33) and comparing with (4.4.12) to give

$$A_m = \frac{\mathrm{i}\pi a}{2N_0h_0} \sum_{n=m}^{\infty} \frac{(-1)^n}{(n-m)!}\, c_n^m (ka)^n \tag{4.4.40}$$

We solve the system by truncating the infinite sums in the expansion of the multipoles as before to take the first N terms and by considering the first $2M+1$ angular modes. The multipoles are symmetric/anti-symmetric according to whether m is even/odd and we find it convenient to consider each separately. So for $m = 0, \ldots, M$ the even problem is given, after some simplification, by

$$\lambda_q^{2m} - \sum_{p=0}^{N} \frac{2m+2q}{2m+2q+1} B_{pq}^{2m} \lambda_p^{2m} = \frac{2m+2q}{2m+2q+1} (ka)^{2m+2q} \qquad q = 0, \ldots, N \tag{4.4.41}$$

where (4.4.32) becomes

$$B_{pq}^{2m} = \frac{1}{2p!(4m+2q)!} \left\{ \frac{\mathrm{i}\pi a}{2N_0h_0} (ka)^{4m+2(p+q)} + \int_0^{\infty} (a\mu)^{4m+2(p+q)} A(\mu) a \,\mathrm{d}\mu \right\} \tag{4.4.42}$$

and for $m = 1, \ldots, M$ the odd problem is given by

$$\lambda_q^{2m-1} - \sum_{p=0}^{N} \frac{2m+2q-1}{2m+2q} B_{pq}^{2m-1} \lambda_p^{2m-1} = -\frac{2m+2q-1}{2m+2q} (ka)^{2m+2q-1} \qquad q = 0, \ldots, N \tag{4.4.43}$$

in which case (4.4.32) becomes

$$B_{pq}^{2m-1} = \frac{1}{2p!(4m+2q-2)!}\left\{\frac{\mathrm{i}\pi a}{2N_0h_0}\,(ka)^{4m+2(p+q-1)} + \int_0^\infty (a\mu)^{4m+2(p+q-1)}A(\mu)a\,\mathrm{d}\mu\right\}. \quad (4.4.44)$$

Calculation of the principal valued integrals proceeds as before with us truncating each of the integrals of the form

$$a\int_{2k}^\infty a(a\mu)^p A(\mu)\,\mathrm{d}\mu \qquad p=0,1,\ldots,4M+2N, \quad (4.4.45)$$

at a value $T(p)$ so where the contribution from the integrand is ϵ. In this case we determine $T(p)$ from the solution of

$$2Th_0/a - p\log T = -\log\epsilon. \quad (4.4.46)$$

4.5 Results

4.5.1 Scattering by a semicircular ridge

Firstly we shall investigate the rate of convergence of the multipole solutions in terms of the truncation parameter N which we recall truncates the infinite sums taking the first $N+1$ symmetric and the first N antisymmetric, multipoles respectively. Table (4.1) shows the rate of convergence of the absolute value of the reflection coefficient for normal scattering by a semicircular ridge whose amplitude is half of the fluid domain's depth. Where a numerical value has converged to a value which does

$kl=$	0.5	1	1.5	2
$N=1$	0.200953954	0.234190524	0.153975563	0.062442503
$N=2$	0.xx1245504	0.xx6689068	0.x61893932	0.x77207676
$N=3$	0.xxxxxx836	0.xxxx91575	0.xxx912458	0.xxxx94690
$N=4$	0.xxxxxxxx7	0.xxxxxxxx7	0.xxxxxxx72	0.xxxxxx794
$N=5$	0.xxxxxxxxx	0.xxxxxxxxx	0.xxxxxxxxx	0.xxxxxxxxx

Table 4.1: Convergence of $|R|$ against truncation size N for normal incidence to a semicircular ridge with radius:depth ratio $a/h_0 = 0.5$

$kl =$	0.5	1	1.5	2
$N = 1$	0.195978328	0.228804676	0.150716980	0.061298505
$N = 2$	0.xx6280365	0.x31322387	0.xx8637025	0.x75944732
$N = 3$	0.xxxxxx856	0.xxxxx5425	0.xxxx56817	0.xx6032205
$N = 4$	0.xxxxxxxx8	0.xxxxxxx31	0.xxxxxxx40	0.xxxxx2331
$N = 5$	0.xxxxxxxxx	0.xxxxxxxxx	0.xxxxxxxxx	0.xxxxxxxxx

Table 4.2: Convergence of $|R|$ against truncation size N for $10°$ oblique incidence to a semi-circular ridge with radius:depth ratio $a/h_0 = 0.5$

$kl =$	0.5	1	1.5	2
$N = 1$	0.426877868	0.617583581	0.670778358	0.657608720
$N = 2$	0.xxxx38514	0.xxx278564	0.x69795829	0.xx5697630
$N = 3$	0.xxxxxx439	0.xxxxxx319	0.xxxxx4992	0.xxxxx4987
$N = 4$	0.xxxxxxxx8	0.xxxxxxxx8	0.xxxxxxxx1	0.xxxxxxxx5
$N = 5$	0.xxxxxxxxx	0.xxxxxxxxx	0.xxxxxxxxx	0.xxxxxxxxx

Table 4.3: Convergence of $|R|$ against truncation size N for $80°$ oblique incidence to a semicircular ridge with radius:depth ratio $a/h_0 = 0.5$

not change with increasing N we replace the value with an x. We see that, in all cases convergence is extremely rapid with our approximations reaching 9 significant figures accuracy at a truncation size of $N = 4$. We now consider oblique incidence for the same topography for both nearly normal $(10°)$ and glancing incidence $(80°)$ over the semicircular ridge of height half the fluid domain depth. Table (4.2) shows the results for $\theta = 10°$ and once again we see that 9 significant figures accuracy is reached with a truncation size of $N = 4$. Similarly, table (4.3) shows the results for $\theta = 80°$ which also achieves 9 significant figures accuracy with a truncation size of $N = 4$. As we have reached 9 significant figures accuracy for typical wavenumbers of interest with a truncation size of $N = 4$, then we choose a truncation size of $N = 5$ in all the results that follow.

Figure (4.1) shows the variation of the reflection coefficient for dimensionless wavenumbers $kl \in [0,\ 5]$ for a range of radii from $a/h_0 = 0.1$ to $a/h_0 = 0.9$. As expected, the greater the radius the more pronounced the variation of the reflec-

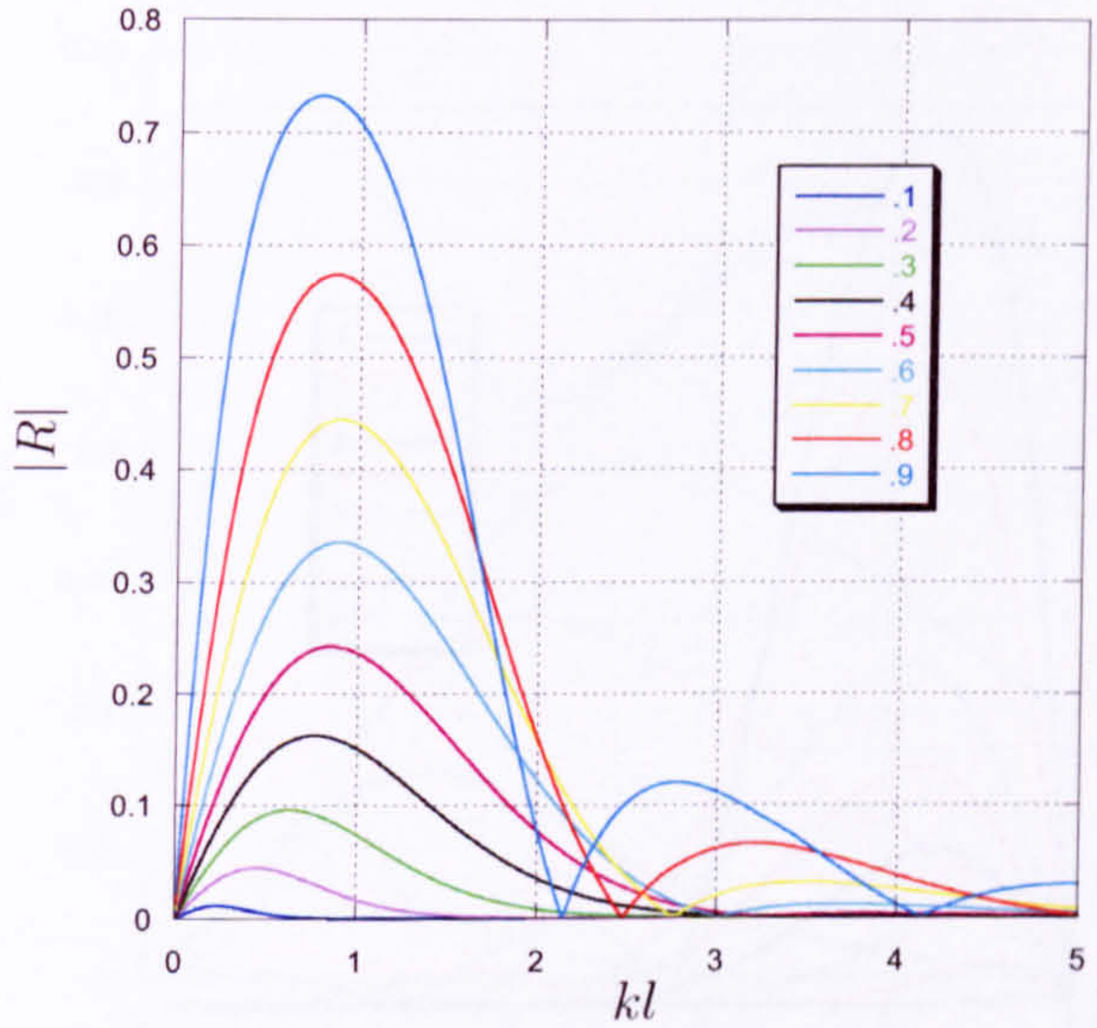

Figure 4.1: Reflection coefficients for scattering at normal incidence by a semicircular ridge for height to depth ratios $a/h_0 = 0.1, \ldots, 0.9$

tion coefficient. We also observe that for a/h_0 greater than approximately 0.4 there are zeros of the reflection coefficient and by the time $a/h_0 = 0.9$ the first peak is very pronounced and a second zero is evident within the range of interest. We find that as the angle of incidence is increased the curves vary smoothly; however, for angles close to normal incidence the same qualitative behaviour occurs. This is evident from figure (4.2) which shows the results for $30°$ incidence where we see the growth of the first peak of $|R|$ as a/h_0 increases and the presence of zeros of reflection for a/h_0 greater than approximately 0.4. It is worth noting that, although the curves in figure (4.2) have the same qualitative shape as those in figure (4.1), we see that maximum value of $|R|$ is lower in the oblique case.

The general trend of decreasing maximium value of $|R|$ with increasing obliqueness is still evident in figure (4.3) which plots results for $45°$ incidence. With this level of obliqueness we observe some different structure to the curves. For instance a first zero of $|R|$ is now evident for $a/h_0 = 0.3$, also we see that for $a/h_0 = 0.8$ and above there is a local minimum of $|R|$ but no longer a zero. For $a/h_0 = 0.9$ this

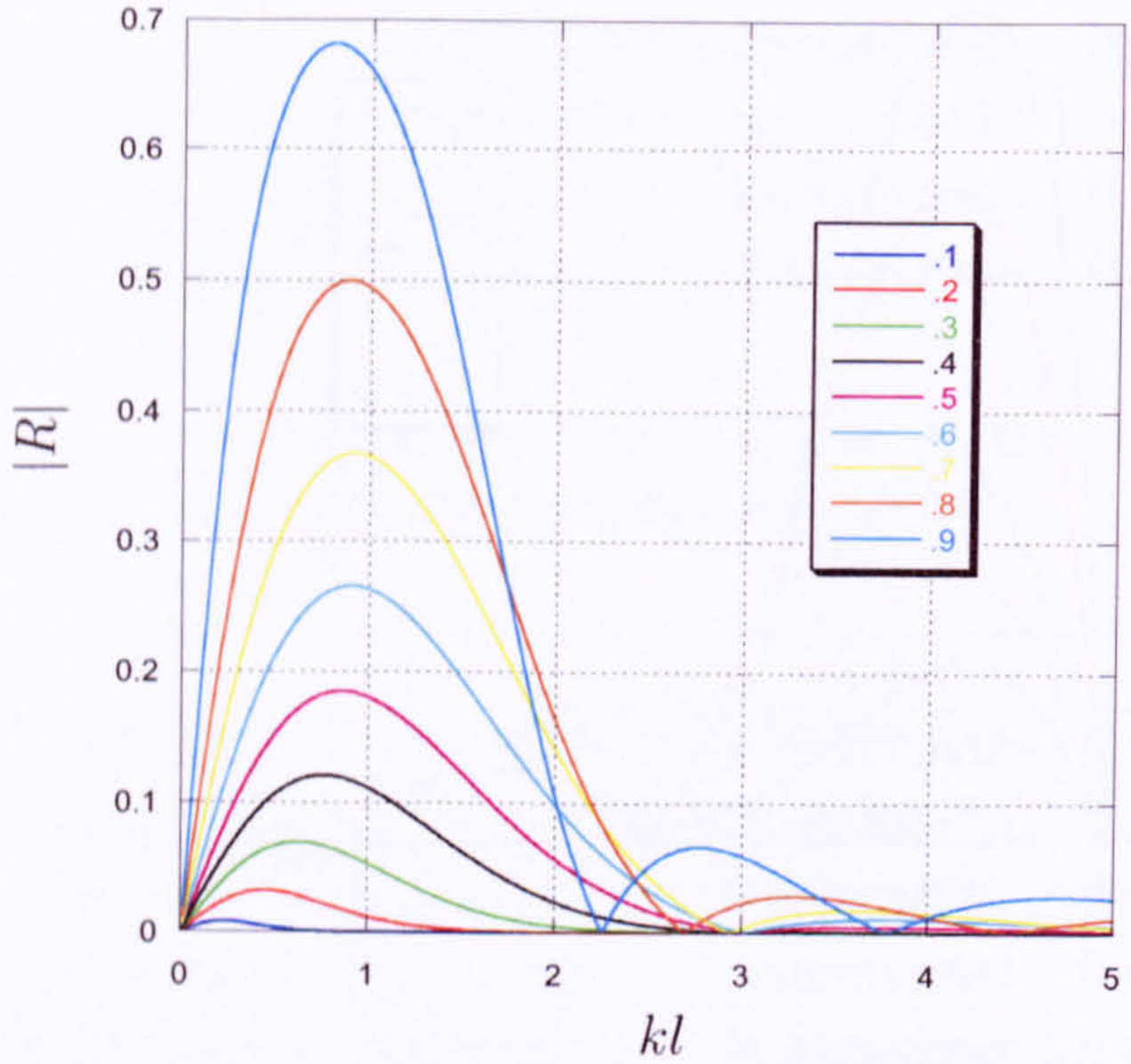

Figure 4.2: Reflection coefficients for scattering at $30°$ incidence by a semicircular ridge for height to depth ratios $a/h_0 = 0.1, \ldots, 0.9$

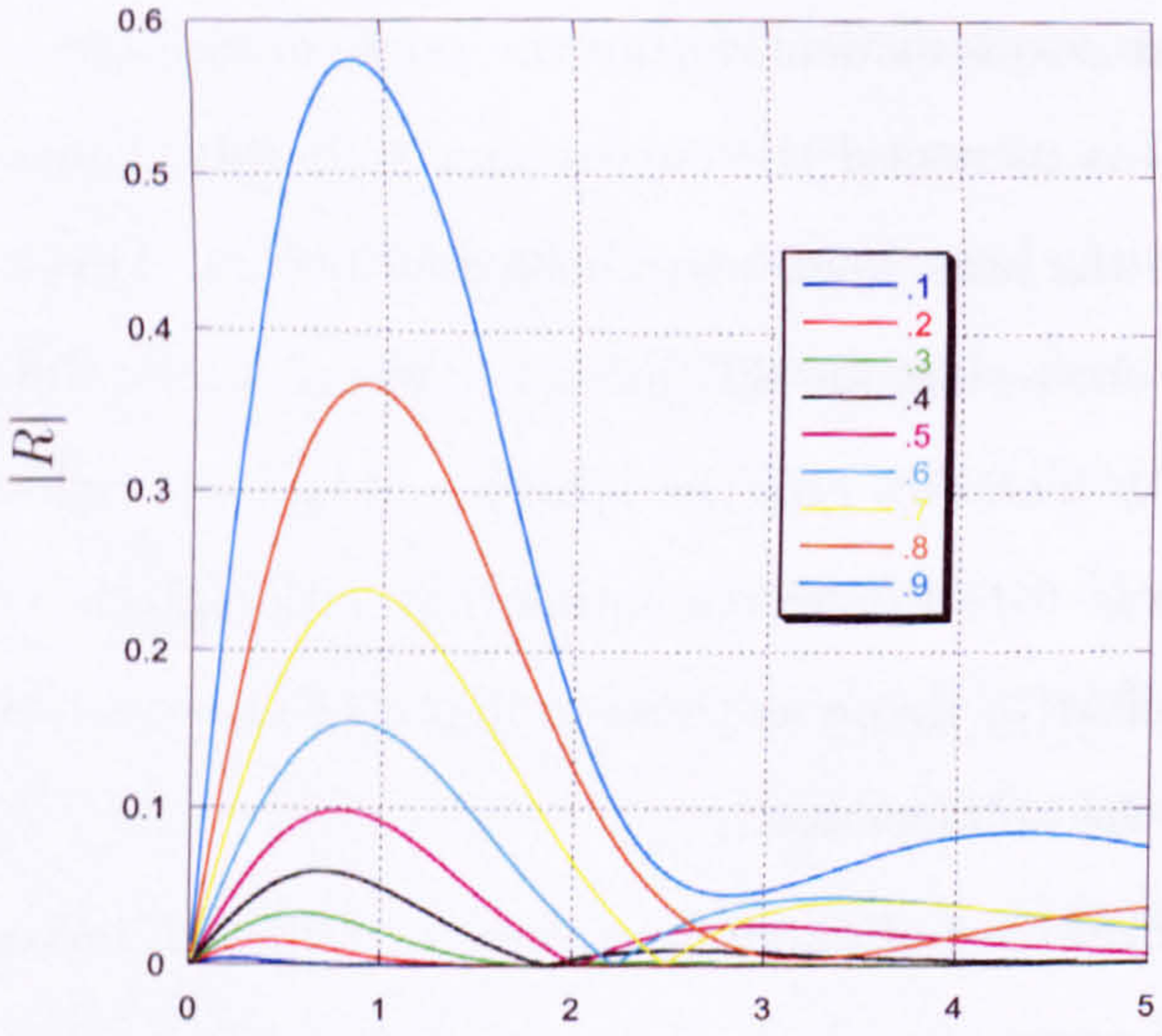

Figure 4.3: Reflection coefficients for scattering at $45°$ incidence by a semicircular ridge for height to depth ratios $a/h_0 = 0.1, \ldots, 0.9$

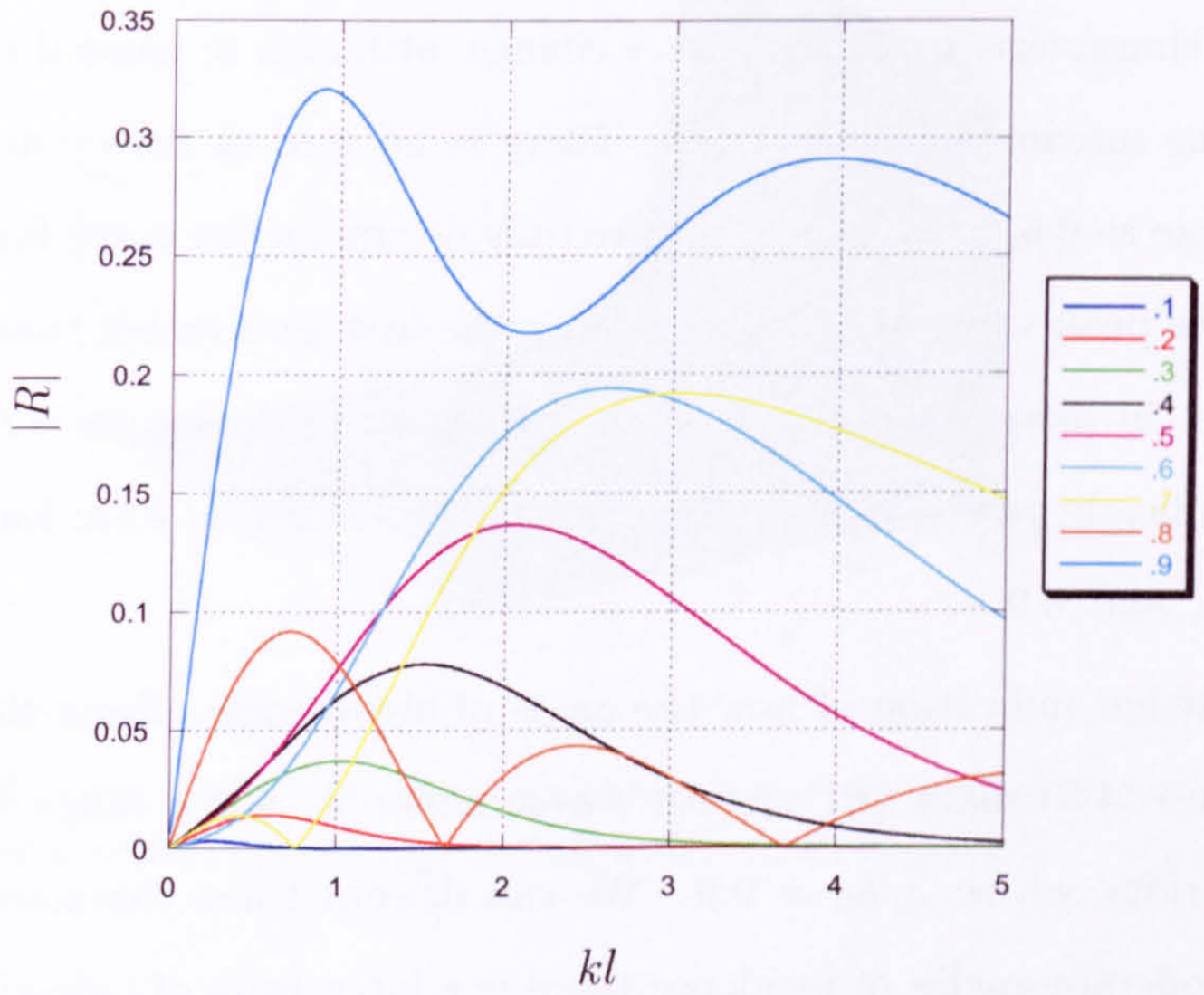

Figure 4.4: Reflection coefficients for scattering at $60°$ incidence by a semicircular ridge for height to depth ratios $a/h_0 = 0.1, \ldots, 0.9$

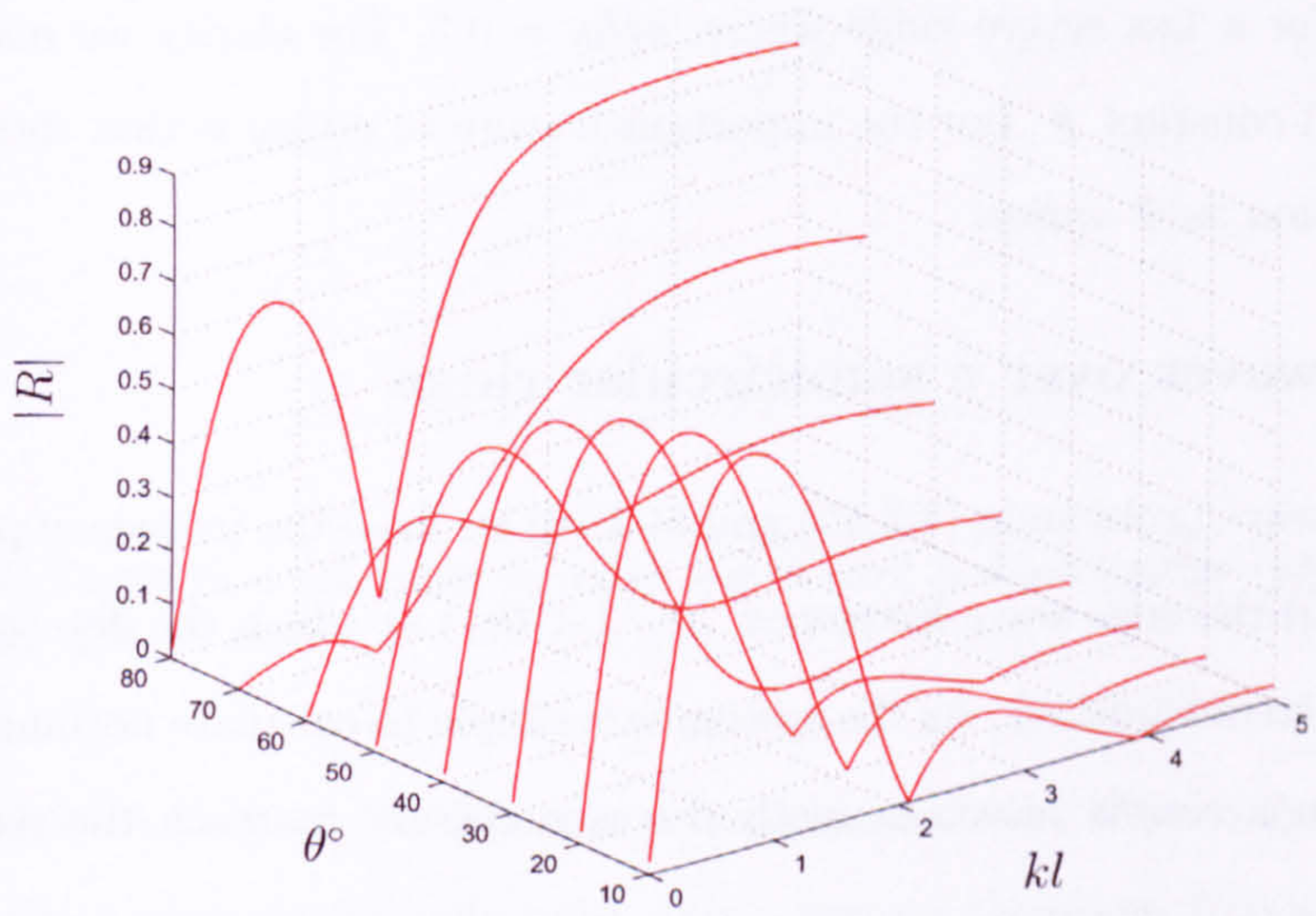

Figure 4.5: Reflection coefficients for oblique scattering at angles of incidence $\theta = 10°, \ldots, 80°$ to a semicircular ridge of height to depth ratio $a/h_0 = 0.9$

local minimum is particularly easy to see. As the obliqueness increases to $60°$ as in figure (4.4) the characteristics of the curves change, although in general there is still a decrease in the maximum value of $|R|$. There is no zero of reflection evident as a/h_0 gets as large as 0.6, in fact the first zero only occurs on the curve for $a/h = 0.7$ but this time the peak value of $|R|$ occurs after the first zero rather than as before. We also see that, at increased obliqueness the behaviour of the curves is rather more sensitive to the height of the ridge with significant difference in form for the values $a/h_0 = 0.7,\ 0.8,\ \text{and}\ 0.9$.

To give a further indication of how the angle of obliqueness affects the reflection coefficient, figure (4.5) plots $|R|$ against wavenumber kl for a range of angles of incidence to a ridge where $a/h_0 = 0.9$. We can discern three characteristic forms of curve; for moderate angles of incidence there is a large peak of reflection followed by successive peaks with zeros of reflection in between. For mid-range angles of incidence there remains an initial peak but there are no zeros of reflection whereas for approaching glancing incidence there is a small peak before a zero reappears and then $|R|$ reaches a higher peak value. Figure (4.6) shows the variation of $|R|$ with $\theta = 1, 2, \ldots, 89$, for a less severe ridge where $a/h_0 = 0.5$. For clarity we mark on the surface lines of constant θ, but the important feature to notice is that there is a continuous transition as θ varies.

4.5.2 Edge waves over a semicircular ridge

To solve the edge wave problem in (4.3.15) and (4.3.16) we fixed the frequency parameter lh_0 and found the edge wave frequency kh_0 $(< lh_0)$ at which the determinant of the resulting system vanished. As the system was simple to calculate nothing more sophisticated than a simple bisection method was necessary to reach the required accuracy.

Figure (4.7) shows the dispersion relation for a semicircular ridge of height 0.95 the fluid depth. The odd numbered modes are found by solving the symmetric problem (4.3.15) and the even numbered modes arise from solving the anti-symmetric

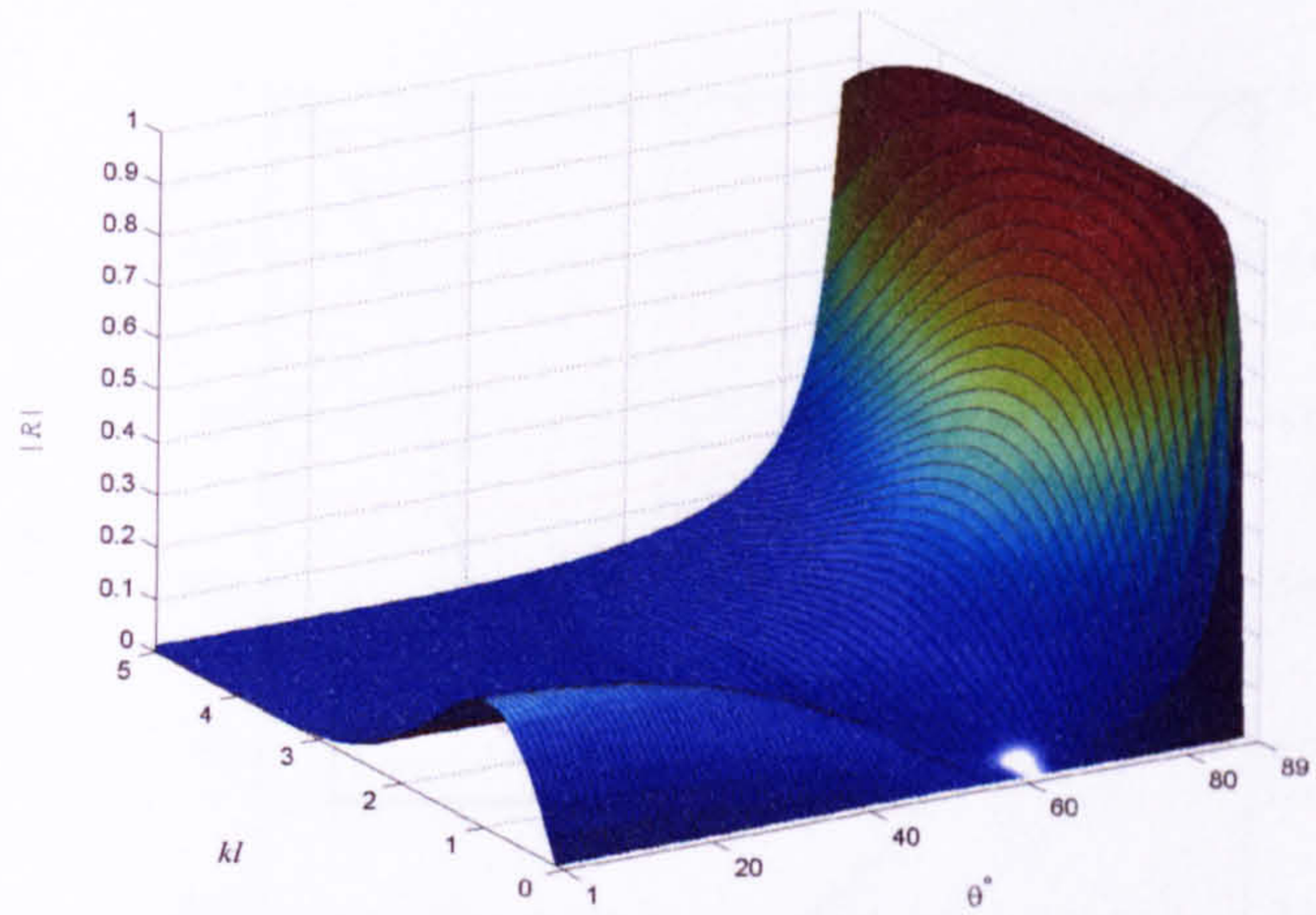

Figure 4.6: Reflection coefficients varying wavenumber kl against incidence angle θ for scattering by a semicircular ridge of height to depth ratio $a/h_0 = 0.5$.

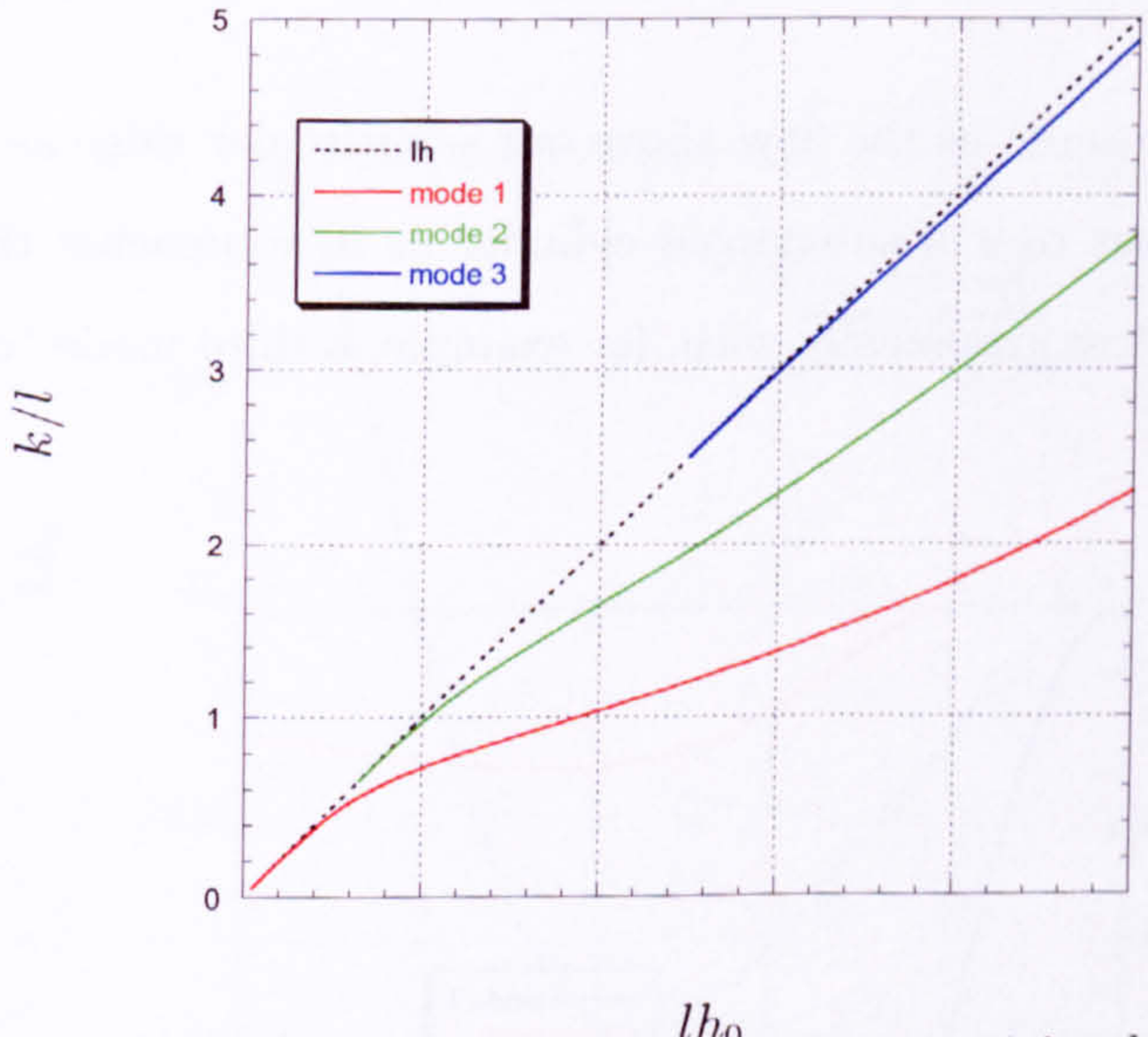

Figure 4.7: Dispersion relations for edge waves over a semicircular ridge of height to depth ratio $a/h_0 = 0.95$.

problem (4.3.16). We see that, in this extreme case we are able to find three modes although the higher modes only exist above certain threshold frequencies. Figure (4.8) is an alternative way of presenting this data where we normalise by the cut-off frequency. We note that this replicates the results in Porter & Evans [76] who solved the edge wave problem for multiple submerged cylinders in infinite depth. We would

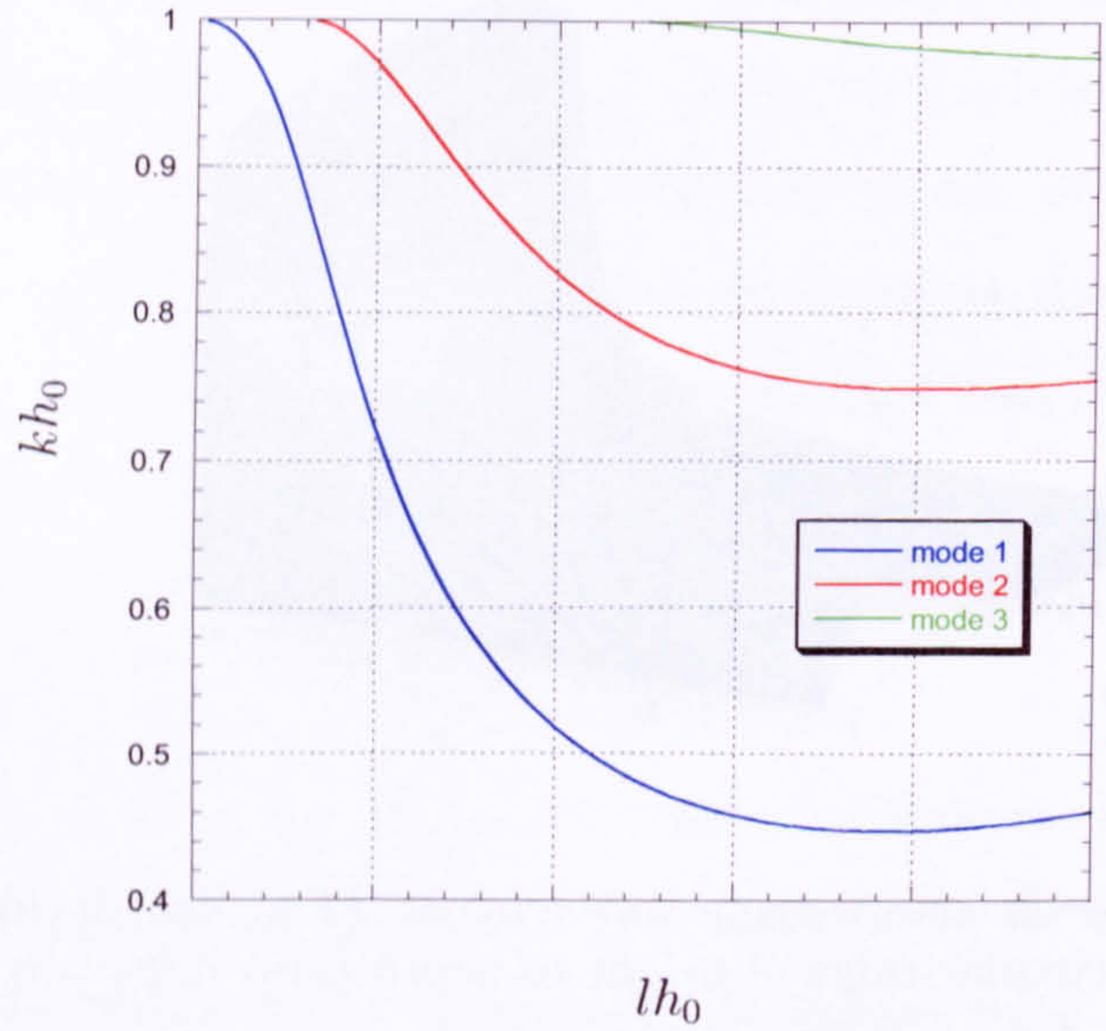

Figure 4.8: Dispersion relations for edge waves over a semicircular ridge of height to depth ratio $a/h_0 = 0.95$.

expect almost identical results as the flow above our semicircular ridge as $a/h_0 \to 1$ is locally identical to that over a submerged cylinder as it approaches the surface, and this is what we observe graphically with, for example, a third mode "cutting in" at around $lh_0 = 2.5$.

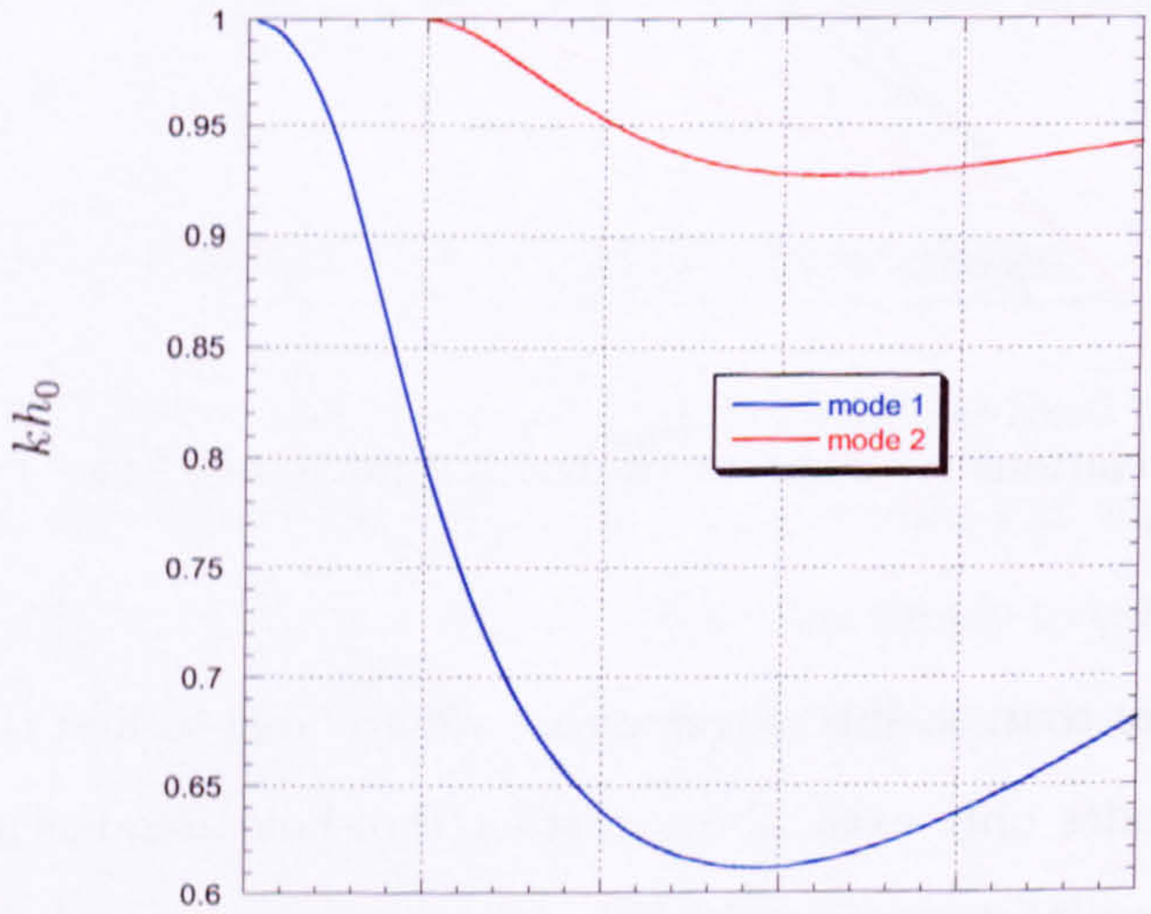

Figure 4.9: Dispersion relations for edge waves over a semicircular ridge of height to depth ratio $a/h_0 = 0.90$.

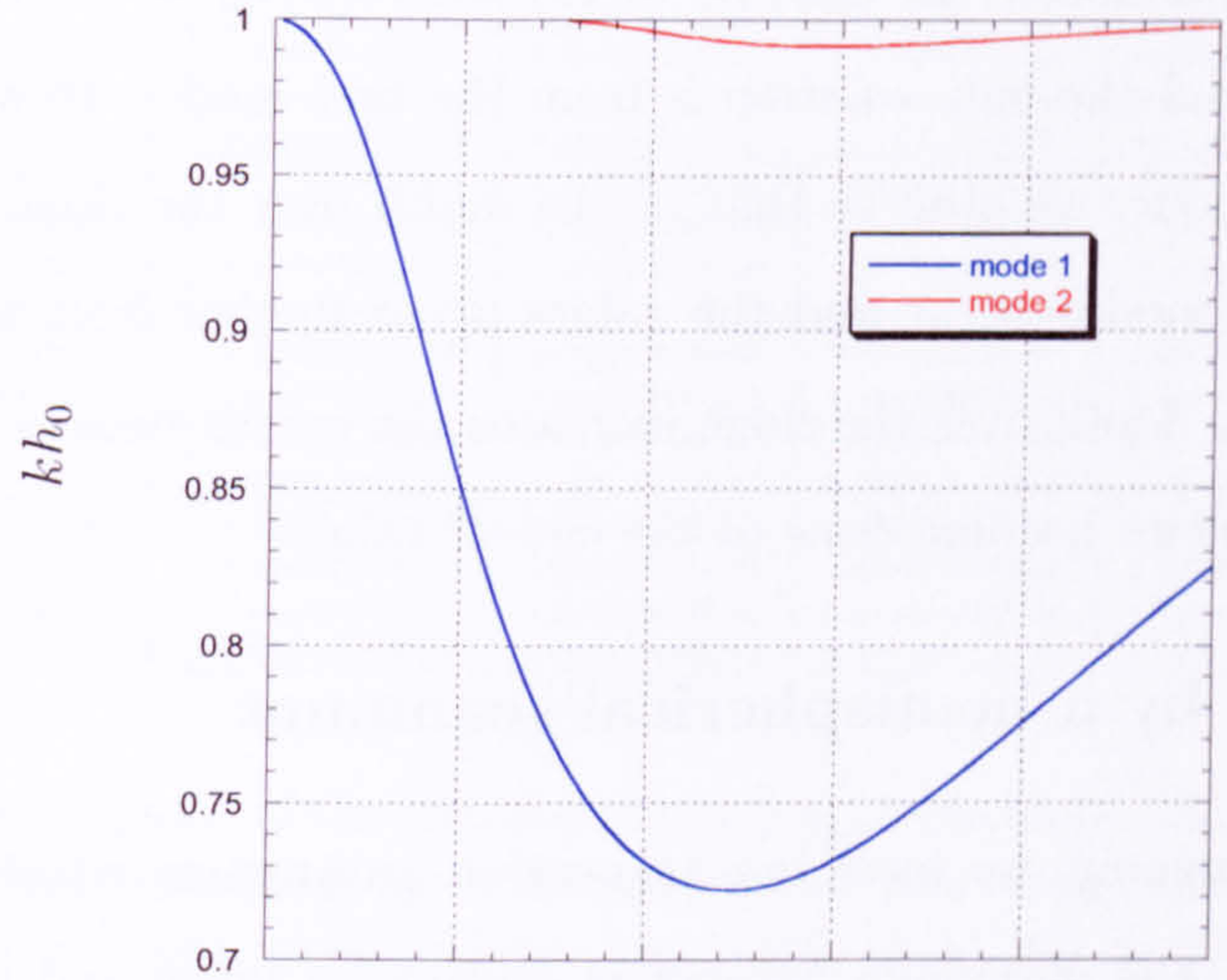

Figure 4.10: Dispersion relations for edge waves over a semicircular ridge of height to depth ratio $a/h_0 = 0.85$.

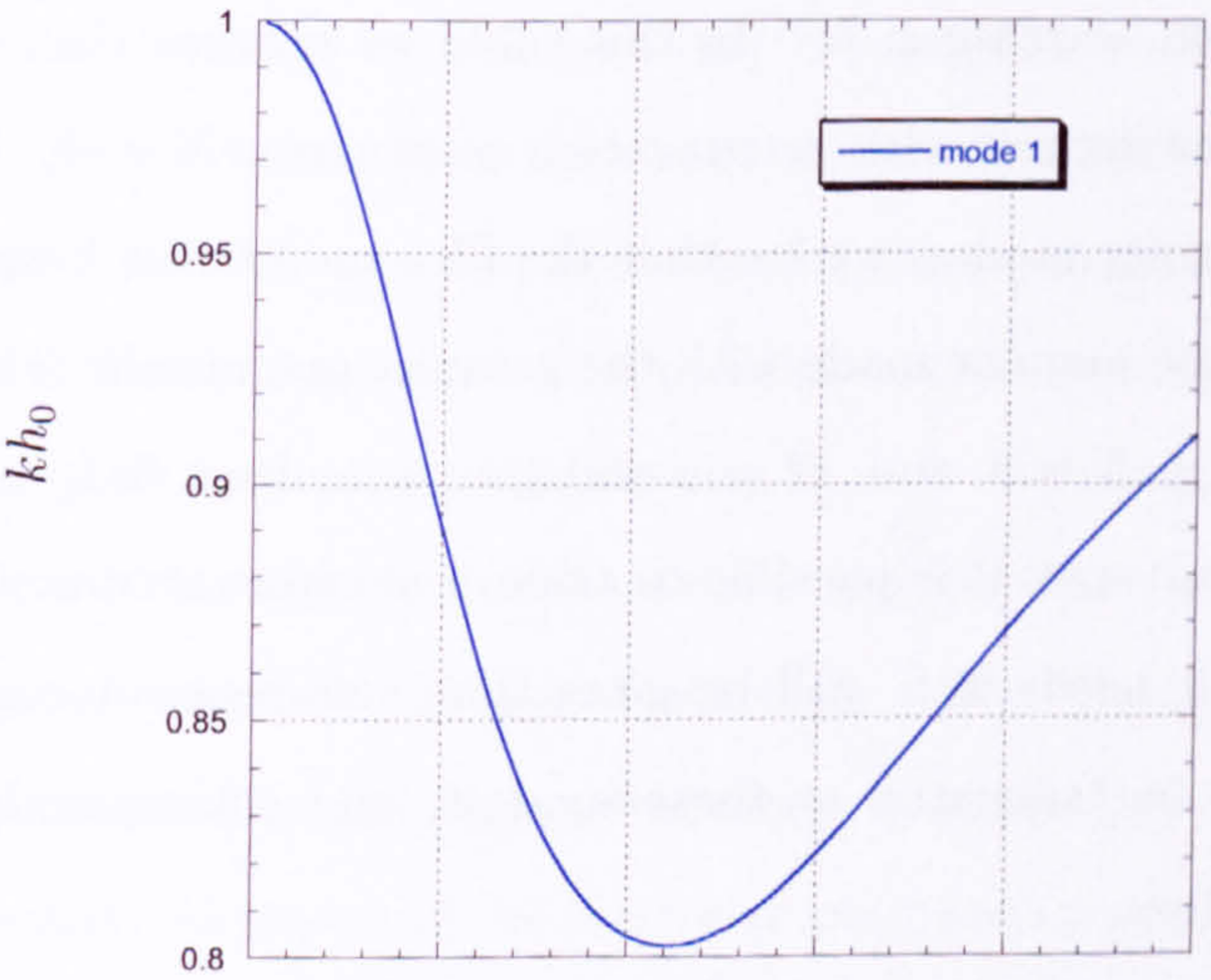

Figure 4.11: Dispersion relations for edge waves over a semicircular ridge of height to depth ratio $a/h_0 = 0.80$.

Figure (4.9) shows the edge wave dispersion relation for a ridge where $a/h_0 = 0.9$, and already it can be seen that we no longer have a third mode. Also the second mode now cuts in for larger values of lh_0 and is becoming less pronounced. By figure (4.10) where $a/h_0 = 0.85$ the second mode now cuts in for even larger values of

lh_0 and is much less pronounced. In fact, by (4.11) where $a/h_0 = 0.8$ the second mode has disappeared and the only solution is from the first mode. To summarise the characteristic behaviour, we observe that as the depth over the ridge decreases ($a/h_0 \to 1$) then more modes occur and the values occur further from the cut-off value. Conversely, as the depth over the ridge increases the curves become shallower as the edge wave frequencies become close to the cut-off value.

4.5.3 Scattering by a hemispherical seamount

For a hemispherical seamount we have two truncation parameters which we must consider; the first is N the maximum number of multipoles taken and the second is M the number of angular modes we take in the expansion of $\mathcal{A}(\theta)$. Table (4.4) displays typical results for scattering by a hemisphere whose radius is half the depth of the fluid domain. Once again we use an x to denote where a value shows no further improvement with increasing N. In this table we observe that each entry has achieved 9 significant figures with a truncation of at most $N = 4$. Likewise if we now consider the angular modes, we see that the fifth mode is at best six orders of magnitude less than the angular mode with the greatest magnitude. Therefore we deduce that truncating at $N = 4$ and $M = 5$ will give us at least 6s.f. accuracy. In fact for modest truncation sizes it is possible to achieve machine accuracy extremely rapidly. However for our needs 6s.f. will be more than sufficient. Accordingly our results that follow will be truncated at these modest, and consequently quick to compute, truncation values.

We now plot the magnitude of the angular variation, $|\mathcal{A}(\theta)|$ for $\theta \in [0, 2\pi]$, for a range of wavenumbers $kh_0 \in [0.5, 5]$ where they have been non-dimensionalised with reference to the fluid domain's depth. Figures (4.12) to (4.17) show the angular variation for a range of seamounts $a/h_0 = 0.5, 0.6, \ldots, 0.9$ and also for $a/h_0 = 0.99$. As we have non-dimensionalised the incident waves with respect to h_0 rather than a, direct comparison may be made between the plots for the different sized seamounts.

In figure (4.12) we plot the results for a seamount where $a/h = 0.5$. In this case

		Mode					
kl	*N*	0	1	2	3	4	5
0.5	1	4.75228954E-04	1.15842144E-02	7.85037750E-05	1.83676472E-07	2.18636706E-10	1.58155096E-13
	2	x.xxx54098E-04	x.xxxxxx65E-02	x.xxxxxxx5E-05	x.xxxxxxxxE-07	x.xxxxxxxxE-10	x.xxxxxxxxE-13
	3	x.xxxxx116E-04	x.xxxxxxxxE-02	x.xxxxxxxxE-05	x.xxxxxxxxE-07	x.xxxxxxxxE-10	x.xxxxxxxxE-13
1	1	5.91946747E-03	3.58118455E-02	9.73400633E-04	9.09440727E-06	4.32891264E-08	1.25241332E-10
	2	x.x2318503E-03	x.xxxx9196E-02	x.xxxxx810E-04	x.xxxxxx64E-06	x.xxxxxx71E-08	x.xxxxxxx3E-10
	3	x.xxxxx619E-03	x.xxxxxxx7E-02	x.xxxxxxx1E-04	x.xxxxxxxxE-06	x.xxxxxxxxE-08	x.xxxxxxxxE-10
	4	x.xxxxxx20E-03	x.xxxxxxxxE-02	x.xxxxxxxxE-04	x.xxxxxxxxE-06	x.xxxxxxxxE-08	x.xxxxxxxxE-10
1.5	1	1.94919769E-02	5.20363420E-02	3.21329201E-03	6.73400391E-05	7.20416700E-07	4.68722008E-09
	2	x.x5501406E-02	x.xxx77890E-02	x.xxx30348E-03	x.xxxx1053E-05	x.xxxxx981E-07	x.xxxxxx96E-09
	3	x.xxxxx762E-02	x.xxxxxxx9E-02	x.xxxxxxxxE-03	x.xxxxxxxxE-05	x.xxxxxxxxE-07	x.xxxxxxxxE-09
	4	x.xxxxxxx3E-02	x.xxxxxxxxE-02	x.xxxxxxxxE-03	x.xxxxxxxxE-05	x.xxxxxxxxE-07	x.xxxxxxxxE-09
2	1	3.39158512E-02	5.23504493E-02	5.70424627E-03	2.11319712E-04	4.00803166E-06	4.62972830E-08
	2	x.42248006E-02	x.xx619526E-02	x.xxx43481E-03	x.xxx21749E-04	x.xxxx4720E-06	x.xxxx3694E-08
	3	x.xxx52553E-02	x.xxxxx629E-02	x.xxxxxx90E-03	x.xxxxxx50E-04	x.xxxxxxx1E-06	x.xxxxxxxxE-08
	4	x.xxxxxxx6E-02	x.xxxxxxxxE-02	x.xxxxxxxxE-03	x.xxxxxxxxE-04	x.xxxxxxxxE-06	x.xxxxxxxxE-08

Table 4.4: Convergence of the angular scattering coefficients $|A_m|$ against truncation size N for wave scattering by a hemispherical seamount with radius:depth ratio $a/h_0 = 0.5$ for incident wavenumbers $kh_0 = 0.5,\ 1.0,\ 2.5\ \&\ 2.0$.

the most interesting structure is for long waves where the seamount causes a rapid change of depth within a single wavelength and we observe a distinct lobe shape for $kh_0 = 0.5, 1.0, 1.5$. However we also note that the amplitude of the angular variation remains small. As the wavenumber increases we see that the lobe structure flattens out and by $kh_0 = 3$ looks more elliptical with the major axis oriented along the axis of propagation of the incident wave. It is possible to discern from the wave $kh_0 = 3.0$ that there is slightly more scattering in the $\theta = 0$ direction than the $\theta = 180°$ direction which is to be expected as the wave is incident from $r = \infty$ along the axis $\theta = 0$. As the wavenumber increases further we expect the effect of the hump to become less pronounced as the higher frequency waves do not 'feel' the submerged seamount as greatly. As expected the scattered amplitude tends to decrease now, and we see that the elliptical shape becomes more circular for higher frequencies.

In figures (4.13) to (4.16) we see clearly the effect of increasing the seamount radius. The longer waves still generate a lobe shape but the transition to a more elliptical shape comes sooner. Also, as would be expected, by inspection of the scales of the plots we see that the amount of scattering increases significantly from for example a maximum of 0.12 in figure (4.12a) for $a/h_0 = 0.5$ to a maximum of 3.0 in figure (4.16a) for $a/h_0 = 0.9$. Also of note is that, as the height of the seamount

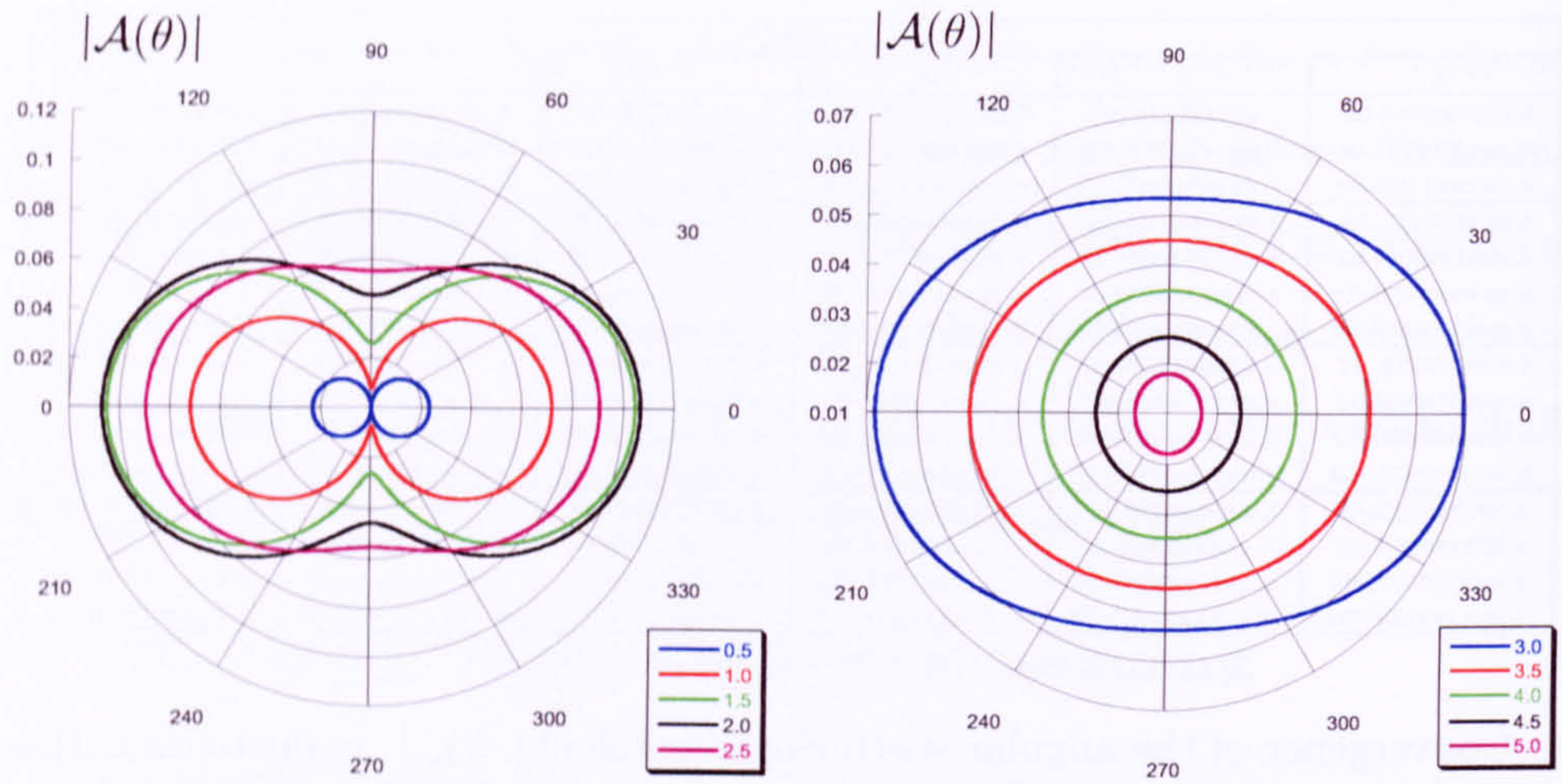

(a) $kh_0 = 0.5, \ldots, 2.5.$ (b) $kh_0 = 3.0, \ldots, 5.0$

Figure 4.12: $|\mathcal{A}(\theta)|$ for scattering by a hemispherical hump where $a/h_0 = 0.5$

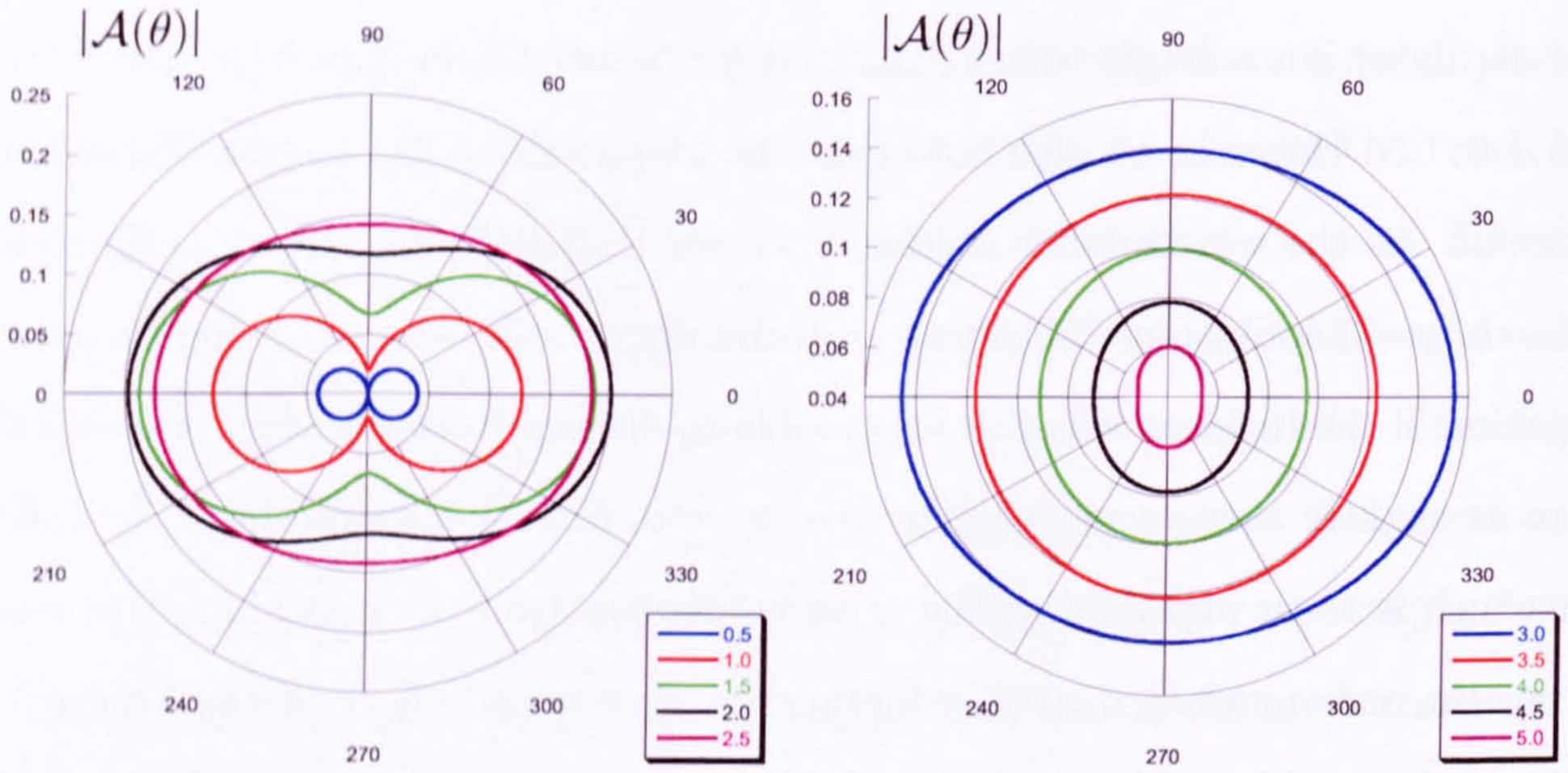

(a) $kh_0 = 0.5, \ldots, 2.5.$ (b) $kh_0 = 3.0, \ldots, 5.0$

Figure 4.13: $|\mathcal{A}(\theta)|$ for scattering by a hemispherical hump where $a/h_0 = 0.6$

increases, the higher frequency waves in the plots (b) start to exhibit more interesting behaviour. The curves become more elongated in a direction perpendicular to the propagation of the incident wave and we see a drop in the reflection on the leeward side of the seamount.

Finally, to show the behaviour in an extreme case we plot the results for scatter-

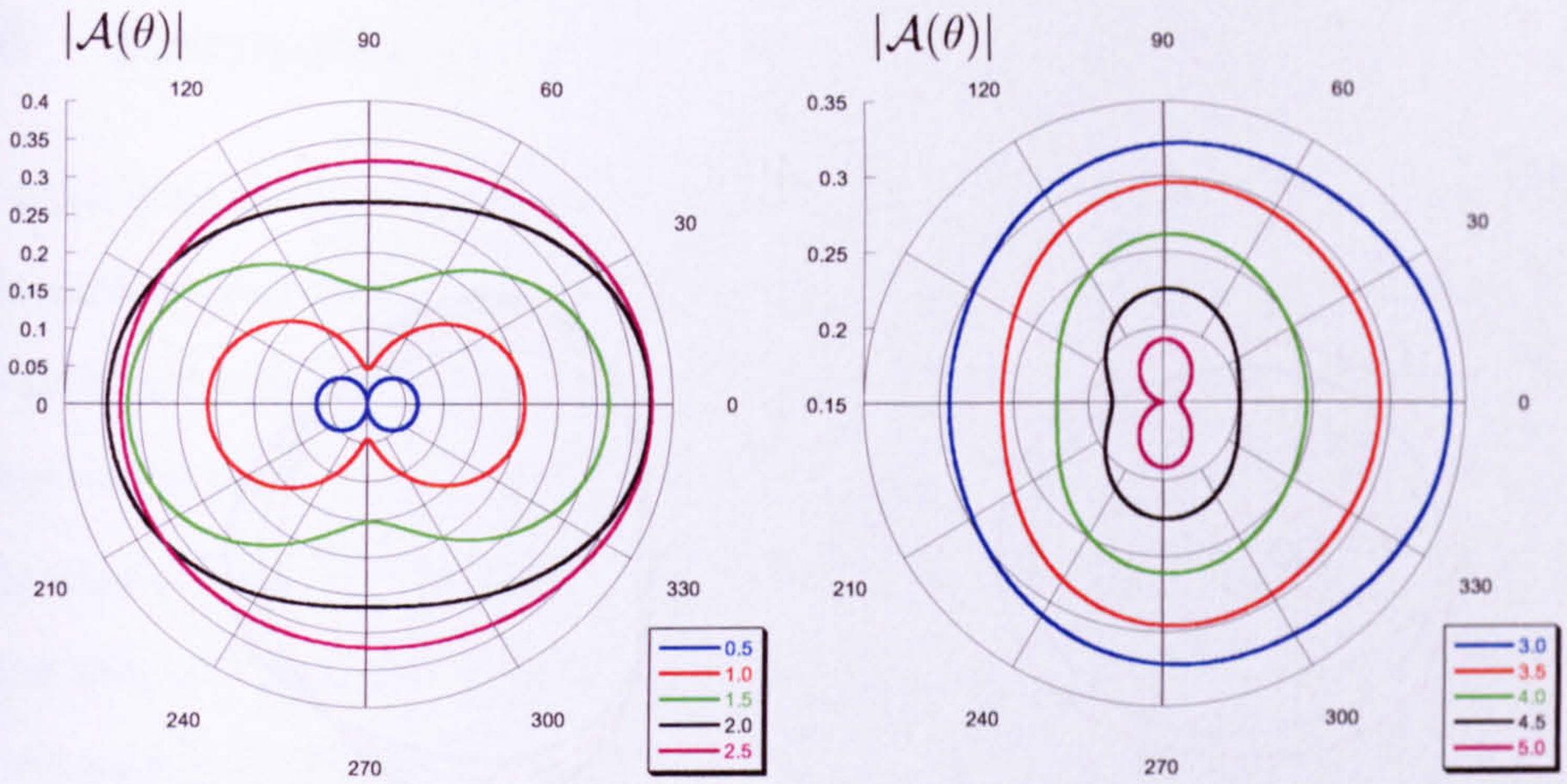

(a) $kh_0 = 0.5, \ldots, 2.5.$ (b) $kh_0 = 3.0, \ldots, 5.0$

Figure 4.14: $|\mathcal{A}(\theta)|$ for scattering by a hemispherical hump where $a/h_0 = 0.7$

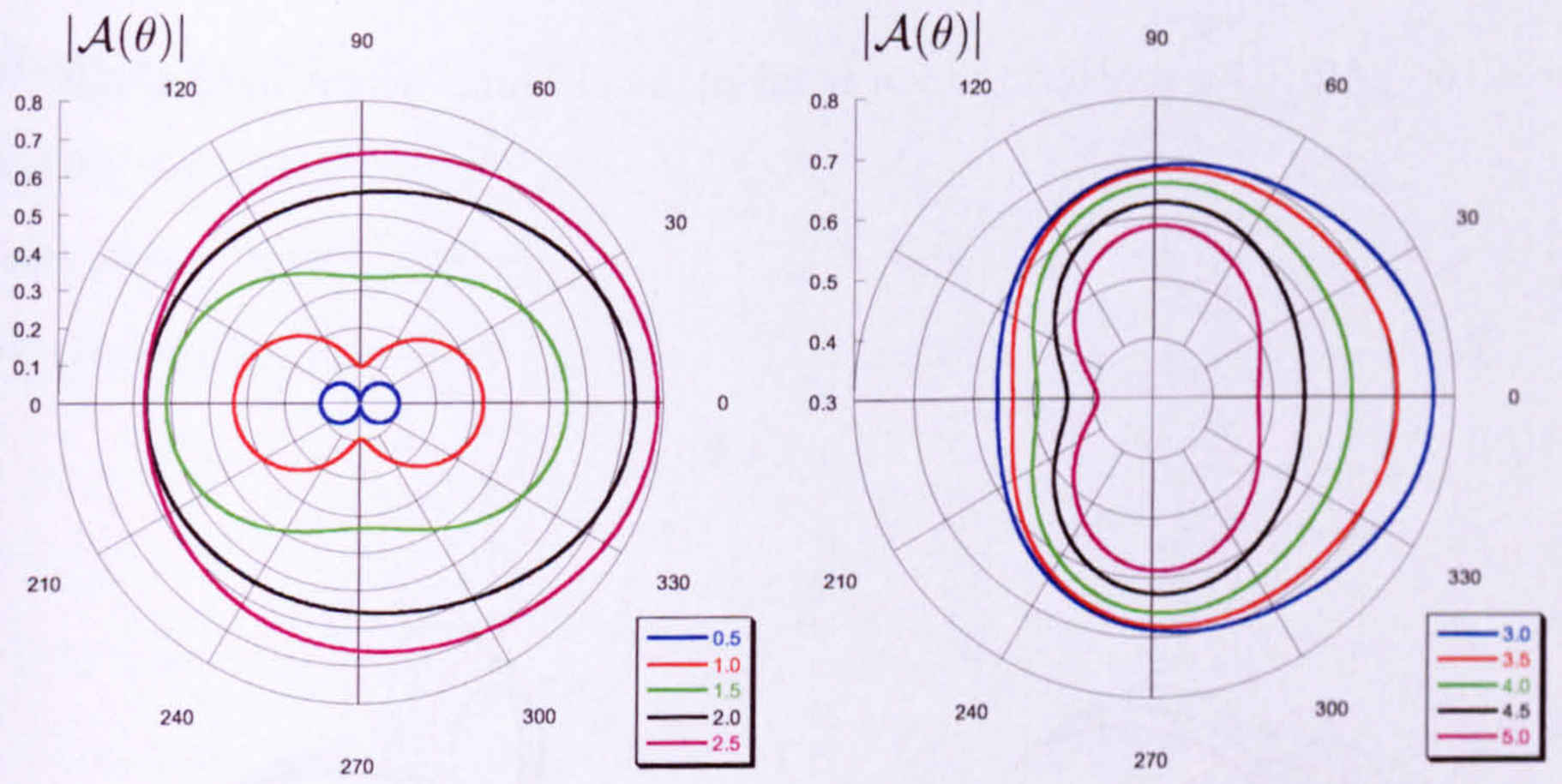

(a) $kh_0 = 0.5, \ldots, 2.5.$ (b) $kh_0 = 3.0, \ldots, 5.0$

Figure 4.15: $|\mathcal{A}(\theta)|$ for scattering by a hemispherical hump where $a/h_0 = 0.8$

ing by a seamount where $a/h_0 = 0.99$. We see that there is significant scattering back along the axis of propagation but also there are two sidelobes scattering energy sideways. There is also relatively little scattered wave to the leeward side of the seamount.

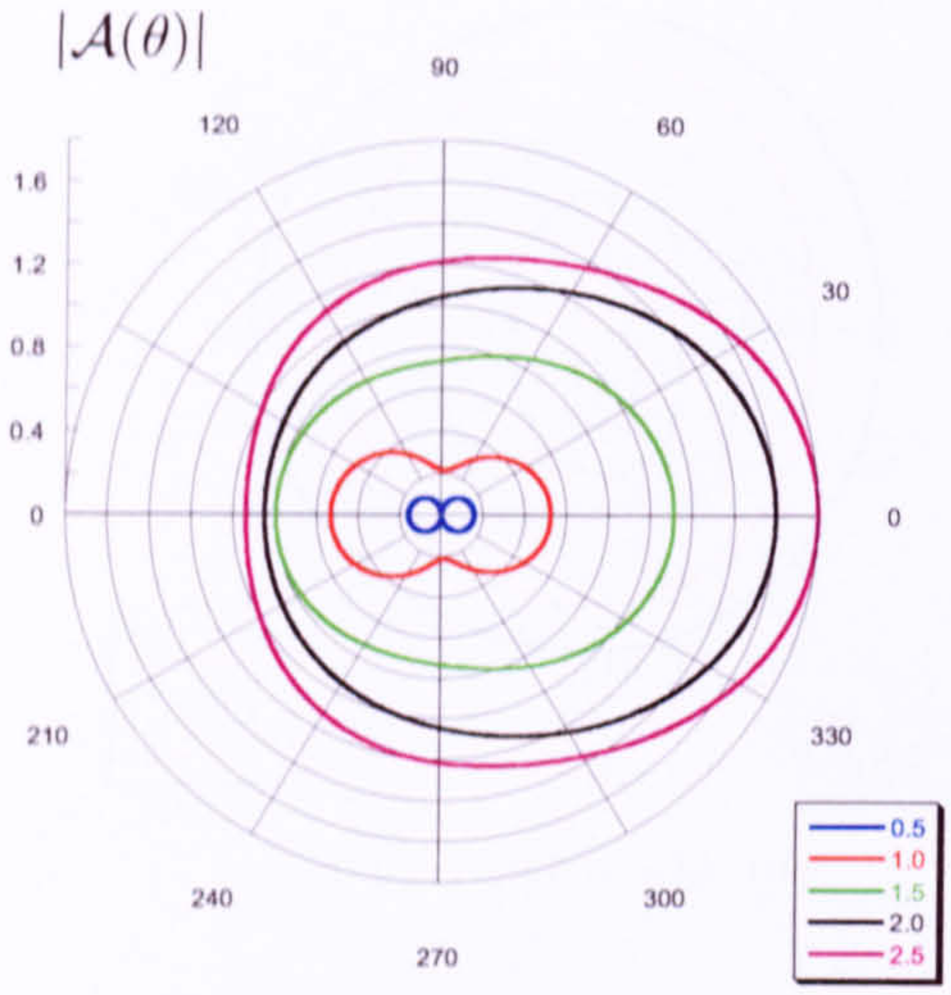

(a) $kh_0 = 0.5, \ldots, 2.5.$

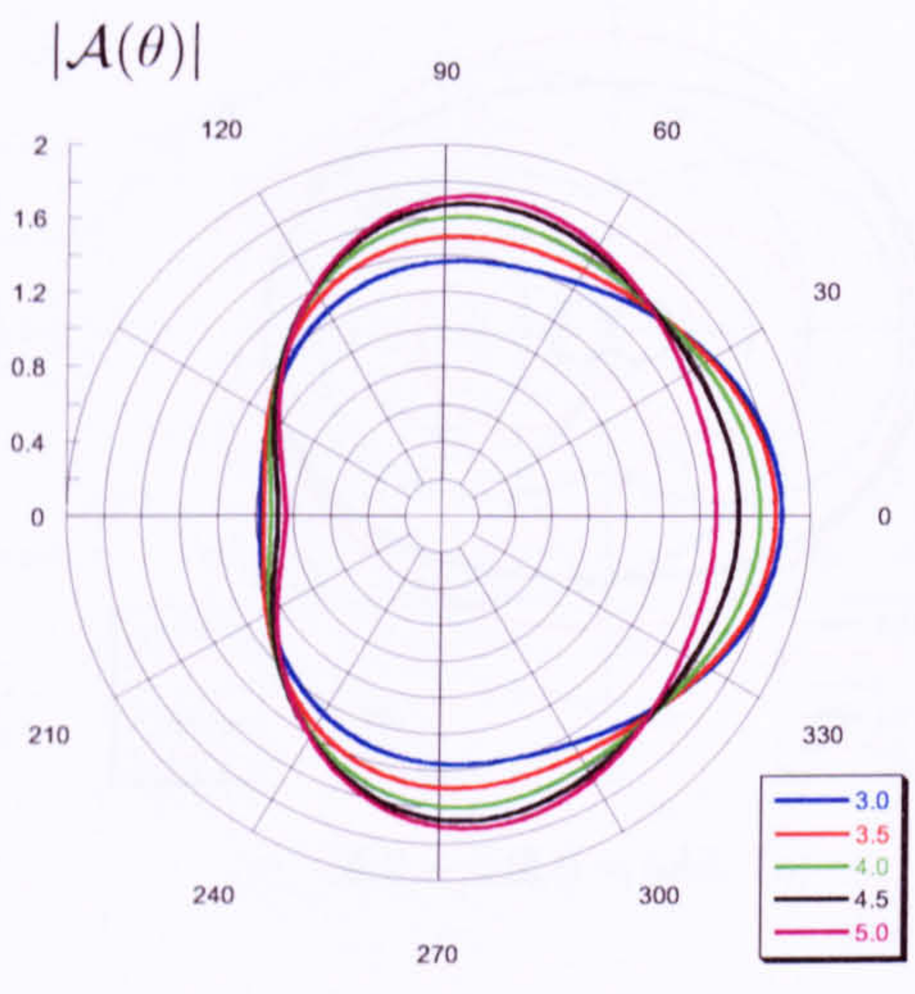

(b) $kh_0 = 3.0, \ldots, 5.0$

Figure 4.16: $|\mathcal{A}(\theta)|$ for scattering by a hemispherical hump where $a/h_0 = 0.9$

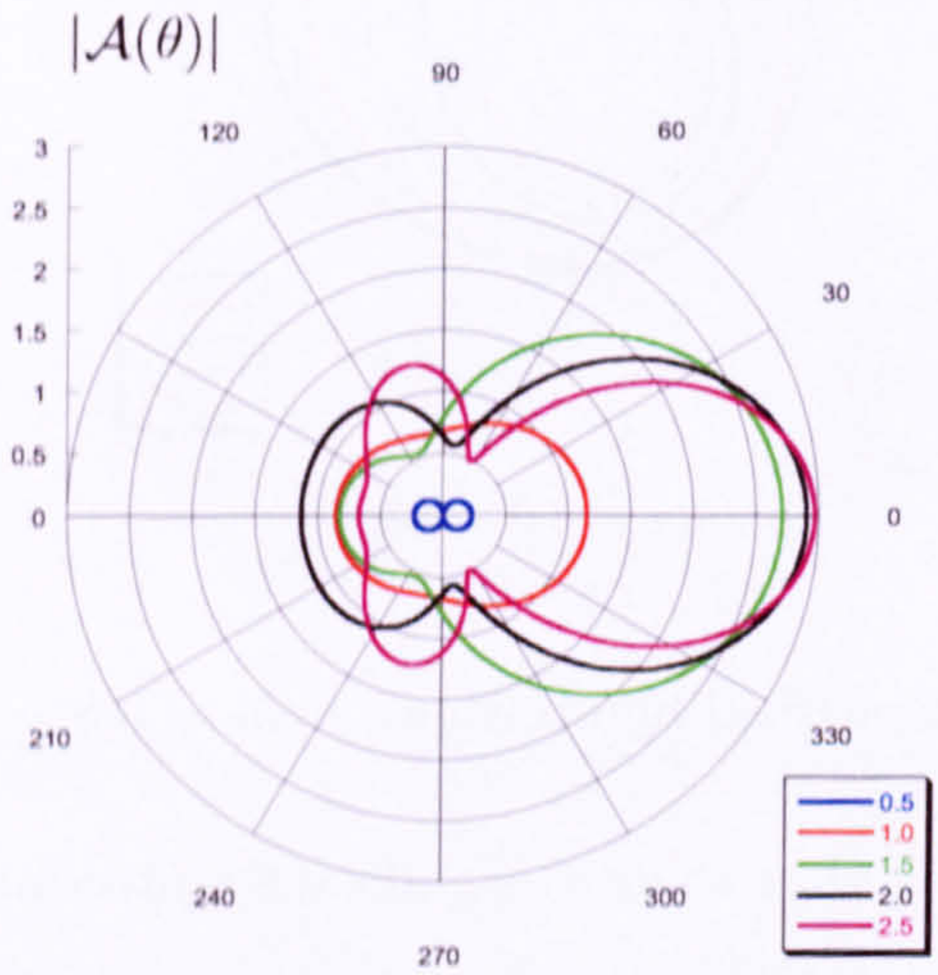

(a) $kh_0 = 0.5, \ldots, 2.5.$

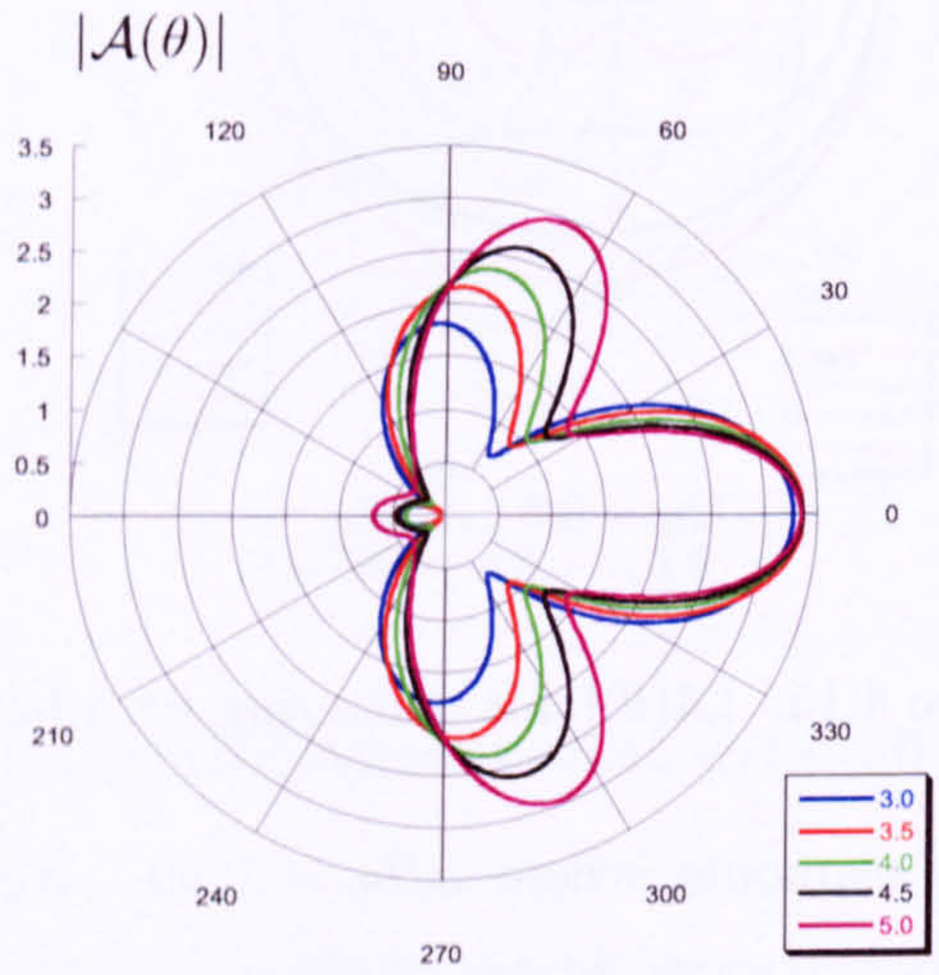

(b) $kh_0 = 3.0, \ldots, 5.0$

Figure 4.17: $|\mathcal{A}(\theta)|$ for scattering by a hemispherical hump where $a/h_0 = 0.99$.

4.6 Remarks

We have seen in this chapter that multipoles have excellent convergence properties with modest truncation sizes of infinite sums reaching a high degree of accuracy. In fact their convergence is so rapid that, to all intents and purposes, these results may be viewed as exact numerical solutions to the problems under consideration.

In this chapter we have solved two particular three-dimensional problems, which to the best of the author's knowledge have not been solved before. This is perhaps not surprising as the geometries under consideration are not particularly physically realistic. Furthermore, as the majority of techniques for dealing with more arbitrary geometries tend to make some sort of assumption of mildness of slope in the topography then these two problems would be unlikely to be considered due to the steep gradients at the join with the domain of constant depth.

As our methods will make no such approximation and deal with the bed condition exactly, then these multipole results will provide useful benchmarks giving exact results for simple geometries against which our later results may be validated.

Chapter 5

Wave interaction with a ridge of arbitrary profile

5.1 Introduction

The three-dimensional problem of wave/body or wave/topography interactions is extremely complicated due primarily to the Neumann boundary condition on an arbitrary curve. As we have seen in Chapter 2 these problems have tended to be solved by making some kind of simplifying assumptions about the topography or body which allows progress to be made with the numerical solution of the problem.

We have seen in Chapter 3 how established techniques for two-dimensional water wave problems that convert from normal to tangential derivatives are capable of producing extremely accurate results. However, in the form in which Chapter 3 is formulated this conversion from $\partial/\partial n$ to $\partial/\partial s$ is really an expression of the Cauchy-Riemann equations which have no analogue in three dimensions. In contrast to our ultimate goal which is to develop solutions to the problem of scattering in three dimensions over arbitrary bed shapes, in Chapter 4 we considered two specific problems of rather specialised bedforms. This will enable us to provide an independent means of verifying the results from this and later chapters.

In this chapter we introduce the key principles behind our techniques for modeling fully three-dimensional wave/body or wave/topography interactions. We do this by formulating the problem as an integral equation and then retaining a formulation that

satisfies the bed condition exactly. The aim is to arrive at an integral equation formulation which is at most log-singular (of course, it is also possible, and mathematically simpler, to arrive at other types of integral equation which are Cauchy-singular or supersingular). We start, in this chapter, by choosing the simplest possible three-dimensional problem of oblique scattering by a submerged infinite ridge of constant cross section, to present the techniques and indicate the main issues underlying their application. In later chapters we will extend the technique to more complicated problems. Some of the work in this chapter was presented, as work in progress, by Chapman and Porter [16] to the 20th International Workshop on Water Waves and Floating Bodies at Spitzbergen.

The two-dimensional (normal incidence) version of this problem was solved by Staziker, Porter and Stirling [89] who formulated the problem as an integral equation and converted from normal to tangential derivatives. This technique has subsequently been used to good effect on a range of problems by Porter, see for example [74] investigating scattering by an arbitrary cylinder or [75] looking at wave trapping by pairs of cylinders. However, this formulation, which we employed in Chapter 3, was strictly two-dimensional with no obvious means of extension. Given the complicated nature of the two-dimensional problem it is not surprising that the three-dimensional case we deal with here has, to the best of our knowledge, received no attention.

Of course approximate techniques such as the mild slope equation have been applied to three-dimensional scattering problems, see for example Porter & Porter [78] who investigated scattering by three-dimensional periodic topography and the phenomenom of Bragg resonance. There is a wide body of literature concerning this specific approach, see Porter & Chamberlain [70] for an overview of two-dimensional wave scattering problems. In contrast we will introduce an approach which makes no approximation whatsoever and applies the full linear theory to a three-dimensional scattering problem.

5.2 Formulation of the scattering problem

Cartesian coordinates (x, y, z) are chosen with the x and y axes lying in the undisturbed free surface of the fluid and z directed vertically downwards. The fluid is bounded below by $S_b : \{z = H(x), -\infty < x, y < \infty\}$ where $H(x)$ is assumed to be a continuous function with $H(x) = h_0$, a constant, for $x \notin (0, \ell)$ and $H(x) = h(x)$ for $x \in (0, \ell)$ and it is assumed that $h(x) \leq h_0$. Thus the topography consists of an infinitely-long ridge with constant cross-section in the (x, z)-plane and which protrudes from an otherwise flat bed of depth h_0. We denote the curve $z = h(x)$ in the (x, z) plane, which defines the edge of a section of the ridge by Γ.

On the lower boundary of the fluid, S_b, we define an orthonormal basis by

$$\left.\begin{aligned} \mathbf{n} &= (-H'(x), 0, 1)/\sigma(x) \\ \mathbf{s} &= (1, 0, H'(x))/\sigma(x) \\ \mathbf{t} &= (0, 1, 0) \end{aligned}\right\}, \qquad \sigma(x) = \sqrt{1 + (H'(x))^2} \tag{5.2.1}$$

representing, respectively, the normal (out of the fluid) and tangential unit vectors, perpendicular and parallel respectively to the y-axis, on the surface S_b.

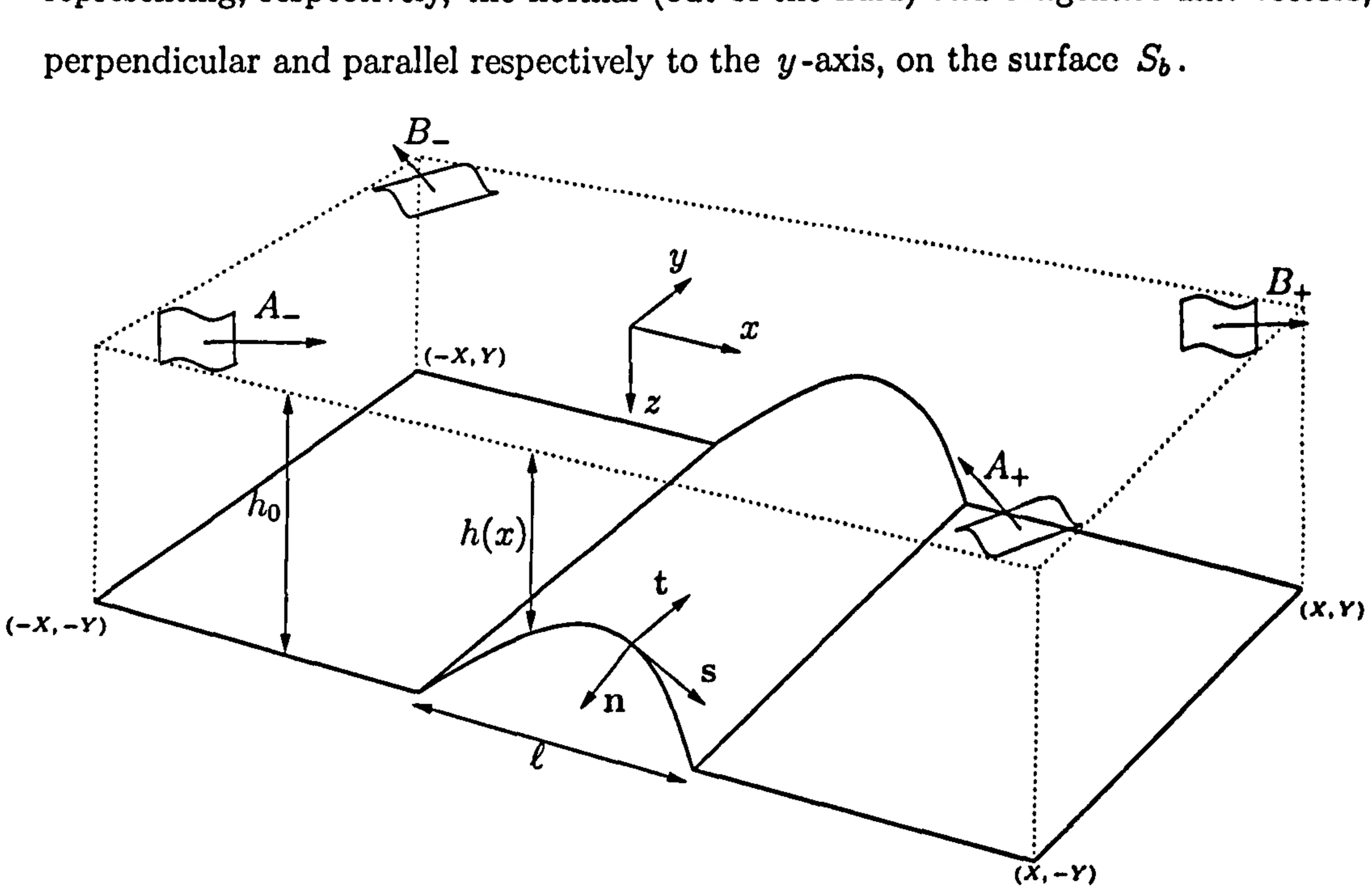

Figure 5.1: Geometrical description of the scattering problem for waves obliquely incident on an infinite uniform ridge in a domain of otherwise constant depth

The fluid potential Φ satisfies

$$\nabla^2\Phi = 0, \qquad \mathbf{r} \in D, \tag{5.2.2}$$

where $D : \{0 < z < H(x), -\infty < x, y < \infty\}$ is the fluid domain which is bounded by the surface ∂D,

$$\mathbf{n}.\nabla\Phi = 0, \qquad \mathbf{r} \in S_b \tag{5.2.3}$$

and

$$\frac{\partial\Phi}{\partial z} + K\Phi = 0, \qquad \text{on } z = 0. \tag{5.2.4}$$

To complete the formulation of the problem, we need radiation conditions at infinity, which are written as

$$\Phi(\mathbf{r}) \sim \begin{cases} A_-\Phi_0^+(\mathbf{r}) + B_-\Phi_0^-(\mathbf{r}), & x \to -\infty, \\ A_+\Phi_0^-(\mathbf{r}) + B_+\Phi_0^+(\mathbf{r}), & x \to \infty. \end{cases} \tag{5.2.5}$$

Here $\Phi_0^\pm(\mathbf{r})$ define waves propagating obliquely towards $x = \pm\infty$ respectively in water of constant depth h_0, whilst $A_\pm$ and $B_\pm$ represent wave amplitudes associated with waves that are incoming and outgoing (respectively) on the ridge from $x = \pm\infty$. More specifically,

$$\Phi_0^\pm(\mathbf{r}) = \mathrm{e}^{\pm\mathrm{i}\alpha x}\mathrm{e}^{\mathrm{i}ly}\psi_0(z) \equiv \phi_0^\pm(x,z)\mathrm{e}^{\mathrm{i}ly} \tag{5.2.6}$$

where $\alpha = k\cos\theta$ and $l = k\sin\theta$ are components of the wavenumber, k, in the x and y directions (respectively) for a wave propagating at an angle $\pm\theta$ with respect to the positive x-axis.

We define reflection and transmission coefficients for waves of unit amplitude incident from $x = -\infty$ by $R_- = B_-/A_-$ and $T_- = B_+/A_-$. Likewise we define reflection and transmission coefficients for waves of unit amplitude incident from $x = +\infty$ by $R_2 = B_+/A_+$ and $T_+ = B_-/A_+$. It follows from (5.2.5) that

$$\begin{pmatrix} B_- \\ B_+ \end{pmatrix} = \mathbf{S}\begin{pmatrix} A_- \\ A_+ \end{pmatrix} \qquad \mathbf{S} = \begin{pmatrix} R_- & T_+ \\ T_- & R_+ \end{pmatrix} \tag{5.2.7}$$

where $\mathbf{S}$ is referred to as the scattering matrix. The scattering matrix is regarded as the principal unknown in this problem see, for example Porter & Chamberlain

[70] who also proved the relation $\mathbf{S}\overline{\mathbf{S}} = \mathbf{I}$, where the overbar denotes complex conjugation. This last relation gives rise to the Kreisel [47] relations which include a statement of conservation of energy. Porter & Chamberlain's elegant proof is entirely independent of formulation and shows that any formulation which incorporates the exact far-field structure of (5.2.5), as ours certainly does, will satisfy energy conservation exactly. Consequently, we remark that energy conservation being satisfied is therefore an unreliable check on the numerical accuracy. In fact our final notation in this specific problem will prove to be more compact if we consider a non-standard form of scattering matrix $\mathbf{M}$ defined by the relation

$$\begin{pmatrix} B_+ \\ B_- \end{pmatrix} = \mathbf{M} \begin{pmatrix} A_- \\ A_+ \end{pmatrix} \qquad \mathbf{M} = \begin{pmatrix} T_- & R_+ \\ R_- & T_+ \end{pmatrix} \tag{5.2.8}$$

Now, due to the lack of dependence of the geometry upon y, the exponential variation in y, namely $\mathrm{e}^{\mathrm{i}ly}$, assumed by the far field waves through (5.2.5) and (5.2.6) is inherited by $\Phi(\mathbf{r})$ allowing us to write

$$\Phi(\mathbf{r}) = \phi(x,z)\mathrm{e}^{\mathrm{i}ly}. \tag{5.2.9}$$

At this point, it is common practice to use this factorisation to reduce the boundary-value problem stated above to a two-dimensional problem for $\phi(x,z)$ in which the field equation is reduced to the modified Helmholtz equation. However, we shall need to use a three-dimensional coordinate system in our solution procedure and therefore we leave it until later before making use of the particular form of Φ assumed above.

The method of solution relies on the use of a Green's function appropriate to this problem. Thus we define $G(\mathbf{r};\mathbf{r}_0)$ where $\mathbf{r}_0 = (x_0, y_0, z_0)$ is to be regarded as the field point and $\mathbf{r}$ the source point, satisfying

$$\nabla^2 G(\mathbf{r};\mathbf{r}_0) = -\delta(x-x_0)\delta(z-z_0)\mathrm{e}^{\mathrm{i}l(y_0-y)}, \qquad \text{in } 0 < z, z_0 < h_0 \tag{5.2.10}$$

with

$$\frac{\partial G}{\partial z} + KG = 0, \qquad \text{on } z = 0 \tag{5.2.11}$$

and

$$\frac{\partial G}{\partial z} = 0, \qquad \text{on } z = h_0 \tag{5.2.12}$$

holding for $-\infty < x, x_0, y, y_0 < \infty$. Thus, G represents a line source along $(x, z) = (x_0, z_0)$ with the same assumed variation along its length as in the problem for Φ. As in the problem for Φ, the dependence can be made explicit by writing

$$G(\mathbf{r}; \mathbf{r}_0) = g(x, z; x_0, z_0)\mathrm{e}^{\mathrm{i}l(y_0 - y)} \tag{5.2.13}$$

Then it is readily shown, using standard Green's function methods (see Appendix A), that

$$g(x, z; x_0, z_0) = \sum_{r=0}^{\infty} \frac{\psi_r(z)\psi_r(z_0)}{2\alpha_r h_0}\mathrm{e}^{-\alpha_r|x - x_0|}, \tag{5.2.14}$$

(or alternatively see, for example, Heins [40]), where $\{\psi_r(z)\}$ are the usual depth eigenfunctions given by (2.1.47) and

$$\alpha_r = \sqrt{k_r^2 + l^2}, \qquad \alpha_0 = -\mathrm{i}\sqrt{l^2 - k^2} = -\mathrm{i}\alpha \tag{5.2.15}$$

with $k_0 = -\mathrm{i}k$ where the k_r are the roots of the dispersion relation (2.1.44). We note that as $|x - x_0| \to \infty$,

$$G \sim \mathrm{e}^{\mathrm{i}l(y_0 - y)}\frac{\mathrm{i}\psi_0(z)\psi_0(z_0)}{2\alpha h_0}\mathrm{e}^{\mathrm{i}\alpha|x - x_0|}. \tag{5.2.16}$$

We will find it convenient to decompose G and consequently, g in the form

$$G = G_0 + \widehat{G} = \mathrm{e}^{\mathrm{i}l(y_0 - y)}(g_0 + \widehat{g}) \tag{5.2.17}$$

where

$$G_0(\mathbf{r}; \mathbf{r}_0) = \mathrm{e}^{\mathrm{i}l(y_0 - y)}\frac{\mathrm{i}\psi_0(z)\psi_0(z_0)}{2\alpha h_0}\cos\alpha(x - x_0) \tag{5.2.18}$$

is the separable component of the wave-like part of the Green's function previously exposed in (5.2.16) and

$$\widehat{G}(\mathbf{r}; \mathbf{r}_0) = \mathrm{e}^{\mathrm{i}l(y_0 - y)}\left\{-\frac{\psi_0(z)\psi_0(z_0)}{2\alpha h_0}\sin\alpha|x - x_0| + \sum_{r=1}^{\infty}\frac{\psi_r(z)\psi_r(z_0)}{2\alpha_r h_0}\mathrm{e}^{-\alpha_r|x - x_0|}\right\}, \tag{5.2.19}$$

is the remainder of G. By 'separable' we mean that G_0 may be decomposed into the product of two functions one depending on the source variables (x, z) and the other on the field variables (x_0, z_0). We decompose the Green's function in this way

so that the property $\overline{\widehat{G}(\mathbf{r}_0;\mathbf{r})} = \widehat{G}(\mathbf{r};\mathbf{r}_0)$ holds. This is a critical step as it means our integral kernels will be self-adjoint, a property which allows extremely accurate solution techniques to be employed. Significantly (in terms of what follows), a similar relation does *not* hold for G_0, although we note that the definitions (5.2.6) can be re-used in (5.2.18) by exploiting its separable form to give

$$G_0(\mathbf{r};\mathbf{r}_0) = \frac{\mathrm{i}}{4\alpha h_0}\left\{\overline{\Phi_0^-}(\mathbf{r})\Phi_0^-(\mathbf{r}_0) + \overline{\Phi_0^+}(\mathbf{r})\Phi_0^+(\mathbf{r}_0)\right\}. \qquad (5.2.20)$$

At this point it is convenient to define functions related to the depth eigenfunctions $\psi_r(z)$ which will play an important role in our formulation. Thus we define

$$\chi_r(z) = -k_r\int_{h_0}^{z}\psi_r(z')dz' = N_r^{-1/2}\sin k_r(h_0-z), \qquad r = 0,1,2,\ldots \qquad (5.2.21)$$

with $k_0 = -ik$ implying that

$$\chi_0(z) = -iN_0^{-1/2}\sinh k(h_0-z) \qquad (5.2.22)$$

which recovers the functions introduced in (3.3.5).

5.3 Derivation of the integral equations

In this section, we set out to develop an exact formulation in terms of integral equations of the solution to the problem, as a means of calculating the scattering matrix M.

The first step is to apply Green's identity to the functions $\Phi(\mathbf{r})$ and $G(\mathbf{r};\mathbf{r}_0)$ in a sub-domain D_{XY} of D, bounded laterally by four vertical planes defined in terms of the four vertices $(\pm X, \pm Y, z)$, $0 < z < h_0$ (see figure 5.1). Here, $Y > 0$ is arbitrary, and it is to be assumed in what follows that the limit $X \to \infty$ is taken. We acknowledge that the introduction of these vertical planes at $\pm Y$ is artificial and we will see later that it may be avoided. However, it provides a three-dimensional domain with closed sides to which Green's identity may be applied. Even more importantly, as we shall see, consideration of the three-dimensional problem is necessary to make headway with the two-dimensional version of the problem.

5.3.1 A three-dimensional formulation

Green's Identity states that

$$\iiint_{D_{XY}} (G\nabla^2\Phi - \Phi\nabla^2 G)\,\mathrm{d}x\,\mathrm{d}y\,\mathrm{d}z = \iint_{S_{XY}} (G\mathbf{n}.\nabla\Phi - \Phi\mathbf{n}.\nabla G)\,\mathrm{d}S \tag{5.3.1}$$

where S_{XY} is the closed boundary of D_{XY}, dS being a surface element on S_{XY} and the definition of $\mathbf{n}$ has been extended to boundaries other than those coinciding with S_b to mean the outward unit normal to S_{XY}. Using the definitions of Φ and G it can be found, after some routine algebra, that

$$\mu\Phi(\mathbf{r}_0) = A_-\Phi_0^+(\mathbf{r}_0) + A_+\Phi_0^-(\mathbf{r}_0) - \frac{1}{2Y}\int\!\!\int_\Sigma \Phi(\mathbf{r})\mathbf{n}.\nabla G(\mathbf{r};\mathbf{r}_0)\,\mathrm{d}S \tag{5.3.2}$$

and Σ is the two-dimensional surface of the ridge confined between the planes $y = \pm Y$. Here $\mu = 1$ for $\mathbf{r}_0 \in D$, $\mu = 1/2$ for $\mathbf{r}_0 \in \partial D$, and $\mu = 0$ for $\mathbf{r}_0 \notin D \cup \partial D$. In the derivation of the above, use has been made of (5.2.3), (5.2.4), (5.2.11) and (5.2.12) to both extract the free terms and to eliminate the contribution from the two parallel sides of S_{XY} which coincide with the planes $y = \pm Y$.

Fundamental to our approach is Noblesse's [67] [68] idea of converting the integral equation to a weakly singular form by defining a vector Green's function $\mathbf{L}$ which is no more singular than G, and will enable the integral equation to be converted to a weakly singular form.

We define a vector Green's function $\mathbf{L}$ related to the Green's function G by

$$\nabla G = \nabla \times \mathbf{L} - \delta(x - x_0)\delta^z(z - z_0)\mathrm{e}^{il(y_0 - y)}\mathrm{k}. \tag{5.3.3}$$

The choice of $\mathbf{L}$ is clearly not unique and, in particular, we note that $\mathbf{L}$ can be replaced by $\mathbf{L} + \nabla\varphi$ for any scalar potential φ. In electromagnetic wave theory, this operation is termed a gauge transformation where φ is called the gauge. The most common gauge to use is the Coulomb gauge in which $\nabla\varphi = 0$ is chosen, although this is dictated by a desire to simplify the final equations as much as possible. In this respect, after inheriting Noblesse's notation so that here, and elsewhere,

$$G_y^z \equiv \int_{h_0}^{z} \frac{\partial}{\partial y} G(x, y, z'; \mathbf{r}_0)\,\mathrm{d}z', \qquad \text{etc...} \tag{5.3.4}$$

we choose (for reasons that will become clear)

$$\mathbf{L} = (G^z_y, -G^z_x, 0), \tag{5.3.5}$$

which was also used by Noblesse; other choices for $\mathbf{L}$ could be $(0, G^x_z, -G^x_y)$ or $(-G^y_z, 0, G^y_x)$. These forms may be verified by direct substitution of (5.3.5), or the alternative forms, in (5.3.3) and by using (5.2.10). In particular, we note that $\mathbf{L}|_{z=h_0} = 0$, an important property which would not have followed from employing the alternative versions of $\mathbf{L}$.

It is worth highlighting that our (5.3.3) differs subtly from its equivalent in Noblesse [67] in that we have included a missing term which involves the delta functions. Although rather technical, this omission in Noblesse's exposition proves to be significant as it serves to highlight that points where the source and field point coalesce need special treatment.

For example, we note that

$$\delta^z(z - z_0) = \int_{h_0}^{z} \delta(t - z_0)\,\mathrm{d}t = -\mathrm{H}(z_0 - z) \tag{5.3.6}$$

where $\mathrm{H}(x)$ is the Heaviside step function. So now (5.3.2) becomes

$$\begin{aligned}\mu\Phi(\mathbf{r}_0) = A_-\Phi_0^+(\mathbf{r}_0) + A_+\Phi_0^-(\mathbf{r}_0) &- \frac{1}{2Y}\iint_{S_b} \Phi(\mathbf{r})\mathbf{n}.\nabla\times\mathbf{L}\,\mathrm{d}S \\ &- \frac{1}{2Y}\iint_{S_b} \Phi(\mathbf{r})\delta(x-x_0)\mathrm{H}(z_0-z)\mathrm{e}^{\mathrm{i}l(y_0-y)}\frac{\mathrm{d}S}{\sigma}\end{aligned} \tag{5.3.7}$$

since $\mathbf{n}.\mathbf{k} = 1/\sigma$. Now to deal with the final term we note that $\mathrm{d}S = \sigma\,\mathrm{d}x\,\mathrm{d}y$ so

$$\begin{aligned}-\iint_{S_b} \Phi(\mathbf{r})\delta(x-x_0)\delta(y-y_0)\mathrm{H}(z_0-z)\frac{\mathrm{d}S}{\sigma} \\ = -\iint_{S_p} \Phi(x,y,h(x,y))\delta(x-x_0)\delta(y-y_0)\mathrm{H}(z_0-h(x,y))\,\mathrm{d}x\,\mathrm{d}y \\ = -\Phi(x_0,y_0,h(x_0,y_))\mathrm{H}(z_0-h(x_0,y_0))\end{aligned} \tag{5.3.8}$$

which is zero for points $\mathbf{r}_0 \in D$, $-\frac{1}{2}\Phi(x_0,y_0,h(x_0,y_0))$ for points $\mathbf{r}_0 \in \partial D$ and

$-\Phi(x_0, y_0, h(x_0, y_0))$ for points $\mathbf{r}_0 \notin D \cup \partial D$. Thus

$$\Phi(\mathbf{r}_0) = A_-\Phi_0^+(\mathbf{r}_0) + A_+\Phi_0^-(\mathbf{r}_0) - \frac{1}{2Y}\iint_{S_b} \Phi(\mathbf{r})\mathbf{n}.\nabla \times \mathbf{L}\, dS \qquad \text{for } \mathbf{r}_0 \in D \cup \partial D \tag{5.3.9}$$

which establishes that, unlike the traditional form (5.3.2), the formulation in (5.3.9) gives a continuous definition of the fluid potential as the field point moves from the fluid domain to a point on the boundary. This property of the weakly singular formulation (5.3.9) is acknowledged by Noblesse who indicates how it may be established by direct consideration of (5.3.9) rather than through any discussion of the additional term we have highlighted.

At this point Noblesse's [67] approach is to perform a three-dimensional analogue of integration by parts using the vector identity

$$\nabla \times (\Phi \mathbf{L}) = \Phi \nabla \times \mathbf{L} + \nabla\Phi \times \mathbf{L}$$

and Stokes' theorem. However, at points where the source and field point coalesce, as they do along the bed, the conditions for the applicability of Stokes' theorem no longer apply. In our formulation we show how this issue is dealt with in two dimensions (later on in this chapter) and also how it may be properly dealt with in a fully three-dimensional context (Chapter 8).

Now, noting that $\mathbf{n} = \mathbf{s} \times \mathbf{t}$,

$$\mathbf{n}.\nabla \times \mathbf{L} = (\mathbf{s} \times \mathbf{t}).(\nabla \times \mathbf{L}) = (\mathbf{s}.\nabla)(\mathbf{L}.\mathbf{t}) - (\mathbf{t}.\nabla)(\mathbf{L}.\mathbf{s}) \equiv \frac{\partial L_2}{\partial s} - \frac{\partial L_1}{\partial t} \tag{5.3.10}$$

using a standard vector identity, where we have employed the abbreviations $\partial/\partial s = \mathbf{s}.\nabla$, $\partial/\partial t = \mathbf{t}.\nabla$ and defined

$$L_1(\mathbf{r}; \mathbf{r}_0) = \mathbf{L}.\mathbf{s} = G_y^z/\sigma(x), \tag{5.3.11}$$

$$L_2(\mathbf{r}; \mathbf{r}_0) = \mathbf{L}.\mathbf{t} = -G_x^z, \tag{5.3.12}$$

from (5.3.4) and (5.2.1). Thus we now find

$$\Phi(\mathbf{r}_0) = A_-\Phi_0^+(\mathbf{r}_0) + A_+\Phi_0^-(\mathbf{r}_0) - \frac{1}{2Y}\iint_{\Sigma} \left(\frac{\partial L_2}{\partial s} - \frac{\partial L_1}{\partial t}\right) \Phi(s,t)\, ds\, dt \tag{5.3.13}$$

where we have written $\Phi(\mathbf{r})|_\Sigma = \Phi(s,t)$ in terms of coordinates aligned with $\mathbf{s}$ and $\mathbf{t}$ lying on the surface of the ridge Σ. Clearly in the transformation that has taken place from (5.3.2) to (5.3.13) we have required to be working in a three-dimensional domain. Also we note that $\mathbf{t} = \mathbf{j}$ so that $\mathrm{d}t = \mathrm{d}y$ and $\partial/\partial t = \partial/\partial y$, but we retain $\mathbf{t}$ to be consistent with later chapters.

Our approach, which is a significant departure from Noblesse [67], is to modify (5.3.13) to put it into a form which allows us to define a self-adjoint integral operator. This crucial step allows us to implement a solution using the Rayleigh-Ritz (equivalent in this context to Galerkin) technique which is well known to have excellent convergence properties (see Chapter 2 and, for example, Porter [73]). With this strategy in mind, we mimic the decomposition of the Green's function G performed in (5.2.7), by writing

$$L_i = L_{0i} + \widehat{L}_i, \qquad i = 1,2, \tag{5.3.14}$$

and the two components of L_i are derived directly from the two components of G in (5.2.7). Thus, in particular, we find

$$\left.\begin{aligned} L_{01} &= \frac{(G_0)_y^z}{\sigma(x)} = \frac{\mathrm{i}}{4\alpha h_0}\left(\frac{l}{k\sigma(x)}\right)\left\{\overline{f}_-(\mathbf{r})\Phi_0^-(\mathbf{r}_0) + \overline{f}_+(\mathbf{r})\Phi_0^+(\mathbf{r}_0)\right\} \\ L_{02} &= -(G_0)_x^z = \frac{\mathrm{i}}{4\alpha h_0}\left(\frac{\alpha}{k}\right)\left\{\overline{f}_-(\mathbf{r})\Phi_0^-(\mathbf{r}_0) - \overline{f}_+(\mathbf{r})\Phi_0^+(\mathbf{r}_0)\right\} \end{aligned}\right\} \tag{5.3.15}$$

in terms of newly-defined functions

$$f_\pm(\mathbf{r}) = \mathrm{e}^{\pm\mathrm{i}\alpha x}\mathrm{e}^{\mathrm{i}ly}\chi_0(z) \tag{5.3.16}$$

where (5.2.19) and (5.2.20) have been used and we note that $\overline{\chi}_0(z) = -\chi_0(z)$.

At this point, we shall introduce some more notation so we define

$$F_\pm(s,t) = \left(\mp\frac{\alpha}{k}\frac{\partial}{\partial s} - \frac{l}{k\sigma(x)}\frac{\partial}{\partial t}\right) f_\pm(\mathbf{r})\Big|_{\mathbf{r}\in\Sigma} \tag{5.3.17}$$

and we also introduce the inner product notation for functions $u(s,t), v(s,t) \in \mathcal{H}$ (where $\mathcal{H}$ is the space of functions whose derivatives belong to $L_2(\Sigma)$)

$$\langle u, v\rangle = \frac{1}{2Y}\int\!\!\int_\Sigma u\overline{v}\,\mathrm{d}s\,\mathrm{d}t. \tag{5.3.18}$$

Then, using the decomposition in (5.3.14) with (5.3.15) in (5.3.9) we find, after some algebra, that

$$\Phi(\mathbf{r}_0) = A_-\Phi_0^+(\mathbf{r}_0) + A_+\Phi_0^-(\mathbf{r}_0) - \frac{1}{2Y}\int\int_\Sigma \left(\frac{\partial \widehat{L}_2}{\partial s} - \frac{\partial \widehat{L}_1}{\partial t}\right)\Phi(s,t)\,\mathrm{d}s\,\mathrm{d}t$$
$$- \frac{\mathrm{i}}{4\alpha h_0}\left\{\Phi_0^-(\mathbf{r}_0)\langle\Phi, F_-\rangle + \Phi_0^+(\mathbf{r}_0)\langle\Phi, F_+\rangle\right\} \quad (5.3.19)$$

This is a good point at which to pause for a moment and go back to (5.3.9) in order to establish relations which arise from consideration of the far field. First, we note that as $|x - x_0| \to \infty$,

$$L_1 \sim \frac{\mathrm{i}}{2\alpha h_0}\left(\frac{l}{k\sigma(x)}\right)\overline{\chi}_0(z)\psi_0(z_0)\mathrm{e}^{\mathrm{i}\alpha|x-x_0|}\mathrm{e}^{\mathrm{i}l(y_0-y)} \quad (5.3.20)$$

and

$$L_2 \sim \frac{\mathrm{i}}{2\alpha h_0}\mathrm{sgn}(x - x_0)\left(\frac{\alpha}{k}\right)\overline{\chi}_0(z)\psi_0(z_0)\mathrm{e}^{\mathrm{i}\alpha|x-x_0|}\mathrm{e}^{\mathrm{i}l(y_0-y)} \quad (5.3.21)$$

which may be determined from (5.2.16), the far-field form of G. Hence, taking $x_0 \to -\infty$ in (5.3.9) and (5.3.13) and using the far-field form of Φ provided by (5.2.5) gives, after considerable algebra,

$$B_- = A_+ - \frac{\mathrm{i}}{2\alpha h_0}\langle\Phi, F_-\rangle, \quad (5.3.22)$$

where the inner product notation (5.3.18) has been invoked and F_- is defined by (5.3.17). In a similar manner, taking the limit $x_0 \to \infty$, we obtain

$$B_+ = A_- - \frac{\mathrm{i}}{2\alpha h_0}\langle\Phi, F_+\rangle. \quad (5.3.23)$$

These last two equations hold the key to the continued development of the formulation, since now they can used to substitute in the second line of (5.3.19), resulting in

$$\Phi(\mathbf{r}_0) = \tfrac{1}{2}(A_- + B_+)\Phi_0^+(\mathbf{r}_0) + \tfrac{1}{2}(A_+ + B_-)\Phi_0^-(\mathbf{r}_0)$$
$$- \frac{1}{2Y}\iint_\Sigma \left(\frac{\partial \widehat{L}_2}{\partial s} - \frac{\partial \widehat{L}_1}{\partial t}\right)\Phi(s,t)\,\mathrm{d}s\,\mathrm{d}t. \quad (5.3.24)$$

Equation (5.3.24) may be regarded as a second-kind integral equation for Φ for points on Σ, by moving the field point $\mathbf{r}_0$ onto $(s_0, t_0) \in \Sigma$. The forcing term is a weighted sum of the two incident wave modes $\Phi_0^\pm$.

5.3.2 A two-dimensional formulation

At this point we may drop the three-dimensional formulation acknowledging the exponential dependence in y, y_0 and substituting (5.3.11), (5.3.12) and (5.3.14) into (5.3.24) to obtain

$$\phi(x_0,z_0) = \tfrac{1}{2}(A_- + B_+)\phi_0^+(x_0,z_0) + \tfrac{1}{2}(A_+ + B_-)\phi_0^-(x_0,z_0) + \int_\Gamma \left(\frac{\partial}{\partial s}\,\widehat{g}_x^z - \frac{l^2}{\sigma}\,\widehat{g}^z\right)\phi(s)\,\mathrm{d}s, \quad (5.3.25)$$

which has reduced our formulation to a two-dimensional representation in a plane of constant y. Here, the normal and tangential vectors are redefined appropriately to give their two-dimensional equivalents so that in coordinates (x,z) (5.2.1) becomes

$$\left.\begin{aligned}\mathbf{n} &= (-h'(x),1)/\sigma(x)\\ \mathbf{s} &= (1,h'(x))/\sigma(x)\end{aligned}\right\}, \qquad \sigma(x) = \sqrt{1+[h'(x)]^2}. \quad (5.3.26)$$

Crucially to our approach (5.3.3) becomes

$$\frac{\partial}{\partial n}g = -\frac{\partial}{\partial s}g_x^z + \frac{l^2}{\sigma}g^z + \frac{1}{\sigma}\delta(x-x_0)H(z_0-z) \quad (5.3.27)$$

and once this relation has been identified we are able to proceed with our techniques in a two-dimensional formulation which proves simpler and clearer for this problem and its extension in Chapter 6.

In Chapter 8 we will see that (5.3.24) may be solved in a fully three-dimensional framework. However, as we see from (5.3.25) this problem is essentially quasi two-dimensional. Therefore we will proceed to solve this problem in its two-dimensional formulation using (5.3.25), but still using all of the principles of the fully three-dimensional approach. This has the advantage of indicating the key features of our theory as well as showing the link between the approach used in Porter & Porter [77] and Chapter 3 and our extension of their approach to three-dimensional problems. In order to proceed in this way, we must redefine some of the notation introduced earlier so that (5.3.16) reduces to

$$f_\pm(x,z) = \mathrm{e}^{\pm \mathrm{i}\alpha x}\chi_0(z) \quad (5.3.28)$$

and consequently (5.3.17) becomes

$$F_{\pm}(x,z) = -\left(\pm\frac{\alpha}{k}\frac{\partial}{\partial s} + \frac{\mathrm{i}l^2}{k\sigma}\right) f_{\pm}, \qquad (x,z) \in \Gamma. \tag{5.3.29}$$

We also redefine the inner product (5.3.18) as

$$\langle u, v\rangle = \int_{\Gamma} u\bar{v}\,\mathrm{d}s \tag{5.3.30}$$

where s is an element of the arclength of Γ.

We present two alternative methods of solving equation (5.3.25) which will provide a useful check on results, as although each is based on (5.3.25) they result in different formulations and approaches to numerical solution. The first approach is to move the field point onto the bed and treat (5.3.25) as a second-kind integral equation for ϕ. Therefore if we define an integral operator

$$(\mathcal{K}_1\phi)(s_0) = \phi(s_0) - \int_{\Gamma}\left(\frac{\partial}{\partial s}\widehat{g}^z_x - \frac{l^2}{\sigma}\widehat{g}^z\right)\phi\,\mathrm{d}s \tag{5.3.31}$$

and then define a pair of functions $\varphi_1^{\pm}$ on Γ such that

$$(\mathcal{K}_1\varphi_1^{\pm})(s_0) = \phi_0^{\pm}, \tag{5.3.32}$$

then it follows that the solution of (5.3.25) is given by

$$\phi = \tfrac{1}{2}(A_- + B_+)\varphi_1^+ + \tfrac{1}{2}(A_+ + B_-)\varphi_1^-. \tag{5.3.33}$$

We note that $\mathcal{K}_1$ is not a self-adjoint integral operator, i.e. for functions $u, v \in \mathcal{H}$ (2.3.21) does not apply.

Alternatively, we may develop the formulation in an analogous manner to that appearing in the two-dimensional scattering problem considered by Porter & Porter [77], anticipating a self-adjoint structure in the final integral equations that is not enjoyed by an integral equation arising directly from (5.3.25). Thus, we first introduce quantities which apply to the field variable $\mathbf{r}_0$, namely

$$\left.\begin{aligned}\mathbf{n}_0 &= (-h'(x_0), 1)/\sigma(x_0)\\ \mathbf{s}_0 &= (1, h'(x_0))/\sigma(x_0)\end{aligned}\right\}, \qquad \nabla_0 \equiv \left(\frac{\partial}{\partial x_0}, \frac{\partial}{\partial z_0}\right), \tag{5.3.34}$$

and extend the definition of the orthonormal basis, $\{\mathbf{n}_0, \mathbf{s}_0\}$ to points away from the curve Γ.

We now apply the operator $\mathbf{n}_0.\nabla_0 \equiv \partial/\partial n_0$ to (5.3.25) for field points off Γ to obtain

$$\frac{\partial}{\partial n_0}\phi = \tfrac{1}{2}(A_- + B_+)\frac{\partial}{\partial n_0}\phi_0^+ + \tfrac{1}{2}(A_+ + B_-)\frac{\partial}{\partial n_0}\phi_0^- + \frac{\partial}{\partial n_0}\int_\Gamma \left(\frac{\partial}{\partial s}\widehat{g}_x^z - \frac{l^2}{\sigma}\widehat{g}^z\right)\phi\,\mathrm{d}s, \quad (5.3.35)$$

Now, in terms of field variables (5.3.27) becomes

$$\frac{\partial}{\partial n_0}g = -\frac{\partial}{\partial s_0}g_{x_0}^{z_0} + \frac{l^2}{\sigma}g^{z_0} \quad (5.3.36)$$

for points off Γ. Using this result we switch from normal to tangential derivatives so that

$$\frac{\partial}{\partial n_0}\phi = \tfrac{1}{2}(A_- + B_+)\frac{\partial}{\partial n_0}\phi_0^+ + \tfrac{1}{2}(A_+ + B_-)\frac{\partial}{\partial n_0}\phi_0^- - \frac{\partial}{\partial s_0}\int_\Gamma \left(\frac{\partial}{\partial s}\widehat{g}_{xx_0}^{zz_0} - \frac{l^2}{\sigma}\widehat{g}_{x_0}^{zz_0}\right)\phi\,\mathrm{d}s + \frac{l^2}{\sigma_0}\int_\Gamma \left(\frac{\partial}{\partial s}\widehat{g}_x^{zz_0} - \frac{l^2}{\sigma}\widehat{g}^{zz_0}\right)\phi\,\mathrm{d}s. \quad (5.3.37)$$

This step is critical and therefore worthy of special note; we were able to take the derivatives under the integration sign and then back out again precisely because the field point is not on the bed thus ensuring convergence of the integrals. Now, it is routine to confirm from (5.2.6), (5.3.29) and (5.3.36) that

$$\frac{\partial}{\partial n_0}\phi_0^\pm = F_\pm \quad (5.3.38)$$

for field points on Γ. Using this result we may now let the field point move on to the bed and apply the bed condition to give

$$0 = \tfrac{1}{2}(A_- + B_+)\frac{\partial}{\partial n_0}F^+ + \tfrac{1}{2}(A_+ + B_-)\frac{\partial}{\partial n_0}F- - \frac{\partial}{\partial s_0}\int_\Gamma \left(\frac{\partial}{\partial s}\widehat{g}_{xx_0}^{zz_0} - \frac{l^2}{\sigma}\widehat{g}_{x_0}^{zz_0}\right)\phi\,\mathrm{d}s + \frac{l^2}{\sigma_0}\int_\Gamma \left(\frac{\partial}{\partial s}\widehat{g}_x^{zz_0} - \frac{l^2}{\sigma}\widehat{g}^{zz_0}\right)\phi\,\mathrm{d}s. \quad (5.3.39)$$

The next step is to perform an integration by parts, however, care must be taken to consider discontinuities of the integrand. This is the two-dimensional analogue of

considering points in the three-dimensional problem where Stokes' theorem does not apply and is an issue not addressed by Noblesse [67]. We will return to this in a three-dimensional context in Chapter 8. Therefore in (5.3.39) we note that $\widehat{g}^{zz_0}_{xx_0}$ is continuous in x whereas $\widehat{g}^{zz_0}_{x}$ contains a factor $\mathrm{sgn}(x-x_0)$ which will throw out an extra term in the integration by parts. Therefore

$$\begin{aligned} 0 &= \tfrac{1}{2}(A_- + B_+)F_+ + \tfrac{1}{2}(A_+ + B_-)F_- \\ &+ \frac{\partial}{\partial s_0}\int_\Gamma \left(\widehat{g}^{zz_0}_{xx_0}\frac{\partial\phi}{\partial s} + \frac{l^2}{\sigma}\widehat{g}^{zz_0}_{x_0}\phi\right)\,\mathrm{d}s - \frac{l^2}{\sigma_0}\int_\Gamma \left(\widehat{g}^{zz_0}_{x}\frac{\partial\phi}{\partial s} + \frac{l^2}{\sigma}\widehat{g}^{zz_0}\phi\right)\,\mathrm{d}s + \frac{l^2}{\sigma_0}\left[\phi\widehat{g}^{zz_0}_{x}\right]^{x_0^-}_{x_0^+} \end{aligned} \tag{5.3.40}$$

where the square brackets denotes the jump in the quantity at $x = x_0$. Thus once again we have obtained a second-kind integral equation for ϕ on Γ although its form and structure is entirely different to (5.3.25).

We pause for an instant to consider the explicit form of the free term which is found to be

$$\left[\phi\,\widehat{g}^{zz_0}_{x}\right]^{x_0^-}_{x_0^+} = \phi(x_0,h(x_0))\sum_{r=0}^{\infty}\frac{\chi_r^2(h(x_0))}{k_r^2 h_0} \tag{5.3.41}$$

after using (5.2.21) in (5.2.14). Now we note from Chapman & Porter [14], or alternatively (3.3.16), that

$$\sum_{n=0}^{\infty}\frac{\chi_n(h(x_0))\psi_n(z_0)}{k_n h_0} = \mathrm{H}(z_0 - h(x_0)) \tag{5.3.42}$$

which, if we integrate between h_0 and z_0, results in

$$\sum_{n=0}^{\infty}\frac{\chi_n(h(x_0))\chi_n(z_0)}{k_n^2 h_0} = h_0 - h(x_0) \tag{5.3.43}$$

for all points in the fluid domain. Therefore if we let $z_0 \longrightarrow h(x_0)$ in (5.3.43) we find that we can sum (5.3.41) explicitly to give

$$\left[\phi\,\widehat{g}^{zz_0}_{x}\right]^{x_0^-}_{x_0^+} = \phi(x_0,h(x_0))\,(h_0 - h(x_0)). \tag{5.3.44}$$

Now we observe that (5.3.40) is a second-kind integro-differential equation for ϕ

defined on the curve Γ. Therefore if we define an integro-differential operator

$$(\mathcal{K}_2\phi)(s_0) = -\frac{l^2}{\sigma_0}\phi(s_0)(h_0 - h(x_0)) - \frac{\partial}{\partial s_0}\int_\Gamma \left(\widehat{g}^{zz_0}_{xx_0}\frac{\partial\phi}{\partial s} + \frac{l^2}{\sigma}\widehat{g}^{zz_0}_{x_0}\phi\right)\,\mathrm{d}s + \frac{l^2}{\sigma_0}\int_\Gamma\left(\widehat{g}^{zz_0}_{x}\frac{\partial\phi}{\partial s} + \frac{l^2}{\sigma}\widehat{g}^{zz_0}\phi\right)\,\mathrm{d}s, \quad (5.3.45)$$

then define a pair of functions $\varphi_2^{\pm}$ on Γ such that

$$(\mathcal{K}_2\,\varphi_2^{\pm})(s_0) = F_{\pm}(s_0), \quad (5.3.46)$$

we see that the solution to (5.3.40) and hence (5.3.25) is given by

$$\phi(s_0) = \tfrac{1}{2}(A_- + B_+)\,\varphi_2^+ + \tfrac{1}{2}(A_+ + B_-)\,\varphi_2^-. \quad (5.3.47)$$

It can be readily shown that $\mathcal{K}_2$ is a self-adjoint operator so that (2.3.21) applies. This fact can be established by repeated integration by parts and use of the symmetry properties of the integrand which we highlighted in the discussion after (5.2.19), although the algebra is somewhat protracted and tedious.

We note that the form of (5.3.40) is entirely different from (5.3.25) therefore each method provides an independent check on the other. However, if we compare (5.3.33) with (5.3.47) we must have $\varphi_1^{\pm} = \varphi_2^{\pm}$ in which case, as the approach to determining the scattering matrix is identical whichever method is used, we drop the suffix on $\varphi^{\pm}$.

5.3.3 Recovery of the scattering matrix

In our two-dimensional notation (5.3.22) and (5.3.23) become

$$B_- = A_+ - \frac{\mathrm{i}}{2\alpha h_0}\langle\phi, F_-\rangle, \quad (5.3.48)$$

and

$$B_+ = A_- - \frac{\mathrm{i}}{2\alpha h_0}\langle\phi, F_+\rangle. \quad (5.3.49)$$

Then using (5.3.33) or (5.3.47) we deduce that

$$\left.\begin{aligned} B_- &= A_+ - \lambda\left\{(A_- + B_+)P_-^+ + (A_+ + B_-)P_-^-\right\} \\ B_+ &= A_- - \lambda\left\{(A_- + B_+)P_+^+ + (A_+ + B_-)P_+^-\right\}. \end{aligned}\right\} \quad (5.3.50)$$

where we have defined

$$P_{\pm}^{\pm} = \langle \varphi^{\pm}, F_{\pm} \rangle, \qquad \text{and} \qquad \lambda = \frac{\mathrm{i}}{4\alpha h_0} \tag{5.3.51}$$

and the superscripts and subscripts on the left-hand side correspond to those that are attached to quantities on the right-hand side. Then rearranging these equations we find

$$(\mathbf{I} + \lambda \mathbf{P}) \begin{pmatrix} B_+ \\ B_- \end{pmatrix} = (\mathbf{I} - \lambda \mathbf{P}) \begin{pmatrix} A_- \\ A_+ \end{pmatrix}, \qquad \text{where} \qquad \mathbf{P} = \begin{pmatrix} P_+^+ & P_+^- \\ P_-^+ & P_-^- \end{pmatrix} \tag{5.3.52}$$

and $\mathbf{I}$ is the 2×2 identity matrix. Finally, comparison with (5.2.8) shows that

$$\mathbf{M} = (\mathbf{I} + \lambda \mathbf{P})^{-1} (\mathbf{I} - \lambda \mathbf{P}). \tag{5.3.53}$$

5.4 Approximation and numerical method

The problem of determining the reflection and transmission coefficients has been reduced to one in which we need to determine the four matrix elements $P_{\pm}^{\pm}$ of P which are defined in (5.3.41) in terms of inner products involving functions $\varphi^{\pm}$ which are the solution of the integral equations in (5.3.25) or the integro-differential equations in (5.3.40). These alternative formulations of the problem call for different styles of approach depending critically upon whether or not the integral operator is self-adjoint.

5.4.1 Boundary element approach

The operator $\mathcal{K}_1$ is not self-adjoint and furthermore the physical nature of the adjoint problem is unclear. Therefore it is not evident how to solve integral equations based on this operator by the Rayleigh-Ritz method. In fact we find that this formulation is particularly amenable to a boundary element approach. In what follows we assume that the bed profile $z = h(x)$ is single-valued in x, that is to say there are no overhangs. This is not unduly restrictive, our main reason for requiring it is simplification of the parameterisation of the curve by projecting the curve Γ onto the

x axis. In any case this is purely a numerical issue in that it affects how we choose to parameterise the surface. If $h(x)$ was no longer single valued the method would not fail, we would choose an alternative parameterisation defined along the curve rather than using projection and parameterising along the x axis.

Projecting (5.3.24) onto the x axis using $\mathrm{d}s = \sigma \mathrm{d}x$ and $\partial/\partial s = \sigma^{-1}\partial/\partial x$ results in

$$(\mathcal{K}_1\phi)(x_0, h(x_0)) = \phi(x_0, h(x_0)) - \int_0^\ell \left(\frac{\mathrm{d}}{\mathrm{d}x}\widehat{g}_x^z - l^2\widehat{g}^z\right)\phi \,\mathrm{d}x \qquad (5.4.1)$$

where the argument of the Green's function terms g^z and g_x^z is $(x, h(x); x_0, h(x_0))$. Therefore defining a pair of functions $\varphi_1^\pm(x)$ for $x \in [0, \ell]$, the integral equation (5.3.25) becomes

$$(\mathcal{K}_1\varphi^\pm)(x_0) = \phi_0^\pm(x_0, h(x_0)), \qquad x_0 \in [0, \ell]. \qquad (5.4.2)$$

We now solve (5.4.2) by a boundary element approach, namely subdividing the x axis into N equal length elements and assuming ϕ takes a specific form on each element. Often in boundary integral approaches increasingly sophisticated choices of the form of ϕ are taken. For example piecewise polynomials, defined on each element so that ϕ and one or more of its derivatives are continuous at the ends of adjacent panels, might be chosen in the hope that they will better approximate the exact solution. In fact we find that, in this formulation, the simplest approximation that ϕ is a constant on each panel is extremely effective. Thus writing (5.4.2) in full using (5.4.1) and assuming φ is a constant on each panel results in the equation

$$\varphi_n^\pm(x_0, h(x_0)) - \sum_{n=1}^{N} \varphi_n^\pm \left(\int_{x_n-\delta}^{x_n+\delta} \left(\frac{\mathrm{d}}{\mathrm{d}x}\widehat{g}_x^z - l^2\widehat{g}^z\right) \mathrm{d}x\right) = \phi_0^\pm(x_0, h(x_0)) \qquad (5.4.3)$$

where $x_n = (2n-1)\delta$ with $\delta = \ell/2N$, defines the position of the midpoint of the $n'th$ panel. In this form it is clear that the main advantage of choosing such a simple form of φ on each panel enables us to integrate out the potentially most singular term in the equation explicitly. Therefore we may write

$$\varphi^\pm(x_0, h(x_0)) - \sum_{n=1}^{N} \varphi_n^\pm \left([\widehat{g}_x^z]_{x_n-\delta}^{x_n+\delta} - l^2\int_{x_n-\delta}^{x_n+\delta} \widehat{g}^z \,\mathrm{d}x\right) = \phi_0^\pm(x_0, h(x_0)) \qquad (5.4.4)$$

We proceed by collocating, i.e. requiring (5.4.4) to hold exactly at the centre point of each panel in x_0, therefore (5.4.4) becomes

$$\varphi_m^{\pm} - \sum_{n=1}^{N} \varphi_n^{\pm} \left(A_{mn} - l^2 B_{mn} \right) = \phi_{0,m}^{\pm}, \qquad m = 1, \ldots, N, \tag{5.4.5}$$

where $\varphi_m^{\pm} = \varphi^{\pm}(x_m, h(x_m))$, $\phi_{0,m}^{\pm} = \phi_0^{\pm}(x_m, h(x_m))$,

$$A_{mn} = [\widehat{g}_x^z(x, h(x); x_m, h(x_m))]_{x_n-\delta}^{x_n+\delta} \tag{5.4.6}$$

and

$$B_{mn} = \int_{x_n-\delta}^{x_n+\delta} \widehat{g}^z(x, h(x); x_m, h(x_m))\, \mathrm{d}x. \tag{5.4.7}$$

We now simply solve (5.4.5) which is a system of two straight forward $N \times N$ matrix equations differing only by the forcing terms on the right hand side.

Finally, using (5.3.33) in (5.3.51) we deduce that

$$P_{\pm}^{\pm} = \sum_{n=1}^{N} \varphi_n^{\pm} F_{n\pm} \tag{5.4.8}$$

where $F_{n\pm}$ is given by

$$F_{n\pm} = \mp \frac{\alpha}{k} \left[f_{\pm}(x, h(x)) \right]_{x_n-\delta}^{x_n+\delta} - \frac{\mathrm{i}l^2}{k} \int_{x_n-\delta}^{x_n+\delta} f_{\pm}(x, h(x))\, \mathrm{d}x \tag{5.4.9}$$

thus giving us all the information we require to calculate the scattering matrix. It should be stressed that there are no numerical difficulties with any of the calculated quantities. The only quantity which would have been expected to cause difficulties, that is A_{mn} for $m = n$, is integrated out explicitly. Although deceptively simple, this approach is extremely powerful and efficient, when it is compared with the amount of effort required to implement the traditional approach using normal derivatives rather than our switch to tangential derivatives (see for example Fenton [34]).

5.4.2 Rayleigh-Ritz approach

Crucially to what follows the integro-differential operator $\mathcal{K}_2$ is self-adjoint. Therefore, in order to solve the integro-differential equation, we use a standard variational

principle applicable to self-adjoint operators and, with $p^{\pm} \in \mathcal{H}$ we define the functional $J_2 : \mathcal{H} \times \mathcal{H} \to \mathbb{C}$ by

$$J_2(p^+, p^-) = \langle p^+, F_- \rangle + \langle F_+, p^- \rangle - \langle \mathcal{K} p^+, p^- \rangle. \tag{5.4.10}$$

It is easily shown that the functional J_2 is stationary with respect to variations in p^+, p^- when $p^+ = \varphi^+$ and $p^- = \varphi^-$ where it takes the value

$$J_2(\varphi^+, \varphi^-) = P_-^+ = \overline{P}_+^-. \tag{5.4.11}$$

A second functional, $J_1 : \mathcal{H} \to \mathbb{R}$ is defined by

$$J_1(p^{\pm}) = \langle p^{\pm}, F_{\pm} \rangle + \langle F_{\pm}, p^{\pm} \rangle - \langle \mathcal{K} p^{\pm}, p^{\pm} \rangle \tag{5.4.12}$$

is designed to be stationary at $p^{\pm} = \varphi^{\pm}$ where its respective values are

$$J_1(\varphi^+) = P_+^+, \qquad J_1(\varphi^-) = P_-^-. \tag{5.4.13}$$

An approximation to $\varphi^{\pm}$, say $\tilde{\varphi}^{\pm}$ gives rise to approximate values of $P_{\pm}^{\pm}$, say $\tilde{P}_{\pm}^{\pm}$. The variational principles above immediately give rise to the estimates

$$|P_{\pm}^{\pm} - \tilde{P}_{\pm}^{\pm}| = O(||\varphi^{\pm} - \tilde{\varphi}^{\pm}||\, ||\varphi^{\pm} - \tilde{\varphi}^{\pm}||) \tag{5.4.14}$$

where the superscripts and subscripts on the left-hand side correspond to the first and second factors on the right-hand side. That is, the approximations to the quantities of interest are second-order accurate with respect to first-order approximations (in an L_2 norm sense) to the exact solutions of the integral equations.

Adopting this principle $\varphi^{\pm}$ is approximated by $\tilde{\varphi}^{\pm} \in \mathcal{H}_{N+1}$, an $(N+1)$-dimensional subspace of $\mathcal{H}$ (as yet undefined), spanned by a set of test functions $p_n(s,t) \in \mathcal{H}_{N+1}$, by writing

$$\varphi^{\pm} \approx \tilde{\varphi}^{\pm} = \sum_{n=0}^{N} a_n^{\pm} p_n(s). \tag{5.4.15}$$

This approximation is substituted in place of $p^{\pm}$ in (5.4.10) and (5.4.13). By making the resulting expressions stationary with respect to $a_n^{\pm}$, we arrive at the two

independent system of equations

$$\sum_{n=0}^{N} a_n^{\pm} \langle \mathcal{K} p_n, p_m \rangle = \langle F_{\pm}, p_m \rangle \tag{5.4.16}$$

where the coefficients a_n^+ are determined by selecting F_+ on the right-hand side, and likewise for a_n^-. The system of equations (5.4.16) are equivalent to direct application of Galerkin's method to the original integral equations in which (5.4.15) is substituted into (5.3.40) and the residual is forced to be orthogonal to the space $\mathcal{H}_{N+1}$ spanned by the functions p_m.

The resulting approximations to $P_{\pm}^{\pm}$ are

$$\tilde{P}_{\pm}^{\pm} = \sum_{n=0}^{N} a_n^{\pm} \langle p_n, F_{\pm} \rangle \tag{5.4.17}$$

where superscripts and subscripts correspond across both sides of the equation. The test functions $p_n(s)$ are defined to model the potential φ over the ridge and although it is possible to do so, we choose not to specify p_n at this point.

Things now become a little complicated as we sift through the details of what (5.4.16) and (5.4.17) imply. We write

$$\langle \mathcal{K} p_n, p_m \rangle \equiv K_{mn} = K_{mn}^{(1)} + K_{mn}^{(2)} + K_{mn}^{(3)} + K_{mn}^{(4)} + K_{mn}^{(5)} \tag{5.4.18}$$

where

$$K_{mn}^{(1)} = -\int_\Gamma p_m(s_0) \frac{\mathrm{d}}{\mathrm{d}s_0} \int_\Gamma \widehat{g}_{xx_0}^{zz_0} \frac{\mathrm{d}p_n(s)}{\mathrm{d}s} \,\mathrm{d}s \,\mathrm{d}s_0, \tag{5.4.19}$$

$$K_{mn}^{(2)} = -l^2 \int_\Gamma p_m(s_0) \frac{\mathrm{d}}{\mathrm{d}s_0} \int_\Gamma \widehat{g}_{x_0}^{zz_0} p_n(s) \,\mathrm{d}s \,\mathrm{d}s_0, \tag{5.4.20}$$

$$K_{mn}^{(3)} = l^2 \int_\Gamma p_m(s_0) \int_\Gamma \widehat{g}_x^{zz_0} \frac{\mathrm{d}p_n(s)}{\mathrm{d}s} \,\mathrm{d}s \frac{\mathrm{d}s_0}{\sigma_0}, \tag{5.4.21}$$

$$K_{mn}^{(4)} = l^4 \int_\Gamma p_m(s_0) \int_\Gamma \widehat{g}^{zz_0} p_n(s) \,\mathrm{d}s \frac{\mathrm{d}s_0}{\sigma_0} \tag{5.4.22}$$

and

$$K_{mn}^{(5)} = -l^2 \int_\Gamma (h_0 - h(x_0)) p_m(s_0) p_n(s_0) \frac{\mathrm{d}s_0}{\sigma_0}. \tag{5.4.23}$$

To simplify matters further, it is assumed that $x(s)$ is monotonic increasing with s (i.e. $h(x)$ is a single-valued function and so the ridge has no overhangs) so that we

may project the integration from the curve Γ onto the interval $x \in [0, \ell]$. Furthermore as $h(x)$ is single valued, the arc-length s may be parameterised by x so that $s = s(x)$, $\mathrm{d}s = \sigma(x)\,\mathrm{d}s$ and also $p_n(s) \equiv p_n(x)$. Then after integrating (5.4.21) and (5.4.22) by parts noting that there are no discontinuities which affect the integration, and that the free terms are zero by construction, we obtain the simplified (and computationally friendly) form

$$K_{mn}^{(1)} = \int_0^\ell \int_0^\ell \widehat{g}_{xx_0}^{zz_0}(x, h(x); x_0, h(x_0)) p_n'(x) p_m'(x_0)\,\mathrm{d}x\,\mathrm{d}x_0, \tag{5.4.24}$$

$$K_{mn}^{(2)} = l^2 \int_0^\ell \int_0^\ell \widehat{g}_{x_0}^{zz_0}(x, h(x); x_0, h(x_0)) p_n(x) p_m'(x_0)\,\mathrm{d}x\,\mathrm{d}x_0, \tag{5.4.25}$$

$$K_{mn}^{(3)} = l^2 \int_0^\ell \int_0^\ell \widehat{g}_{x}^{zz_0}(x, h(x); x_0, h(x_0)) p_n'(x) p_m(x_0)\,\mathrm{d}x\,\mathrm{d}x_0, \tag{5.4.26}$$

$$K_{mn}^{(4)} = l^4 \int_0^\ell \int_0^\ell \widehat{g}^{zz_0}(x, h(x); x_0, h(x_0)) p_n(x) p_m(x_0)\,\mathrm{d}x\,\mathrm{d}x_0, \tag{5.4.27}$$

and

$$K_{mn}^{(5)} = -l^2 \int_0^\ell (h_0 - h(x_0)) p_n(x_0) p_m(x_0)\,\mathrm{d}x_0. \tag{5.4.28}$$

Without loss of generality we may assume that $p_n(x)$ is real so that K_{mn} in turn is a real matrix. Furthermore the individual kernels have the following symmetry properties

$$K_{mn}^{(1)} = K_{nm}^{(1)}, \tag{5.4.29}$$

$$K_{mn}^{(2)} = K_{nm}^{(3)}, \tag{5.4.30}$$

$$K_{mn}^{(4)} = K_{nm}^{(4)}, \tag{5.4.31}$$

$$K_{mn}^{(5)} = K_{nm}^{(5)}, \tag{5.4.32}$$

which are easily deduced from (5.4.23) to (5.4.27) by switching variables. Hence it follows that K_{mn} is a real symmetric matrix, a property which is a direct consequence of the self-adjointness of $\mathcal{K}_2$.

Let us now consider the right-hand side terms in (5.4.16) and develop them in a similar manner. Thus from the definition of $F_\pm$ in (5.3.29), and integrating by parts,

$$\langle F_\pm, p_m \rangle \equiv F_m^\pm = \int_\Gamma \left\{ \pm \left(\frac{\alpha}{k}\right) \frac{\partial \overline{p}_m}{\partial s} - \left(\frac{\mathrm{i}l^2}{k\sigma}\right) \overline{p}_m \right\} f_\pm(x, z)|_{(x,z)\in\Gamma}\,\mathrm{d}s. \tag{5.4.33}$$

Projecting onto the x axis and, as $p_n(x)$ is real,

$$F_m^{\pm} = \int_0^{\ell} \left\{ \pm \frac{\alpha}{k} p_m'(x) - \frac{\mathrm{i}l^2}{k} p_m(x) \right\} \mathrm{e}^{\pm \mathrm{i}\alpha x} \chi_0(h(x)) \, \mathrm{d}x. \tag{5.4.34}$$

It follows that $F_m^{\mp} = \overline{F}_m^{\pm}$ and on account of K_{mn} being real, $a_n^{\mp} = \overline{a_n}^{\pm}$. Thus only one complex set of equations in (5.4.16) needs to be solved. Alternatively, a pair of systems of *real* equations for the real and imaginary parts of the right-hand side terms, $F_m^{\pm}$ could be solved to generate $a_n^{\pm}$.

All that is required of the functions $p_n(x)$ is that they define a complete set in the interval $(0, \ell)$. However, functions which incorporate the local fluid behaviour at the end points of Γ will in general provide better results. For topographies where the join with the region of constant depth is not continuous, the flow at the join is locally like potential flow within a wedge and hence the bed flux must vanish at the join. In such cases therefore we choose $p_n(x) = \cos n\pi x/\ell$ which gives the required behaviour at the join. In the case of smooth joins Legendre polynomials, or a full Fourier series, would be appropriate.

The case of normal incidence requires more careful thought because, when $l = 0$ and $p_0(x) = 1$ then the matrix K_{mn} becomes degenerate with zero entries in the first row and column. This is because we formulate the problem in terms of the potentials $p_n(x)$ and then find the flux $q_n(x) = p_n'(x)$, whereas the normal incidence problem is determined by the bed flux (see for example, Porter & Porter [77] or Staziker *et al* [89]) . Thus in the case of normal incidence the correct approach is to expand the flux functions $q_n(x)$ as a complete set and then the $p_n(x)$ do not appear. In fact, using this approach we recover Porter & Porter's [77] formulation exactly, thus showing how our approach generalises theirs to three-dimensional problems.

Let us briefly discuss some of the issues surrounding the computation of the solution. There are five separate elements, $K_{mn}^{(i)}$, $i = 1, 5$ which make up K_{mn}. Although symmetry implies only half the elements need to be computed, and that they are real, each factor requires the evaluation of a double-integral in which the kernel is not separable. The infinite sums in the kernels decrease exponentially away from the line

$x = x_0$ where convergence is only algebraic, therefore the kernels are relatively easy to compute. It is worth noting that, in $K_{mn}^{(1)}$ it is easy to see, with reference to Porter & Porter [77], that the kernel $g_{xx_0}^{zz_0}$ contains a logarithmic singularity. Thus we write

$$\widehat{g}_{xx_0}^{zz_0}(x,z;x_0,z_0) = \widehat{g}_{xx_0}^{\prime zz_0}(x,z;x_0,z_0) - \frac{1}{2\pi}\ln T(x,z;x_0,z_0) \tag{5.4.35}$$

where

$$\widehat{g}_{xx_0}^{\prime zz_0}(x,z;x_0,z_0) = \frac{\alpha\chi_0(z)\chi_0(z_0)}{2k^2h_0}\sin\alpha|x-x_0|$$
$$-\sum_{r=1}^{\infty}\left\{\frac{\alpha_r\chi_r(z)\chi_r(z_0)}{2k_r^2h_0}\mathrm{e}^{-\alpha_r|x-x_0|} - \frac{\sin(r\pi z/h_0)\sin(r\pi z_0/h_0)}{r\pi}\mathrm{e}^{-r\pi|x-x_0|/h_0}\right\} \tag{5.4.36}$$

and

$$T(x,z;x,z_0) = \left[\frac{\sin^2\frac{1}{2}\pi(z+z_0)/h_0 + \sinh^2\frac{1}{2}\pi(x-x_0)/h_0}{\sin^2\frac{1}{2}\pi(z-z_0)/h_0 + \sinh^2\frac{1}{2}\pi(x-x_0)/h_0}\right]^{\frac{1}{2}} \tag{5.4.37}$$

The sum in (5.4.36) above is now convergent for all $x-x_0$ and Abramowitz & Stegun [1] has been used to sum the series explicitly.

5.5 Edge waves over a ridge

We turn to the edge wave problem, where much of the analysis carries forward from the scattering problem. Again, to be specific, let us write the boundary value problem to be considered in the quasi two-dimensional formulation. We seek $\phi(x,z)$ satisfying

$$(\nabla^2 - l^2) = 0, \qquad \text{in } D, \tag{5.5.1}$$

with

$$\frac{\partial\phi}{\partial z} = 0, \qquad x \in (-\infty,0)\cup(\ell,\infty) \tag{5.5.2}$$
$$\frac{\partial\phi}{\partial n} = 0, \qquad (x,z)\in\Gamma, \tag{5.5.3}$$

with the "edge-wave" condition

$$\phi \to 0, \qquad |x| \to \infty. \tag{5.5.4}$$

As in Section (4.3.1), we consider l to be the given parameter of the problem and seek a value of k (below the cutoff so $k < l$) for which edge waves are found.

The edge wave condition necessitates a modification to the Green's function in (5.2.14) which we may continue to write as

$$g(x,z;x_0,z_0) = \sum_{r=0}^{\infty} \frac{\psi_r(z)\psi_r(z_0)}{2\alpha_r h_0} \mathrm{e}^{-\alpha_r|x-x_0|}, \tag{5.5.5}$$

provided we modify the α_r in (5.2.15) so that

$$\alpha_r = \sqrt{l^2 + k_r^2} \qquad \alpha_0 = \sqrt{l^2 + k_r^2} = \alpha. \tag{5.5.6}$$

This has the effect of changing what was a propagating mode before, into an evanescent mode thus ensuring that the Green's function satisfies the edge-wave condition.

We proceed, as before by applying Green's identity to the functions g and ϕ and switch from normal to tangential derivatives using (5.3.27) to give

$$\phi(x_0,z_0) = \int_\Gamma \left(\frac{\partial}{\partial s} g_x^z - \frac{l^2}{\sigma} g^z \right) \phi(s)\, \mathrm{d}s. \tag{5.5.7}$$

This is a simplified version of (5.3.25) in that there are no forcing terms. Once again we may solve it in two different ways according to how we formulate the integral equation. Thus solving (5.5.7) directly via a boundary integral approach we would define an integral operator $\mathcal{E}_1$ as

$$(\mathcal{E}_1\phi)(s_0) = \phi(s_0) - \int_\Gamma \left(\frac{\partial}{\partial s} g_x^z - \frac{l^2}{\sigma} g^z \right) \phi(s)\, \mathrm{d}s \tag{5.5.8}$$

in which case the problem to be solved is

$$(\mathcal{E}_1\phi)(s_0) = 0. \tag{5.5.9}$$

The boundary integral equation approach proceeds exactly as before, therefore we do not present the detail, but note that it results in a matrix equation of the form

$$E^{(1)}_{mn}\phi_n = 0 \qquad m,n = 1,\ldots,N. \tag{5.5.10}$$

We solve the equation by finding the value of k for which the determinant of the matrix vanishes thus identifying the particular frequency which supports edge waves.

Alternatively we may reformulate (5.5.8) in a form suitable for solution by the Rayleigh-Ritz method. Thus, taking the normal derivative and proceeding as before we arrive at the integral equation

$$\frac{\partial}{\partial s_0}\int_\Gamma \left(g_{xx_0}^{zz_0}\frac{\partial\phi}{\partial s}+\frac{l^2}{\sigma}g_{x_0}^{zz_0}\phi\right)\,\mathrm{d}s-\frac{l^2}{\sigma_0}\int_\Gamma\left(g_x^{zz_0}\frac{\partial\phi}{\partial s}+\frac{l^2}{\sigma}g^{zz_0}\phi\right)\,\mathrm{d}s$$
$$-\frac{l^2}{\sigma_0}\phi(s_0)(h_0-h(x_0))=0 \quad (5.5.11)$$

which, if we define $\mathcal{E}_2$ as

$$(\mathcal{E}_2\phi)(s_0)=\frac{l^2}{\sigma_0}\phi(s_0)(h_0-h(x_0))-\frac{\partial}{\partial s_0}\int_\Gamma\left(g_{xx_0}^{zz_0}\frac{\partial\phi}{\partial s}+\frac{l^2}{\sigma}g_{x_0}^{zz_0}\phi\right)\,\mathrm{d}s$$
$$+\frac{l^2}{\sigma_0}\int_\Gamma\left(g_x^{zz_0}\frac{\partial\phi}{\partial s}+\frac{l^2}{\sigma}g^{zz_0}\phi\right)\,\mathrm{d}s, \quad (5.5.12)$$

may be written as

$$(\mathcal{E}_2\phi)(s_0)=0. \quad (5.5.13)$$

Solution of this equation follows exactly as before with no new issues introduced by the slightly modified Green's function, thus once again we arrive at a matrix equation of the form

$$E_{mn}^{(2)}c_n=0 \qquad m,n=0,\ldots,N. \quad (5.5.14)$$

Again, we solve this by finding the values of $k<l$ for which the determinant vanishes.

5.6 Results

Let us first consider the convergence properties of the boundary element (BE) method and the Rayleigh-Ritz (RR) method by comparing them with exact results for a semicircular ridge found by multipole techniques. We solved the problem for a semicircular ridge where the radius to depth ration $a/h=0.5$ truncating the multipole system at $N=16$ which by reference to Chapter 4 can be viewed as giving exact solutions, certainly to the number of figures displayed below. We then varied the number of panels in the BE method for a range of incidence angles presenting the results for $\theta=0°$, $30°$, $45°$ and $60°$ in tables (5.1) to (5.4) respectively. We extrapolated to

the results for $N = \infty$ by interpolating the data against $1/N$ and finding the interpolated value for $1/N = 0$ using the standard cubic spline interpolating routine in Matlab version 6.5 Release 13. It should be stressed that there is no mathematical basis for supposing that this method will converge to the correct answer. The extrapolation was done simply to investigate whether it did improve the convergence of the system.

	kl				
N	1	2	3	4	5
20	0.237085	0.080225	0.004956	0.002579	0.000847
40	0.237068	0.078341	0.004503	0.002447	0.000769
60	0.237051	0.077868	0.004398	0.002412	0.000750
80	0.237041	0.077670	0.004356	0.002397	0.000742
100	0.237036	0.077565	0.004333	0.002388	0.000738
120	0.237032	0.077502	0.004320	0.002383	0.000736
140	0.237030	0.077460	0.004312	0.002380	0.000734
160	0.237028	0.077431	0.004306	0.002378	0.000733
180	0.237026	0.077410	0.004301	0.002376	0.000732
200	0.237025	0.077394	0.004298	0.002375	0.000731
⋮	⋮	⋮	⋮	⋮	⋮
∞	0.237018	0.077294	0.004278	0.002367	0.000727
exact	0.236692	0.077295	0.004282	0.002367	0.000728

Table 5.1: Convergence of $|R|$ by the Boundary Element Method for scattering at normal incidence by a semicircular ridge where $a/h_0 = 0.5$.

It should be noted that we anticipate the semicircular ridge problem to be a severe test of our numerical approximation. This is simply because, in both BE and RR we have projected our integrals down onto the x axis. This technique breaks down when the gradient is infinite as occurs at the joins of a semicircular ridge to the constant depth domain. To resolve this numerically one would instead parameterise in terms of arclength at the expense of complicating the numerics somewhat. Alternatively as we have done, we restrict our applications to topographies where the gradient does not become infinite (or contain any overhangs). In our numerical integration schemes we use a 10 point Gaussian quadrature scheme which performs the quadrature at

internal points of the interval therefore enabling us to investigate the semicircular ridge numerically as we never calculate quantities of interest at the end points where the gradient is infinite.

We see from table 5.1 that normal incidence provides a severe test in that, at best, 200 panels gives 2-3 s.f. accuracy. We also note that extrapolation does not improve the convergence. Further increases in the number of panels does not change the convergence significantly, but increases the running time markedly. The main reason is that, on the end panels, the slope of the topography changes significantly and therefore there is significant fluid motion that cannot be resolved by assuming the potential is a constant on the panel.

	kl				
N	1	2	3	4	5
20	0.180226	0.059298	0.001009	0.004151	0.001679
40	0.180382	0.057664	0.000437	0.004115	0.001613
60	0.180409	0.057251	0.000300	0.004104	0.001596
80	0.180419	0.057077	0.000243	0.004098	0.001589
100	0.180423	0.056985	0.000214	0.004095	0.001585
120	0.180425	0.056930	0.000196	0.004094	0.001583
140	0.180427	0.056893	0.000185	0.004092	0.001582
160	0.180428	0.056868	0.000176	0.004092	0.001581
180	0.180429	0.056849	0.000171	0.004091	0.001580
200	0.180429	0.056835	0.000166	0.004090	0.001579
⋮	⋮	⋮	⋮	⋮	⋮
∞	0.180431	0.056746	0.000138	0.004087	0.001576
exact	0.180431	0.056752	0.000140	0.004087	0.001576

Table 5.2: Convergence of the Boundary Element Method for scattering at 30° incidence by a semicircular ridge where $a/h_0 = 0.5$.

Interestingly we see in Table 5.2 that obliqueness appears to help the convergence of the system. Most values converge to values where only the fifth decimal place changes above a value of 100 panels. Furthermore the extrapolation appears to be successful giving four significant places in most cases. The results for $kl = 3$ are the only exception as they only achieve 1 s.f. and then only after a large number of

	kl				
N	1	2	3	4	5
20	0.091132	0.003878	0.024234	0.015633	0.006520
40	0.091391	0.002509	0.024899	0.015723	0.006492
60	0.091446	0.002161	0.025062	0.015742	0.006485
80	0.091468	0.002014	0.025130	0.015750	0.006482
100	0.091478	0.001936	0.025166	0.015754	0.006480
120	0.091485	0.001889	0.025187	0.015756	0.006479
140	0.091489	0.001858	0.025202	0.015758	0.006478
160	0.091491	0.001836	0.025211	0.015759	0.006478
180	0.091493	0.001820	0.025219	0.015760	0.006477
200	0.091495	0.001808	0.025224	0.015760	0.006477
⋮	⋮	⋮	⋮	⋮	⋮
∞	0.091504	0.001733	0.025258	0.015764	0.006475
exact	0.091503	0.001738	0.025256	0.015764	0.006476

Table 5.3: Convergence of the Boundary Element Method for scattering at $45°$ incidence by a semi-circular ridge where $a/h_0 = 0.5$.

panels is taken. This arises because there happens to be a zero of reflection at 3.0788 which is so close to the value 3 that the BE method cannot resolve the "bounce" sufficiently accurately.

The results in tables 5.3 and 5.4 all seem to confirm that an element of obliqueness helps convergence of the system. At $45°$ and for $kl \geq 3$, 140 panels suffices to give 4 d.p. accuracy and the effort in extrapolating gives 5 or 6 d.p. accuracy. At $60°$ incidence 100 panels generally suffices for 4 d.p. accuracy and the extrapolation generally gives 5-6 d.p. accuracy. These results are particularly impressive for such a simple collocation scheme when tested against such a demanding topography. Undoubtedly they are able to achieve these results because the switch to tangential derivatives enables us to integrate the most singular part of the kernel explicitly.

Table 5.5 presents results for the RR method applied to the same scattering problem namely oblique incidence to a semicircular ridge of radius to depth ratio $a/h_0 = 0.5$. We ran results for a range of truncation sizes N of the trial space to investigate the convergence properties of the RR method. It is worth noting that for

	kl				
N	1	2	3	4	5
20	0.076042	0.134630	0.104805	0.055917	0.024469
40	0.075837	0.135734	0.105513	0.056136	0.024508
60	0.075793	0.136015	0.105688	0.056188	0.024517
80	0.075776	0.136134	0.105761	0.056209	0.024520
100	0.075767	0.136197	0.105800	0.056220	0.024522
120	0.075762	0.136235	0.105823	0.056227	0.024523
140	0.075759	0.136260	0.105838	0.056232	0.024524
160	0.075756	0.136277	0.105849	0.056235	0.024524
180	0.075755	0.136290	0.105857	0.056237	0.024524
200	0.075753	0.136300	0.105862	0.056238	0.024525
⋮	⋮	⋮	⋮	⋮	⋮
∞	0.075746	0.136361	0.105899	0.056249	0.024526
exact	0.075747	0.136357	0.105897	0.056248	0.024526

Table 5.4: Convergence of $|R|$ by the Boundary element method for scattering at $60°$ incidence by a semicircular ridge where $a/h_0 = 0.5$.

all values of N the RR method was noticeably quicker than the BE for greater than 100 panels. We see that through most of the runs convergence is rapid to typically 3sf with a trial space of around 10. The exceptions are for $30°$ when $kl = 3$ which as we have already seen that the proximity of a zero of reflection affects the convergence. With this in mind we investigate $45°$ and $kl = 2$ where convergence is not as good and it transpires that there is a zero of reflection at 2.026416.

Thus it appears that, in general, the RR method is characterised by rapid convergence with modest truncation sizes. However, the end effects of our projection method are evident in that increase in dimension of the trial space does not appear to change the convergence significantly. In essence the RR method uses a Fourier cosine series to model the potential, and from Fourier theory it is well known that the Gibbs' phenomenom affects the convergence at the end points of the range. This, in conjunction with the limitations of the projection method for infinite gradients, must be the prime reason for no further significant improvement in results.

Despite providing a severe test, the semicircular ridge problem confirms that the

		kl				
θ	N	1	2	3	4	5
0°	5	0.237009	0.077260	0.004294	0.002353	0.000747
	10	0.237017	0.077292	0.004281	0.002364	0.000728
	15	0.237018	0.077293	0.004279	0.002366	0.000727
	20	0.237018	0.077294	0.004278	0.002366	0.000727
	25	0.237018	0.077294	0.004278	0.002366	0.000727
	30	0.237018	0.077294	0.004278	0.002366	0.000727
	Exact	0.236692	0.077295	0.004282	0.002367	0.000728
30°	5	0.181811	0.059348	0.000019	0.004621	0.001677
	10	0.180657	0.057252	0.000001	0.004267	0.001622
	15	0.180571	0.057027	0.000106	0.004156	0.001592
	20	0.180493	0.056888	0.000109	0.004131	0.001587
	25	0.180477	0.056848	0.000126	0.004113	0.001582
	30	0.180457	0.056812	0.000126	0.004107	0.001581
	Exact	0.180431	0.056752	0.000140	0.004087	0.001576
45°	5	0.092749	0.004323	0.024976	0.016205	0.006680
	10	0.091693	0.002239	0.025300	0.015925	0.006545
	15	0.091620	0.002007	0.025249	0.015824	0.006503
	20	0.091549	0.001867	0.025265	0.015804	0.006493
	25	0.091535	0.001826	0.025258	0.015788	0.006486
	30	0.091517	0.001790	0.025262	0.015783	0.006484
	Exact	0.091503	0.001738	0.025256	0.015764	0.006476
60°	5	0.074471	0.133630	0.104954	0.056326	0.024707
	10	0.075553	0.135829	0.105792	0.056334	0.024594
	15	0.075637	0.136084	0.105826	0.056276	0.024553
	20	0.075710	0.136232	0.105877	0.056274	0.024545
	25	0.075725	0.136277	0.105884	0.056265	0.024539
	30	0.075744	0.136315	0.105897	0.056265	0.024537
	Exact	0.075747	0.136357	0.105897	0.056248	0.024526

Table 5.5: Convergence of $|R|$ by the Rayleigh-Ritz method for oblique scattering by a semicircular ridge where $a/h_0 = 0.5$.

method of switching from normal to tangential derivatives and its implementation in both RR and BE work. This is important given the lack of published exact results for fully three-dimensional scattering problems. Our final check on the accuracy of the methods is to compare results from BE and RR methods against each other for oblique scattering by a topography where the gradient is nowhere infinite. This will provide the final confirmation of the methods as, although they are derived from the same integral equation, their formulation and implementation are entirely distinct.

In figure (5.2) we plot results for oblique scattering by a ridge whose profile is a single period of a sine function with a maximum height $h_{max} = 0.5h_0$ and the length to depth ratio $l/h_0 = 1$. Results for the RR method were produced with a truncation size of $N = 32$ which was chosen to avoid convergence issues. We will return to the issue of the rate of convergence of the RR method later. The results for the BE method were produced with a modest number $(N = 100)$ of panels. We plot the results for the RR method as solid lines with no marker; the BE results for the same problem are overlaid as markers of the same colour. It is evident from the plots that the two sets of results are visibly indistinguishable. In fact for almost all of the range of values the results agree to at least 5 d.p. and in many cases to 6 d.p. The only area where the error is greater is in the immediate vicinity of zeros as we have already seen.

This is the final confirmation that both methods and their implementations give accurate results. Accordingly, from now we shall concentrate on investigating the effect of the truncation size N upon convergence of the Rayleigh-Ritz method. Tables 5.6 to 5.8 all show results for the same topography, identical to that used to produce figure 5.2, namely a ridge for which $h(x) = h_0(1 - 0.5\sin(\pi x/l)$ and $l/h_0 = 1$. For normal incidence it is clear from table 5.6 that convergence is rapid with 4 d.p. being achieved typically with $N = 4 - 6$ and 5 d.p. by $N = 10$ although improvement of the sixth decimal place is somewhat slower.

The position is generally the same for angles of incidence 30° and 60° in tables 5.7 and 5.8 respectively. Therefore we conclude that the Rayleigh-Ritz method is extremely quick to converge to accurate results with an even higher degree of accuracy obtained by only a modest truncation size. Accordingly for the figures that follow we use a truncation size of $N = 10$ as any larger would not produce a change in results that would be discernable from the plots.

We now plot results for oblique scattering by a ridge in the shape of a hump defined by a single period of a cosine functiom so that $h(x) = h_0 - h_{max}(1 - \cos \pi x/l)$. This

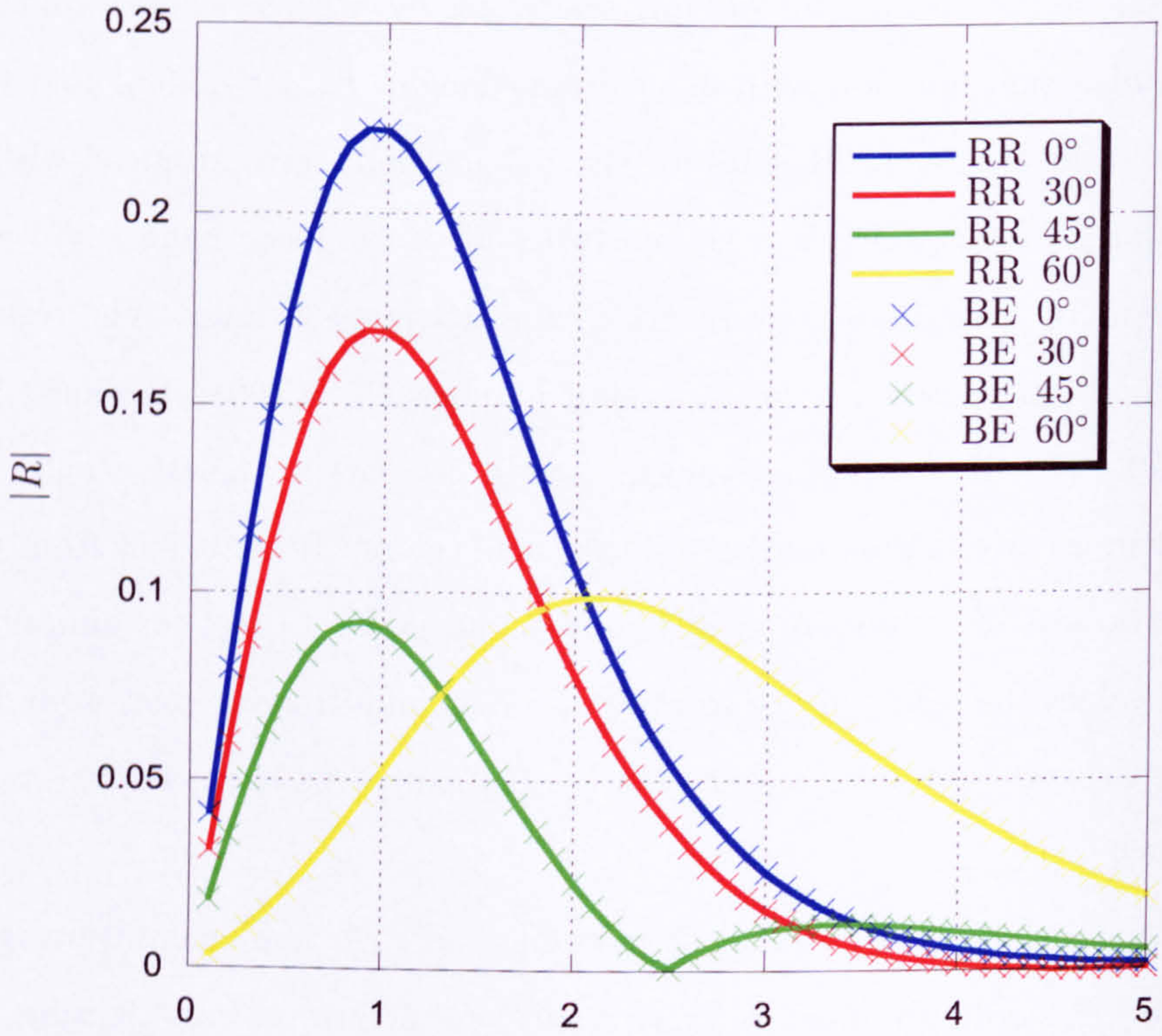

Figure 5.2: Comparison of BE and RR methods for oblique scattering by a ridge where $h(x) = h_0(1 - 0.5\sin(\pi x/l))$ and $l/h_0 = 1$

topography is characterised by a smooth join with the domain of constant depth. Figure 5.3 shows how, for this particular topography when $h_{max}/h_0 = 0.75$, the reflection coefficient varies against the angle of incidence for a fixed wavenumber kl the value of which is marked in the legend. In contrast figure 5.4 shows the effect of altering h_{max}/h_0 for this same topography, this time plotting the reflection coefficient $|R|$ against wavenumber kl.

Finally we turn to the edge wave problem, which for variety we choose to solve using the boundary element formulation. Results are presented for edge waves over a ridge for which $h(x) = h_0 - 0.95h_0(1 - \cos\pi x/l)$ at figure 5.5 and were produced using a system with 100 panels. The numerical problem involves finding frequencies $kh_0 < lh_0$ for a given lh_0 such that the determinant in (5.5.13) vanishes. The values

	kl				
N	1	2	3	4	5
2	0.223104	0.110831	0.032456	0.011015	0.004754
4	0.222076	0.105698	0.025625	0.005701	0.001800
6	0.222036	0.105636	0.025632	0.005608	0.001577
8	0.222026	0.105614	0.025629	0.005610	0.001578
10	0.222023	0.105607	0.025628	0.005611	0.001578
12	0.222021	0.105603	0.025628	0.005611	0.001578
14	0.222021	0.105602	0.025628	0.005612	0.001578
16	0.222021	0.105601	0.025628	0.005612	0.001578
18	0.222020	0.105600	0.025628	0.005612	0.001578
⋮	⋮	⋮	⋮	⋮	⋮
32	0.222020	0.105600	0.025628	0.005612	0.001578

Table 5.6: Convergence of $|R|$ against truncation size N for scattering of normally incident waves by a ridge where $h(x) = h_0(1 - 0.5\sin(\pi x/l))$ and $l/h_0 = 1$

	kl				
N	1	2	3	4	5
2	0.169307	0.073674	0.006435	0.006869	0.005044
4	0.169188	0.077948	0.015823	0.001472	0.000334
6	0.169180	0.077890	0.015805	0.001490	0.000226
8	0.169177	0.077870	0.015809	0.001498	0.000222
10	0.169175	0.077861	0.015810	0.001500	0.000221
12	0.169175	0.077857	0.015810	0.001501	0.000221
14	0.169174	0.077855	0.015809	0.001501	0.000221
16	0.169174	0.077853	0.015809	0.001501	0.000220
18	0.169174	0.077852	0.015809	0.001502	0.000220
⋮	⋮	⋮	⋮	⋮	⋮
32	0.169174	0.077850	0.015809	0.001502	0.000220

Table 5.7: Convergence of $|R|$ against truncation size N for scattering of oblique waves incident at $30°$ to a ridge where $h(x) = h_0(1 - 0.5\sin(\pi x/l))$ and $l/h_0 = 1$

of kh_0 inevitably have to be found by a bisection method which searches for changes in sign of the determinant between two values of kh_0 and reduces the interval until a required tolerance is achieved. We optimise the numerical system by applying a routine which calculates the determinant at a range of vales kh_0 for the largest value of lh_0 of interest and is used to find coarse intervals in which edge wave frequencies may be found. These intervals are then used as seed values for calculation of the edge

	kl				
N	1	2	3	4	5
2	0.052524	0.100347	0.082467	0.046529	0.021832
4	0.052628	0.098438	0.077827	0.042036	0.018972
6	0.052621	0.098483	0.077851	0.042038	0.018947
8	0.052620	0.098498	0.077857	0.042038	0.018946
10	0.052619	0.098504	0.077860	0.042038	0.018946
12	0.052619	0.098507	0.077861	0.042038	0.018946
14	0.052619	0.098508	0.077862	0.042039	0.018946
16	0.052619	0.098509	0.077862	0.042039	0.018946
18	0.052619	0.098510	0.077862	0.042039	0.018946
20	0.052619	0.098510	0.077863	0.042039	0.018946
⋮	⋮	⋮	⋮	⋮	⋮
32	0.052619	0.098511	0.077863	0.042039	0.018946

Table 5.8: Convergence of $|R|$ against truncation size N for scattering of oblique waves incident at $60°$ to a ridge where $h(x) = h_0(1 - 0.5\sin(\pi x/l)$ and $l/h_0 = 1$

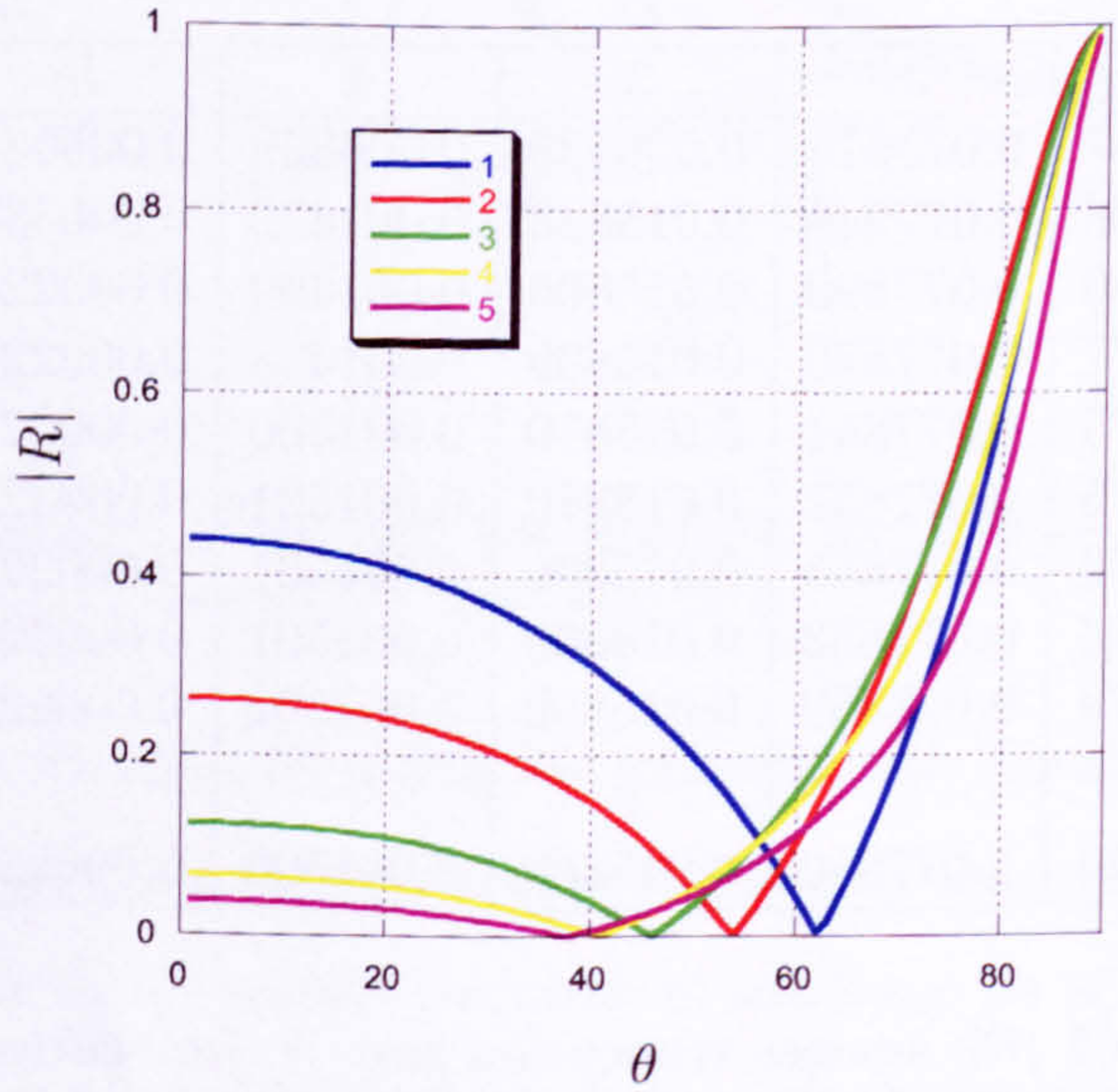

Figure 5.3: Oblique scattering by a ridge for which $h(x) = h_0 - 0.75h_0(1 - \cos\pi x/l)$ - $|R|$ against θ for fixed wavenumber kl.

wave frequencies for all lh_0 of interest by Ridder's method. The underlying approach in Ridder's method is still to find roots by bisection, however, it uses earlier values to forecast an approximate value and squeeze the interval so that after around 3 steps, only a couple of bisections is required. This provides significant efficiency, particularly if the Rayleigh-Ritz method were to be used as in this method the calculation of the

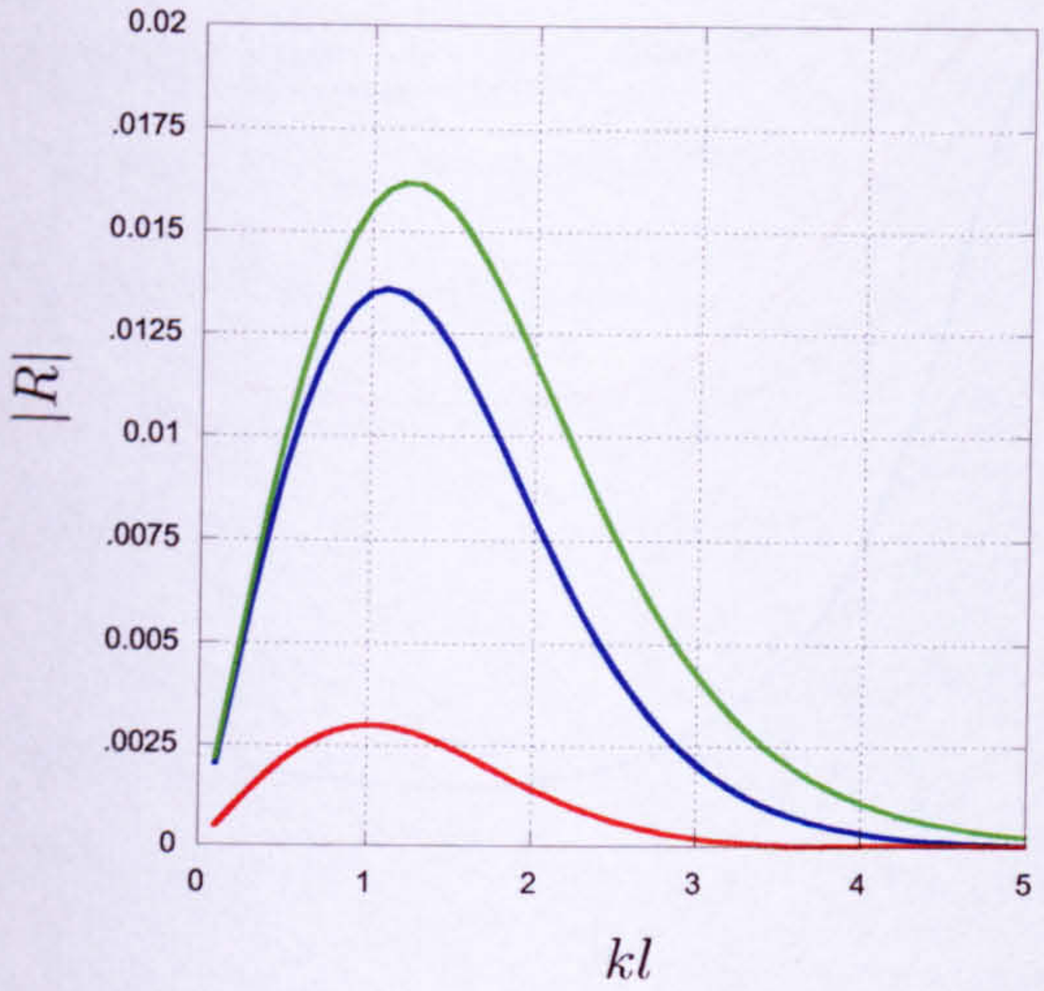

(a) $h_{max} = 0.1$, 30° (—), 45° (—) and 60° (—).

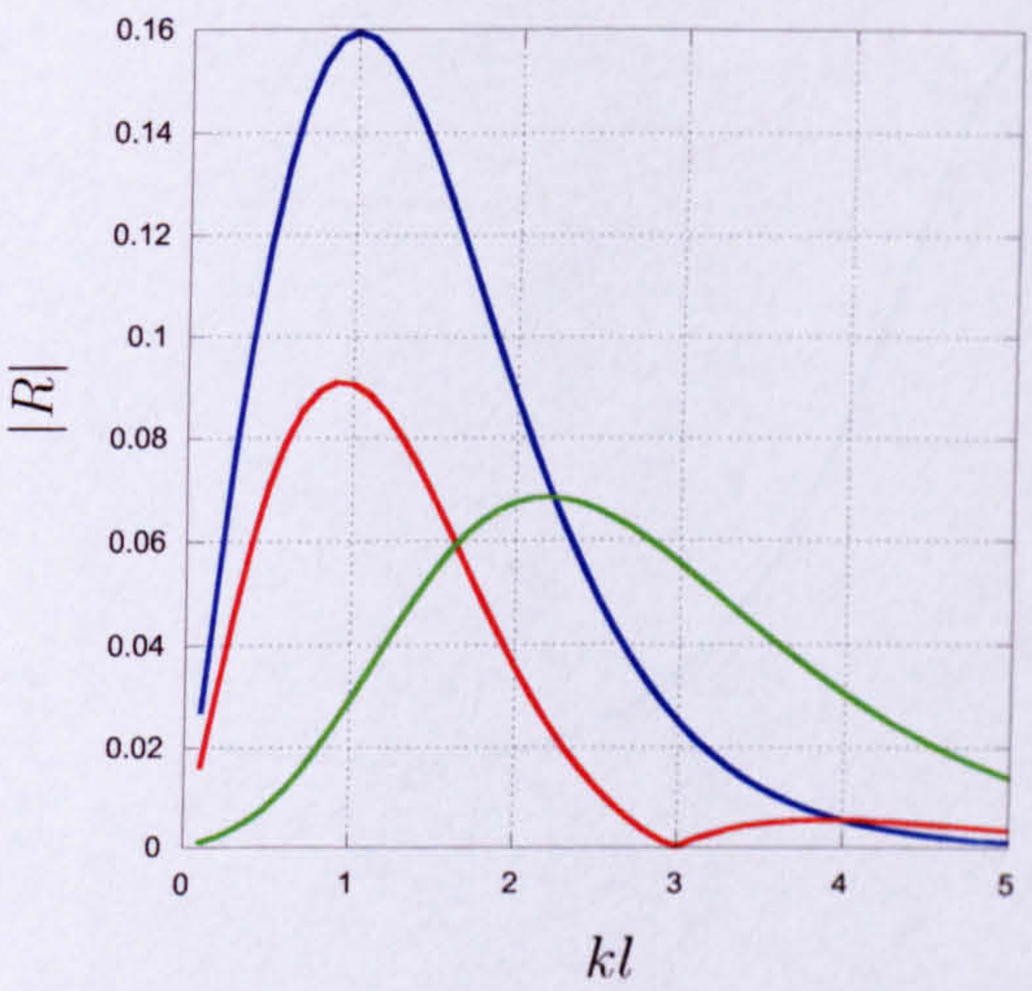

(b) $h_{max} = 0.5$, 30° (—), 45° (—) and 60° (—).

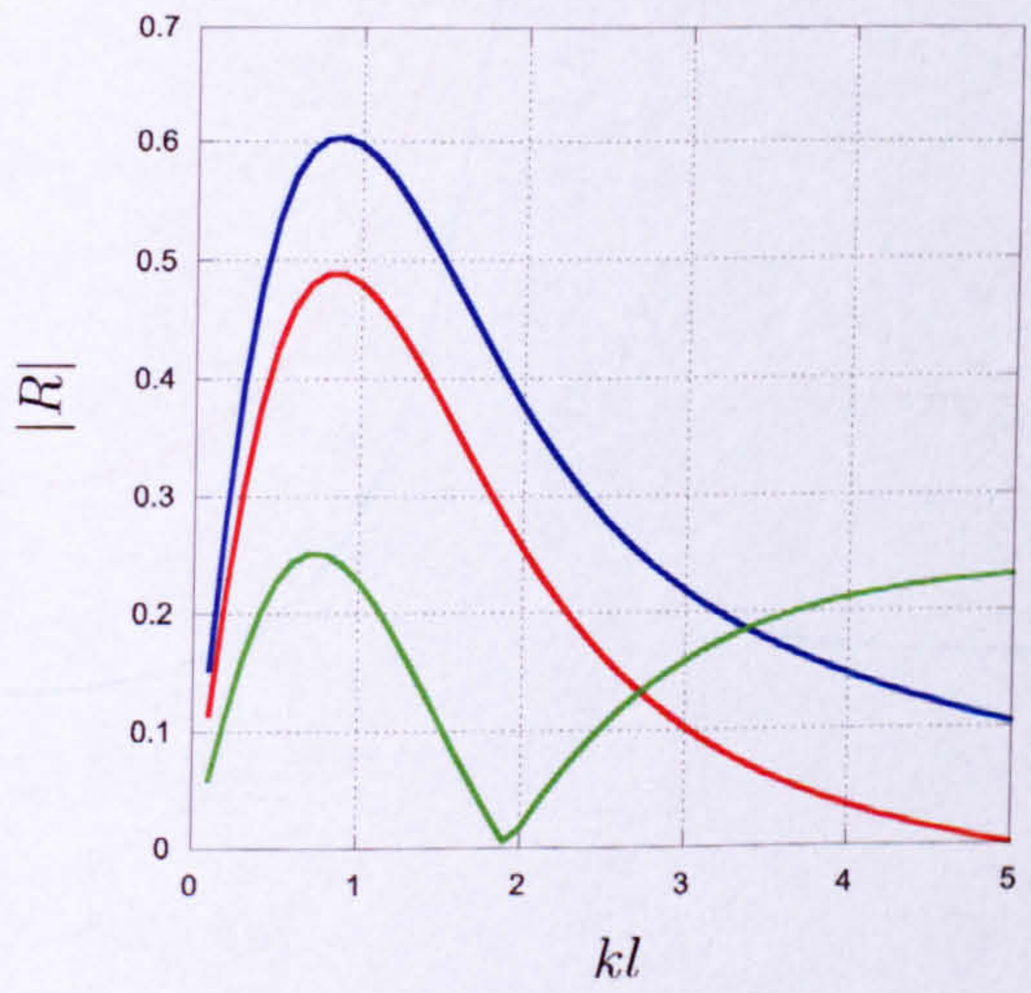

(c) $h_{max} = 0.9$ 30° (—), 45° (—) and 60° (—).

Figure 5.4: Oblique scattering by a ridge for which $h(x) = h_0 - h_{max}(1 - \cos \pi x/l)$ - $|R|$ against wavenumber kl.

determinant is computationally expensive.

5.7 Remarks

In this chapter we have shown how to formulate a three-dimensional problem as an integral equation which satisfies the fixed boundary condition exactly. It provides

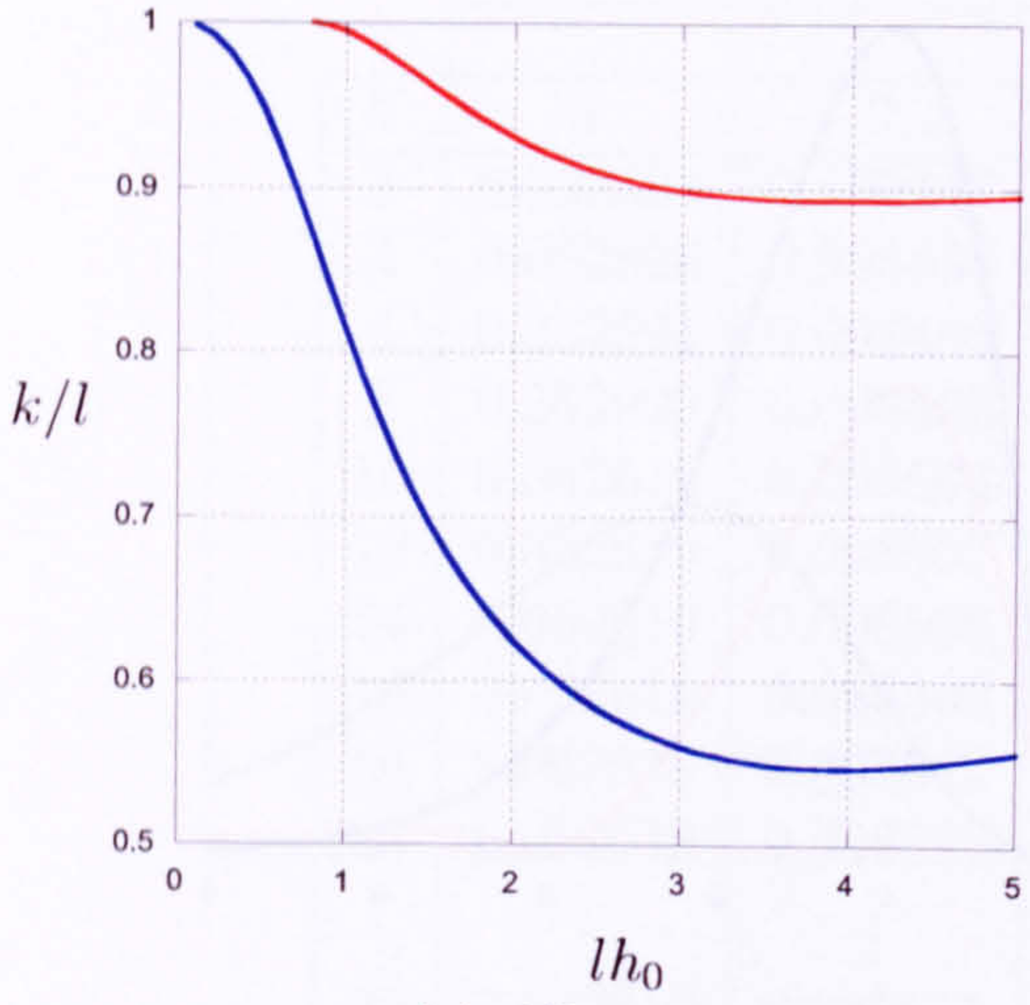

(a) $\ell/h_0 = 2$

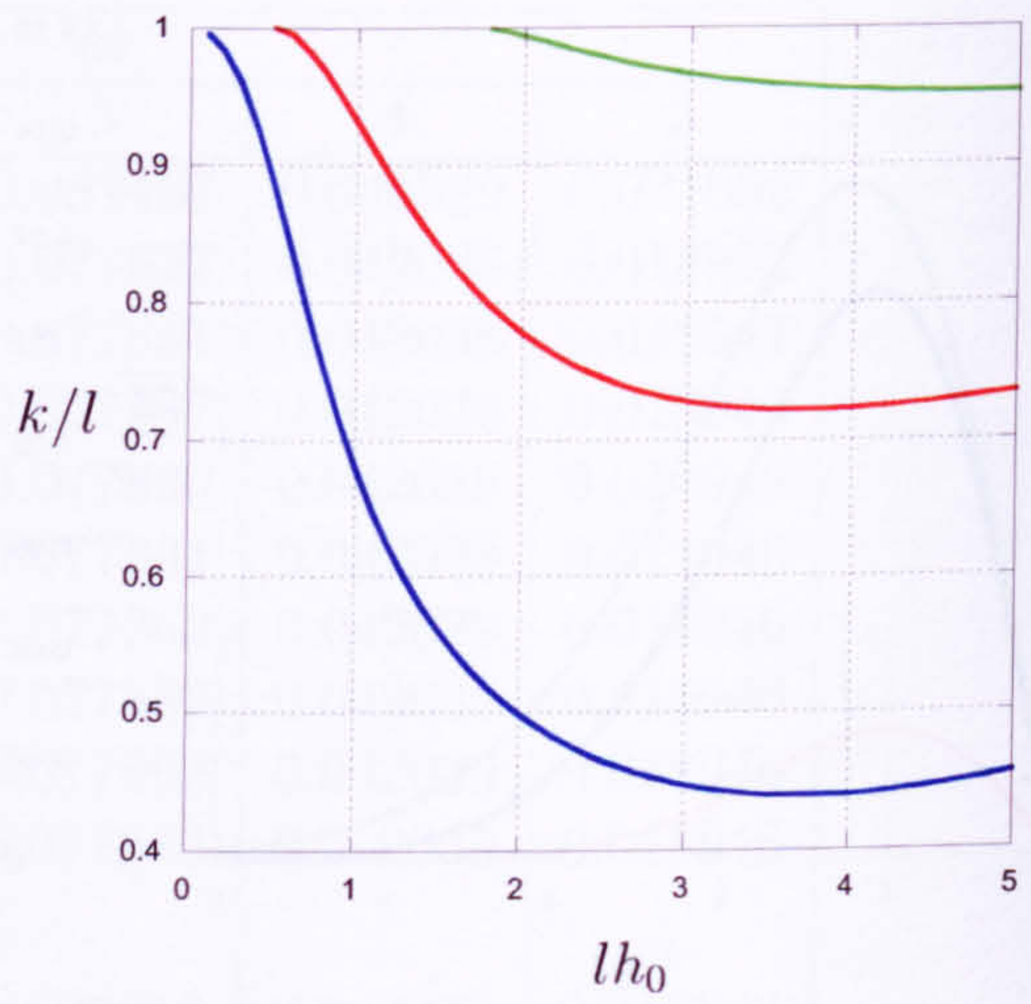

(b) $\ell/h_0 = 3$

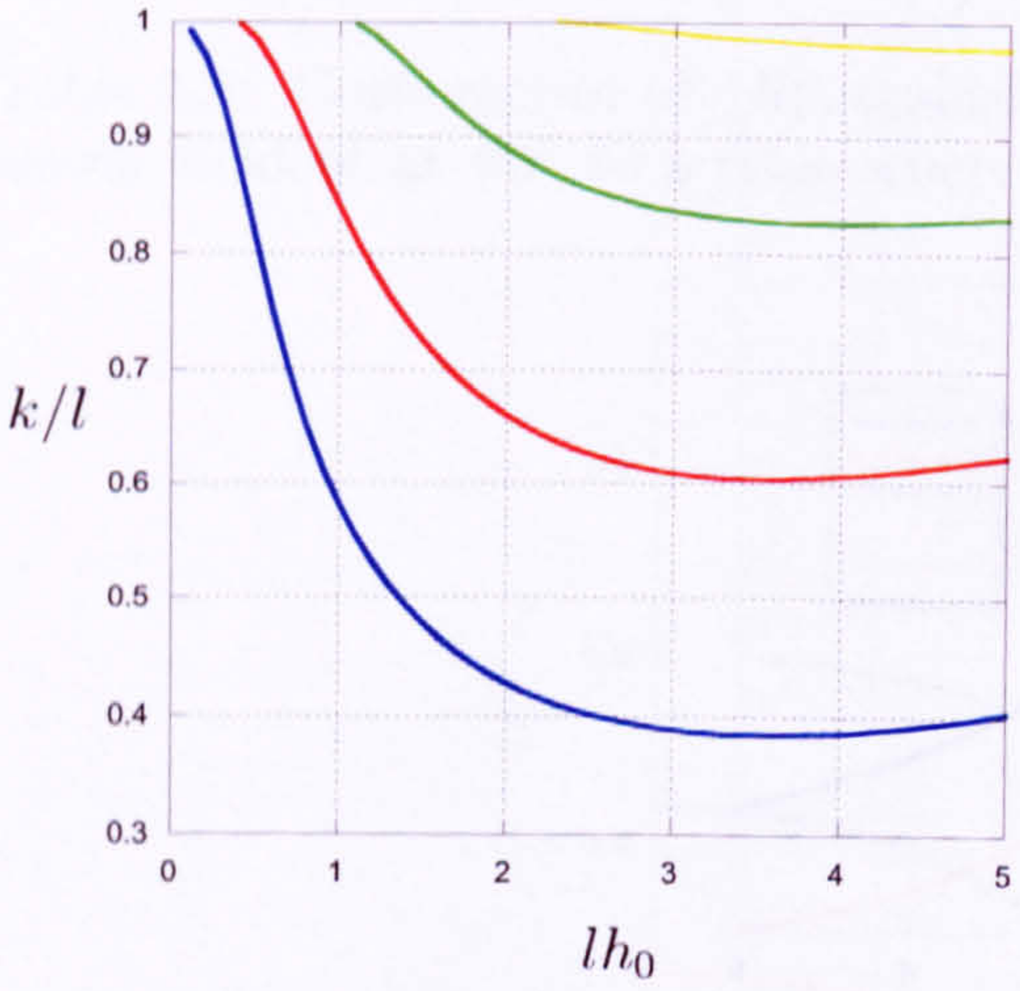

(c) $\ell/h_0 = 4$

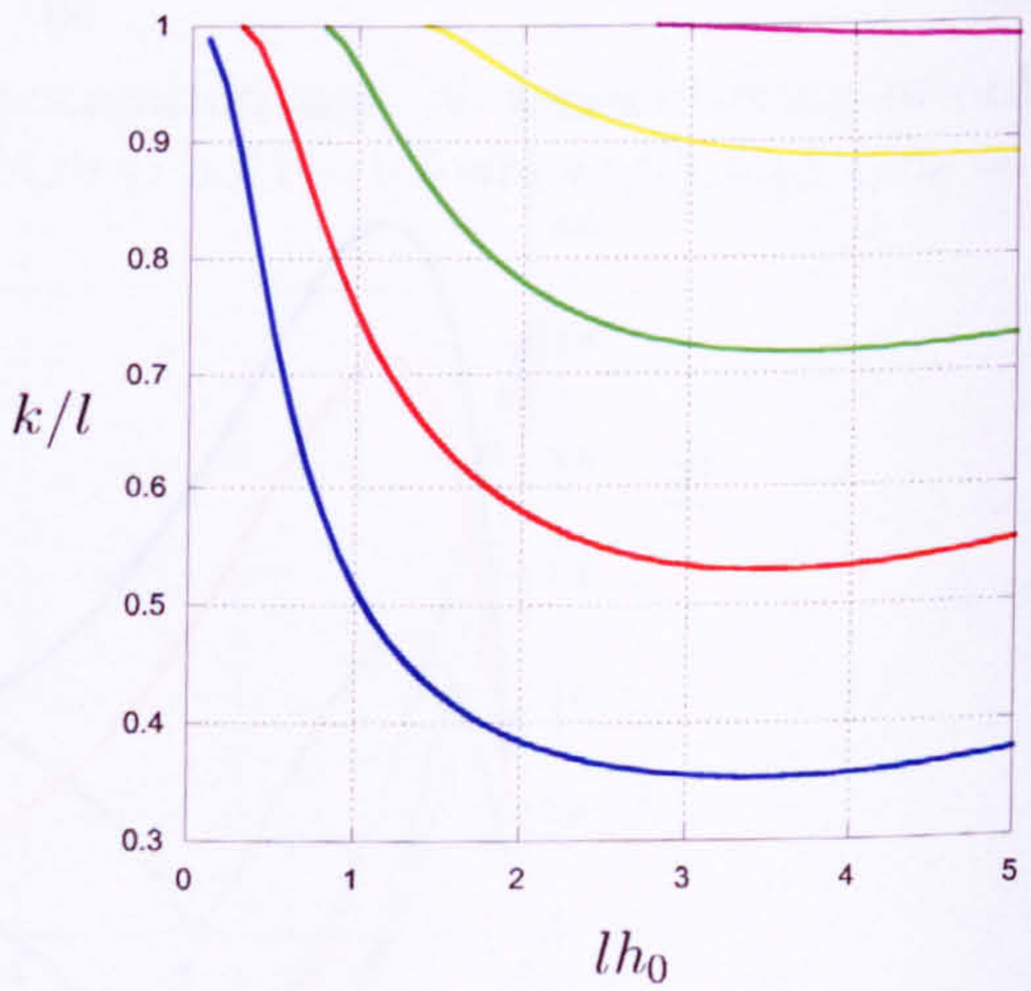

(d) $\ell/h_0 = 5$

Figure 5.5: Edge wave dispersion relations for a ridge where $h(x) = h_0 - 0.95h_0(1 - \cos \pi x/l)$.

a generalisation of the two-dimensional Cauchy-Riemann equation based approach highlighted in Chapter 3. The switch to tangential derivatives in both 2 and 3 dimensions is critical as it is this which transforms the system to a weakly singular form which allows explicit treatment of the singularity.

We have offered a choice of two methods, both of which allow the most singular part of the integral equation, which in any case is at worst weakly singular, to be integrated explicitly. The boundary element method provides an easy to implement

system which typically reaches engineering accuracy (3-4 s.f.) by typically solving a 100×100 system of equations. The Rayleigh-Ritz method is numerically more demanding, but in contrast achieves at least 5-6 s.f. by solving a 10×10 system.

The main advantage of these methods is that the switch to tangential derivatives produces simpler numerical schemes than traditional Cauchy-singular formulations. This is evident in our boundary element method where the switch means that no further special treatment is needed to evaluate the derivatives of the Green's function. The additional effort in the analysis for our other approach is rewarded by allowing us to employ the Rayleigh-Ritz method and to retain an exact formulation.

Chapter 6

Scattering of obliquely incident waves by a step of arbitrary profile

6.1 Introduction

In this chapter we show how the ideas from Chapter 5 may be used to tackle the more realistic, and substantially more demanding, problem of oblique scattering by a step of arbitrary profile. The problem of scattering by a step between two domains of constant but different depth is of great practical interest and continues to receive attention, even in two dimensions. A brief overview of the background to this problem is presented below.

Lamb [49] first dealt with the shallow-water (or very long wavelength) problem of wave scattering by a vertical step, an approach which is repeated in Mei [61]. Miles [62] used a variational approach to solve an eigenfunction matching technique to deal with this same problem and also introduced the scattering matrix formulation that we employ in these problems. Mei & Black [59] extended these ideas to deal with scattering by rectangular obstacles whereas Kirby & Dalrymple [46] solved the similar problem of oblique diffraction by a rectangular trench. Porter [73] revisited Miles' [62] problem developing Miles' eigenfunction approach and solving it by a Galerkin method. More recently Rhee [82] and [83] has looked at the transmission of oblique waves over a shelf to second-order. The natural extension of the vertical step is the linear slope joining two domains of different depth, a problem considered by Booij

[8] who used it to assess the accuracy of the mild slope equations. The Booij profile continues to be used as a canonical test of a wave scattering theory, see for example Ehrenmark & Williams [24].

Turning to arbitrary profiles, Evans & Linton [27] present a novel technique whereby the two-dimensional arbitrary step problem is mapped into a uniform strip where the effect of the step manifests itself as a more complicated free-surface condition which is then discretised, hence the step approximation. Athanassoulis & Belibassakis [3] present what is essentially an extended version of the mild slope equations with an additional term to deal with the bed slope to tackle with the two-dimensional scattering problem. Porter & Porter [77] tackle the two-dimensional problem by forming an integral equation and switching from normal to tangential derivatives to finally solve the integral equation by the Galerkin method. As for the ridge problem discussed in Chapter 5, the oblique arbitrary step scattering problem has, to the best of our knowledge, received no attention in the literature.

This chapter, investigating the scattering of obliquely incident waves by a step of arbitrary profile, provides a full generalisation of Porter & Porter's [77] equivalent problem for normal incidence. We keep our notation as close as possible to Porter & Porter's so that the nature of the extension is made as transparent as possible. Accordingly we solve this problem in its quasi two-dimensional formulation, switching to tangential derivatives using equation (5.3.27) which we deduced from the three-dimensional formulation of the oblique problem. This chapter therefore serves to illustrate how the ideas applied to a simple problem in Chapter 5 may be extended to more complicated, and physically more realistic, problems.

The significant difference from Chapter 5 is that, instead of a ridge of arbitrary profile, we now have a step of arbitrary profile joining two regions of constant, but different depth. The bed profile, which is uniform along the y axis, is determined by

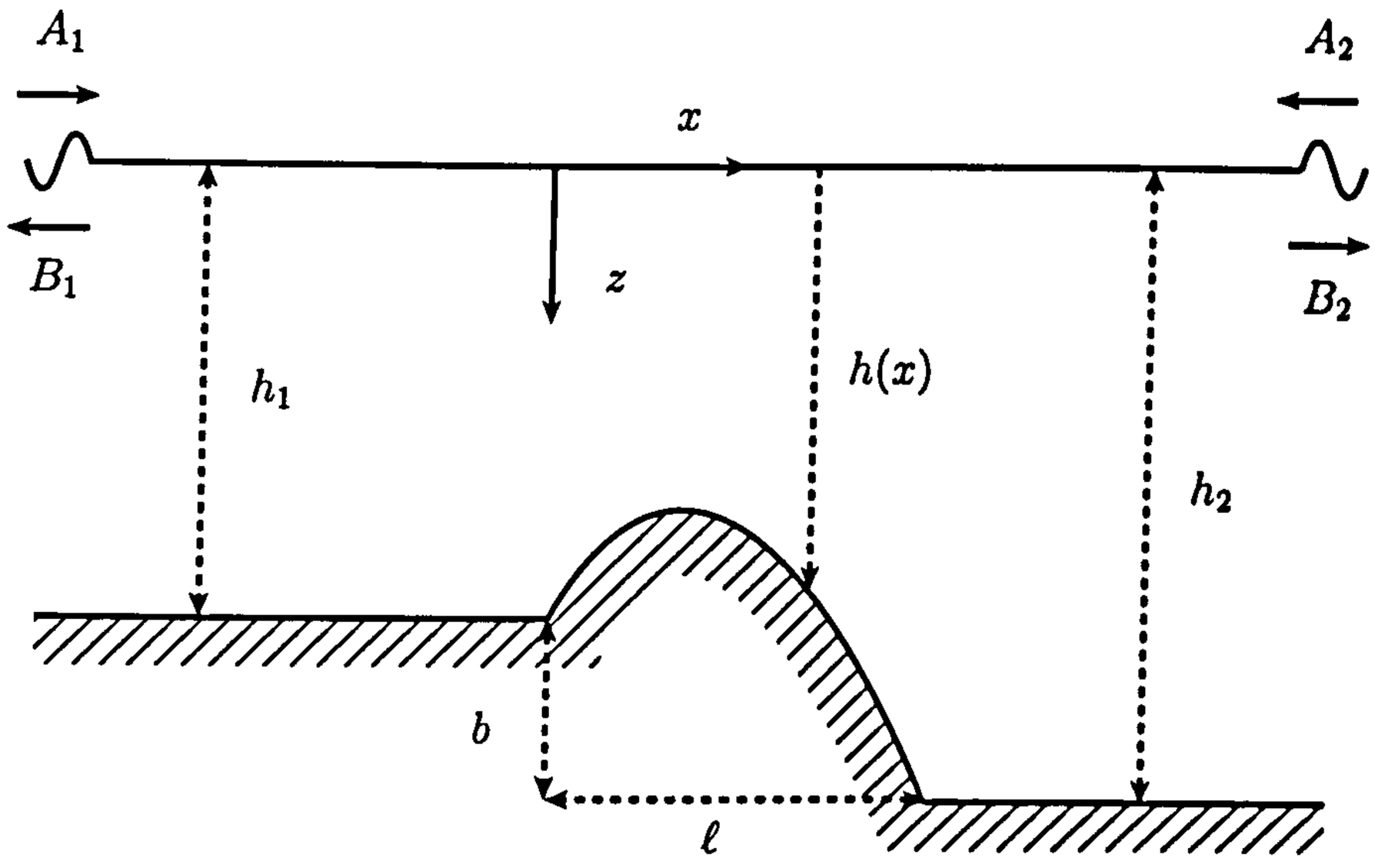

Figure 6.1: Geometrical description of the scattering problem for waves obliquely incident on an infinite step joining two domains of otherwise constant depth

$z = H(x)$ for $-\infty < x < \infty$ where

$$H(x) = \begin{cases} h_1, & x < 0, \\ h(x), & 0 \le x \le \ell, \\ h_2, & \ell \le x, \end{cases} \tag{6.1.1}$$

with h_1 and h_2 constant. We present the case of scattering by a step whose profile does not dip below the deeper of the two domains of constant depth. The case of a step with a depression is more complicated, but does not add any new understanding to the problem. By following the methods in this chapter and referring to Porter & Porter [77] the extension to a step with depression should be straightforward.

6.2 Formulation and preliminaries

We proceed as before having reduced the three-dimensional problem to a quasi two-dimensional problem. The boundary value problem we will solve is

$$(\nabla^2 - l^2)\phi = 0 \qquad \text{in } D : -\infty < x < \infty,\ 0 < z < H(x), \tag{6.2.1}$$

$$\frac{\partial \phi}{\partial z} + K\phi = 0 \qquad \text{on } z = 0 \tag{6.2.2}$$

with $K = \omega^2/g$ as usual,

$$\frac{\partial \phi}{\partial z} = 0 \qquad \text{on} \qquad \begin{cases} z = h_1 & x < 0 \\ z = h_2 & x > \ell \end{cases} \tag{6.2.3}$$

and

$$\frac{\partial \phi}{\partial n} = 0 \qquad \text{on } \Gamma : 0 < x < \ell,\ z = h(x). \tag{6.2.4}$$

We modify our notation from the previous chapter to recognise that we have two regions of differing constant depth. So, now the far field behaviour of ϕ is given by

$$\phi(x,z) \sim -\{A_1 \mathrm{e}^{\mathrm{i}\alpha_1 x} + B_1 \mathrm{e}^{-\mathrm{i}\alpha_1 x}\}\psi_{1,0}(z), \qquad x \to -\infty \tag{6.2.5}$$

$$\sim \{A_2 \mathrm{e}^{\mathrm{i}\alpha_2 x} + B_2 \mathrm{e}^{-\mathrm{i}\alpha_2 x}\}\psi_{2,0}(z), \qquad x \to \infty \tag{6.2.6}$$

where A_i and B_i are the wave amplitudes associated with incoming and outgoing waves (respectively) propagating at angles $\pm\theta_i$ to the x axis. Thus $\alpha_i = k_i \cos\theta_i$, $l = k_i \sin\theta_i$ are the components of the wavenumbers k_i, defined by the dispersion relations

$$K = k_i \tanh k_i h_i, \qquad i = 1, 2. \tag{6.2.7}$$

We also define the depth modes according to the depth of the region under consideration so that

$$\psi_{i,n} = N_{i,n}^{-1/2} \cos k_{i,n}(h_i - z), \qquad N_{i,n} = \frac{1}{2}\left(1 + \frac{\sin 2k_{i,n}h_i}{2k_{i,n}h_i}\right) \tag{6.2.8}$$

and

$$\alpha_{i,n} = \sqrt{l^2 + k_{i,n}^2}, \qquad \alpha_{i,0} = -\mathrm{i}\alpha_i \tag{6.2.9}$$

where $k_{i,0} = -\mathrm{i}k_i$ and $k_{i,n}$, $n = 1, \ldots$ are the positive roots of

$$K = -k_{i,n} \tan k_{i,n} h_i. \tag{6.2.10}$$

The principal unknown of this problem is the scattering matrix $\mathbf{S}$ introduced at (5.2.7) which given the form of the far-field in (6.2.5) and (6.2.6) takes the form

$$\mathbf{S} = \begin{pmatrix} R_1 & -T_2 \\ -T_1 & R_2 \end{pmatrix} \tag{6.2.11}$$

where $R_1 = B_1/A_1$, $T_1 = -B_2/A_1$, $R_2 = B_2/A_2$ and $T_1 = -B_2/A_1$. We note that to recover the transmission coefficients for the free surface displacements we must take into account the different depths into which the transmitted waves propagate so that

$$\tilde{T}_1 = T_1\psi_{2,0}(0)/\psi_{1,0}(0) \qquad \tilde{T}_2 = T_2\psi_{1,0}(0)/\psi_{2,0}(0),$$

see Miles [62].

Analogously to (5.2.20) we introduce a set of functions related to $\psi_{i,n}(z)$ by

$$\chi_{i,n}(z) = -k_{i,n}\int_{h_i}^{z}\psi_{i,n}(z')\,\mathrm{d}z' = N_{i,n}^{-1/2}\sin k_{i,n}(h_i - z), \qquad n = 0, 1, \ldots \tag{6.2.12}$$

with $k_{i,0} = -\mathrm{i}k_i$ implying

$$\chi_{i,0}(z) = -\mathrm{i}N_{i,0}^{-1/2}\sinh k_i(h_i - z), \tag{6.2.13}$$

The oblique incidence Green's functions g_i for regions of constant depth h_i are given by

$$g_i = \sum_{n=0}^{\infty}\frac{\psi_{i,n}(z)\psi_{i,n}(z_0)}{2\alpha_{i,n}h_i}\mathrm{e}^{-\alpha_{i,n}|x-x_0|}, \qquad (x,z) \neq (x_0,z_0) \tag{6.2.14}$$

as in (5.2.13) so that

$$g_i \sim \mathrm{i}\frac{\psi_{i,0}(z)\psi_{i,0}(z_0)}{2\alpha_i h_i}\mathrm{e}^{\mathrm{i}\alpha_i|x-x_0|}, \qquad |x - x_0| \to \infty. \tag{6.2.15}$$

6.3 Oblique scattering by a step of arbitrary profile

When the profile of the step does not dip below the depth of the deeper region of constant depth we solve the problem by considering two regions of constant depth and applying appropriate matching conditions at the intersection of the two regions. Region 1 is defined by $x < 0$, $0 < z < h_1$ and region 2 as $0 < x$, $0 < z < h_2$.

We start by defining a Green's function g_- where

$$g_- = g_1(x, z; x_0, z_0) + g_1(-x, z; x_0, z_0) \tag{6.3.1}$$

which satisfies (6.2.1) in $x < 0, 0 < z < h_1$, (6.2.2) on $z = 0, x < 0$, and (6.2.3) on $z = h_1, x < 0$. It is constructed so that

$$\frac{\partial g_-}{\partial x} = 0 \qquad \text{on } x = 0,\ 0 \le z \le h_1. \tag{6.3.2}$$

We now apply Green's identity to the domain $-X < x_0, x < 0,\ 0 < z < h_1$ and evaluate the limit $X \to \infty$ from (6.2.5) and (6.2.15) to give

$$\phi(x_0, z_0) = -2A_1 \cos(\alpha_1 x_0)\psi_{1,0}(z_0) + \int_0^{h_1} g_-(0, z; x_0, z_0)\phi_x(0, z)\,\mathrm{d}z,$$
$$x_0 < 0, 0 < z < h_1. \tag{6.3.3}$$

Then using the far-field forms of ϕ from (6.2.5) and g_1 from (6.2.15) in (6.3.3) we deduce that A_1 and B_1 are related by

$$B_1 = A_1 - \frac{\mathrm{i}}{\alpha_1 h_1}\int_0^{h_1} \psi_{1,0}(z)\phi_x(0, z)\,\mathrm{d}z. \tag{6.3.4}$$

Similarly we define a Green's function g_+ where

$$g_+ = g_2(x, z; x_0, z_0) + g_2(-x, z; x_0, z_0) \tag{6.3.5}$$

which satisfies (6.2.1) in $x > 0,\ 0 < z < h_2$, (6.2.2) on $z = 0, x > 0$, and (6.2.3) on $z = h_2,\ 0 < x$ and is constructed so that

$$\frac{\partial g_+}{\partial x} = 0 \qquad \text{on } x = 0,\ 0 \le z \le h_2. \tag{6.3.6}$$

Again we apply Green's identity, this time to the domain $0 < x_0, x < X,\ 0 < z < h_2$ and evaluate the limit $X \to \infty$ from (6.2.6) and (6.2.15) to give

$$\phi(x_0, z_0) = 2A_2 \cos(\alpha_2 x_0)\psi_{2,0}(z_0) - \int_0^{h_1} g_+(0, z; x_0, z_0)\phi_x(0, z)\,\mathrm{d}z$$
$$- \int_\Gamma \phi(x, z)\frac{\partial}{\partial n} g_+(x, z; x_0, z_0)\,\mathrm{d}s, \qquad 0 < x_0, 0 < z < H(x_0). \tag{6.3.7}$$

Then using the far-field forms of ϕ from (6.2.5) and g_2 from (6.2.15) in (6.3.7) we deduce that A_2 and B_2 are related by

$$B_2 = A_2 - \frac{\mathrm{i}}{\alpha_2 h_2}\int_0^{h_1} \psi_{2,0}(z)\phi_x(0, z)\,\mathrm{d}z - \frac{\mathrm{i}}{\alpha_2 h_2}\int_\Gamma \phi(x, z)\frac{\partial}{\partial n}(\psi_{2,0}(z)\cos\alpha_2 x)\,\mathrm{d}x. \tag{6.3.8}$$

We now find it convenient to decompose the Green's functions so that

$$g_i = g_i^0 + \widehat{g}_i \tag{6.3.9}$$

and consequently

$$g_\pm = g_\pm^0 + \widehat{g}_\pm \tag{6.3.10}$$

where

$$g_i^0 = \mathrm{i}\frac{\psi_{i,0}(z)\psi_{i,0}(z_0)}{2\alpha_i h_i}\cos\alpha_i(x - x_0) \tag{6.3.11}$$

and

$$\widehat{g}_i = -\frac{\psi_{i,0}(z)\psi_{i,0}(z_0)}{2\alpha_i h_i}\sin\alpha_i|x - x_0| + \sum_{n=1}^{\infty}\frac{\psi_{i,n}(z)\psi_{i,n}(z_0)}{2\alpha_{i,n}h_i}\mathrm{e}^{-\alpha_{i,n}|x-x_0|}. \tag{6.3.12}$$

Using (6.3.9) and (6.3.11) in (6.3.2) and (6.3.5), we deduce that

$$g_-^0(0, z; x_0, z_0) = \mathrm{i}\frac{\psi_{1,0}(z)\psi_{1,0}(z_0)}{\alpha_1 h_1}\cos\alpha_1 x_0 \tag{6.3.13}$$

and

$$g_+^0(0, z; x_0, z_0) = \mathrm{i}\frac{\psi_{2,0}(z)\psi_{2,0}(z_0)}{\alpha_2 h_2}\cos\alpha_2 x_0. \tag{6.3.14}$$

Then using (6.3.10), (6.3.13) and (6.3.4) in (6.3.3) we find that we may write

$$\phi(x_0, z_0) = -(A_1 + B_1)\cos(\alpha_1 x_0)\psi_{1,0}(z_0) + \int_0^{h_1}\widehat{g}_-(0, z; x_0, z_0)\phi_x(0, z)\,\mathrm{d}z,$$
$$x_0 < 0, 0 < z_0 < h_1 \tag{6.3.15}$$

and similarly, using (6.3.10), (6.3.14) and (6.3.8) in (6.3.7) we find

$$\phi(x_0, z_0) = (A_2 + B_2)\cos(\alpha_2 x_0)\psi_{2,0}(z_0) - \int_0^{h_1}\widehat{g}_+(0, z; x_0, z_0)\phi_x(0, z)\,\mathrm{d}z$$
$$- \int_\Gamma \phi(x, z)\frac{\partial}{\partial n}\widehat{g}_+(x, z; x_0, z_0)\,\mathrm{d}s, \qquad 0 < x_0,\ 0 < z < H(x_0). \tag{6.3.16}$$

Before proceeding further we convert the normal derivative in the integral along Γ in (6.3.16) to tangential derivatives using (5.3.23) to give

$$\phi(x_0, z_0) = (A_2 + B_2)\cos(\alpha_2 x_0)\psi_{2,0}(z_0) - \int_0^{h_1}\widehat{g}_+(0, z; x_0, z_0)\phi_x(0, z)\,\mathrm{d}z$$
$$- \int_\Gamma \phi(x, z)\left(-\frac{\partial}{\partial s}(\widehat{g}_+)_x^z(x, z; x_0, z_0) + \frac{l^2}{\sigma}(\widehat{g}_+)^z(x, z; x_0, z_0)\right)\mathrm{d}s,$$
$$0 < x_0,\ 0 < z < H(x_0). \tag{6.3.17}$$

We obtain our first integral equation by matching the expressions for $\phi(0,z_0)$ from (6.3.15) and (6.3.17) for $0 \le z_0 \le h_1$. The first step is to take the limit $x_0 \to 0$ in (6.3.17) and then integrate by parts by parts so that

$$\phi(0,z_0) = (A_2+B_2)\psi_{2,0}(z_0) - \int_0^{h_1} \widehat{g}_+(0,z;0,z_0)\phi_x(0,z)\,\mathrm{d}z$$
$$- \int_\Gamma \frac{\partial}{\partial s}\phi(x,z)(\widehat{g}_+)_x^z(x,z;0,z_0) + \phi(x,z)\frac{l^2}{\sigma}(\widehat{g}_+)^z(x,z;0,z_0)\,\mathrm{d}s,$$
$$0 \le z_0 \le h_1. \quad (6.3.18)$$

The free terms at the end of Γ vanish because $(\widehat{g}_+)^z(\ell,h_2;0,z_0)=0$ and likewise for $(\widehat{g}_+)_x^z$. The free terms at the beginning of Γ vanish because, from (3.3.16)

$$(\widehat{g}_+)_x^z(0,h_1;0,z_0) = \sum_{n=0}^{\infty} \frac{\chi_{2,n}(h_1)\psi_{2,n}(z_0)}{k_{2,n}h_2} = f(z_0) \equiv \begin{cases} 0, & 0<z_0<h_1, \\ 1, & h_1<z_0<h_2. \end{cases} \quad (6.3.19)$$

The fact that the value of the summation is undetermined at $z_0 = 0, h_1$ does not present a problem because we will solve the integral equations as integral operator equations in a Hilbert space which is required to be L_2 integrable. So this requirement is not affected by the summation only being defined almost everywhere (see for example Porter & Stirling [72] and Weir [102]). In fact we use (6.3.18) to define the values of $\phi(0,0)$ and $\phi(0,h_1)$, hence our extension of the range of validity to $0 \le z_0 \le h_1$.

Therefore matching (6.3.18) with (6.3.15) evaluated at $x_0 = 0$ we find, after some rearrangement

$$\int_0^{h_1} \{\widehat{g}_-(0,z;0,z_0) + \widehat{g}_+(0,z;0,z_0)\}\phi_x(0,z)\,\mathrm{d}z + \int_\Gamma \frac{\partial}{\partial s}\phi(x,z)(\widehat{g}_+)_x^z(x,z;0,z_0) + \cdots$$
$$+ \frac{l^2}{\sigma}(\widehat{g}_+)^z(x,z;0,z_0)\phi(x,z)\,\mathrm{d}s = (A_1+B_1)\psi_{1,0}(z_0) + (A_2+B_2)\psi_{2,0}(z_0),$$
$$0 \le z_0 \le h_1. \quad (6.3.20)$$

In order to simplify (6.3.20) and expose the structure of the integral equations we define

$$\left.\begin{aligned} p(x) &= \phi(s(x)), \quad (x,z)\in\Gamma, \\ q(z) &= \phi_x(0,z), \quad 0 \le z < h_1, \end{aligned}\right\} \quad (6.3.21)$$

so that $p'(x) = \sigma^{-1}\partial\phi/\partial s$ for $(x,z) \in \Gamma$. Then using (6.3.21) in (6.3.20) and with $\mathrm{d}s = \sigma(x)\,\mathrm{d}x$ for $(x,z) \in \Gamma$ we have

$$\int_0^{h_1} k_{11}(z_0,z)q(z)\,\mathrm{d}z + \int_0^{\ell} k_{12a}(z_0,x)p'(x) + l^2 k_{12b}(z_0,x)p(x)\,\mathrm{d}x = (A_1+B_1)\psi_{1,0}(z_0) + (A_2+B_2)\psi_{2,0}(z_0), \qquad 0 \le z_0 \le h_1, \quad (6.3.22)$$

where the real valued kernels are given by

$$k_{12a}(z_0,x) = (\widehat{g}_+)_x^z(x,h(x);0,z_0), \quad (6.3.23)$$

$$k_{12b}(z_0,x) = (\widehat{g}_+)^z(x,h(x);0,z_0) \quad (6.3.24)$$

and

$$k_{11}(z,z_0) = \widehat{g}_-(0,z;0,z_0) + \widehat{g}_+(0,z;0,z_0). \quad (6.3.25)$$

The explicit forms of the kernels (6.3.23) to (6.3.23) are given by

$$k_{12a}(z_0,x) = \frac{\mathrm{i}}{k_2 h_2}\psi_{2,0}(z_0)\chi_{2,0}(h(x))\cos(\alpha_2 x) + \sum_{n=1}^{\infty}\frac{\psi_{2,n}(z_0)\chi_{2,n}(h(x))}{k_{2,n}h_2}\mathrm{e}^{-\alpha_{2,n}x}, \quad (6.3.26)$$

$$k_{12b}(z_0,x) = \frac{\mathrm{i}}{\alpha_2 k_2 h_2}\psi_{2,0}(z_0)\chi_{2,0}(h(x))\sin(\alpha_2 x) - \sum_{n=1}^{\infty}\frac{\psi_{2,n}(z_0)\chi_{2,n}(h(x))}{\alpha_{2,n}k_{2,n}h_2}\mathrm{e}^{-\alpha_{2,n}x}, \quad (6.3.27)$$

and

$$k_{11}(z,z_0) = \sum_{n=1}^{\infty}\left\{\frac{\psi_{1,n}(z)\psi_{1,n}(z_0)}{\alpha_{1,n}h_1} + \frac{\psi_{2,n}(z)\psi_{2,n}(z_0)}{\alpha_{2,n}h_2}\right\}. \quad (6.3.28)$$

A second integral equation will be obtained by applying the bcd condition to (6.3.17), therefore as in Chapter 5, we extend the definitions of n_0 to field points off the curve and take the normal derivative to obtain

$$\frac{\partial}{\partial n_0}\phi(x_0,z_0) = (A_2+B_2)\frac{\partial}{\partial n_0}(\cos(\alpha_2 x_0)\psi_{2,0}(z_0)) - \frac{\partial}{\partial n_0}\int_0^{h_1}\widehat{g}_+(0,z;x_0,z_0)\phi_x(0,z)\mathrm{d}z - \frac{\partial}{\partial n_0}\int_\Gamma \phi(x,z)\left(-\frac{\partial}{\partial s}(\widehat{g}_+)_x^z(x,z;x_0,z_0) + \frac{l^2}{\sigma}(\widehat{g}_+)^z(x,z;x_0,z_0)\right)\mathrm{d}s, \quad 0 < x_0,\ 0 < z < H(x_0). \quad (6.3.29)$$

We now switch from normal to tangential derivatives using (5.3.36), so that

$$\frac{\partial}{\partial n_0}(\cos(\alpha_2 x_0)\psi_{2,0}(z_0)) = -\frac{\alpha_2}{k_2}\frac{\partial}{\partial s_0}(\mathrm{i}\chi_{2,0}(z_0)\sin(\alpha_2 x_0)) - \frac{l^2}{k_2\sigma_0}(\mathrm{i}\chi_{2,0}(z_0)\cos(\alpha_2 x_0)) \quad (6.3.30)$$

and also

$$\frac{\partial}{\partial n_0}\int_0^{h_1}\widehat{g}_+(0,z;x_0,z_0)\phi_x(0,z)\,\mathrm{d}z = -\frac{\partial}{\partial s_0}\int_0^{h_1}(\widehat{g}_+)^{z_0}_{x_0}(0,z;x_0,z_0)\phi_x(0,z)\,\mathrm{d}z + \frac{l^2}{\sigma_0}\int_0^{h_1}(\widehat{g}_+)^{z_0}(0,z;x_0,z_0)\phi_x(0,z)\,\mathrm{d}z. \quad (6.3.31)$$

The final term in (6.3.29) includes those appearing in (5.3.37) to (5.3.45) and so we do not repeat the details. We now move the field point onto the bed and apply the bed condition to give an integro-differential equation

$$\begin{aligned}0 = (A_2+B_2)&\left\{-\frac{\alpha_2}{k_2}\frac{\partial}{\partial s_0}(\mathrm{i}\chi_{2,0}(z_0)\sin(\alpha_2 x_0)) - \frac{l^2}{k_2\sigma_0}(\mathrm{i}\chi_{2,0}(z_0)\cos(\alpha_2 x_0))\right\}\\ &+\frac{\partial}{\partial s_0}\int_0^{h_1}(\widehat{g}_+)^{z_0}_{x_0}(0,z;x_0,z_0)\phi_x(0,z)\,\mathrm{d}z - \frac{l^2}{\sigma_0}\int_0^{h_1}(\widehat{g}_+)^{z_0}(0,z;x_0,z_0)\phi_x(0,z)\,\mathrm{d}z\\ &\quad+\frac{\partial}{\partial s_0}\int_\Gamma\left((\widehat{g}_+)^{zz_0}_{xx_0}(x,z;x_0,z_0)\frac{\partial\phi}{\partial s}+\frac{l^2}{\sigma}(\widehat{g}_+)^{zz_0}_{x_0}(x,z;x_0,z_0)\phi\right)\,\mathrm{d}s\\ &\quad-\frac{l^2}{\sigma_0}\int_\Gamma\left((\widehat{g}_+)^{zz_0}_{x}(x,z;x_0,z_0)\frac{\partial\phi}{\partial s}+\frac{l^2}{\sigma}(\widehat{g}_+)^{zz_0}(x,z;x_0,z_0)\phi\right)\,\mathrm{d}s\\ &\qquad+\frac{l^2}{\sigma_0}\phi(s_0)(h_2-h(x_0)) \qquad (x_0,z_0)\in\Gamma. \quad (6.3.32)\end{aligned}$$

This may be rewritten as

$$\begin{aligned}0 = (A_2+B_2)&\left\{-\frac{\alpha_2}{k_2}\frac{\partial}{\partial s_0}(\mathrm{i}\chi_{2,0}(z_0)\sin(\alpha_2 x_0)) - \frac{l^2}{k_2\sigma_0}(\mathrm{i}\chi_{2,0}(z_0)\cos(\alpha_2 x_0))\right\}\\ &+\frac{\partial}{\partial s_0}\int_0^{h_1}k_{21a}(x_0,z_0;z)q(z)\,\mathrm{d}z - \frac{l^2}{\sigma_0}\int_0^{h_1}k_{21b}(x_0,z_0;z)q(z)\,\mathrm{d}z\\ &\quad+\frac{\partial}{\partial s_0}\int_0^{\ell}\left(k_{22a}(x_0,z_0;z)p'(x)+l^2k_{22b}(x_0,z_0;z)p(x)\right)\,\mathrm{d}x\\ &\quad-\frac{l^2}{\sigma_0}\int_0^{\ell}\left(k_{22c}(x_0,z_0;z)p'(x)+l^2k_{22d}(x_0,z_0;z)p(x)\right)\,\mathrm{d}x\\ &\qquad+\frac{l^2}{\sigma_0}\phi(s_0)(h_2-h(x_0)), \qquad (x_0,z_0)\in\Gamma, \quad (6.3.33)\end{aligned}$$

where

$$\left.\begin{aligned}k_{21a}(x_0,z_0;z) &= (\widehat{g}_+)^{z_0}_{x_0}(0,z;x_0,z_0),\\ k_{21b}(x_0,z_0;z) &= (\widehat{g}_+)^{z_0}(0,z;x_0,z_0),\\ k_{22a}(x_0,z_0;x) &= (\widehat{g}_+)^{zz_0}_{xx_0}(x,h(x);x_0,z_0)\\ k_{22b}(x_0,z_0;x) &= (\widehat{g}_+)^{zz_0}_{x_0}(x,h(x);x_0,z_0),\\ k_{22c}(x_0,z_0;x) &= (\widehat{g}_+)^{zz_0}_{x}(x,h(x);x_0,z_0)\\ k_{22d}(x_0,z_0;x) &= (\widehat{g}_+)^{zz_0}(x,h(x);x_0,z_0),\end{aligned}\right\}(x_0,z_0)=\in\Gamma. \quad (6.3.34)$$

By comparing (6.3.34) with (6.3.23) and (6.3.24) it is immediately evident that

$$k_{21a}(x_0;x) = k_{12a}(z;x_0), \tag{6.3.35}$$

$$k_{21b}(x_0;x) = k_{12b}(z;x_0), \tag{6.3.36}$$

where, we have recognised that the arguments for $(x_0,z_0)\in\Gamma$ depend solely on x and x_0.

The explicit forms of the remaining kernels are

$$k_{22a}(x_0;x) = \frac{\chi_{2,0}(h(x))\chi_{2,0}(h(x_0))\alpha_2}{2h_2(k_2)^2}\{\sin\alpha_2|x-x_0| - \sin\alpha_2(x+x_0)\}$$
$$-\sum_{n=1}^{\infty}\frac{\chi_{2,n}(h(x))\chi_{2,n}(h(x_0))\alpha_{2,n}}{2h_2(k_{2,n})^2}\{\mathrm{e}^{-\alpha_{2,n}|x-x_0|} - \mathrm{e}^{-\alpha_{2,n}(x+x_0)}\}, \tag{6.3.37}$$

$$k_{22b}(x_0;x) = \frac{\chi_{2,0}(h(x))\chi_{2,0}(h(x_0))}{2h_2(k_2)^2}\{-\mathrm{sgn}(x-x_0)\cos\alpha_2|x-x_0| + \cos\alpha_2(x+x_0)\}$$
$$-\sum_{n=1}^{\infty}\frac{\chi_{2,n}(h(x))\chi_{2,n}(h(x_0))}{2h_2(k_{2,n})^2}\{-\mathrm{sgn}(x-x_0)\mathrm{e}^{-\alpha_{2,n}|x-x_0|} + \mathrm{e}^{-\alpha_{2,n}(x+x_0)}\}, \tag{6.3.38}$$

$$k_{22c}(x;x_0) = k_{22b}(x_0;x) \tag{6.3.39}$$

and

$$k_{22d}(x_0;x) = \frac{\chi_{2,0}(h(x))\chi_{2,0}(h(x_0))}{2\alpha_2 h_2(k_2)^2}\{\sin\alpha_2|x-x_0| + \sin\alpha_2(x+x_0)\}$$
$$+\sum_{n=1}^{\infty}\frac{\chi_{2,n}(h(x))\chi_{2,n}(h(x_0))}{2\alpha_{2,n}h_2(k_{2,n})^2}\{\mathrm{e}^{-\alpha_{2,n}|x-x_0|} + \mathrm{e}^{-\alpha_{2,n}(x+x_0)}\}. \tag{6.3.40}$$

Finally, as in Porter & Porter [77] we employ a more succinct notation to expose the structure of the integral equations. We keep our notation identical to that in Porter & Porter so the extension of the structure to the oblique case is clear. Thus we introduce integro-differential operators K_{ij} defined by

$$(K_{11}q)(z_0) = \int_0^{h_1} k_{11}(z_0,z)q(z)\,\mathrm{d}z, \tag{6.3.41}$$

$$(K_{12}p)(z_0) = \int_0^{\ell} k_{12a}(z_0,x)p'(x) + l^2 k_{12b}(z_0,x)p(x)\,\mathrm{d}x, \tag{6.3.42}$$

both defined for $0\le z_0\le h_1$ whereas, for $(x_0,z_0)\in\Gamma$, we have

$$(K_{21}q)(x_0) = -\frac{\partial}{\partial s_0}\int_0^{h_1} k_{21a}(x_0,z)q(z)\,\mathrm{d}z + \frac{l^2}{\sigma_0}\int_0^{h_1} k_{21b}(x_0,z)q(z)\,\mathrm{d}z \tag{6.3.43}$$

and

$$(K_{22}p)(x_0) = -\frac{\partial}{\partial s_0}\int_0^\ell \left(k_{22a}(x_0;x)p'(x) + l^2 k_{22b}(x_0;x)p(x)\right)\,\mathrm{d}x$$
$$+\frac{l^2}{\sigma_0}\int_0^\ell \left(k_{22c}(x_0;x)p'(x) + l^2 k_{22d}(x_0;x)p(x)\right)\,\mathrm{d}x - \frac{l^2}{\sigma_0}\phi(s_0)(h_0 - h(x_0)). \quad (6.3.44)$$

We also introduce the inner products

$$(q_1,q_2)_1 = \int_0^{h_1} q_1(z)\overline{q_2(z)}\,\mathrm{d}z, \qquad (p_1,p_2)_2 = \int_\Gamma p_1(s)\overline{p_2(s)}\,\mathrm{d}s. \quad (6.3.45)$$

If we now write

$$f_{1i}(z) = \psi_{i,0}(z), \qquad 0 \le z \le h_i, \quad i = 1,2, \quad (6.3.46)$$
$$f_{21}(s) = 0, \qquad (x,z) \in \Gamma \quad (6.3.47)$$
$$f_{22}(s) = -\frac{\mathrm{i}\alpha_2}{k_2}\frac{\partial}{\partial s}(\chi_{2,0}(z)\sin(\alpha_2 x)) - \frac{\mathrm{i}l^2}{k_2\sigma}(\chi_{2,0}(z)\cos(\alpha_2 x)) \quad (6.3.48)$$

then the integro-differential equations (6.3.22) and (6.3.33) may be rewritten as the operator equations

$$K_{11}q + K_{12}p = (A_1+B_1)f_{11} + (A_2+B_2)f_{12} \quad (6.3.49)$$
$$K_{21}q + K_{22}p = (A_1+B_1)f_{21} + (A_2+B_2)f_{22}. \quad (6.3.50)$$

These can be further simplified to the equation

$$\mathbf{K}\mathbf{v} = (A_1+B_1)\mathbf{f}_1 + (A_2+B_2)\mathbf{f}_2 \quad (6.3.51)$$

in $L_2(0,h_1)\oplus L_2(0,\ell)$ where

$$\mathbf{K} = \begin{pmatrix} K_{11} & K_{12} \\ K_{21} & K_{22} \end{pmatrix}, \qquad \mathbf{v} = \begin{pmatrix} q \\ p \end{pmatrix}, \qquad f_i = \begin{pmatrix} f_{1i} \\ f_{2i} \end{pmatrix} \quad (6.3.52)$$

and we define a composite inner product

$$\langle \mathbf{v}^{(1)}, \mathbf{v}^{(2)} \rangle = (q^{(1)}, q^{(2)})_1 + (p^{(1)}, p^{(2)})_2. \quad (6.3.53)$$

The solution of (6.3.51) is given by

$$\mathbf{v} = (A_1+B_1)\mathbf{v}^{(1)} + (A_2+B_2)\mathbf{v}^{(2)}, \quad (6.3.54)$$

where

$$\mathbf{K}\mathbf{v}^{(i)} = \mathbf{f}_i, \qquad i = 1, 2. \tag{6.3.55}$$

The equations (6.3.4) and (6.3.8) can now be written as

$$B_1 = A_1 - \frac{i}{\alpha_1 h_1}\langle \mathbf{v}, \mathbf{f}_1 \rangle, \qquad B_2 = A_2 - \frac{i}{\alpha_2 h_2}\langle \mathbf{v}, \mathbf{f}_2 \rangle, \tag{6.3.56}$$

so that, when we insert (6.3.54) into these expressions we find that the scattering matrix is given by

$$\mathbf{S} = (\mathbf{D} + \mathrm{i}\mathbf{V})^{-1}(\mathbf{D} - \mathrm{i}\mathbf{V}) \tag{6.3.57}$$

in which

$$\mathbf{D} = \begin{pmatrix} \alpha_1 h_1 & 0 \\ 0 & \alpha_2 h_2 \end{pmatrix}, \qquad \mathbf{V} = \begin{pmatrix} \langle \mathbf{v}^{(1)}, \mathbf{f}_1 \rangle & \langle \mathbf{v}^{(2)}, \mathbf{f}_1 \rangle \\ \langle \mathbf{v}^{(1)}, \mathbf{f}_2 \rangle & \langle \mathbf{v}^{(2)}, \mathbf{f}_2 \rangle \end{pmatrix}. \tag{6.3.58}$$

6.4 Approximation and numerical method

The integral equations we have derived extend those obtained for the normal incidence case to a more general oblique case. Therefore, although the equations involved for oblique incidence are inevitably more complicated than those for normal incidence, when framed as operator equations they possess the same overall structure. As we have kept our notation consistent with Porter & Porter [77] and our integro-differential equations in operator form have the same structure, we follow their discussion of the approximation exactly. Thus we seek to approximate the real quantities

$$\mathbf{V}_{ij} = \langle \mathbf{v}^{(i)}, \mathbf{f}_j \rangle, \qquad i, j = 1, 2, \tag{6.4.1}$$

where

$$\mathbf{K}\mathbf{v}^{(i)} = \mathbf{f}_i, \qquad i, j = 1, 2, \tag{6.4.2}$$

and $\mathbf{K}$ is a self-adjoint operator on $\mathcal{H} = L_2(0, h_1) \oplus L_2(0, \ell)$, which is equipped with an inner product $\langle ., . \rangle$.

The functional $J_2 : \mathcal{H} \times \mathcal{H} \to \mathbb{C}$ defined by

$$J_2(\mathbf{p}^{(1)}, \mathbf{p}^{(2)}) = \langle \mathbf{p}^{(1)}, \mathbf{f}_2 \rangle + \langle \mathbf{f}_1, \mathbf{p}^{(2)} \rangle - \langle \mathbf{K}\mathbf{p}^{(1)}, \mathbf{p}^{(2)} \rangle \tag{6.4.3}$$

is easily seen to be stationary at $\mathbf{p}^{(i)} = \mathbf{v}^{(i)}$, for $i = 1, 2$ and the stationary value is $J_2(\mathbf{v}^{(1)}, \mathbf{v}^{(2)}) = \mathbf{V}_{12} = \mathbf{V}_{21}$. The reduced functional $J_1 : \mathcal{H} \to \mathbb{R}$ where

$$J_1(\mathbf{p}^{(i)}) = \langle \mathbf{p}^{(i)}, \mathbf{f}_i \rangle + \langle \mathbf{f}_i, \mathbf{p}^{(i)} \rangle - \langle \mathbf{K}\mathbf{p}^{(i)}, \mathbf{p}^{(i)} \rangle \tag{6.4.4}$$

is also stationary at $\mathbf{p}^{(i)} = \mathbf{v}^{(i)}$, for $i = 1, 2$ and $J_1(\mathbf{v}^{(i)}) = \mathbf{V}_{ii}$ is the stationary value. We can therefore obtain estimates $\tilde{\mathbf{V}}_{i,j}$ say of $\mathbf{V}_{i,j}$ by approximating $\mathbf{v}^{(i)}$ by $\tilde{\mathbf{v}}^{(i)} \in \mathcal{H}_{N+1}$, a chosen $N+1$ dimensional subspace of $\mathcal{H}$; these will be second-order accurate in the sense that

$$|\mathbf{V}_{ij} - \tilde{\mathbf{V}}_{ij}| = O(||\mathbf{v}^{(i)} - \tilde{\mathbf{v}}^{(i)}||\ ||\mathbf{v}^{(i)} - \tilde{\mathbf{v}}^{(i)}||). \tag{6.4.5}$$

Suppose then that $\mathcal{H}_{N+1}$ is spanned by the given functions $\mathbf{p}_0, \ldots, \mathbf{p}_N$, and hence that

$$\tilde{\mathbf{v}}^{(i)} = \sum_{n=0}^{N} c_n^{(i)} \mathbf{p}_n, \qquad i = 1, 2. \tag{6.4.6}$$

Then the stationary points $\tilde{\mathbf{v}}^{(i)} \approx \mathbf{v}^{(i)}$ of both $J_1(\tilde{\mathbf{v}}^{(i)})$ and $J_2(\tilde{\mathbf{v}}^{(1)}, \tilde{\mathbf{v}}^{(2)})$ are given by solving

$$\langle \mathbf{K}\tilde{\mathbf{v}}^{(i)} - \mathbf{f}_i, \mathbf{p}_m \rangle = 0, \qquad m = 0, \ldots, N, \tag{6.4.7}$$

for $c_0^{(i)}, \ldots c_N^{(i)}$ with $i = 1, 2$. The equations (6.4.6) and (6.4.7) are also equivalent to Galerkin's method in this case. Combining them gives a system which determines the coefficients in (6.4.6) explicitly in the form

$$\sum_{n=0}^{N} c_n^{(i)} \langle \mathbf{K}\mathbf{p}_n, \mathbf{p}_m \rangle = \langle \mathbf{f}_i, \mathbf{p}_m \rangle, \qquad m = 0, \ldots, N, \tag{6.4.8}$$

for $i = 1, 2$. The approximations to $\mathbf{V}_{ij}$ are given by

$$\tilde{\mathbf{V}}_{ij} = \sum_{n=0}^{N} c_n^{(i)} \langle \mathbf{p}_n, \mathbf{f}_j \rangle, \qquad i, j = 1, 2. \tag{6.4.9}$$

We now present the implementation of this approximation for which it is clearer to revert to a system which considers the components relating to $q(z)$ and $p(s)$ separately. Thus, instead of (6.4.6) we write

$$\left.\begin{aligned} \tilde{q}^{(i)}(z) &= \sum_{n=0}^{N_1} c_n^{(1i)} q_n(z) \quad 0 < z < h_1 \\ \tilde{p}^{(i)}(s) &= \sum_{n=0}^{N_2} c_n^{(2i)} p_n(s) \quad s \in \Gamma \end{aligned}\right\} \qquad i = 1, 2, \tag{6.4.10}$$

where the choice of test functions $\{q_n\}$ and p_n remains arbitrary, but will be discussed later, and the coefficients $c_n^{(1i)}$ and $c_n^{(2i)}$ are to be determined.

Once we apply the Galerkin approximation (6.4.8) to our system, the resulting matrix system inevitably differs from Porter & Porter's due to our differing definitions of the underlying integral operators. Thus, from here on we diverge from Porter & Porter's exposition.

Before we apply the Galerkin approximation (6.4.8) we define additional terms which we shall use to show the structure of the integral equations. Again we try to keep our notation consistent with Porter & Porter's thus we define

$$F_{nr}^{(1i)} = (q_n, \psi_{i,r})_1, \qquad r = 0, 1, 2, \ldots, \qquad n = 0, 1, \ldots, N_1, \qquad i = 1, 2 \quad (6.4.11)$$

and

$$E_{nr}^{(22)} = \int_0^\ell \chi_{2,r}(h(x)) \mathrm{e}^{-\alpha_{2,r}x} p_n(x)\, \mathrm{d}x, \qquad r = 1, 2, \ldots, \quad n = 0, 1, \ldots, N_1, \quad (6.4.12)$$

$$F_{nr}^{(22)} = \int_0^\ell \chi_{2,r}(h(x)) \mathrm{e}^{-\alpha_{2,r}x} p_n'(x)\, \mathrm{d}x, \qquad r = 1, 2, \ldots, \quad n = 0, 1, \ldots, N_1. \quad (6.4.13)$$

The term $F_{nr}^{(ij)}$ correspond to the equivalently named terms in Porter & Porter, whereas $E_{nr}^{(22)}$ is a new term arising from the obliqueness. We also define

$$a_n = \int_0^\ell \mathrm{i}\chi_{2,0}(h(x)) \sin(\alpha_2 x) p_n'(x)\, \mathrm{d}x, \qquad n = 0, 1, \ldots, N_1, \quad (6.4.14)$$

$$b_n = \int_0^\ell \mathrm{i}\chi_{2,0}(h(x)) \cos(\alpha_2 x) p_n'(x)\, \mathrm{d}x, \qquad n = 0, 1, \ldots, N_1, \quad (6.4.15)$$

$$d_n = \int_0^\ell \mathrm{i}\chi_{2,0}(h(x)) \sin(\alpha_2 x) p_n(x)\, \mathrm{d}x, \qquad n = 0, 1, \ldots, N_1, \quad (6.4.16)$$

$$e_n = \int_0^\ell \mathrm{i}\chi_{2,0}(h(x)) \cos(\alpha_2 x) p_n(x)\, \mathrm{d}x, \qquad n = 0, 1, \ldots, N_1, \quad (6.4.17)$$

where the a_n and b_n correspond to the equivalent terms in Porter & Porter and the d_n and e_n are additional terms arising from the obliqueness. Then, the Galerkin approximation transforms the system into a coupled system of equations for the

unknown coefficients which is given by

$$\sum_{n=0}^{N_1} c_n^{(1i)} K_{mn}^{(11)} + \sum_{n=0}^{N_2} c_n^{(2i)} K_{mn}^{(12)} = F_{m0}^{(1i)}, \quad m = 0, \ldots, N_1 \tag{6.4.18}$$

$$\sum_{n=0}^{N_1} c_n^{(1i)} K_{mn}^{(21)} + \sum_{n=0}^{N_2} c_n^{(2i)} K_{mn}^{(22)} = F_{m0}^{(2i)}, \quad m = 0, \ldots, N_2 \tag{6.4.19}$$

for $i = 1, 2$, and from (6.4.9)

$$\tilde{\mathbf{V}}_{ij} = \sum_{n=0}^{N_1} c_n^{(1i)} F_{n0}^{(1j)} + \sum_{n=0}^{N_2} c_n^{(2i)} F_{n0}^{(2j)}, \qquad i, j = 1, 2. \tag{6.4.20}$$

The elements of the system are defined as follows

$$\left.\begin{array}{lll} K_{mn}^{(11)} = (K_{11} q_n, q_m)_1, & m, n = 0, \ldots, N_1, & \\ K_{mn}^{(12)} = (K_{12} p_n, q_m)_1, & m = 0, \ldots, N_1, & n = 0, \ldots, N_2, \\ K_{mn}^{(21)} = K_{nm}^{(12)} & m = 0, \ldots, N_2, & n = 0, \ldots, N_1, \\ K_{mn}^{(22)} = (K_{22} p_n, p_m)_2, & m, n = 0, \ldots, N_2, & \\ F_{mr}^{(1i)} = (\psi_{i,r}, q_m)_1, & m = 0, \ldots, N_1, & \\ F_{m0}^{(2i)} = (f_{2i}, p_m)_2, & m = 0, \ldots, N_2, & \end{array}\right\} \tag{6.4.21}$$

We note from (6.3.47) that $F_{m0}^{(21)} = 0$ and on using (6.4.14) and (6.4.17) that

$$F_{m0}^{(22)} = \frac{\alpha_2}{k_2} a_n - \frac{l^2}{k_2} e_n, \tag{6.4.22}$$

where to obtain this last result we have integrated by parts once and projected the integral onto the x axis as we are, by now, well used to doing.

We can now expose the structure of the individual kernels so that

$$K_{mn}^{(11)} = \sum_{r=1}^{\infty} \left\{ \frac{F_{nr}^{(11)} F_{mr}^{(11)}}{\alpha_{1,r} h_1} + \frac{F_{nr}^{(12)} F_{mr}^{(12)}}{\alpha_{2,r} h_2} \right\} \tag{6.4.23}$$

and

$$K_{mn}^{(12)} = K_{nm}^{(21)} = \frac{b_n F_{m0}^{(12)}}{k_2 h_2} + \frac{l^2 d_n F_{m0}^{(12)}}{\alpha_2 k_2 h_2} + \sum_{r=1}^{\infty} \left\{ \frac{F_{nr}^{(22)} F_{mr}^{(12)}}{k_{2,r} h_2} - \frac{l^2 E_{nr}^{(22)} F_{mr}^{(12)}}{\alpha_{2,r} k_{2,r} h_2} \right\}. \tag{6.4.24}$$

The matrix $K_{mn}^{(22)}$ is composed of five individual kernels so that

$$K_{mn}^{(22)} = K_{mn}^{(22a)} + l^2 (K_{mn}^{(22b)} + K_{mn}^{(22c)}) + l^4 K_{mn}^{(22d)} - l^2 K_{mn}^{(22e)} \tag{6.4.25}$$

where

$$K_{mn}^{(22a)} = \int_0^\ell \int_0^\ell k_{22a}(x;x_0)p_n'(x)p_m'(x_0)\,\mathrm{d}x\,\mathrm{d}x_0, \tag{6.4.26}$$

$$K_{mn}^{(22b)} = \int_0^\ell \int_0^\ell k_{22b}(x;x_0)p_n(x)p_m'(x_0)\,\mathrm{d}x\,\mathrm{d}x_0, \tag{6.4.27}$$

$$K_{mn}^{(22c)} = \int_0^\ell \int_0^\ell k_{22c}(x;x_0)p_n'(x)p_m(x_0)\,\mathrm{d}x\,\mathrm{d}x_0, \tag{6.4.28}$$

$$K_{mn}^{(22d)} = \int_0^\ell \int_0^\ell k_{22d}(x;x_0)p_n(x)p_m(x_0)\,\mathrm{d}x\,\mathrm{d}x_0, \tag{6.4.29}$$

$$K_{mn}^{(22e)} = \int_0^\ell (h_2 - h(x_0))p_n(x_0)p_m(x_0)\,\mathrm{d}x_0, \tag{6.4.30}$$

and in these last results we have integrated by parts where appropriate and projected all integrals onto the x axis. We note that (6.4.26) to (6.4.30) correspond to equations (5.4.24) to (5.4.28).

For completeness the structure of the remaining elements is

$$K_{mn}^{(22a)} = -w_{mn}^{(a)} - e_{mn}^{(a)} + \frac{\alpha_2}{k_2}\frac{a_nb_m + a_mb_n}{2k_2h_2} + \sum_{r=1}^{\infty}\frac{\alpha_{2,r}}{k_{2,r}}\frac{F_{nr}^{(22)}F_{mr}^{(22)}}{2k_{2r}h_2} \tag{6.4.31}$$

$$K_{mn}^{(22b)} = w_{mn}^{(b)} + e_{mn}^{(b)} + \frac{d_na_m - e_nb_m}{2(k_2)^2h_2} - \sum_{r=1}^{\infty}\frac{E_{nr}^{(22)}F_{mr}^{(22)}}{2(k_{2r})^2h_2} \tag{6.4.32}$$

$$K_{mn}^{(22d)} = -w_{mn}^{(d)} + e_{mn}^{(d)} - \frac{d_ne_m + d_me_n}{2\alpha_2(k_2)^2h_2} + \sum_{r=1}^{\infty}\frac{E_{nr}^{(22)}E_{mr}^{(22)}}{2\alpha_{2,r}(k_{2r})^2h_2} \tag{6.4.33}$$

where we define

$$w_{mn}^{(a)} = \frac{\alpha_2}{2(k_2)^2h_2}\int_0^\ell \mathrm{i}\chi_{2,0}(h(x_0))p_m'(x_0)\int_0^\ell \mathrm{i}\chi_{2,0}(h(x))\sin(\alpha_2|x-x_0|)p_n'(x)\,\mathrm{d}x\,\mathrm{d}x_0, \tag{6.4.34}$$

$$w_{mn}^{(b)} = \frac{1}{2(k_2)^2h_2}\int_0^\ell \mathrm{i}\chi_{2,0}(h(x_0))p_m'(x_0)\int_0^\ell \mathrm{i}\chi_{2,0}(h(x))\mathrm{sgn}\cos(\alpha_2|x-x_0|)p_n(x)\,\mathrm{d}x\,\mathrm{d}x_0, \tag{6.4.35}$$

$$w_{mn}^{(d)} = \frac{1}{2\alpha_2(k_2)^2h_2}\int_0^\ell \mathrm{i}\chi_{2,0}(h(x_0))p_m(x_0)\int_0^\ell \mathrm{i}\chi_{2,0}(h(x))\sin(\alpha_2|x-x_0|)p_n(x)\,\mathrm{d}x\,\mathrm{d}x_0, \tag{6.4.36}$$

and

$$e^{(a)}_{mn} = \sum_{r=1}^{\infty} \frac{\alpha_{2,r}}{2(k_{2,r})^2 h_2} \int_0^{\ell} \chi_{2,r}(h(x_0)) p'_m(x_0) \int_0^{\ell} \chi_{2,r}(h(x)) \mathrm{e}^{-\alpha_{2,r}|x-x_0|} p'_n(x)\, \mathrm{d}x\, \mathrm{d}x_0, \tag{6.4.37}$$

$$e^{(b)}_{mn} = \sum_{r=1}^{\infty} \frac{1}{2(k_{2,r})^2 h_2} \int_0^{\ell} \chi_{2,r}(h(x_0)) p'_m(x_0) \int_0^{\ell} \chi_{2,r}(h(x)) \mathrm{sgn}\, \mathrm{e}^{-\alpha_{2,r}|x-x_0|} p_n(x)\, \mathrm{d}x\, \mathrm{d}x_0, \tag{6.4.38}$$

$$e^{(d)}_{mn} = \sum_{r=1}^{\infty} \frac{1}{2\alpha_{2,r}(k_{2,r})^2 h_2} \int_0^{\ell} \chi_{2,r}(h(x_0)) p_m(x_0) \int_0^{\ell} \chi_{2,r}(h(x)) \mathrm{e}^{-\alpha_{2,r}|x-x_0|} p_n(x)\, \mathrm{d}x\, \mathrm{d}x_0. \tag{6.4.39}$$

and for compactness we have written sgn for $\mathrm{sgn}(x - x_0)$.

6.5 Boundary element approach

As usual it is possible to solve the integral equations via the boundary element approach and we proceed to do so in order to provide an independent check on the results from the Rayleigh-Ritz approach. In this case we subdivide the vertical boundary $x = 0,\ z \in [0, h_1]$ into N_1 panels and the horizontal axis defined by $x \in [0, \ell]$ into N_2 panels. The process follows in a similar manner to before therefore we just present the key steps. Firstly we define some notation

$$I_m = [(m-1)h_1/N_1, mh_1/N_1] \qquad m = 1, \ldots, N_1, \tag{6.5.1}$$

$$I_n = [(n-1)\ell/N_2, n\ell/N_2] \qquad n = 1, \ldots, N_2, \tag{6.5.2}$$

$$z_j = (j - 0.5)h_1/N_1 \qquad j = 1, \ldots, N_1, \tag{6.5.3}$$

$$x_i = (i - 0.5)\ell/N_2 \qquad i = 1, \ldots, N_2, \tag{6.5.4}$$

$$h_i = h(x_i) \qquad i = 1, \ldots, N_2, \tag{6.5.5}$$

$$\psi^j_{10} = \psi_{1,0}(z_j), \tag{6.5.6}$$

$$\psi^j_{20} = \psi_{2,0}(z_j) \tag{6.5.7}$$

and we collocate assuming that the quantities of interest, are constant over a panel so that

$$\frac{\partial \phi}{\partial x}(0, z_m) = q_m \qquad m = 1, \ldots, N_1 \tag{6.5.8}$$

and

$$\phi(x_n, h_n) = p_n \qquad n = 1, \ldots, N_2. \tag{6.5.9}$$

Our first boundary element equation is derived from equation matching (6.3.15) and (6.3.17) on $x_0 = 0$ so that, after some manipulation which we are now used to we have

$$\sum_{m=1}^{N_1} K_{jm}^{(11)} q_m + \sum_{n=1}^{N_2} K_{jn}^{(12)} p_n = (A_1 + B_1)\psi_{10}^j + (A_2 + B_2)\psi_{20}^j \qquad j = 1, \ldots, N_1 \tag{6.5.10}$$

where

$$K_{jm}^{(11)} = \int_{I_m} g_-(0, z, 0, z_j) + g_+(0, z, 0, z_j)\, \mathrm{d}z \tag{6.5.11}$$

and

$$K_{jn}^{(12)} = [-g_+ {}_x^z(x, h(x); 0, z_j)]_{I_n} + l^2 \int_{I_n} g_+^z(x, h(x); 0, z_j)\, \mathrm{d}x. \tag{6.5.12}$$

Our second boundary element equation is found from (6.3.17) so that

$$\sum_{m=1}^{N_1} K_{im}^{(21)} q_m + \sum_{n=1}^{N_2} K_{in}^{(22)} p_n = (A_2 + B_2)\cos\alpha_2 x_i \psi_{20}(h_i) \qquad i = 1, \ldots, N_2 \tag{6.5.13}$$

where

$$K_{im}^{(21)} = \int_{I_m} g_+(0, z, x_i, h_i)\, \mathrm{d}z \tag{6.5.14}$$

and

$$K_{jn}^{(22)} = \delta_{ij} + [-g_+ {}_x^z(x, h(x); x_i, h_i)]_{I_n} + l^2 \int_{I_n} g_+^z(x, h(x); x_i, h_i)\, \mathrm{d}x. \tag{6.5.15}$$

We combine these into one system so that

$$\underline{\underline{\mathbf{K}}}.\mathbf{v} = (A_1 + B_1)\mathbf{f_1} + (A_2 + B_2)\mathbf{f_2} \tag{6.5.16}$$

where

$$\underline{\underline{\mathbf{K}}} = \begin{pmatrix} K_{11}^{(11)} & \dots & K_{1N_1}^{(11)} & K_{11}^{(12)} & \dots & K_{1N_2}^{(11)} \\ \vdots & \ddots & \vdots & \vdots & \ddots & \vdots \\ K_{N_1 1}^{(11)} & \dots & K_{N_1 N_1}^{(11)} & K_{N_1 1}^{(11)} & \dots & K_{N_1 N_2}^{(11)} \\ K_{11}^{(21)} & \dots & K_{1N_1}^{(21)} & K_{11}^{(22)} & \dots & K_{1N_2}^{(22)} \\ \vdots & \ddots & \vdots & \vdots & \ddots & \vdots \\ K_{N_2 1}^{(21)} & \dots & K_{N_2 N_1}^{(21)} & K_{N_2 1}^{(22)} & \dots & K_{N_2 N_2}^{(22)} \end{pmatrix}, \tag{6.5.17}$$

$$\mathbf{v} = \begin{pmatrix} q_1 \\ \vdots \\ q_{N_1} \\ \\ p_1 \\ \vdots \\ p_{N_2} \end{pmatrix}, \quad \mathbf{f_1} = \begin{pmatrix} \psi_{10}^1 \\ \vdots \\ \psi_{10}^{N_1} \\ \\ 0 \\ \vdots \\ 0 \end{pmatrix} \quad \text{and} \quad \mathbf{f_2} = \begin{pmatrix} \psi_{20}^1 \\ \vdots \\ \psi_{20}^{N_1} \\ \\ \cos(\alpha_2 x_1)\psi_{20}(h_1) \\ \vdots \\ \cos(\alpha_2 x_{N_2})\psi_{20}(h_{N_2}) \end{pmatrix}. \tag{6.5.18}$$

In this form we see that the system has an identical structure to that in (6.3.51) and (6.3.52) and therefore it is now routine to deduce the scattering coefficients by following (6.3.54) to (6.3.58).

6.6 Results

In the results that follow we use the Legendre polynomials to model the bed flux along the varying slope. This is in contrast to Porter & Porter [77] who suggest the Jacobi polynomials for profiles which do not join the domains of constant depth smoothly at the end points. The discussion in Porter & Porter [77] concerning convergence of the system according to the choice of trial functions carries forward to the oblique problem unchanged, therefore we will not labour this point further. We would anticipate slower convergence rates with the choice of Legendre functions for non-smooth joins rather than a set which incorporated the singular behaviour at the end points and our numerical experiments confirmed this. In all of the results we non-dimensionalise the profile of the step by using the transformation

$$\hat{h}(x) = (h_2 - h(\ell x))/b, \qquad 0 \le x \le 1, \qquad b = h_2 - h_1, \tag{6.6.1}$$

so that $\hat{h}(0) = 1$ and $\hat{h}(1) = 0$.

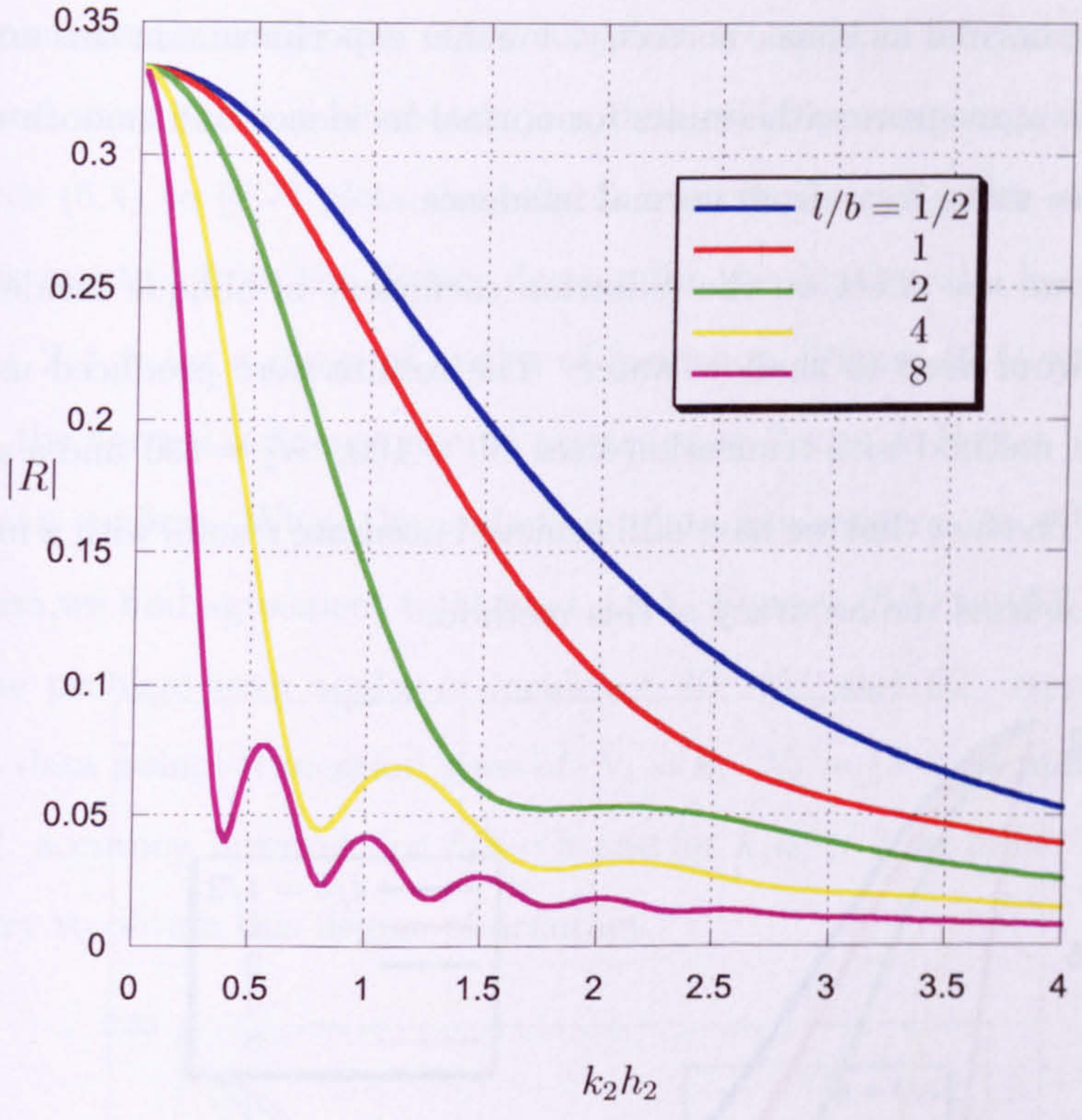

Figure 6.2: Reflection coefficient, $|R_2|$, against wavenumber k_2h_2 for almost normal incidence ($\theta = 0.01°$) to the plane slope profile $\hat{h}(x) = 1 - x$, $h_1/h_2 = \frac{1}{4}$ for various values of l/b as indicated in the legend.

Figure 6.2 shows the reflection coefficients for the linear sloping profile $\hat{h}(x) = 1-x$ as in Porter & Porter [77], figure 5 where we have used identical parameters and are very close to normal incidence ($\theta = 0.01°$). We note that for exactly normal incidence, with some minor modification to the trial functions our formulation reduces exactly to that in Porter & Porter [77]. Accordingly we present results for almost normal incidence to demonstrate that our results approach those for normal incidence in the limit. In fact figure 6.2 (produced using Legendre polynomials and $N_1 = 10$, $N_2 = 15$) is identical to the published results for normal incidence, with the data points agreeing to at least 4 s.f. with the published results. The high truncation sizes were chosen to ensure accurate results for the case of $l/b = 8$. We note also that the boundary element results agree with the published results to 3 s.f. using truncation sizes $N_1 = 100$, $N_2 = 100$. This extreme case confirms that both of our

methods deal with normal incidence correctly. Further experiments on this and other topographies show agreement with results for normal incidence and smooth changes to the curves as we move away from normal incidence.

Figure 6.3 shows the effect on the reflection coefficient of oblique incidence, for waves travelling from deep to shallow water. The results were produced using the boundary element method with truncation sizes $N_1 = 100$, $N_2 = 100$ and a step-size of $\delta k_2 h_2 = 0.05$. The fact that we have still achieved accurate results with a moderate trial space size confirms the accuracy of this method.

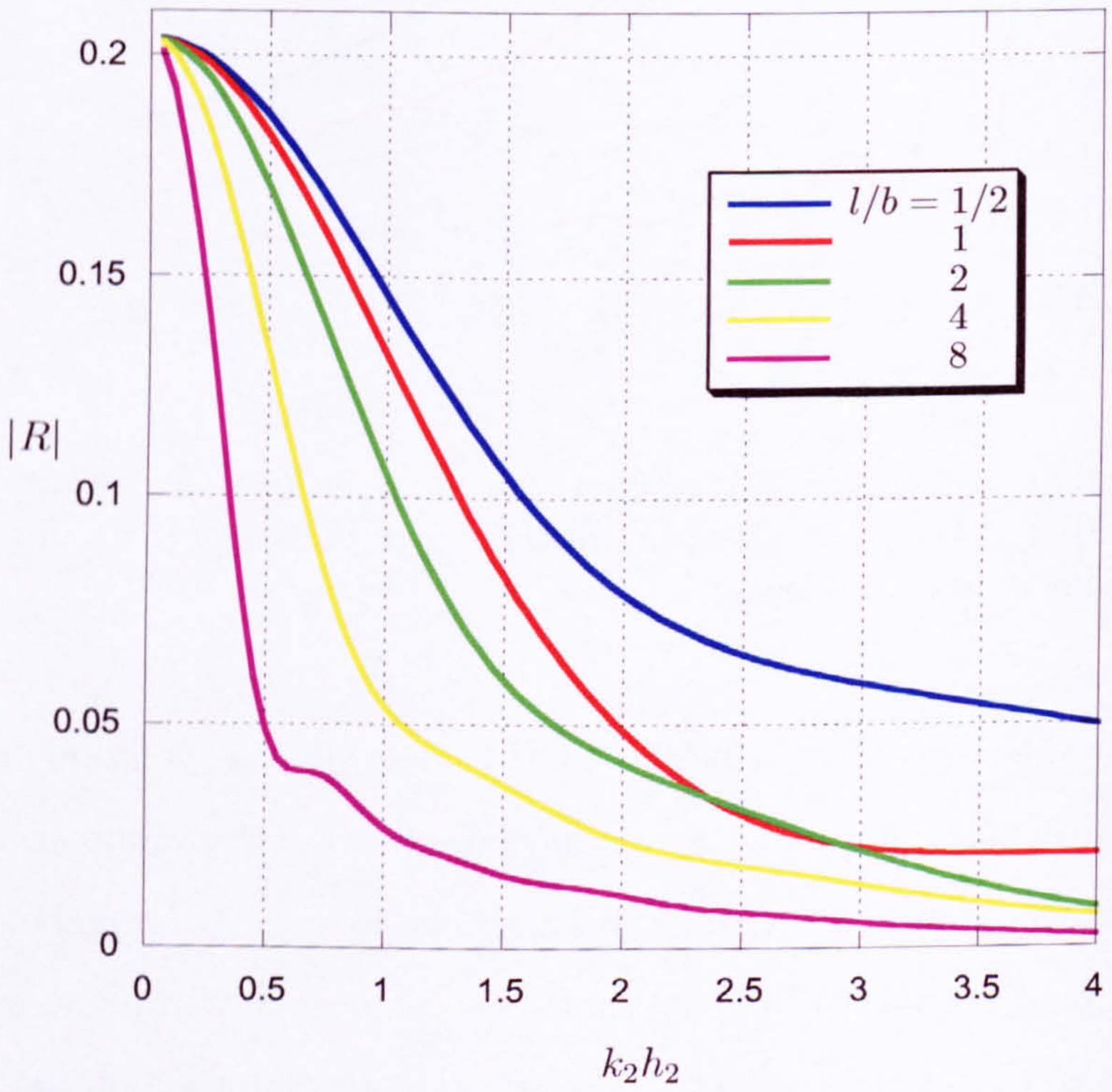

Figure 6.3: Reflection coefficient, $|R_2|$, against wavenumber k_2h_2 for $\theta = 45°$ incidence to the plane slope profile $\hat{h}(x) = 1 - x$, $h_1/h_2 = \frac{1}{4}$ for various values of l/b as indicated in the legend.

We now consider results for a smoothly varying bed form defined by

$$\hat{h}(x) = 1 - 3x^2 + 2x^3 \tag{6.6.2}$$

which joins the domains of constant depth smoothly. In this case the choice of Leg-

endre polynomials (as would any other complete set such as a Fourier series) is appropriate and, now there is a smooth join, has rapid convergence with truncation size. Figures (6.4) to (6.7) plots the reflection coefficient $|R_2|$ for oblique scattering of waves incident from the deeper domain for the depth ratio $h_1/h_2 = 1/4$ and $\ell/b = 1/2, 1, 2, 4, 8$ for a range of angles of incidence. Figure (6.4) where $\theta = 0.1°$ agrees with the normal incidence results presented in Porter & Porter [77] as a visual inspection can confirm. When the underlying data is compared, as with the infinite ridge problem,we find agreement to at least 4 s.f.. Figures (6.5) to (6.7) show results for the same problem with angles of incidence $30°, 45°$ and $60°$ respectively. For most of the data points truncation sizes of $N_1 = 8,\ N_2 = 12$ were sufficient to give at least 4 s.f. accuracy, however, for $\ell/b = 8$ and for $k_1 h_1 > 3$ we found that $N_2 = 15$ was necessary to obtain this degree of accuracy.

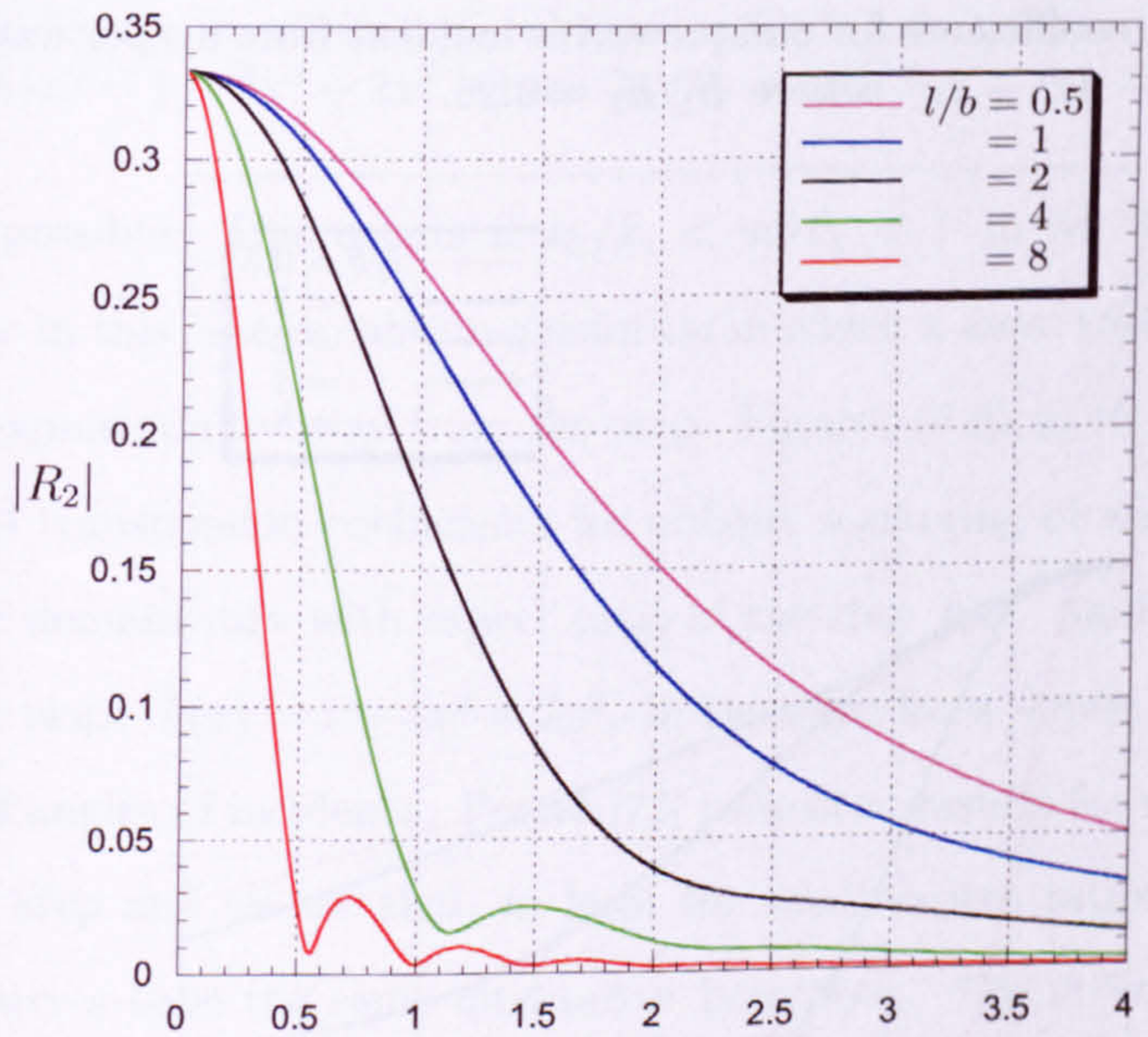

Figure 6.4: Reflection coefficients for oblique waves incident from deeper water at $0.1°$ to the step $\hat{h}(x) = 1 - 3x^2 + 2x^3$ where $h_1/h_2 = 0.25$.

Using $l = k_i \sin\theta_i$ which in turn implies $k_1 \sin\theta_1 = k_2 \sin\theta_2$ the famous Snell's law of refraction, we find that for waves travelling from shallow to deeper water, total

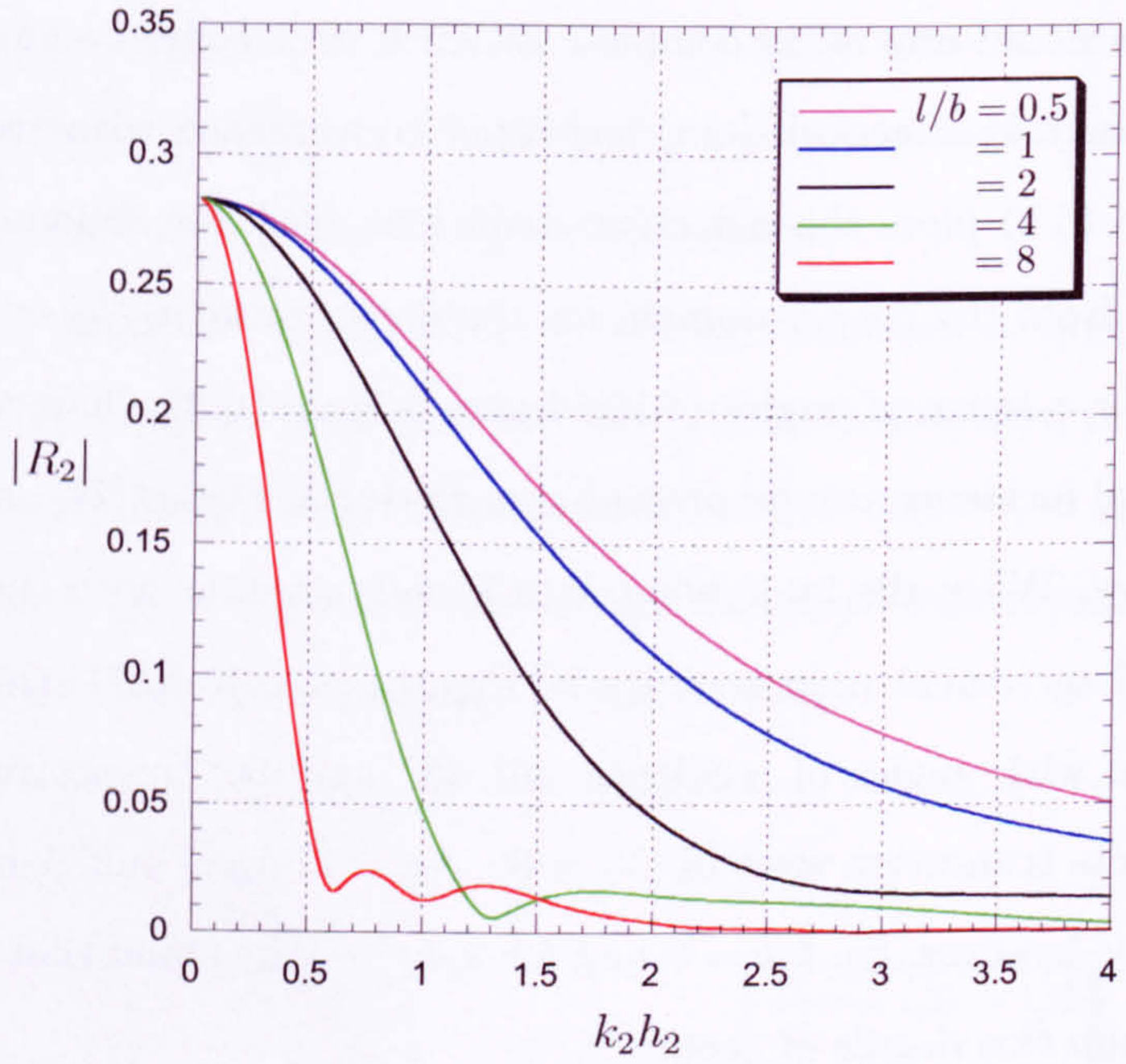

Figure 6.5: Reflection coefficients for oblique waves incident from deeper water at $30°$ to the step $\hat{h}(x) = 1 - 3x^2 + 2x^3$ where $h_1/h_2 = 0.25$.

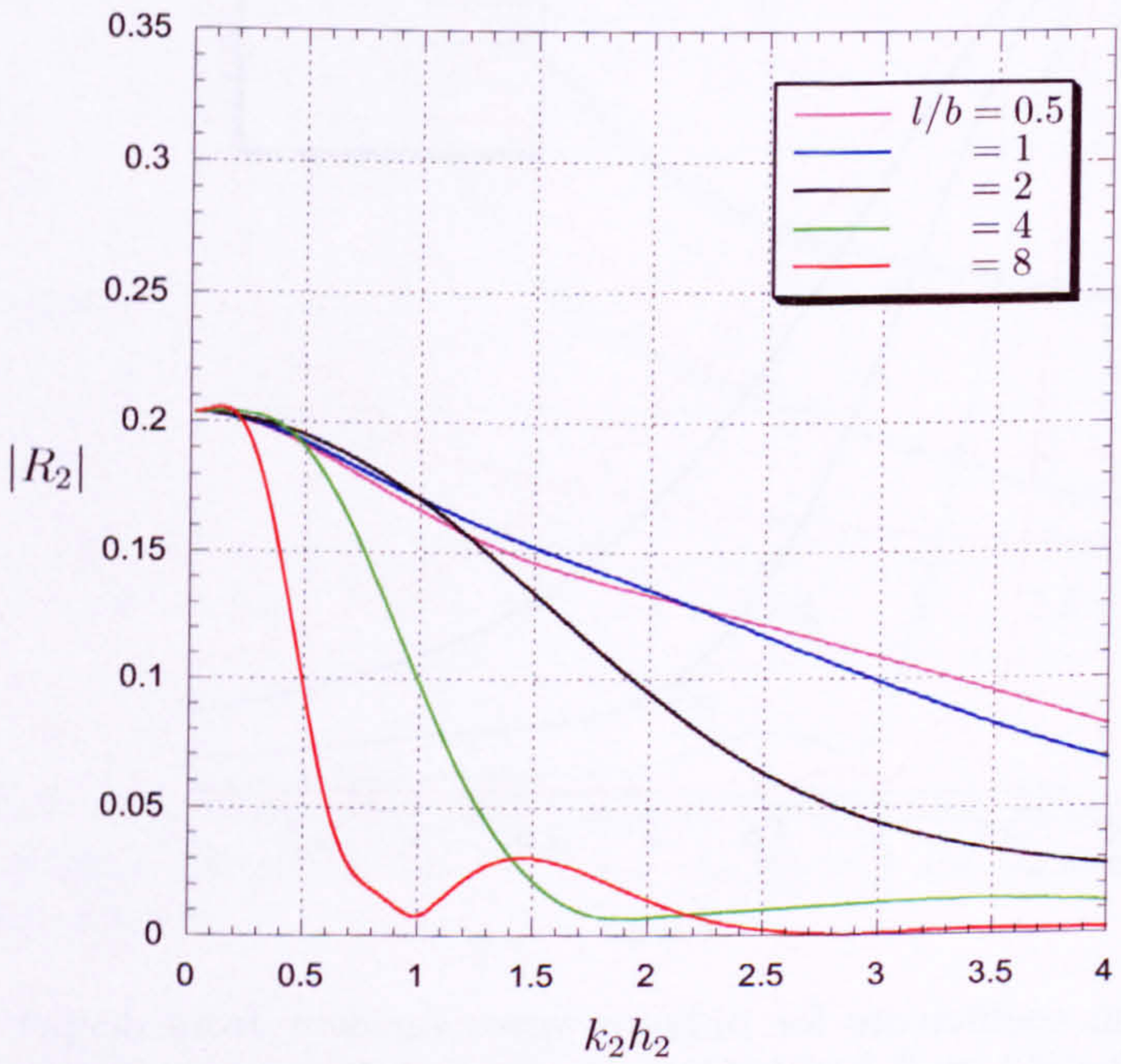

Figure 6.6: Reflection coefficients for oblique waves incident from deeper water at $45°$ to the step $\hat{h}(x) = 1 - 3x^2 + 2x^3$ where $h_1/h_2 = 0.25$.

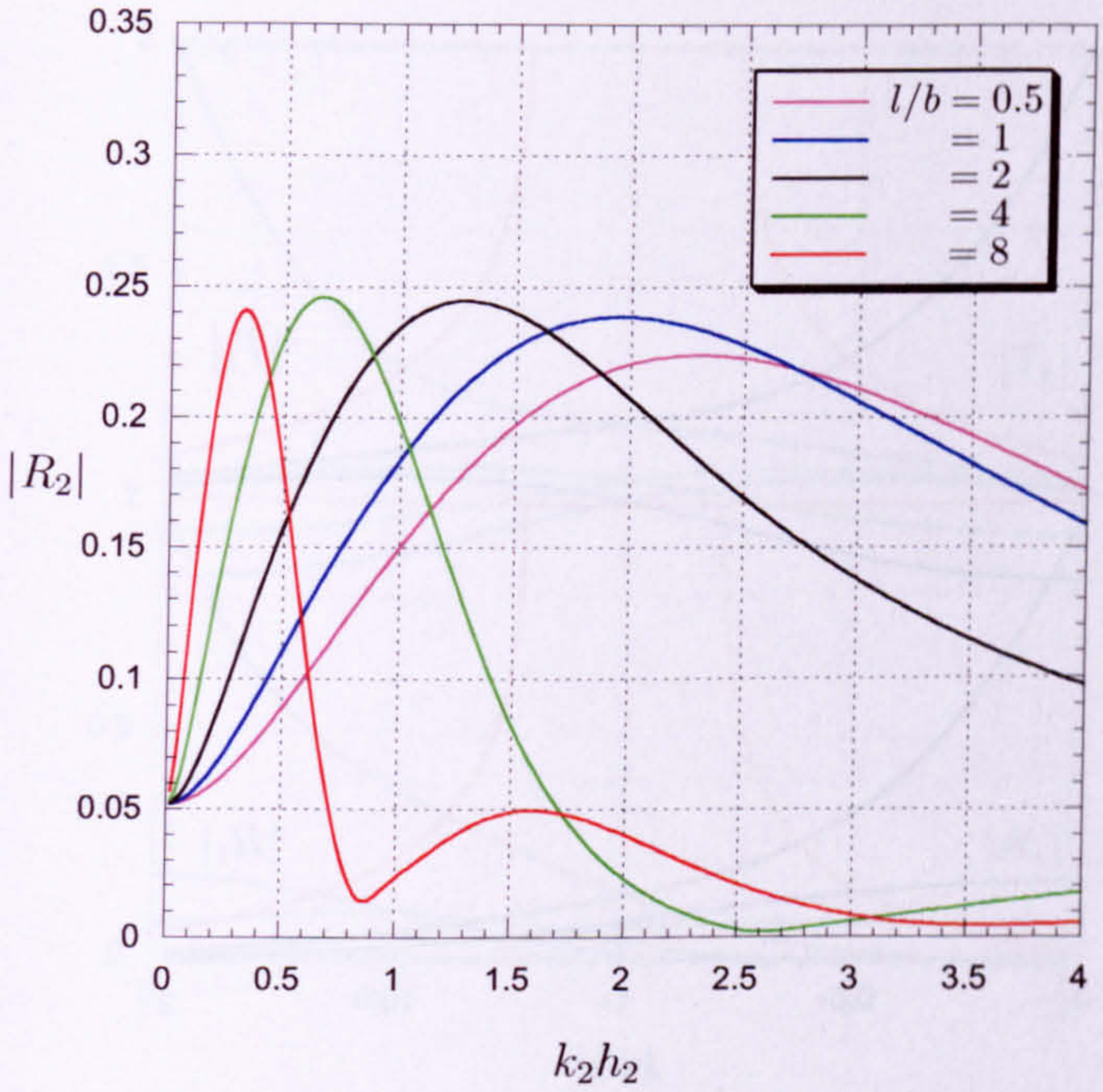

Figure 6.7: Reflection coefficients for oblique waves incident from deeper water at $60°$ to the step $\hat{h}(x) = 1 - 3x^2 + 2x^3$ where $h_1/h_2 = 0.25$.

reflection is possible. This occurs if $k_2/k_1 < \sin\theta_1 < 1$ in which case there is no transmission. In this case we obtain a solution in which a wave travels along the step and decays exponentially away from the step. Figures (6.8) to (6.11) show how the reflection and transmission coefficients for oblique scattering of waves incident from the shallower domain vary with aspect ratio of the step ℓ/b. Again we consider the smooth cubic slope $\hat{h}(x) = 1 - 3x^2 + 2x^3$, in this case for a depth ratio $h_1/h_2 = 0.5$ for a range of angles of incidence. Porter [73] presented results for oblique scattering by a vertical step and we see that, at least for small aspect ratios of the arbitrary profile, the curves have the same qualitative behaviour. The critical angle depends solely on the depth difference b as the figures show; whatever the value of ℓ, the critical angle occurs at the same point. Apart from in figure (6.11) and to a lesser extent (6.10) it is not clear how changes in the step profile affect the reflection and transmission curves. To make this more obvious we replot the data for fixed angles of $30°$ and $60°$ in figures (6.12) and (6.13) respectively.

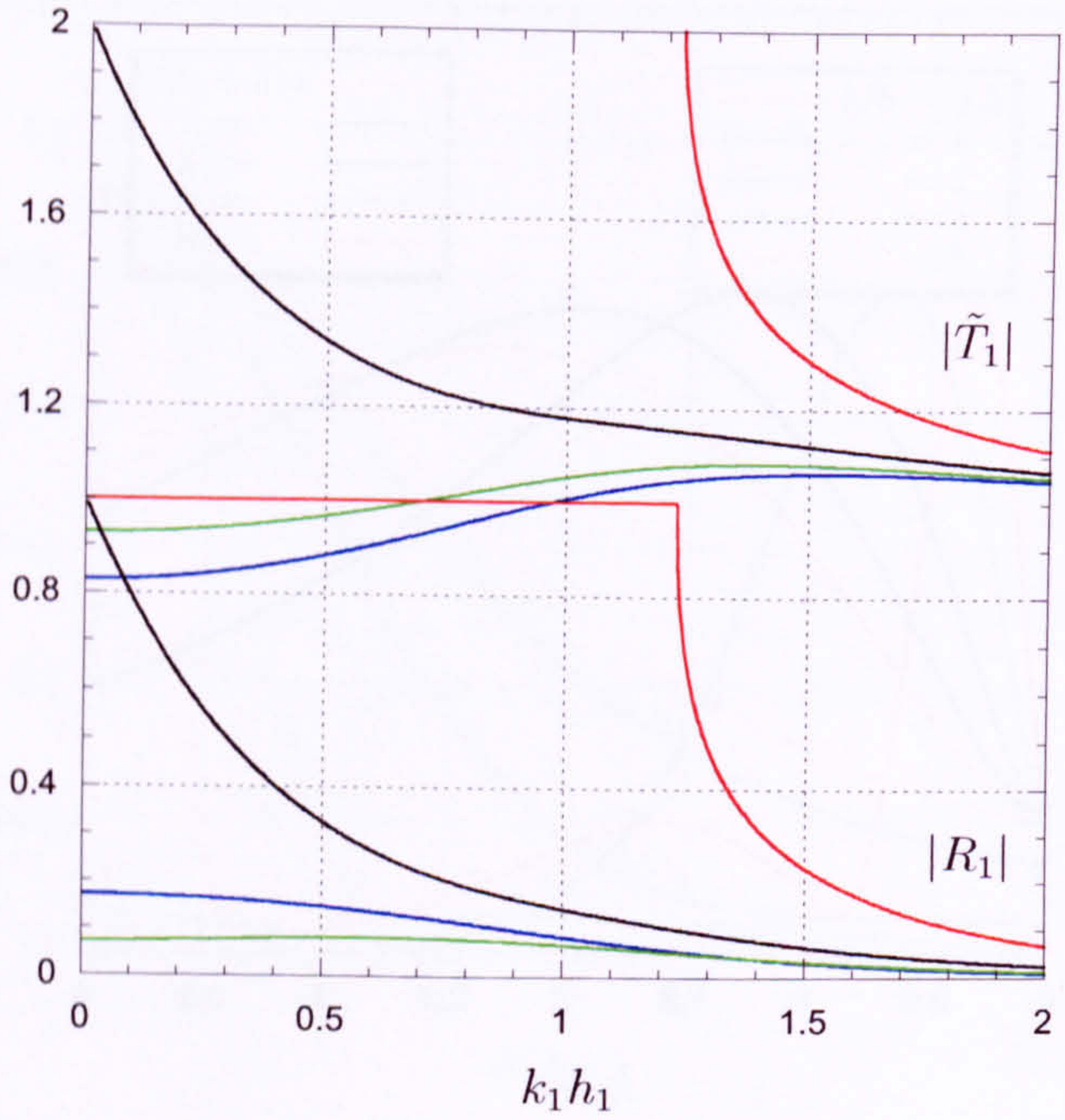

Figure 6.8: Reflection and transmission coefficients for oblique waves incident from the shallower domain onto the step $\hat{h}(x) = 1 - 3x^2 + 2x^3$, $h_1/h_2 = 0.5$, $\ell/b = 1$. $0.1°$ (—), $30°$ (—), $45°$ (—), $60°$ (—).

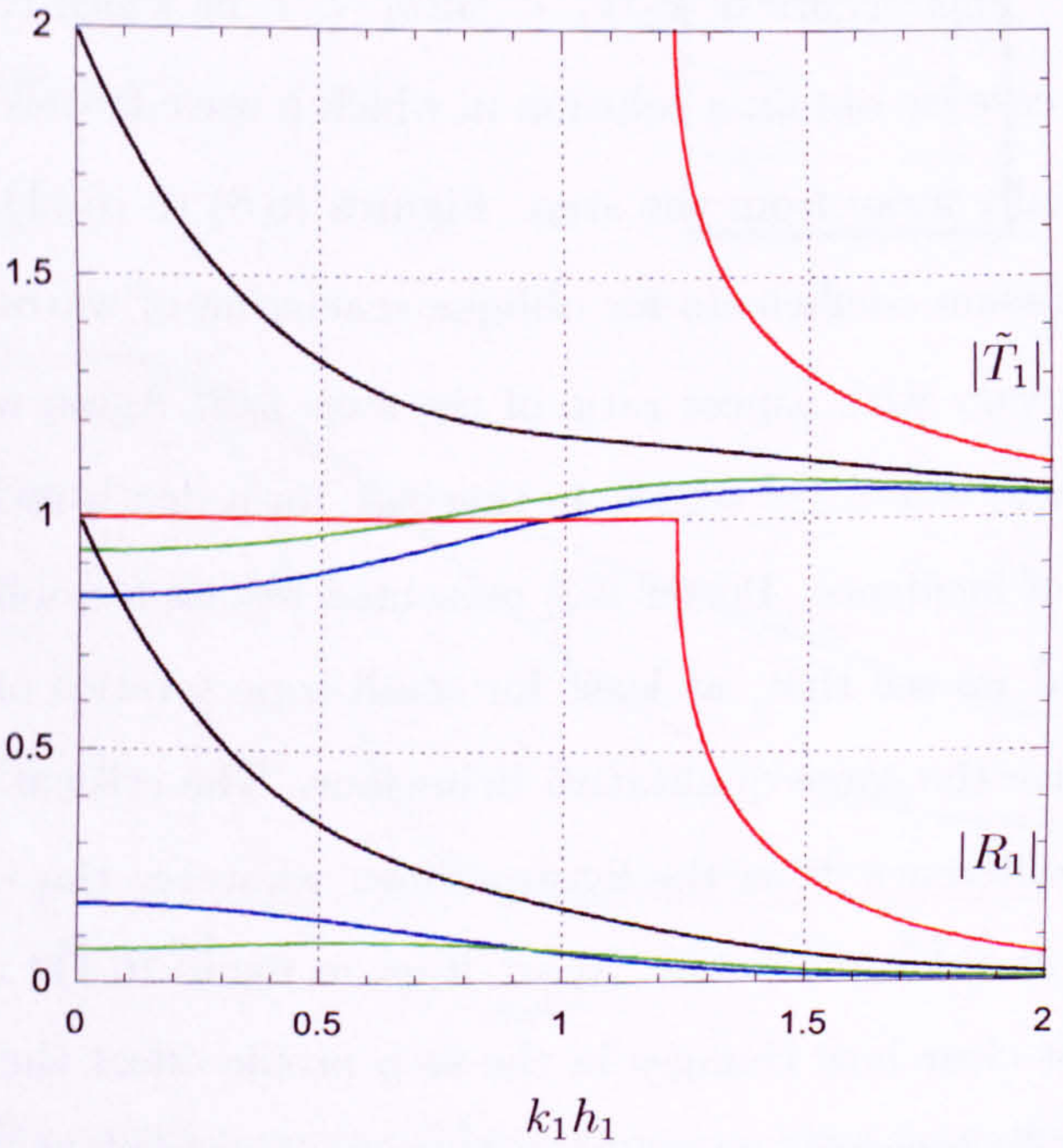

Figure 6.9: Reflection and transmission coefficients for oblique waves incident from the shallower domain onto the step $\hat{h}(x) = 1 - 3x^2 + 2x^3$, $h_1/h_2 = 0.5$, $\ell/b = 2$. $0.1°$ (—), $30°$ (—), $45°$ (—), $60°$ (—).

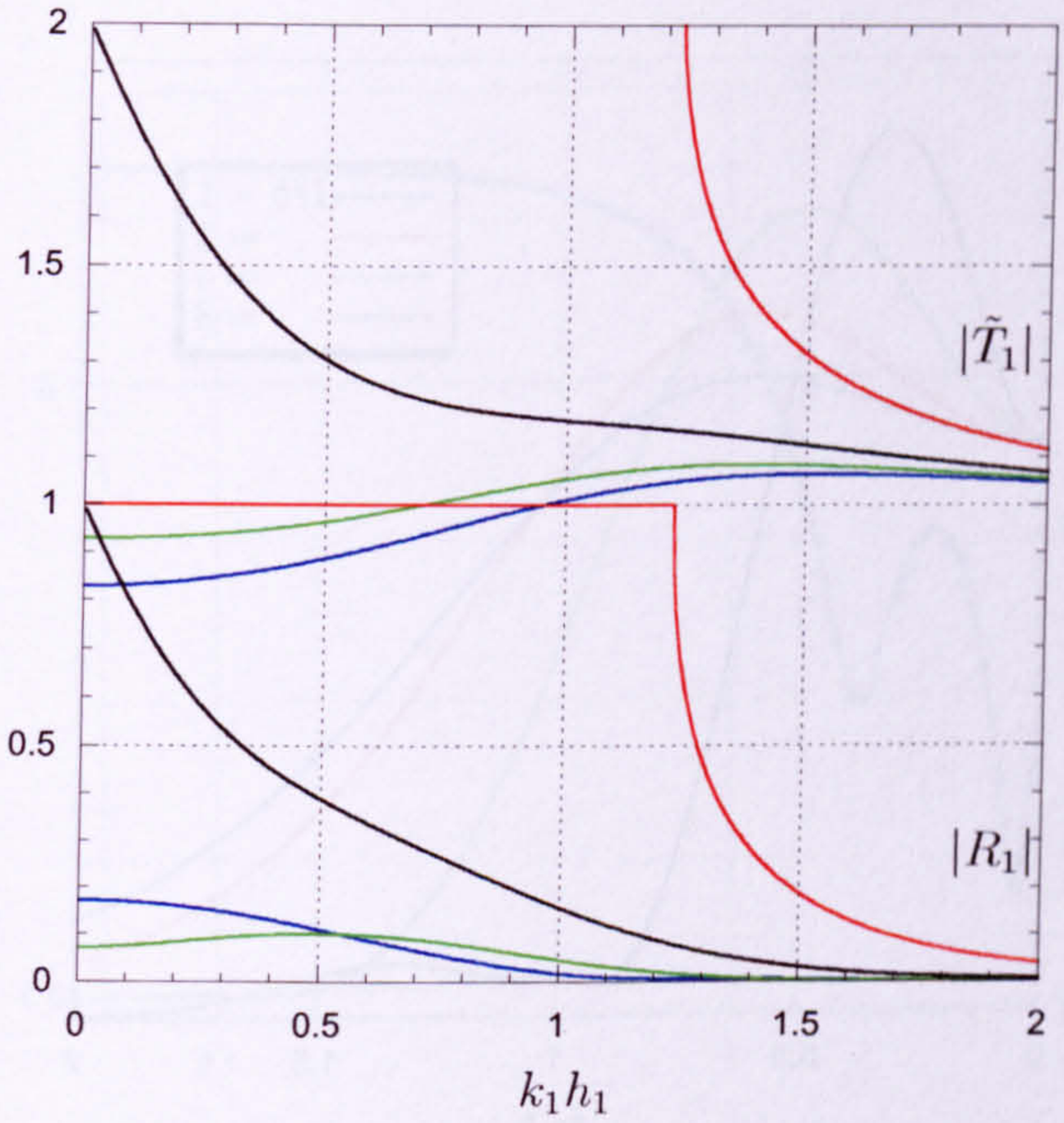

Figure 6.10: Reflection and transmission coefficients for oblique waves incident from the shallower domain onto the step $\hat{h}(x) = 1 - 3x^2 + 2x^3$, $h_1/h_2 = 0.5$, $\ell/b = 4$. $0.1°$ (—), $30°$ (—), $45°$ (—), $60°$ (—).

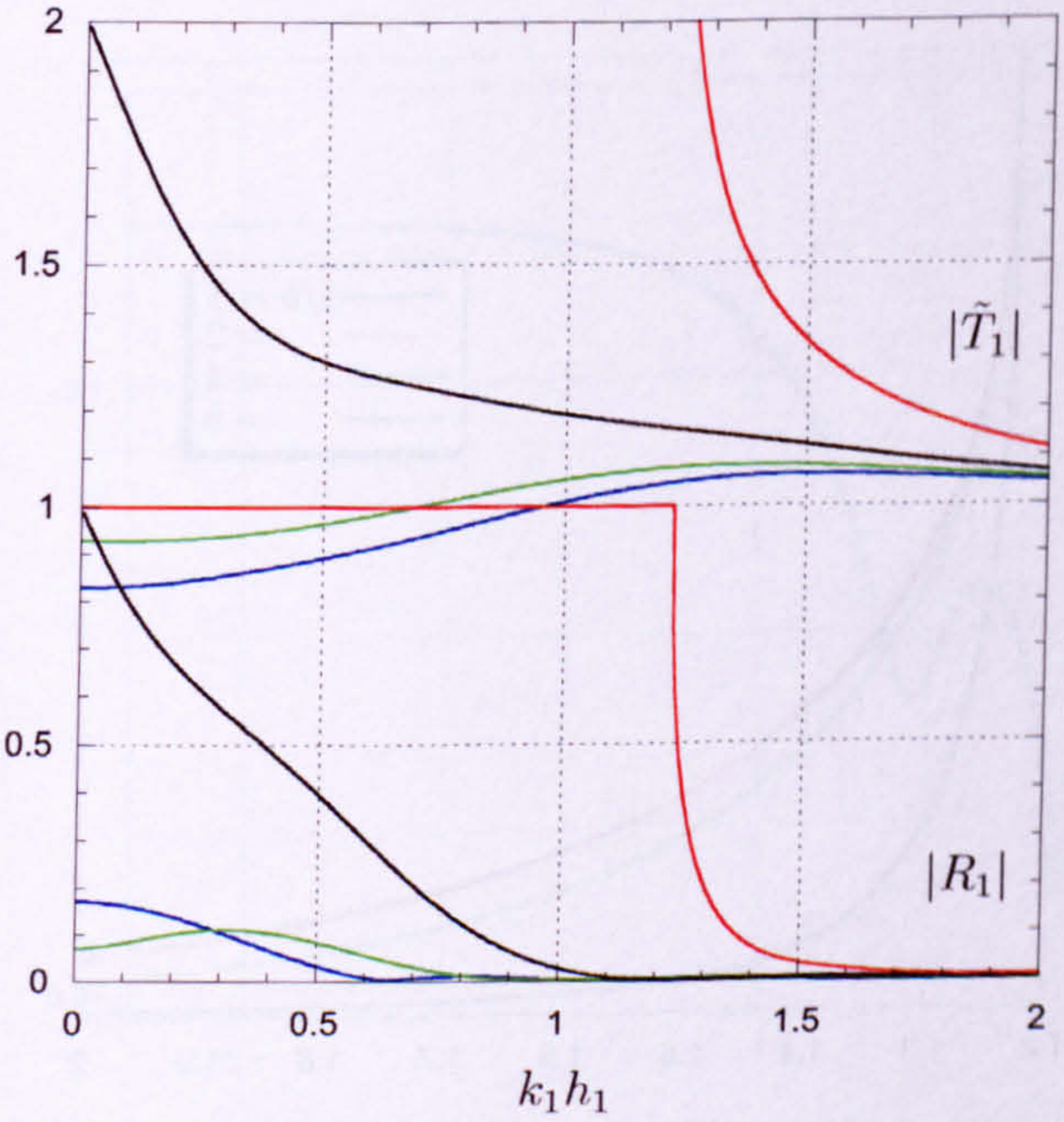

Figure 6.11: Reflection and transmission coefficients for oblique waves incident from the shallower domain onto the step $\hat{h}(x) = 1 - 3x^2 + 2x^3$, $h_1/h_2 = 0.5$, $\ell/b = 8$. $0.1°$ (—), $30°$ (—), $45°$ (—), $60°$ (—).

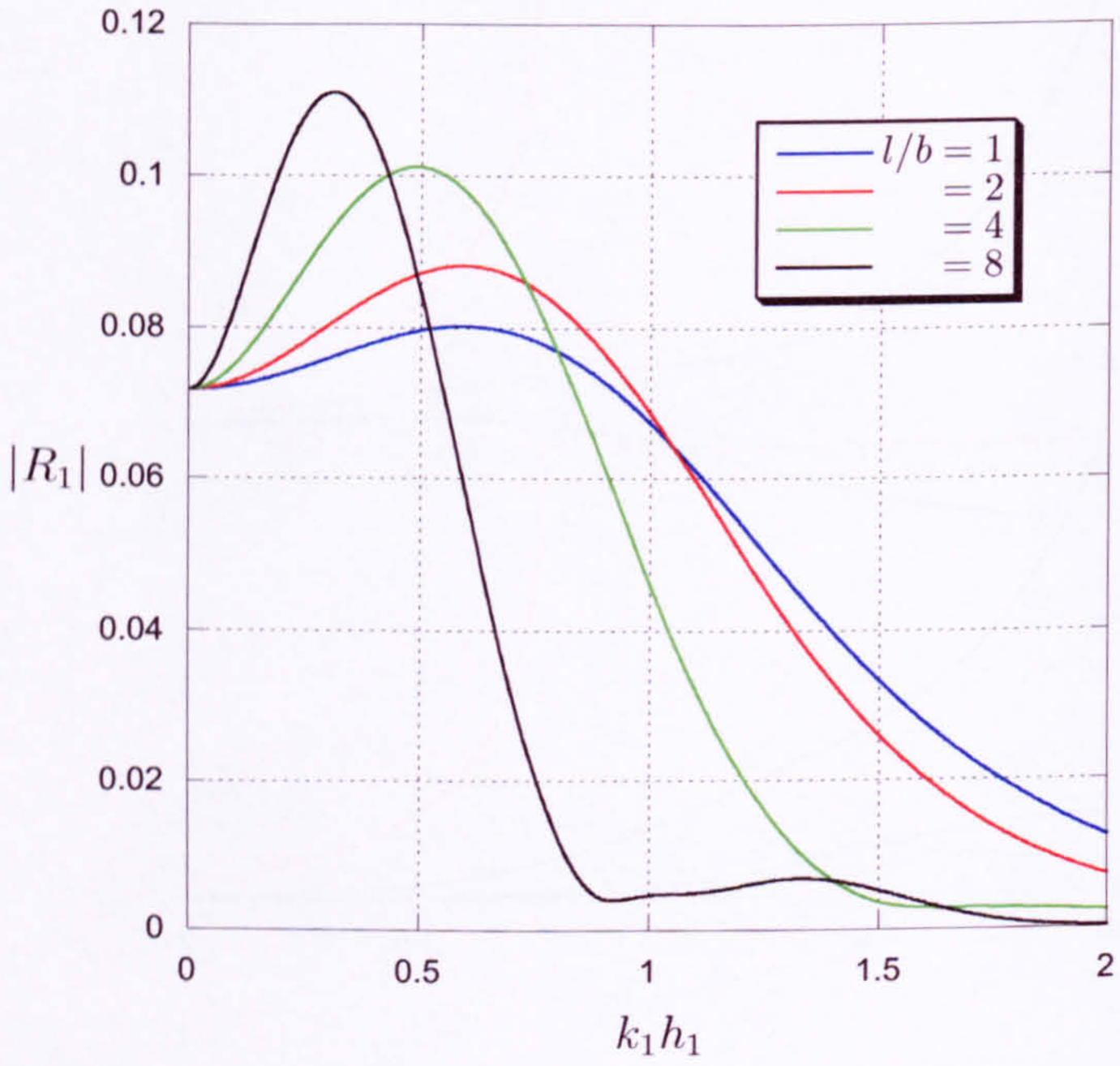

Figure 6.12: Reflection coefficients for oblique waves incident from the shallower domain onto the step $\hat{h}(x) = 1 - 3x^2 + 2x^3$, $h_1/h_2 = 0.5$, $\theta = 30°$.

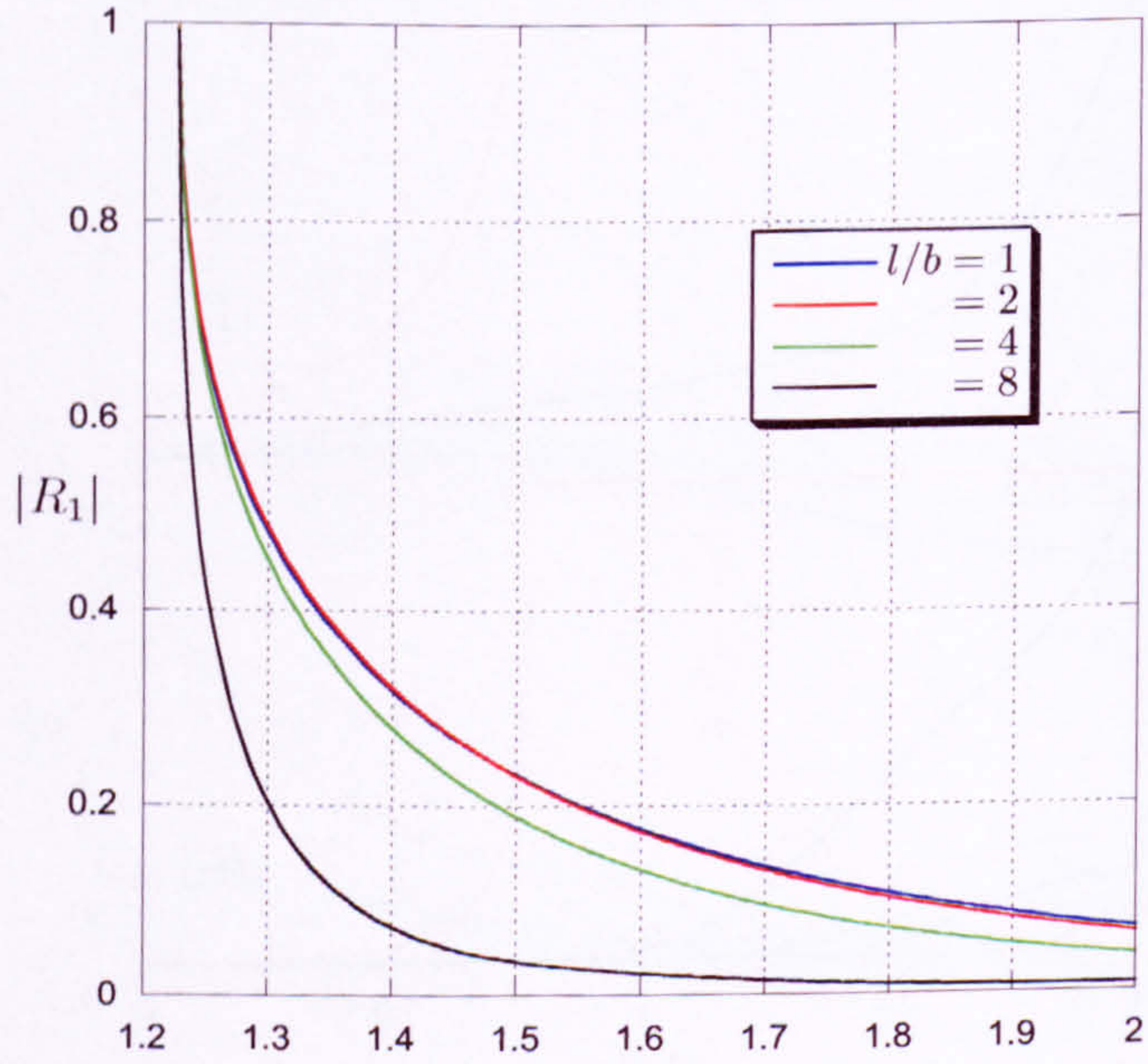

Figure 6.13: Reflection coefficients for oblique waves incident from the shallower domain onto the step $\hat{h}(x) = 1 - 3x^2 + 2x^3$, $h_1/h_2 = 0.5$, $\theta = 60°$.

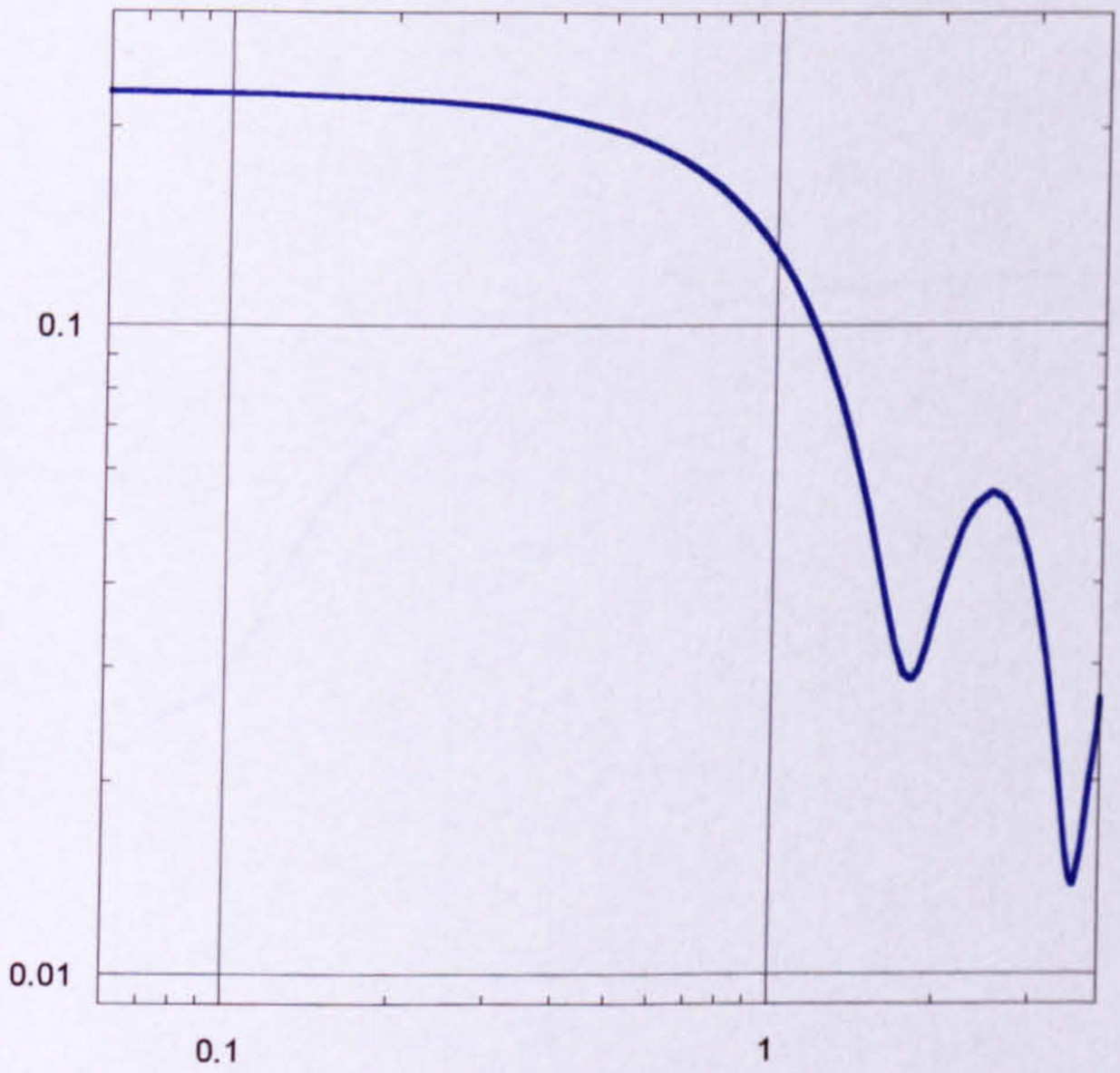

Figure 6.14: Reflection coefficients for Booij' test problem at $0.01°$ incidence

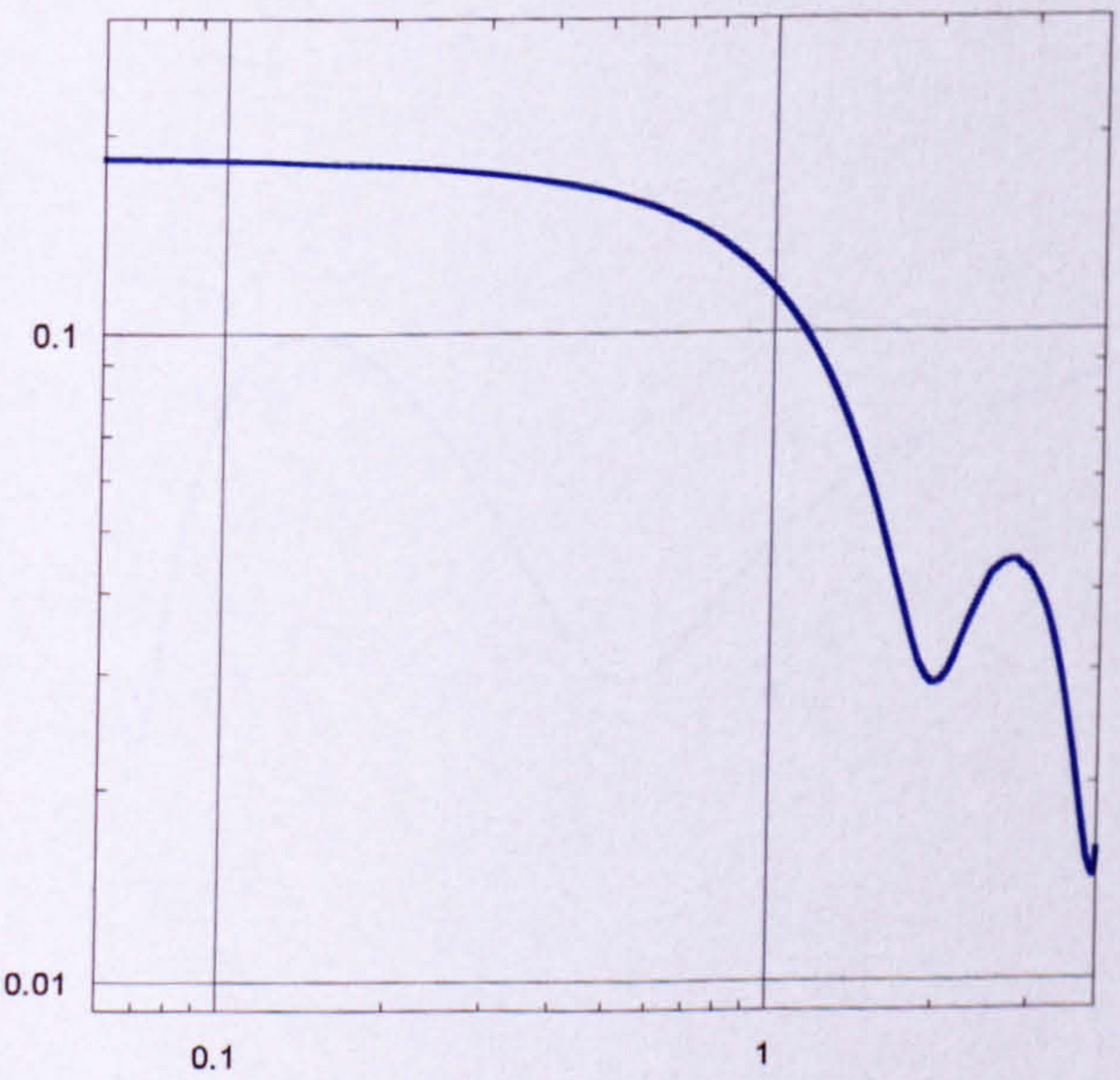

Figure 6.15: Reflection coefficients for Booij' test problem at $30°$ incidence

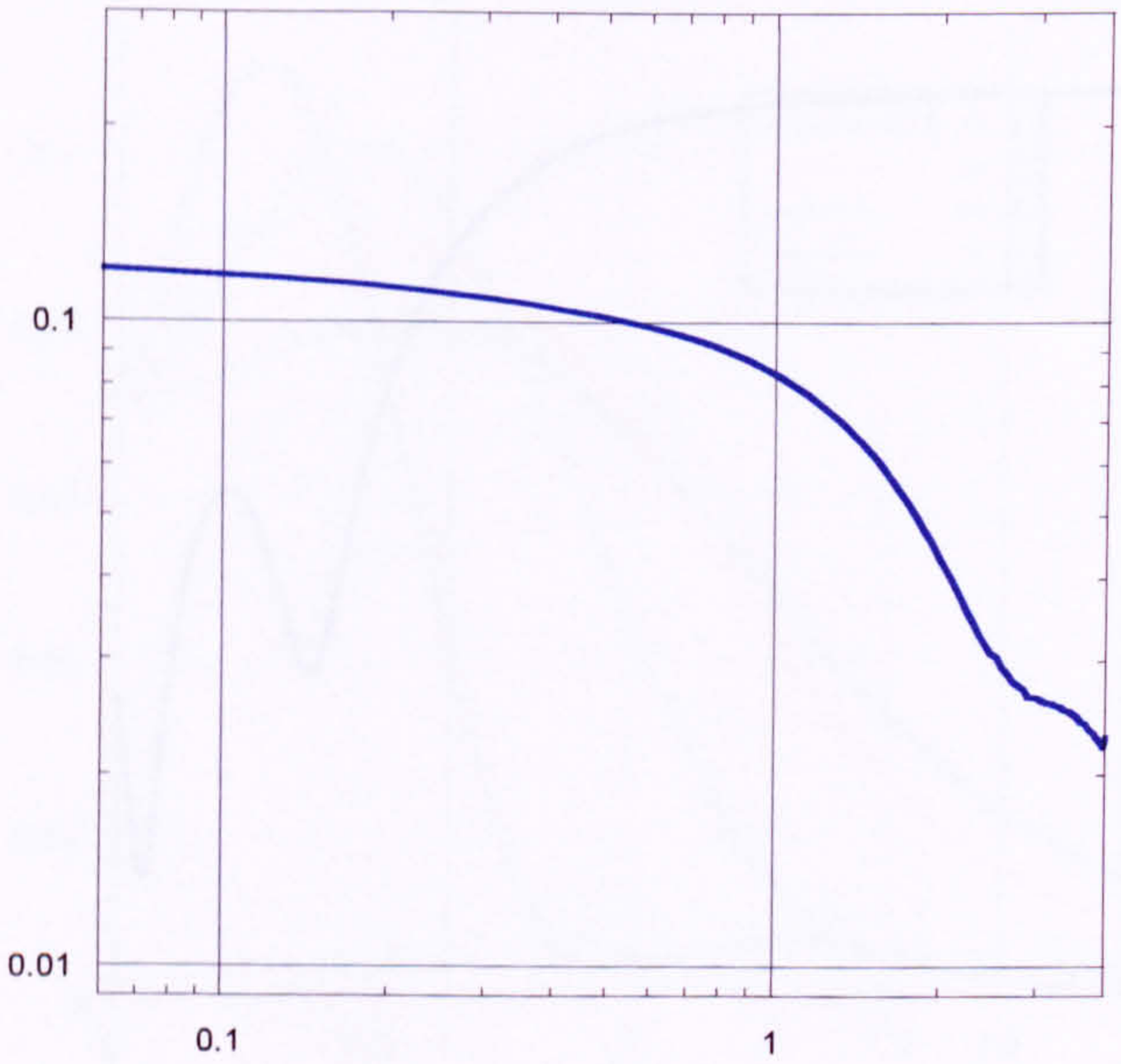

Figure 6.16: Reflection coefficients for Booij' test problem at 45° incidence

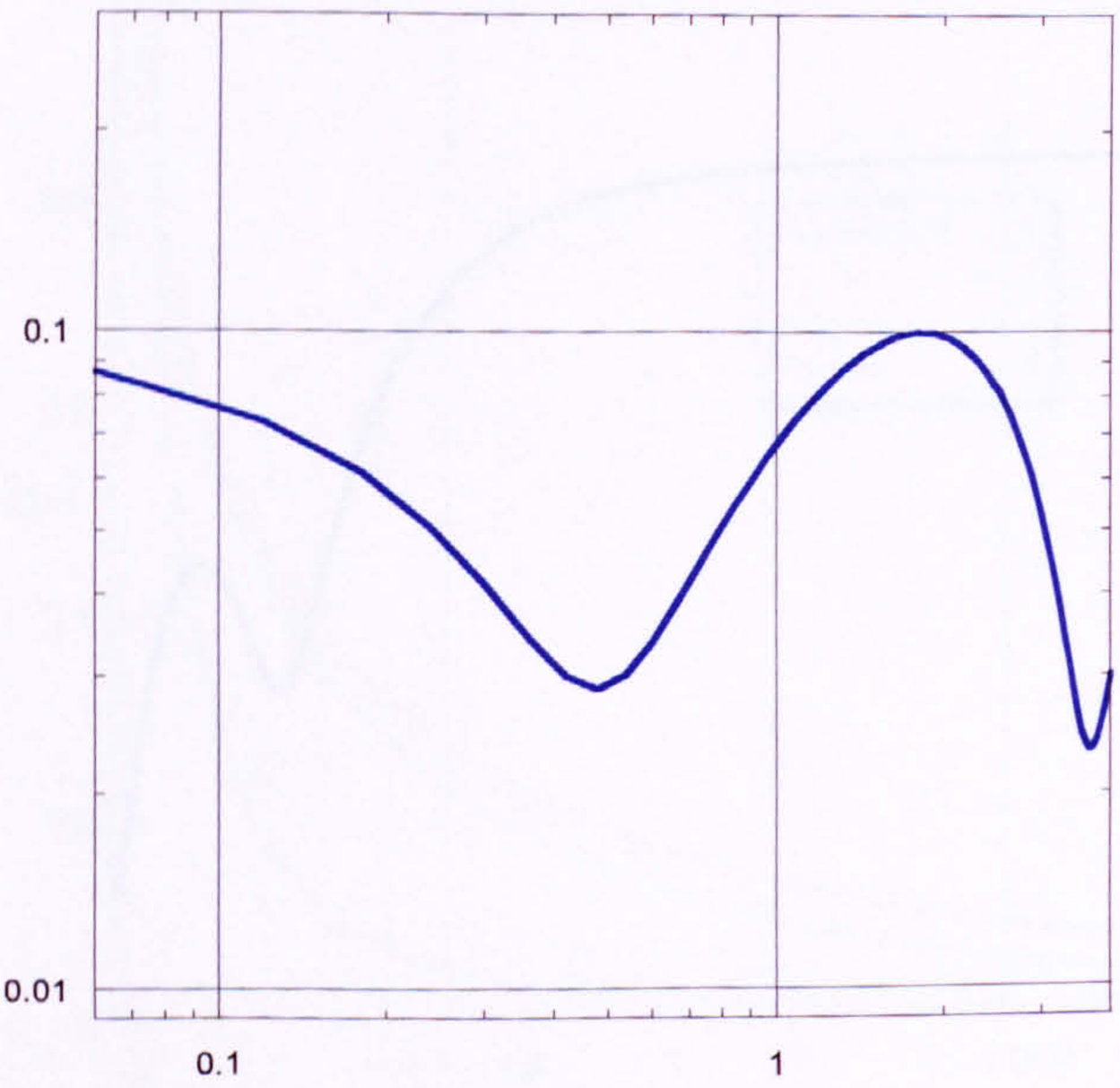

Figure 6.17: Reflection coefficients for Booij' test problem at 60° incidence

6.7 Remarks

In this chapter we have shown how our techniques of converting from normal to tangential derivatives motivated by ideas from three-dimensional vector calculus enable us to generalise the two-dimensional problem of scattering by an arbitrary step considered by Porter & Porter [77]. Although we have presented our approach in its quasi two-dimensional form we stress that all of the analysis could have been done in its natural three-dimensional form. However, it would have appeared more complicated than necessary and the link with Porter & Porter might not have been quite as clear.

Chapter 7

Scattering of plane waves by an axially symmetric seamount

7.1 Introduction

In this chapter we apply the techniques of Chapters 5 and 6 to problems involving surface water wave scattering by axisymmetric topography. This problem has received considerable attention and an overview of some of the key papers is presented below.

In a key paper Longuet-Higgins [52] used shallow water theory to conduct a thorough investigation of the trapping of wave energy around axisymmetric islands. In this investigation he considered the interaction with a circular sill and found that, for certain frequencies, the theory predicted large responses. Barnard, Pritchard & Provis [4] conducted experiments to search for these "near-resonances" but were unable to find any sign of their existence. Accordingly Renardy [81] applied the full linear theory to Longuet-Higgins' [52] sill problem and established that "the nearly resonant frequencies differ significantly ..." and "the observed amplitudes at a given frequency differ greatly." Shen, Meyer and Keller [85] used a geometrical optics approach to calculate the spectra of waves around conical islands, and for this problem too, experiments by Provis [80] found markedly different results to the theoretical results.

Smith and Sprinks [86] also looked at the scattering of surface waves by a conical island using essentially the mild slope equations which they had developed indepen-

dently from Berkhoff [6]. In the course of developing this paper they communicated with Provis so that they could compare their results against those of Barnard *et al.* [4] experiments. As we have discussed, Barnard *et al.* were unable to confirm the near-resonances which were also predicted by Smith & Sprinks' theory [86]. Moving forward Chamberlain & Porter[12] revisited the axisymmetric topography problem using the MMSE (see Chamberlain & Porter, [11]), and an improved matching condition at the join of the topography with the constant depth domain (see Porter & Staziker [71]). In this paper Chamberlain & Porter also found near-resonances but they proved to be extremely difficult to locate. In an entirely different approach Bender & Dean [5] solve axisymmetric problems by discretising the topography as a series of steps and matching constant depth separation solutions at the interface between the regions of constant depth.

As in Chapters 5 and 6 although we consider three-dimensional problems, these problems are quasi two-dimensional in that they may be reduced to a problem depending on only two dimensions by factoring out the angular dependence (noting that the extra dimension manifests itself by modifying the field equation). Thus the techniques of the last two chapters may be applied, albeit in polar coordinates, to solve problems involving axisymmetric geometries. Instead we choose this problem to demonstrate the three-dimensional nature of our solution technique by retaining a three-dimensional formulation throughout. This approach serves to illustrate some aspects of the general theory which will be developed further in Chapter 8. Of course, once we have formulated the integral equations and performed all of the switches from normal to tangential derivatives, we still factor out the angular dependence to give the identical system of equations had we followed the quasi two-dimensional approach. It is interesting to note the following quote from Chamberlain & Porter [12],

> "An investigation of this problem using full linear theory would be formidable .... As far as we are aware, there is no full linear solution available for axisymmetric scattering which will serve to examine the accuracy of the

modified mild-slope equation for such geometry."

which, to the best of the author's knowledge remains the case. Given the lack of exact results we present two alternative *fully-linear* formulations of the same problem which will serve as independent checks against each other. As in the ridge problem of Chapter 5 we also compare our results with those derived from the multipole approach of Chapter 4 in the specific case of a hemispherical bed protrusion .

7.2 Formulation and preliminaries

Cylindrical polar coordinates (r, θ, z) are chosen with z directed vertically downwards. The origin is placed in the undisturbed free surface of the fluid, and the z axis is chosen to coincide with the axis of symmetry of the seamount. The fluid is

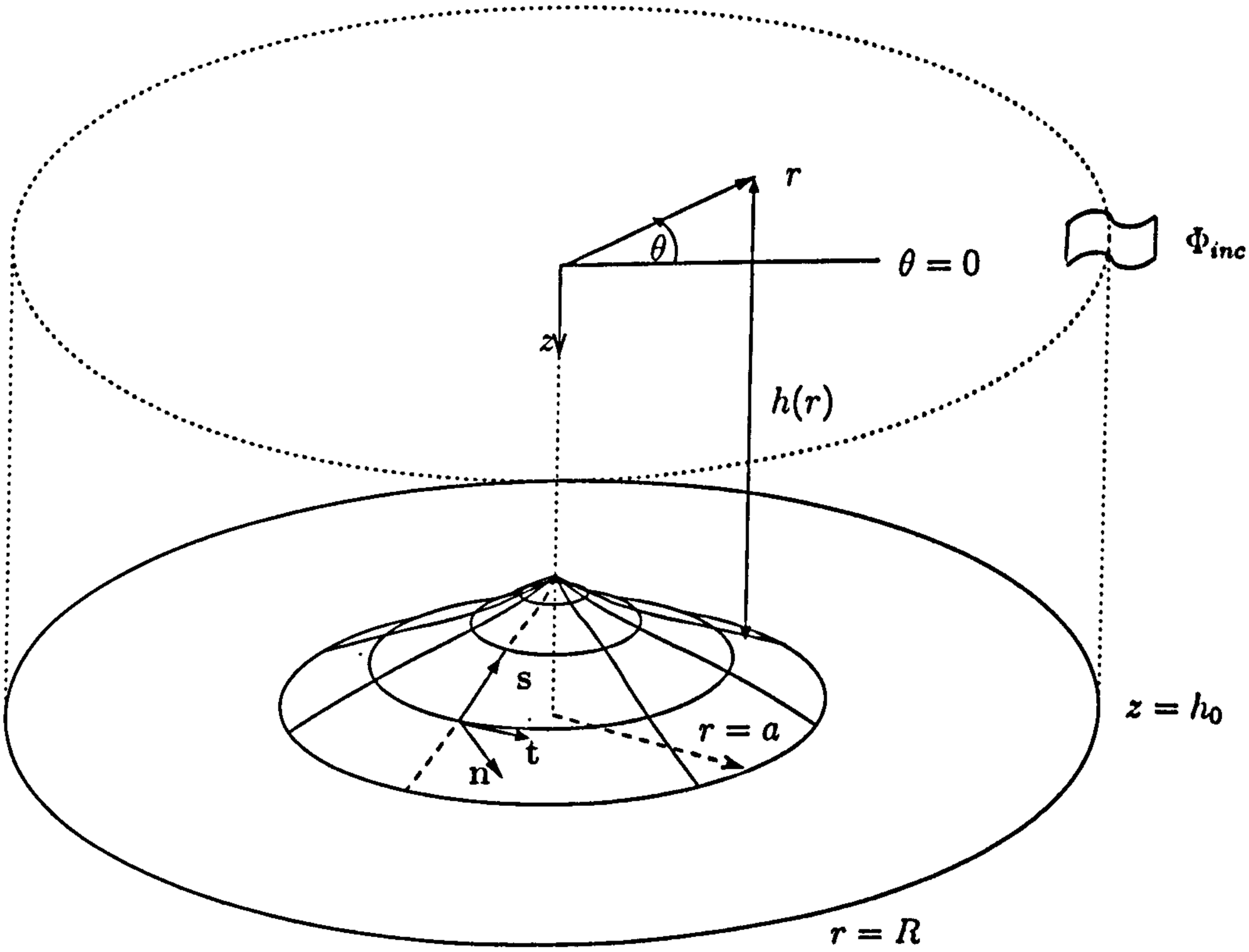

Figure 7.1: Geometrical description of the axially symmetric scattering problem

bounded below by $S_b : \{z = H(r), 0 \leq r < \infty, \theta \in [0, 2\pi)\}$ where $H(r)$ is assumed to be a continuous function with $H(r) = h_0$, a constant, for $r \notin [0, a)$ and $H(r) = h(r)$ for $r \in [0, a)$. Furthermore, it is assumed that $h(r) \leq h_0$ for $r \in [0, a)$, and we define h_1 as the maximum height of the seamount ie $h_1 = h_0 - \min(h(r))$, $r \in [0, a]$. Thus the topography consists of an axially symmetric seamount with constant cross-section in the (r, z)-plane as θ varies and which protrudes from an otherwise flat bed of depth h_0. The profile of the cross section is denoted by Γ defined by $z = h(r)$.

As we work in cylindrical coordinates we write vectors in the form $\mathbf{F} = (F_r, F_\theta, F_z) \equiv F_r\hat{\mathbf{r}} + F_\theta\hat{\boldsymbol{\theta}} + F_z\mathbf{k}$ where $\hat{\mathbf{r}}$, $\hat{\boldsymbol{\theta}}$ and $\mathbf{k}$ are the conventional cylindrical coordinate system unit vectors. On the lower boundary of the fluid, S_b, we define an orthonormal basis by

$$\left.\begin{aligned} \mathbf{n} &= (-h'(r), 0, 1)/\sigma(r) \\ \mathbf{s} &= (1, 0, h'(r))/\sigma(r) \\ \mathbf{t} &= (0, 1, 0) \end{aligned}\right\}, \qquad \sigma(r) = \sqrt{1 + (h'(r))^2} \tag{7.2.1}$$

representing, respectively, the normal (out of the fluid) and tangential unit vectors, perpendicular and parallel to the θ-axis, on the surface S_b. In this problem $\mathbf{t} = \boldsymbol{\theta}$ although we will use the notation $\mathbf{t}$ for consistency and to maintain the link with the fully three-dimensional theory.

As usual the flow is described in terms of a time-harmonic velocity potential, $\Phi(\mathbf{r})$ (see Chapter 2). Here, $\mathbf{r} = (r, \theta, z)$ and fluid motion assumes a time-harmonic variation of angular frequency ω. Then Φ satisfies

$$\nabla^2\Phi = 0, \qquad \mathbf{r} \in D \tag{7.2.2}$$

where $D : \{0 < z < h(r), -\infty < r < \infty, \theta \in [0, 2\pi]\}$ is the fluid domain,

$$\mathbf{n}.\nabla\Phi = 0, \qquad \mathbf{r} \in S_b \tag{7.2.3}$$

and

$$\frac{\partial\Phi}{\partial z} + K\Phi = 0, \qquad \text{on } z = 0 \tag{7.2.4}$$

where $K = \omega^2/g$ and g is gravitational acceleration. In this co-ordinate system the

gradient operator is defined as

$$\nabla = \left(\frac{\partial}{\partial r}, \frac{1}{r}\frac{\partial}{\partial \theta}, \frac{\partial}{\partial z}\right) \tag{7.2.5}$$

We assume an incident plane wave Φ_{inc} from infinity whose direction of propagation may be taken, without loss of generality, to be the line $\theta = 0$. To complete the formulation of the problem, we impose a Sommerfeld radiation condition requiring the scattered wave Φ^S to be outgoing at infinity, and which may be written as

$$(kr)^{\frac{1}{2}}\left(\frac{\partial}{\partial r} - \mathrm{i}k\right)\Phi^S \to 0, \quad kr \to \infty. \tag{7.2.6}$$

The potentials are related by

$$\Phi = \Phi_{inc} + \Phi^S \tag{7.2.7}$$

where the incoming plane wave Φ_{inc} may be expressed using the Jacobi-Anger expansion, as

$$\begin{aligned}\Phi_{inc} &= \mathrm{e}^{\mathrm{i}kx}\psi_0(z) \\ &= \sum_{m=-\infty}^{\infty} \mathrm{i}^m \mathrm{J_m}(kr)\mathrm{e}^{\mathrm{i}m\theta}\psi_0(z) \equiv \sum_{m=-\infty}^{\infty} \Phi_{0m}\end{aligned} \tag{7.2.8}$$

which we alternatively write as

$$= \sum_{m=-\infty}^{\infty} \phi_{0m}\mathrm{e}^{\mathrm{i}m\theta} \tag{7.2.9}$$

where

$$\phi_{0m} = \mathrm{i}^m \mathrm{J_m}(kr)\psi_0(z). \tag{7.2.10}$$

In the far field the scattered potential Φ^S, may be expressed in the form

$$\Phi^S \sim \sum_{m=-\infty}^{\infty} A_m \mathrm{i}^m H_m^{(1)}(kr)\mathrm{e}^{\mathrm{i}m\theta}\psi_0(z), \quad kr \to \infty \tag{7.2.11}$$

which implies, and is implied by, the radiation condition.

The method of solution relies on the use of a Green's function appropriate to this problem. Thus we define $G(\mathbf{r};\mathbf{r}_0)$ where $\mathbf{r}_0 = (r_0, \theta_0, z_0)$ is regarded as the field point and $\mathbf{r}$ the source point, as satisfying

$$\nabla^2 G(\mathbf{r};\mathbf{r}_0) = -\delta(\mathbf{r} - \mathbf{r}_0), \qquad \text{in } D \tag{7.2.12}$$

with

$$\frac{\partial G}{\partial z} + KG = 0, \qquad \text{on } z = 0 \tag{7.2.13}$$

and

$$\frac{\partial G}{\partial z} = 0, \qquad \text{on } z = h_0 \tag{7.2.14}$$

holding for $0 \leq r, r_0 < \infty \quad 0 \leq \theta, \theta_0 < 2\pi$. We present the derivation of the appropriate Green's function in Appendix A and for further details the reader is referred to Hulme [43]. We show that the Green's function separates out the θ dependence by expanding as

$$G(\mathbf{r}; \mathbf{r}_0) = \sum_{m=-\infty}^{\infty} G_m(\mathbf{r}; \mathbf{r}_0) \tag{7.2.15}$$

where

$$G_m(\mathbf{r}; \mathbf{r}_0) = g_m(r, z; r_0, z_0) \mathrm{e}^{-\mathrm{i}m(\theta - \theta_0)} \tag{7.2.16}$$

and the specific form of g_m is

$$g_m = \frac{\mathrm{i}}{4} \mathrm{J_m}(kr_<) \mathrm{H_m}(kr_>) \frac{\psi_0(z)\psi_0(z_0)}{h_0} + \frac{1}{2\pi} \sum_{n=0}^{\infty} \mathrm{I_m}(k_n r_<) \mathrm{K_m}(k_n r_>) \frac{\psi_n(z)\psi_n(z_0)}{h_0}. \tag{7.2.17}$$

where we have employed the compact notation

$$r_< = \min\{r, r_0\} \quad \text{and} \quad r_> = \max\{r, r_0\}.$$

Due to the lack of dependence of the geometry upon θ, it is common practice to reduce the boundary-value problem stated above to a two-dimensional problem for $\phi(r, z)$ in which the field equation is reduced to the modified Helmholtz equation in polar coordinates. Hulme [43] does exactly this, taking advantage of the axial symmetry to reduce the dimension of the problem by integrating over θ to remove the angular dependence and make use of so-called ring sources. However, the strategy we have decided to adopt in tackling this problem uses a three-dimensional coordinate system and leaves it until the end of the formulation before removing the θ dependence.

As in (5.2.17) we decompose G into a form which will enable us to construct a self adjoint integral operator. In effect this separates the Green's function into its real and imaginary parts so that

$$G = G_0 + \hat{G} \tag{7.2.18}$$

where

$$G_0 \equiv \sum_{m=-\infty}^{\infty} G_{0m} \equiv \sum_{m=-\infty}^{\infty} g_{0m} \mathrm{e}^{-\mathrm{i}m(\theta-\theta_0)} \tag{7.2.19}$$

and

$$g_{0m} = \frac{\mathrm{i}}{4} \mathrm{J_m}(kr)\mathrm{J_m}(kr_0)\frac{\psi_0(z)\psi_0(z_0)}{h_0} \tag{7.2.20}$$

is the separable component of the wave-like part of the Green's function previously exposed in (7.2.14). Also

$$\hat{G} = \sum_{m=-\infty}^{\infty} \hat{g}_m \mathrm{e}^{-\mathrm{i}m(\theta-\theta_0)} \tag{7.2.21}$$

is the remainder of G, where

$$\hat{g}_m = -\frac{1}{4}\mathrm{J_m}(kr_<)\mathrm{Y_m}(kr_>)\frac{\psi_0(z)\psi_0(z_0)}{h_0} + \frac{1}{2\pi}\sum_{n=1}^{\infty} \mathrm{I_m}(k_n r_<)\mathrm{K_m}(k_n r_>)\frac{\psi_n(z)\psi_n(z_0)}{h_0}. \tag{7.2.22}$$

As in Chapter 5 we now have the property $\overline{\hat{G}(\mathbf{r}_0;\mathbf{r})} = \hat{G}(\mathbf{r};\mathbf{r}_0)$ which will result in a self-adjoint integral operator which is crucial to our main solution technique.

7.3 Derivation of the integral equations

In this section, we set out to develop an exact formulation in terms of integral equations of the solution to the problem, as a means of calculating the far-field of the scattered potential, and also for finding the free surface elevation.

The first step is to apply Green's identity to the functions $\Phi(\mathbf{r})$ and $G(\mathbf{r};\mathbf{r}_0)$ in a subdomain D_R of D, bounded laterally by a vertical boundary of radius R (see figure 7.1). Here, $R > a > 0$ is arbitrary, and it is to be assumed in what follows

that the limit $R \to \infty$ is taken. Now Green's identity states

$$\iiint_{D_R} (G\nabla^2\Phi - \Phi\nabla^2 G)\,\mathrm{d}V = \iint_{S_R} (G\mathbf{n}.\nabla\Phi - \Phi\mathbf{n}.\nabla G)\,\mathrm{d}S \tag{7.3.1}$$

where S_R is the closed boundary of D_R, dS being a surface element on S_R and the definition of $\mathbf{n}$ has been extended to boundaries other than those coinciding with S_b to mean the outward unit normal to S_R.

Green's identity applied first to Φ_{inc} and G for a domain of constant depth without a seamount gives

$$\iiint_{D_R} \{G\nabla^2\Phi_{inc} - \Phi_{inc}\nabla^2 G\}\,\mathrm{d}V = \iint_{\Sigma_R} \{G\nabla\Phi_{inc} - \Phi_{inc}\nabla G\}.\mathbf{n}\,\mathrm{d}S \tag{7.3.2}$$

which implies

$$\Phi_{inc}(\mathbf{r}_0) = \iint_{\Sigma_R} \{G\nabla\Phi_{inc} - \Phi_{inc}\nabla G\}.\mathbf{n}\,\mathrm{d}S, \tag{7.3.3}$$

where we have used the fact that Φ_{inc} satisfies the Sommerfeld radiation condition and Σ_R denotes the cylindrical surface at $r = R$.

Now apply Green's identity to G and Φ

$$\begin{aligned} \mu\Phi(\mathbf{r}_0) &= \iint_{\Sigma} \{G\nabla\Phi - \Phi\nabla G.\}\mathbf{n}\,\mathrm{d}S \\ &+ \iint_{\Sigma_R} \{G\nabla\Phi^S - \Phi_s\nabla G.\}\mathbf{n}\,\mathrm{d}S \\ &+ \iint_{\Sigma_R} \{G\nabla\Phi_{inc} - \Phi_{inc}\nabla G.\}\mathbf{n}\,\mathrm{d}S \end{aligned} \tag{7.3.4}$$

where the second term on the right had side is zero in the limit $R \to \infty$ as both G and Φ^S satisfy Sommerfeld radiation conditions and so are outgoing wave potentials. Furthermore the third term is Φ_{inc} from equation (7.3.3). Here, as in Chapter 5, $\mu = 1$ for $\mathbf{r}_0 \in D$, $\mu = 1/2$ for $\mathbf{r}_0 \in \partial D$, and $\mu = 0$ for $\mathbf{r}_0 \notin D \cup \partial D$. Now $\nabla\Phi.\mathbf{n}$ vanishes on Σ so we have

$$\mu\Phi(\mathbf{r}_0) = \Phi_{inc}(\mathbf{r}_0) - \iint_{\Sigma} \Phi(\mathbf{r})\nabla G(\mathbf{r}|\mathbf{r}_0; K).\mathbf{n}\,\mathrm{d}S. \tag{7.3.5}$$

and Σ is the two-dimensional surface of the topography.

At this point it is convenient to consider the equation satisfied by the m'th mode in the expansion

$$\Phi(\mathbf{r}_0) = \sum_{m=-\infty}^{+\infty} \Phi_m(r_0, \theta_0, z_0) = \sum_{m=-\infty}^{+\infty} \phi_m(r_0, z_0) \mathrm{e}^{\mathrm{i}m\theta_0} \tag{7.3.6}$$

and which on substitution in (7.3.5) is found to be

$$\mu\Phi_m(\mathbf{r}_0) = \Phi_{0m}(\mathbf{r}_0) - \iint_{\Sigma} \Phi_m(\mathbf{r}) \nabla\{G_m(\mathbf{r}|\mathbf{r}_0; K).\mathbf{n}\, \mathrm{d}S. \tag{7.3.7}$$

Henceforth we concentrate on solving for the m'th mode, leaving the summation over m unstated, noting that we must perform the summation over m to recover the solution for the total potential Φ.

As in the previous two chapters, we follow the main idea of Noblesse [67] and define a vector Green's function $\mathbf{L}_m$ related to the Green's function G_m and which satisfies

$$\nabla G = \nabla \times \mathbf{L} - \frac{1}{r}\delta(r - r_0)\delta(\theta - \theta_0)\delta^z(z - z_0)\mathbf{k}. \tag{7.3.8}$$

Here $\mathbf{L}_m = (\frac{1}{r}(G_m)^z_\theta, -(G_m)^z_r, 0)$ and as we are now used to $F^z_r = \int_{h_0}^z \partial F/\partial r \, \mathrm{d}z$. Equation (7.3.8) may be verified by substitution so that

$$\nabla G_m = \left(\frac{\partial G_m}{\partial r}, \frac{1}{r}\frac{\partial G_m}{\partial \theta}, \frac{\partial G_m}{\partial z}\right) = \frac{1}{r}\begin{vmatrix} \hat{\mathbf{r}} & r\hat{\boldsymbol{\theta}} & \mathbf{k} \\ \dfrac{\partial}{\partial r} & \dfrac{\partial}{\partial \theta} & \dfrac{\partial}{\partial z} \\ \frac{1}{r}(G_m)^z_\theta & -r(G_m)^z_r & 0 \end{vmatrix}$$
$$- \frac{1}{r}\delta(r - r_0)\delta(\theta - \theta_0)\delta^z(z - z_0)\mathbf{k}. \tag{7.3.9}$$

The first two elements of ∇G work out trivially whereas the third uses

$$(G_m)^z_{zz} = -\frac{1}{r}(r(G_m)^z_r)_r - \frac{1}{r^2}(G_m)^z_{\theta\theta} - \frac{1}{r}\delta(r - r_0)\delta(\theta - \theta_0)\delta^z(z - z_0) \tag{7.3.10}$$

which follows from integrating (7.2.12) with respect to z. Then using (5.3.6) in

(7.3.9) we have

$$\mu\Phi(\mathbf{r}_0) = \Phi_{inc}(\mathbf{r}_0) - \iint_{S_b} \Phi(\mathbf{r})\mathbf{n}\nabla\times\mathbf{L}\,\mathrm{d}S$$
$$- \iint_{S_b} \Phi(\mathbf{r})\frac{1}{r}\delta(r-r_0)\delta(\theta-\theta_0)\mathrm{H}(z_0-z)\frac{\mathrm{d}S}{\sigma} \quad (7.3.11)$$

since $\mathbf{n}.\mathbf{k} = 1/\sigma$. Now to deal with the final term we note that $\mathrm{d}S = r\sigma\,\mathrm{d}r\,\mathrm{d}\theta$ so that,analogously to (5.3.8)

$$- \iint_{S_b} \Phi(\mathbf{r})\frac{1}{r}\delta(r-r_0)\delta(\theta-\theta_0)\mathrm{H}(z_0-z)\frac{\mathrm{d}S}{\sigma} =$$
$$- \Phi(r_0,\theta_0,h(r_0,\theta_0))\mathrm{H}(z_0-h(r_0,\theta_0)) \quad (7.3.12)$$

which is zero for points $\mathbf{r}_0 \in D$, $-\frac{1}{2}\Phi(r_0,\theta_0,h(r_0,\theta_0))$ for points $\mathbf{r}_0 \in \partial D$ and $-\Phi(r_0,\theta_0,h(r_0,\theta_0))$ for points $\mathbf{r}_0 \notin D\cup\partial D$. Thus

$$\Phi(\mathbf{r}_0) = \Phi_{inc}(\mathbf{r}_0) - \iint_{S_b} \Phi(\mathbf{r})\mathbf{n}.\nabla\times\mathbf{L}\,\mathrm{d}S \qquad \text{for } \mathbf{r}_0 \in D\cup\partial D \qquad (7.3.13)$$

which establishes that, unlike the traditional form (7.3.7), the formulation in (7.3.13) gives a continuous definition of the fluid potential as the field point moves from the fluid domain to a point on the boundary. As in earlier Chapters, the choice of $\mathbf{L}_m$ is not unique, however, we have chosen the form which gives the important property that $\mathbf{L}_m = 0$ on $z = h_0$.

As in earlier chapters we use the relation $\mathbf{n} = \mathbf{s}\times\mathbf{t}$ to switch from normal to tangential derivatives. So

$$\mathbf{n}.(\nabla\times\mathbf{L}_m) = (\mathbf{s}\times\mathbf{t}).(\nabla\times\mathbf{L}_m), \qquad (7.3.14)$$

then using

$$\mathbf{t}\times\nabla\times\mathbf{L}_m = \nabla(\mathbf{t}.\mathbf{L}_m) - \mathbf{L}_m\times(\nabla\times\mathbf{t}) - (\mathbf{t}.\nabla)\mathbf{L}_m - (\mathbf{L}_m.\nabla)\mathbf{t} \qquad (7.3.15)$$

we find, after some algebra, that

$$\mathbf{n}.(\nabla\times\mathbf{L}_m) = \frac{1}{r}(\mathbf{s}.\nabla)(r\mathbf{L}_m.\mathbf{t}) - (\mathbf{t}.\nabla)(\mathbf{L}_m.\mathbf{s}) \equiv \frac{1}{r}\frac{\partial}{\partial s}(rL_{m2}) - \frac{\partial}{\partial t}L_{m1} \qquad (7.3.16)$$

where we have employed the abbreviations $\partial/\partial s = \mathbf{s}.\nabla$, $\partial/\partial t = \mathbf{t}.\nabla$ and defined

$$L_{1m}(\mathbf{r};\mathbf{r}_0) = \mathbf{L}_m.\mathbf{s} = \frac{1}{r\sigma(r)}(G_m)^z_\theta \tag{7.3.17}$$

$$L_{2m}(\mathbf{r};\mathbf{r}_0) = \mathbf{L}_m.\mathbf{t} = -(G_m)^z_r \tag{7.3.18}$$

from (7.3.9) and (7.2.1). Thus we now find

$$\Phi_m(\mathbf{r}_0) = \Phi_{0m}(\mathbf{r}_0) - \iint_\Sigma \left(\frac{1}{r}\frac{\partial}{\partial s}(rL_{2_m}) - \frac{\partial L_{1m}}{\partial t}\right)\Phi_m(s,t)\ \mathrm{d}S \tag{7.3.19}$$

where we have written $\Phi_m(\mathbf{r})|_\Sigma = \Phi_m(s,t)$ in terms of coordinates aligned with $\mathbf{s}$ and $\mathbf{t}$ lying on the surface of the seamount Σ.

Before proceeding any further, we mimic the decomposition of the Green's function G_m performed in (7.2.18), by writing

$$L_{i_m} = L_{0i_m} + \widehat{L}_{i_m}, \qquad i = 1,2, \tag{7.3.20}$$

and the two components of L_{i_m} are derived directly from the two components of G_m in (7.2.18). Thus, in particular, we find

$$L_{01m} = \frac{1}{r\sigma(r)}(G_{0m})^z_\theta = \frac{1}{4kh_0}\left(\frac{im}{r\sigma(r)}\right)\overline{f_m}(\mathbf{r})\Phi_{0m}(\mathbf{r}_0) \tag{7.3.21}$$

$$L_{02m} = -(G_0)^z_r \qquad = \frac{1}{4kh_0}\frac{\partial}{\partial r}\overline{f_m}(\mathbf{r})\ \Phi_{0m}(\mathbf{r}_0) \tag{7.3.22}$$

in terms of the newly-defined function

$$f_m(\mathbf{r}) = \mathrm{i}^m \mathrm{J_m}(kr)\chi_0(z)\mathrm{e}^{\mathrm{i}m\theta} \tag{7.3.23}$$

where we have acknowledged that $\mathbf{t} = \hat{\theta}$ and the result $\overline{\chi}_0(z) = -\chi_0(z)$.

At this point, we shall introduce some more new notation and first define

$$F_m(s,t) = \frac{1}{4kh_0}\left(\frac{1}{r}\frac{\partial}{\partial s}\left(r\frac{\partial f_m(\mathbf{r})}{\partial r}\right) + \frac{im}{r\sigma(r)}\frac{\partial f_m(\mathbf{r})}{\partial t}\right)\Bigg|_{\mathbf{r}\in\Sigma}. \tag{7.3.24}$$

We also introduce the inner product notation for functions $u(s,t), v(s,t) \in \mathcal{H}$ (where $\mathcal{H}$ is the space of functions whose derivatives belong to $L_2(\Sigma)$)

$$\langle u, v\rangle = \iint_\Sigma u\,\overline{v}\ \mathrm{d}S \tag{7.3.25}$$

We now substitute the decomposed form of $\mathbf{L}_m$ into (7.3.19) to obtain, after some algebra

$$\Phi_m(\mathbf{r}_0) = \Phi_{0_m}(\mathbf{r}_0)(1 - \langle \Phi_m, F_m \rangle) - \iint_\Sigma \left(\frac{1}{r} \frac{\partial}{\partial s} \left(r \widehat{L}_{2_m} \right) - \frac{\partial \widehat{L}_{1_m}}{\partial t} \right) \Phi_m(s,t) \, \mathrm{d}S. \tag{7.3.26}$$

Here, the L_{01m} and L_{02m} are separable and have contributed to the inner product term $-\Phi_{0m}\langle \Phi_m, F_m \rangle$. As in Chapter 5 we find that consideration of the far field in (7.3.19) enables us to relate this inner product term to the scattering coefficients A_m. First, we note that as $(r_0 - r) \to \infty$,

$$L_{1_m} \sim \frac{1}{4kh_0} \left(\frac{\mathrm{i}m}{r\sigma(x)} \right) \mathrm{J_m}(kr)\mathrm{H_m}(kr_0)\overline{\chi}_0(z)\psi_0(z_0)\mathrm{e}^{-\mathrm{i}m(\theta-\theta_0)} \tag{7.3.27}$$

and

$$L_{2_m} \sim \frac{1}{4kh_0} \frac{\partial}{\partial r} \mathrm{J_m}(kr)\mathrm{H_m}(kr_0)\overline{\chi}_0(z)\psi_0(z_0)\mathrm{e}^{-\mathrm{i}m(\theta-\theta_0)} \tag{7.3.28}$$

which may be determined from the far-field form of G_m by using (7.2.19). Hence, taking $r_0 \to \infty$ in (7.3.19) and using (7.3.27) and (7.3.28) in conjunction with the far-field form of Φ provided by equations (7.2.7) and (7.2.11) gives, after some algebra,

$$A_m = -\langle \Phi_m, F_m \rangle \tag{7.3.29}$$

where A_m are the coefficients in (7.2.7). In fact, if we are seeking the far field of the scattered potential these $\{A_m\}$ may be viewed as the principal unknowns in our problem. This last equation holds the key to the continued development of the formulation, since now it can used to substitute in (7.3.26), resulting in

$$\Phi_m(\mathbf{r}_0) = (1 + A_m)\Phi_{0_m}(\mathbf{r}_0) - \iint_\Sigma \left(\frac{1}{r} \frac{\partial}{\partial s} \left(r \widehat{L}_{2_m} \right) - \frac{\partial \widehat{L}_{1_m}}{\partial t} \right) \Phi_m(s,t) \, \mathrm{d}S. \tag{7.3.30}$$

Now (7.3.30) may be regarded as a second-kind integral equation for Φ_m for points on Σ, by moving the field point $\mathbf{r}_0$ onto $(s_0, t_0) \in \Sigma$. As in Chapter 5, this lends itself to a boundary integral/collocation approach. So we define an integral operator

$$(\mathcal{K}_1\Phi_m)(s_0,t_0) = \Phi_m(s_0,t_0) + \iint_\Sigma \left(\frac{1}{r} \frac{\partial}{\partial s} \left(r \widehat{L}_{2_m} \right) - \frac{\partial \widehat{L}_{1_m}}{\partial t} \right) \Phi_m(s,t) \, \mathrm{d}S \tag{7.3.31}$$

and a set of functions $\varphi_m^{(1)}$, $m = 0, 1, \ldots,$ such that

$$(\mathcal{K}_1 \varphi_m^{(1)})(s_0, t_0) = \Phi_{0m} \tag{7.3.32}$$

then the solution to the m'th mode problem is given by

$$\Phi_m = (1 + A_m)\varphi_m^{(1)}, \tag{7.3.33}$$

and consequently, on substituting (7.3.33) in (7.3.29) we deduce that

$$A_m = \frac{-\langle \varphi_m^{(1)}, F_m \rangle}{1 + \langle \varphi_m^{(1)}, F_m \rangle} \tag{7.3.34}$$

Alternatively we may develop the formulation anticipating a self-adjoint structure in the final integral equations that is not enjoyed by an integral equation arising directly from (7.3.31). Thus, we first introduce quantities which apply to the field variable $\mathbf{r}_0$, namely

$$\left.\begin{aligned} \mathbf{n}_0 &= (-h'(r_0), 0, 1)/\sigma(r_0) \\ \mathbf{s}_0 &= (1, 0, h'(r_0))/\sigma(r_0) \\ \mathbf{t}_0 &= (0, 1, 0) \end{aligned}\right\}, \qquad \nabla_0 \equiv \left(\frac{\partial}{\partial r_0}, \frac{1}{r}\frac{\partial}{\partial \theta_0}, \frac{\partial}{\partial z_0}\right). \tag{7.3.35}$$

The definition of the orthonormal basis $\{\mathbf{n}_0, \mathbf{s}_0, \mathbf{t}_0\}$ is extended to points away from the surface Σ where we apply the operator $\mathbf{n}_0.\nabla_0$ to (7.3.30) for points off Σ to obtain

$$\begin{aligned} \mathbf{n}_0.\nabla_0\Phi_m = (1 + A_m)\mathbf{n}_0.\nabla_0\Phi_{0_m} \\ - \mathbf{n}_0.\nabla_0 \iint_\Sigma \left(\frac{1}{r}\frac{\partial}{\partial s}\left(r\widehat{L}_{2m}\right) - \frac{\partial \widehat{L}_{1m}}{\partial t}\right)\Phi_m(s,t)\,\mathrm{d}S \end{aligned} \tag{7.3.36}$$

Results analogous to (7.3.8) can be established so that vector potentials, $\mathbf{H}_{im}$ and $\Psi_{0m}^{\pm}$, are defined, for points off Σ by

$$\nabla_0 \widehat{L}_{im} = \nabla_0 \times \mathbf{H}_{im}, \qquad (i = 1, 2), \qquad \text{and} \qquad \nabla_0 \Phi_{0m} = \nabla_0 \times \Psi_{0m}, \tag{7.3.37}$$

which, for similar reasons as chosen earlier, are defined by

$$\mathbf{H}_{im}(\mathbf{r}; \mathbf{r}_0) = \left(\tfrac{1}{r_0}(\widehat{L}_{im})_{\theta_0}^{z_0}, -(\widehat{L}_{im})_{r_0}^{z_0}, 0\right), \qquad i = 1, 2 \tag{7.3.38}$$

and

$$\Psi_{0m}(\mathbf{r}_0) = \left(\tfrac{1}{r_0}(\Phi_{0m})^{z_0}_{\theta_0}, -(\Phi_{0m})^{z_0}_{r_0}, 0\right). \tag{7.3.39}$$

As earlier, the convention of subscripts and superscripts implying differentiation and integration (respectively) apply here.

Thus, using $\mathbf{n}_0 = \mathbf{s}_0 \times \mathbf{t}_0$ we find, in a similar manner to before, that

$$\mathbf{n}_0.\nabla_0 \widehat{L}_{im} = \frac{1}{r_0}\frac{\partial}{\partial s_0}(r_0 H_{i2m}) - \frac{\partial H_{i1m}}{\partial t_0} \tag{7.3.40}$$

where $\partial/\partial s_0 = \mathbf{s}_0.\nabla_0$, $\partial/\partial t_0 = \mathbf{t}_0.\nabla_0$. Here,

$$H_{11,m}(\mathbf{r};\mathbf{r}_0) = \mathbf{H}_{1m}.\mathbf{s}_0 = \frac{(\widehat{G}_m)^{zz_0}_{\theta\theta_0}}{r\sigma(r)r_0\sigma(r_0)} \equiv \frac{m^2 e^{im(\theta_0-\theta)}}{r\sigma(r)r_0\sigma(r_0)} h_{11,m}(r,z;r_0,z_0) \tag{7.3.41}$$

$$H_{12,m}(\mathbf{r};\mathbf{r}_0) = \mathbf{H}_{1m}.\mathbf{t}_0 = \frac{-(\widehat{G}_m)^{zz_0}_{\theta r_0}}{r\sigma(r)} \equiv \frac{ime^{im(\theta_0-\theta)}}{r\sigma(r)} h_{12,m}(r,z;r_0,z_0) \tag{7.3.42}$$

$$H_{21,m}(\mathbf{r};\mathbf{r}_0) = \mathbf{H}_{2m}.\mathbf{s}_0 = \frac{-(\widehat{G}_m)^{zz_0}_{r\theta_0}}{r_0\sigma(r_0)} \equiv \frac{-ime^{im(\theta_0-\theta)}}{r_0\sigma(r_0)} h_{21,m}(r,z;r_0,z_0) \tag{7.3.43}$$

$$H_{22,m}(\mathbf{r};\mathbf{r}_0) = \mathbf{H}_{2m}.\mathbf{t}_0 = (\widehat{G}_m)^{zz_0}_{rr_0} \equiv e^{im(\theta_0-\theta)} h_{22,m}(r,z;r_0,z_0) \tag{7.3.44}$$

where

$$h_{11,m}(r,z;r_0,z_0) = \hat{g}_m|^{zz_0} = \frac{1}{4}\mathrm{J_m}(kr_<)\mathrm{Y_m}(kr_>)\frac{\chi_0(z)\chi_0(z_0)}{k^2 h_0} + \frac{1}{2\pi}\sum_{n=1}^{\infty}\mathrm{I_m}(k_n r_<)\mathrm{K_m}(k_n r_>)\frac{\chi_n(z)\chi_n(z_0)}{k_n^2 h_0} \tag{7.3.45}$$

$$h_{12,m}(r,z;r_0,z_0) = \hat{g}_m|^{zz_0}_{r_0} = \frac{\partial}{\partial r_0} h_{11_m}(r,z;r_0,z_0) \tag{7.3.46}$$

$$h_{21,m}(r,z;r_0,z_0) = \hat{g}_m|^{zz_0}_{r} = \frac{\partial}{\partial r} h_{11_m}(r,z;r_0,z_0) = h_{12_m}(r_0,z_0;r,z) \tag{7.3.47}$$

$$h_{22,m}(r,z;r_0,z_0) = \hat{g}_m|^{zz_0}_{rr_0} = \frac{1}{4}\mathrm{J'_m}(kr_<)\mathrm{Y'_m}(kr_>)\frac{\chi_0(z)\chi_0(z_0)}{h_0} + \frac{1}{2\pi}\sum_{n=1}^{\infty}\mathrm{I'_m}(k_n r_<)\mathrm{K'_m}(k_n r_>)\frac{\chi_n(z)\chi_n(z_0)}{h_0} \tag{7.3.48}$$

Notice from above that

$$H_{ijm}(\mathbf{r};\mathbf{r}_0) = \overline{H}_{jim}(\mathbf{r}_0;\mathbf{r}), \qquad i,j = 1,2 \tag{7.3.49}$$

a property which holds as a direct consequence of the original decomposition of G_m in (7.2.18).

Less complicated, but along the same lines,

$$\mathbf{n}_0.\nabla_0\Phi_{0m} = \frac{1}{r_0}\frac{\partial}{\partial s_0}(r_0\Psi_{2m}) - \frac{\partial\Psi_{1m}}{\partial t_0} \tag{7.3.50}$$

where

$$\Psi_{1m}(\mathbf{r}_0) = \Psi_{0m}.\mathbf{s}_0 = \frac{(\Phi_{0m})^{z_0}_{\theta_0}}{r_0\sigma(r_0)} = \frac{m}{kr_0\sigma(r_0)}f_m(\mathbf{r}_0) \tag{7.3.51}$$

$$\Psi_{2m}(\mathbf{r}_0) = \Psi_{0m}.\mathbf{t}_0 = -(\Phi_{0_m})^{z_0}_{r_0} = \frac{\mathrm{i}}{k}\frac{\partial}{\partial r_0}f_m(\mathbf{r}_0) \tag{7.3.52}$$

and $f_m(\mathbf{r})$ is defined in (7.3.23).

We now substitute (7.3.40) and (7.3.50) into (7.3.36) and let the field point $\mathbf{r}_0 \rightarrow (s_0, t_0)$, a point on Σ, to obtain

$$\begin{aligned} 0 = 4\mathrm{i}h_0(1+A_m)F_m(s_0,t_0) - \frac{1}{r_0}\frac{\partial}{\partial s_0}\left(r_0\iint_\Sigma\left(\frac{1}{r}\frac{\partial}{\partial s}(rH_{22,m}) - \frac{\partial}{\partial t}H_{12,m}\right)\Phi_m(s,t)\,\mathrm{d}S\right) \\ + \frac{\partial}{\partial t_0}\iint_\Sigma\left(\frac{1}{r}\frac{\partial}{\partial s}(rH_{21,m}) - \frac{\partial}{\partial t}H_{11,m}\right)\Phi_m\,\mathrm{d}S \end{aligned} \tag{7.3.53}$$

and the bed condition (7.2.3) has been applied to render the left-hand side zero.

Thus (7.3.53) now represents an integro-differential equation for the function Φ_m. It proves convenient to define the integro-differential operator in (7.3.53) as

$$\begin{aligned} (\mathcal{K}_2\Phi_m)(s_0,t_0) \equiv \frac{1}{r_0}\frac{\partial}{\partial s_0}\left(r_0\iint_\Sigma\left(\frac{1}{r}\frac{\partial}{\partial s}(rH_{22,m}) - \frac{\partial}{\partial t}H_{12,m}\right)\Phi_m(s,t)\,\mathrm{d}S\right) \\ - \frac{\partial}{\partial t_0}\iint_\Sigma\left(\frac{1}{r}\frac{\partial}{\partial s}(rH_{21,m}) - \frac{\partial}{\partial t}H_{11,m}\right)\Phi_m\,\mathrm{d}S. \end{aligned} \tag{7.3.54}$$

If a set of functions $\varphi_m^{(2)}(s,t)$ is defined on Σ to satisfy

$$(\mathcal{K}_2\varphi_m^{(2)})(s_0,t_0) = F_m(s_0,t_0), \qquad (s_0,t_0)\in\Sigma \tag{7.3.55}$$

then it follows that the solution of (7.3.53) is given by

$$\Phi_m(s,t) = 4\mathrm{i}h_0(1+A_m)\varphi_m^{(2)}(s,t). \tag{7.3.56}$$

Using (7.3.52) in (7.3.29) gives, after some rearrangement

$$A_m = \frac{-4ih_0 \langle \varphi_m^{(2)}, F_m \rangle}{1 + 4ih_0 \langle \varphi_m^{(2)}, F_m \rangle} \tag{7.3.57}$$

thus effectively solving the problem for the m'th mode.

7.4 Approximation and numerical method

The problem of determining the angular variation of the scattered wavefield has been reduced to one in which we need to determine the constants A_m in terms of inner products (7.3.30) and (7.3.53) involving functions $\varphi_m^{(i)}$ which for $i = 1, 2$ are the solutions of the integral equations (7.3.28) and (7.3.51) respectively. As in Chapter 5, each of the integral equations is amenable to different approaches, depending upon whether the underlying integral operator, is, or is not, self-adjoint.

7.4.1 Boundary element approach

We have already seen that non self-adjoint operators such as $\mathcal{K}_1$ are best suited to the boundary element approach in this weakly singular formulation and this is the course we follow now. Until this point we have not taken advantage of the axial symmetry to reduce the dimension of the problem retaining a three-dimensional formulation so we may operate on the equation using vector differential calculus. At this point we acknowledge that the factors $e^{im\theta}$ and $e^{im(\theta_0-\theta)}$ are embedded in the definitions of Φ_m and G_m etc and so we simplify the integral equation (7.3.30) to give its two-dimensional form

$$\phi_m(r_0, z_0) = \phi_{0m}(r_0, z_0)(1 + A_m) - 2\pi \int_\Gamma \left(\frac{\partial}{\partial s}(-r(\widehat{g}_m)_r^z) + \frac{m^2}{r\sigma}(\widehat{g}_m)^z \right) \phi_m(r, z)\, \mathrm{d}s. \tag{7.4.1}$$

The associated integral operator $\mathcal{K}_1$ reduces to

$$(\mathcal{K}_1\phi)(s_0) \equiv \phi_m(r_0, z_0) + 2\pi \int_\Gamma \left(\frac{\partial}{\partial s}(-r(\widehat{g}_m)_r^z) + \frac{m^2}{r\sigma}(\widehat{g}_m)^z \right) \phi_m(r, z)\, \mathrm{d}s \tag{7.4.2}$$

and on defining the real quantity

$$R(s_0) = \mathrm{i}^{-m}\phi_{0m}(s_0), \tag{7.4.3}$$

we obtain a real integral equation

$$(\mathcal{K}_1\varphi_m^{(1)})(s_0) = R(s_0) \tag{7.4.4}$$

gives the solution in the form

$$\phi_m = \mathrm{i}^m(1 + A_m)\varphi_m^{(1)}. \tag{7.4.5}$$

We solve this equation by projecting the curve Γ down onto the r axis dividing the interval $[0, a]$ into N intervals of equal length. Thus we define

$$\begin{aligned} r_i &= \text{the mid point of the i'th panel,} \\ I_i &= \text{the i'th interval on the } r \text{ axis,} \\ \Gamma_i &= \text{the i'th panel on the } \Gamma \text{ projecting onto } I_i, \\ \varphi_i^m &= \varphi_m \text{ at the mid point of the i'th panel,} \end{aligned}$$

in which the collocation scheme becomes

$$\varphi_i^m + 2\pi\sum_{j=1}^{N}\varphi_j^m \int_{\Gamma_j} \frac{\partial}{\partial s}\left(-r\hat{g}_m|_r^z(r, h(r); r_j, h(r_j))\right) + \frac{m^2}{r\sigma}\hat{g}_m|^z(r, h(r); r_j, h(r_j))\,\mathrm{d}s = R_i, \qquad i = 1, \ldots, N. \tag{7.4.6}$$

Then upon projecting, and integrating the first term in the integral explicitly it becomes

$$\varphi_i^m - (M_{i,j}^{1m} - M_{i,j}^{2m})\varphi_j^m = R_i, \qquad i, j = 1, \ldots, N \tag{7.4.7}$$

where

$$M_{i,j}^{1m} = 2\pi\left[r\hat{g}_m|_r^z(r, h(r); r_i, h(r_i))\right]_{I_j} \tag{7.4.8}$$

and

$$M_{i,j}^{2m} = 2\pi m^2 \int_{I_j} \frac{1}{r}\hat{g}_m|^z(r, h(r); r_i, h(r_i))\,\mathrm{d}r. \tag{7.4.9}$$

Also, in order to calculate the A_m using (7.3.29) we need

$$F_i^m = (-\mathrm{i})^m \frac{\pi}{2kh_0} \int_{\Gamma_i} \frac{\partial}{\partial s}\left(-r\chi_0(h(r))\frac{\partial J_m(kr)}{\partial r}\right) + \frac{m^2}{r\sigma} J_m(kr)\chi_0(h(r))\,\mathrm{d}s$$

$$= -(-\mathrm{i})^{m+1}\,\frac{\pi}{2kh_0 N_0^{1/2}}\left\{ [-kr J_m'(kr)\sinh k(d-h(r))]_{I_i} + \right.$$

$$\left. m^2 \int_{I_i} \frac{1}{r} J_m(kr)\sinh k(d-h(r))\,\mathrm{d}r \right\}$$

$$= -(-\mathrm{i})^{m+1} f_i^m, \tag{7.4.10}$$

which also serves to define the real quantities f_i^m. The using (7.4.5), (7.4.10) and (7.3.29) we find, after some rearrangement that

$$A_m = \frac{-\mathrm{i}\sum_{i=1}^{N} \varphi_i^m f_i^m}{1 + \mathrm{i}\sum_{i=1}^{N} \varphi_i^m f_i^m} \tag{7.4.11}$$

where the products under the summation are real quantities.

7.4.2 Rayleigh-Ritz approach

The integral operator $\mathcal{K}_2$ is self-adjoint and therefore amenable to solution by the Rayleigh-Ritz method. In order to solve this integral equation, we use a standard variational principle applicable to self-adjoint operators. So, with $p_m \in \mathcal{H} = L_2(\Sigma)$, we define the functional $J : \mathcal{H} \to \mathbb{C}$ by

$$J(p_m) = \langle p_m, F_m\rangle + \langle F_m, p_m\rangle - \langle \mathcal{K}_2 p_m, p_m\rangle \tag{7.4.12}$$

where we have used the inner product notation of (7.3.25). This functional is designed to be stationary at $p_m = \varphi_m^{(2)}$ where its value is

$$J(\varphi_m^{(2)}) \equiv \langle \varphi_m^{(2)}, F_m\rangle = P_m. \tag{7.4.13}$$

An approximation to $\varphi_m^{(2)}$, say $\widetilde{\varphi}_m^{(2)}$ gives rise to approximate values of P_m, say $\widetilde{P}_m$. The variational principles above immediately give rise to the estimate

$$|P_m - \widetilde{P}_m| = O(||\varphi_m^{(2)} - \widetilde{\varphi}_m^{(2)}||)^2. \tag{7.4.14}$$

That is, the approximations to the quantities of interest are second-order accurate with respect to first-order approximations (in an L_2 norm sense) to the exact solutions of the integral equations.

Adopting this principle $\varphi_m^{(2)}$ is approximated by $\tilde{\varphi}_m^{(2)} \in \mathcal{H}_{N+1}$, an $N+1$-dimensional subspace of $\mathcal{H}$, spanned by a set of test functions $v_i(s,t) \in \mathcal{H}_{N+1}$, by writing

$$\varphi_m^{(2)} \approx \tilde{\varphi}_m^{(2)} = \sum_{i=0}^{N} a_i^{(m)} v_i^{(m)}(s,t). \tag{7.4.15}$$

This approximation is substituted in place of p_m in (7.4.12). By making the resulting expression stationary with respect to $a_i^{(m)}$, we arrive at the system of equations

$$\sum_{j=0}^{N} a_j^{(m)} \langle \mathcal{K} v_i^{(m)}, v_j^{(m)} \rangle = \langle F_m, v_i^{(m)} \rangle. \qquad i = 0, 1, \ldots, N \tag{7.4.16}$$

The system of equations at (7.4.16) is equivalent to direct application of Galerkin's method to the original integral equations and the resulting approximation to P_m is

$$\tilde{P}_m = \sum_{i=0}^{N} a_i^{(m)} \langle v_i^{(m)}, F_m \rangle. \tag{7.4.17}$$

The test functions are defined to model the potential Φ_m over the ridge, so that it is sensible to write (noting, for the first time, that in fact $\theta \equiv t$)

$$v_i^{(m)}(s,t) = e^{imt} q_i(s) \tag{7.4.18}$$

and although it is possible, we choose not to specify q_i at this point, but we note that, without loss of generality, we may assume that q_i is real.

Things now become rather complicated as we sort through the implications of (7.4.16). We write

$$\langle \mathcal{K}_2 v_i, v_j \rangle \equiv K_{ij}^{(m)} = K_{ij,m}^{(11)} + K_{ij,m}^{(12)} + K_{ij,m}^{(21)} + K_{ij,m}^{(22)} \tag{7.4.19}$$

in a notation which is implied (in an obvious way) by the four separate components

of $\mathcal{K}_2$ so that

$$K_{ij,m}^{(22)} = \iint_{\Sigma} \overline{v_j^{(m)}}(s_0,t_0)\frac{1}{r_0}\frac{\partial}{\partial s_0}\left(r_0\iint_{\Sigma}\left(\frac{1}{r}\frac{\partial}{\partial s}(rH_{22,m})\right)v_i^{(m)}(s,t)\,\mathrm{d}S\right)\,\mathrm{d}S_0, \tag{7.4.20}$$

$$K_{ij,m}^{(12)} = \iint_{\Sigma} \overline{v_j^{(m)}}(s_0,t_0)\frac{1}{r_0}\frac{\partial}{\partial s_0}\left(r_0\iint_{\Sigma}\left(-\frac{\partial}{\partial t}H_{12,m}\right)v_i^{(m)}(s,t)\,\mathrm{d}S\right)\,\mathrm{d}S_0, \tag{7.4.21}$$

$$K_{ij,m}^{(21)} = \iint_{\Sigma} \overline{v_j^{(m)}}(s_0,t_0)\frac{\partial}{\partial t_0}\iint_{\Sigma}\left(-\frac{1}{r}\frac{\partial}{\partial s}(rH_{21,m})\right)v_i^{(m)}(s,t)\,\mathrm{d}S\,\mathrm{d}S_0, \tag{7.4.22}$$

and

$$K_{ij,m}^{(11)} = \iint_{\Sigma} \overline{v_j^{(m)}}(s_0,t_0)\frac{\partial}{\partial t_0}\iint_{\Sigma}\frac{\partial}{\partial t}H_{11,m}v_i^{(m)}(s,t)\,\mathrm{d}S\,\mathrm{d}S_0. \tag{7.4.23}$$

At this point, we acknowledge the fact that $\theta \equiv \mathrm{t}$, so consequently $\partial/\partial t \equiv r^{-1}\partial/\partial\theta$ and $\mathrm{d}S = r\,\mathrm{d}\theta\,\mathrm{d}s$. We then exploit the dependence on the θ coordinate in v_i and H_{ij} (see (7.3.41)–(7.3.44), (7.4.18)), to reduce (7.4.20)–(7.4.23) to

$$K_{ij,m}^{(22)} = 4\pi^2\int_{\Gamma} q_j(s_0)\frac{\partial}{\partial s_0}\left(r_0\int_{\Gamma}\left(\frac{\partial}{\partial s}(rh_{22,m})\right)q_i(s)\,\mathrm{d}s\right)\,\mathrm{d}s_0, \tag{7.4.24}$$

$$K_{ij,m}^{(12)} = -4\pi^2m^2\int_{\Gamma} q_j(s_0)\frac{\partial}{\partial s_0}\left(r_0\int_{\Gamma}h_{12,m}\frac{q_i(s)}{r}\frac{\mathrm{d}s}{\sigma}\right)\,\mathrm{d}s_0, \tag{7.4.25}$$

$$K_{ij,m}^{(21)} = -4\pi^2m^2\int_{\Gamma}\frac{q_j(s_0)}{r_0}\int_{\Gamma}\left(\frac{\partial}{\partial s}(rh_{21,m})\right)q_i(s)\,\mathrm{d}s\frac{\mathrm{d}s_0}{\sigma_0}, \tag{7.4.26}$$

and

$$K_{ij,m}^{(11)} = 4\pi^2m^4\int_{\Gamma}\frac{q_j(s_0)}{r_0}\int_{\Gamma}h_{11,m}\frac{q_i(s)}{r}\frac{\mathrm{d}s}{\sigma}\frac{\mathrm{d}s_0}{\sigma_0}. \tag{7.4.27}$$

At this point we may integrate by parts, taking care to deal with any discontinuities in the integrands. In fact, only $h_{12,m}$ and $h_{12,m}$ are affected and in (7.4.26) we apply integration by parts to the integral of a discontinuous function which is smooth, so throws up no additional term. In contrast only (7.4.26) requires special treatment as

$h_{21,m}$ is discontinuous along $r = r_0$. Therefore we deduce that

$$K_{ij,m}^{(22)} = 4\pi^2 \int_\Gamma \int_\Gamma h_{22,m} r q_i'(s) r_0 q_j'(s_0)\, \mathrm{d}s\, \mathrm{d}s_0, \tag{7.4.28}$$

$$K_{ij,m}^{(12)} = 4\pi^2 m^2 \int_\Gamma \int_\Gamma h_{12,m} \frac{q_i(s)}{r} r_0 q_j'(s_0) \frac{\mathrm{d}s}{\sigma}\, \mathrm{d}s_0, \tag{7.4.29}$$

$$K_{ij,m}^{(11)} = 4\pi^2 m^4 \int\int h_{11,m} \frac{q_i(s)}{r} \frac{q_j(s_0)}{r_0} \frac{\mathrm{d}s}{\sigma} \frac{\mathrm{d}s_0}{\sigma_0}, \tag{7.4.30}$$

while

$$K_{ij,m}^{(21)} = 4\pi^2 m^2 \int_\Gamma \int_\Gamma h_{21,m} r q_i'(s) \frac{q_j(s_0)}{r_0}\, \mathrm{d}s \frac{\mathrm{d}s_0}{\sigma_0} - 4\pi^2 m^2 \int_\Gamma q_i(s_0) q_j(s_0) \left[h_{21,m}\right]_{r_0-}^{r_0+} \mathrm{d}s_0. \tag{7.4.31}$$

We find, using (5.3.35) that

$$\left[h_{21,m}\right]_{r_0-}^{r_0+} = \frac{1}{2\pi r_0}(h_0 - h(r_0)) \tag{7.4.32}$$

which can be used to simplify (7.4.31) further.

The integral equation has now been reduced to one which is determined by four integral kernels which are at worst only weakly singular. The kernels $K_{ij,m}^{(11)}$ and $K_{ij,m}^{(22)}$ relate to the self interactions of the flows along and across the seamount respectively, whereas $K_{ij}^{(12)}$ and $K_{ij}^{(21)}$ relate to the cross interactions between these two flow directions

As in earlier chapters, it is assumed that $h(r)$ is a single-valued function and so the seamount has no overhangs, allowing us to project the integration from the curve Γ onto the interval $r \in [0, a]$. This implies the simplified (and computationally friendly) form

$$K_{ij,m}^{(11)} = 4\pi^2 m^4 \int_0^a \int_0^a h_{11,m}(r, h(r); r_0, h(r_0)) \frac{q_i(r) q_j(r_0)}{r r_0}\, \mathrm{d}r\, \mathrm{d}r_0 \tag{7.4.33}$$

where

$$q_i(r) \equiv q_i(s), \qquad \mathrm{d}s = \sigma(r)\, \mathrm{d}r. \tag{7.4.34}$$

We note that boundedness at the origin is guaranteed as, either $m = 0$ or $h_{ij,m}$ behaves like r^m, or r_0^m as $r \to 0$ or $r_0 \to 0$ respectively . We also note from (7.4.33) that $K_{ij,m}^{(11)} = K_{ji,m}^{(11)}$ and by assumption, $K_{ij,m}^{(11)}$ is real.

A similar procedure is followed for the remaining elements $K_{ij,m}^{(\alpha\beta)}$ $\alpha, \beta = 1, 2$ and the details are omitted. We find that

$$K_{ij,m}^{(12)} = 4\pi^2 m^2 \int_0^a \int_0^a h_{12,m}(r, h(r); r_0, h(r_0)) \frac{q_i(r)}{r} r_0 q_j'(r_0)\, \mathrm{d}r\, \mathrm{d}r_0 \qquad (7.4.35)$$

$$K_{ij,m}^{(21)} = 4\pi^2 m^2 \int_0^a \int_0^a h_{21,m}(r, h(r); r_0, h(r_0)) r q_i'(r) \frac{q_j(r_0)}{r_0}\, \mathrm{d}r\, \mathrm{d}r_0$$

$$- 4\pi^2 m^2 \int_0^a q_i(r_0) q_(r_0) \frac{(h_0 - h(r_0))}{2\pi r_0}\, \mathrm{d}r_0 \qquad (7.4.36)$$

$$K_{ij,m}^{(22)} = 4\pi^2 \int_0^a \int_0^a h_{22,m}(r, h(r); r_0, h(r_0)) r q_i'(r) r_0 q_j'(r_0)\, \mathrm{d}r\, \mathrm{d}r_0 \qquad (7.4.37)$$

so that $K_{ij,m}^{(21)} = K_{ji,m}^{(12)}$ and $K_{ij,m}^{(22)} = K_{ji,m}^{(22)}$ are all real and convergence at the origin is guaranteed by the structure of the kernels. Hence, the matrix of elements $K_{ij}^{(m)}$ in (7.4.19) is real and symmetric. Furthermore we note that

$$K_{ij}^{(m)} = K_{ij}^{(-m)} \qquad (7.4.38)$$

which may be easily shown using the standard results

$$\begin{aligned} \mathrm{J_m}(z) &= (-1)^m \mathrm{J_{-m}}(z), \\ \mathrm{Y_m}(z) &= (-1)^m \mathrm{Y_{-m}}(z), \\ \mathrm{I_m}(z) &= \mathrm{I_{-m}}(z), \\ \mathrm{K_m}(z) &= \mathrm{K_{-m}}(z). \end{aligned}$$

Let us now turn to the the right-hand side terms in (7.4.16). Thus from the definition of F_m in (7.3.24)

$$\langle F_m, v_j^{(m)} \rangle \equiv F_{j,m} = \frac{\mathrm{i}^m}{4kh_0} \iint_\Sigma \left(\frac{1}{r} \frac{\partial}{\partial s} (kr J_m'(kr) \chi_0(z)) - \frac{m^2}{r^2 \sigma} J_m(kr) \chi_0(z) \right) q_i(s)\, \mathrm{d}S, \qquad (7.4.39)$$

then projecting onto the r axis gives

$$F_{j,m} = \frac{\pi \mathrm{i}^{m+1}}{2kh_0 N_0^{1/2}} \int_0^a \sinh k(d - h(r)) \left\{ kr \mathrm{J_m'}(kr) q_j'(r) + m^2 \mathrm{J_m}(kr) \frac{q_j(r)}{r} \right\} \mathrm{d}r \qquad (7.4.40)$$

It follows that $F_{j,m} = F_{j,-m}$ and therefore we deduce that $\phi_m = \phi_{-m}$ where the ϕ_m are defined in (7.3.6). Thus to obtain the sum from $-M \rightarrow M$ we only need to solve the first $M+1$ equations i.e. for $m = 0, 1, \ldots, M$ and use the result that $A_m = A_{-m}$. This is as expected since the incident wave has $\theta_{inc} = 0$ which implies symmetry in θ.

Let us now briefly turn to some of the numerical issues surrounding the computation of the solution. Firstly the main requirement on the test functions $q_i(r)$ is that they form a complete set on the interval $[0, a]$. If we also require that they be orthogonal with respect to the inner product, this implies that the Bessel functions of the first kind of order m, $J_m(k_{m,n}r/a)$ $n = 1, \ldots$ are the natural choice, where k_{mn} is the n'th zero of either $J_m(r)$ (Fourier-Bessel series) or $J'_m(r)$ (Dini series). As discussed earlier, trial functions which incorporate the local fluid behaviour are likely to provide better approximations for a fixed truncation size; in this respect $J_m(\lambda_i r/a)$ has the correct behaviour as $r \rightarrow 0$. The behaviour at $r = a$ depends upon whether, or not, the patch of topography joins the domain of constant depth smoothly. If the join is smooth then the Fourier Bessel series is appropriate, whereas for a join with discontinuous slope, then the Dini series is more appropriate. If the join has a discontinuous slope then the local fluid motion is like that within a wedge and consequently the bed flux must vanish at the join where a wedge flow has a stagnation point. In this respect the potential should be modeled by a Dini series so that the flux will vanish. The only additional complexity with a Dini series is that the set of test functions for the $m = 0$ mode must include a constant term which is not required for higher order modes. In fact our numerical experiments demonstrated that, even for a smooth join, the Fourier Bessel series offered no advantages over the Dini series. Accordingly, for all results that follow we used the Dini series.

Before turning to some of the numerical issues we note that in our approach we non-dimensionalize the bedform using the transformation

$$\hat{h}(r) = \frac{h_0 - h(ar)}{h_1} \qquad 0 \leq r \leq 1 \tag{7.4.41}$$

so that $\hat{h}(1) = 0$ and $\hat{h}(r) = 1$ where $h_0 - h(r) = h_1$. Thus $\hat{h}$ effectively scales the bedform to fit into a unit square. Now there are four separate elements, $K_{ij}^{\alpha\beta}$, $\alpha, \beta = 1, 2$ which are real and make up K_{ij} and, although symmetry implies only half the elements need to be computed, each factor requires the evaluation of a double-integral in which the kernel is not separable. It is illustrative to consider the asymptotic behaviour of the infinite sums arising in each $h_{\alpha\beta,m}$. For this we use the following asymptotic results from Watson [100] §7.23

$$I_m(z) \sim \frac{\mathrm{e}^z}{\sqrt{2\pi z}} \tag{7.4.42}$$

$$K_m(z) \sim \sqrt{\frac{\pi}{2z}}\mathrm{e}^{-z} \tag{7.4.43}$$

and the similar forms for their derivatives

$$I'_m(z) \sim \frac{\mathrm{e}^z}{\sqrt{2\pi z}} \tag{7.4.44}$$

$$K'_m(z) \sim -\sqrt{\frac{\pi}{2z}}\mathrm{e}^{-z}. \tag{7.4.45}$$

Furthermore we note that the dispersion relation (2.1.44) implies (2.1.46) i.e. $k_n d \sim n\pi$ as $n \to \infty$ and therefore we also deduce that

$$\chi_n(h(r)) \sim \sqrt{2}\sin(n\pi h_1 \hat{h}(ar)/h_0). \tag{7.4.46}$$

Using these results we see that the summands in the $h_{\alpha\beta_m}$ all include the term

$$\mathrm{e}^{-n\pi|r-r_0|/h_0} \tag{7.4.47}$$

in their asymptotic form. Therefore the kernels are relatively easy to compute apart from along the line $r = r_0$ where convergence is only algebraic. We anticipate the severest problems in the kernel h_{22}, where along the line $r = r_0$ we see that the summand behaves like

$$\sum_{n=1}^{\infty} \frac{1}{n\pi} \tag{7.4.48}$$

and which is indicative of the logarithmic singularity. Thus following the approach of Porter & Porter [77], we write

$$e_{ij} = \int_0^a q'_j(r_0) \int_0^a q'_i(r) \sum_{n=1}^{\infty} I'_m(k_n r_<) K'_m(k_n r_>) \frac{\chi_n(r)\chi_n(r_0)}{h_0} r r_0 \,\mathrm{d}r \,\mathrm{d}r_0 \tag{7.4.49}$$

then using (7.4.44), (7.4.45) and (7.4.46) we rewrite the infinite sum in (7.4.49) as

$$\sum_{n=1}^{\infty}\Bigg[\frac{\chi_n(h(r))\chi_n(h(r_0))}{h_0}\mathrm{I}'_{\mathrm{m}}(k_n r_<)\mathrm{K}'_{\mathrm{m}}(k_n r_>) + \frac{\mathrm{e}^{-n\pi|r-r_0|/d}}{n\pi\sqrt{rr_0}}\sin(n\pi h_1\hat{h}(r)/h_0)\sin(n\pi h_1\hat{h}(r)/h_0)\Bigg] - \sum_{n=1}^{\infty}\frac{\mathrm{e}^{-n\pi|r-r_0|/h_0}}{n\pi\sqrt{rr_0}}\sin(n\pi h_1\hat{h}(r)/d)\sin(n\pi h_1\hat{h}(r)/h_0) \quad (7.4.50)$$

The sum in the square brackets, which we now call $S(r,r_0)$, now converges for $0 \leq r, r_0 \leq a$, as we have removed the asymptotic leading order contribution (convergence of the integrand at $r, r_0 = 0$ is ensured as the infinite sum is multiplied by rr_0). We call the corresponding integral $e_{ij}^{(1)}$ so that

$$e_{ij}^{(1)} = \int_0^a q_j'(r_0)\int_0^a q_i'(r)S(r,r_0)rr_0\ \mathrm{d}r\,\mathrm{d}r_0. \quad (7.4.51)$$

The asymptotic leading order contribution, which appears as the last term in (7.4.50) can be summed explicitly (Gradshteyn & Ryzhik [37], §1.462) to

$$\frac{1}{2\pi(rr_0)^{1/2}}\ln T(r,r_0) \quad (7.4.52)$$

where

$$T(r;r_0) = \left[\frac{\sin^2\{\frac{1}{2}\pi h_1(\hat{h}(r/a)+\hat{h}(r_0/a))/h_0\}+\sinh^2\{\frac{1}{2}\pi(r-r_0)/h_0\}}{\sin^2\{\frac{1}{2}\pi h_1(\hat{h}(r/a)-\hat{h}(r_0/a))/h_0\}+\sinh^2\{\frac{1}{2}\pi(r-r_0)/h_0\}}\right]^{\frac{1}{2}} \quad (7.4.53)$$

The logarithmic singularities are now contained in the integral

$$-\frac{1}{2\pi}\int_0^a q_j'(r_0)\int_0^a q_i'(r)(rr_0)^{1/2}\ln[T(r,r_0)]\ \mathrm{d}r\,\mathrm{d}r_0 = e_{ij}^{(2)} + e_{ij}^{(3)} \quad (7.4.54)$$

where

$$e_{ij}^{(2)} = -\frac{1}{2\pi}\int_0^a q_j'(r_0)\int_0^a q_i'(r)(rr_0)^{1/2}\ln[a^{-1}|r-r_0|T(r,r_0)]\ \mathrm{d}r\,\mathrm{d}r_0 \quad (7.4.55)$$

and

$$e_{ij}^{(3)} = \frac{a}{2\pi}\int_0^1 q_j'(ar_0)r_0^{1/2}\int_0^1 (r^{1/2}q_i'(ar) - r_0^{1/2}q_i'(ar_0))\ln|r-r_0|\ \mathrm{d}r\,\mathrm{d}r_0 + \frac{a}{2\pi}\int_0^1 q_j'(ar)q_i'(ar)r[r\ln(r)+(1-r)\ln(1-r)-1]\ \mathrm{d}r. \quad (7.4.56)$$

Notice that, as in Porter & Porter [77], we have dealt with the logarithmic singularity in such a way that it has been integrated out analytically. The resulting contributions are such that $e_{ij}^{(3)}$ is independent of all parameters, so only needs to be calculated once, and $e_{ij}^{(2)}$ is independent of frequency so only needs to be calculated once for each specific geometry.

The Bessel functions were calculated by the standard SLATEC routines, taking into account the exponential factors in I_m and K_m so that their product could be calculated without loss of precision. We remark that these routines also allow us to create the kernel matrices for each angular mode in one step without adding significant computational overhead.

7.4.3 Conservation of energy

A discussion of the approximation would be incomplete without a consideration of how well the approximation handles the conservation of energy. A statement equivalent to the conservation of energy in this problem is given by

$$\frac{1}{\pi}\int_0^{2\pi} |\mathcal{A}(\theta)|^2 \,\mathrm{d}\theta = -2\mathrm{Re}\mathcal{A}(0) \tag{7.4.57}$$

where

$$\mathcal{A}(\theta) = A_0 + 2\sum_{m=1}^{\infty} A_m \cos m\theta \tag{7.4.58}$$

represents the normalised angular variation of the scattered wave amplitude. This relation, first derived by Maruo [53], is discussed extensively in Mei [61] who presents a derivation of this and a range of similar results for scattering problems in both two and three dimensions. In our approximation we take a finite sum in (7.4.58) so that

$$\mathcal{A}(\theta) \sim \tilde{\mathcal{A}}(\theta) \equiv A_0 + 2\sum_{m=1}^{M} A_m \cos m\theta. \tag{7.4.59}$$

Therefore

$$-2\mathrm{Re}\tilde{\mathcal{A}}(0) = -2\mathrm{Re}\left(A_0 + 2\sum_{m=1}^{M} A_m\right) \tag{7.4.60}$$

and

$$|\mathcal{A}(\theta)|^2 = \left(A_0 + 2\sum_{m=1}^{M} A_m \cos(m\theta)\right)\left(A_0^* + 2\sum_{n=1}^{M} A_n^* \cos(n\theta)\right)$$
$$= A_0 A_0^* + 2A_0 \sum_{n=1}^{M} A_n^* \cos(n\theta) + 2A_0^* \sum_{m=1}^{M} A_m \cos(m\theta) + \ldots$$
$$\ldots 2\sum_{m=1}^{M}\sum_{n=1}^{M} A_m A_n^* \left(\cos(m+n)\theta + \cos(m-n)\theta\right). \quad (7.4.61)$$

Therefore using (7.4.60) and (7.4.61) in (7.4.57) we deduce that energy is conserved if

$$|A_0|^2 + 2\sum_{m=1}^{M} |A_m|^2 = -\mathrm{Re}\left(A_0 + 2\sum_{m=1}^{M} A_m\right). \quad (7.4.62)$$

Now equations (7.3.53) and (7.4.11) show that whatever formulation we choose the far-field coefficient A_m has the form

$$A_m = \frac{-\mathrm{i}a_m}{1 + \mathrm{i}a_m} \quad (7.4.63)$$

where a_m is a real quantity. Therefore it is routine to deduce that

$$|A_m|^2 = -\mathrm{Re}A_m \quad \forall m \quad (7.4.64)$$

thus establishing that both of our formulations satisfy energy conservation exactly on a mode by mode basis.

7.5 Results

We first consider the scattering of plane waves by a hemisphere, a problem which was solved in Chapter 4 by a multipole approach. As before, this will provide quite a severe test of our approach because of the steep gradients near the join of the seamount with the constant depth domain. We will investigate how the convergence properties of each system vary with the two main truncation parameters which are M the maximum number of angular modes and N, the number of panels for the Boundary Element method or the truncation limit of the set of test functions in the Rayleigh-Ritz method.

For clarity and compactness of presentation, rather than present tables of convergence for each of the A_m for a given problem, we consider convergence of $|\mathcal{A}(\theta)|$ for the values $\theta = 0,\ \pi/2$ and π. These values of θ are chosen to provide different combinations of the A_m and our numerical experiments show that this approach accurately represents the convergence of the real and imaginary components of the underlying A_m.

	M			
N	0	1	2	3
50	0.005894	0.077478	0.079420	0.079438
100	0.005913	0.077521	0.079466	0.079484
150	0.005918	0.077532	0.079477	0.079495
200	0.005920	0.077536	0.079482	0.079500

Table 7.1: Convergence of $|\mathcal{A}(0)|$ $(= 0.079509)$ using BE method for scattering by a hemisphere of radius $a/h_0 = 0.5$ for $kh_0 = 1$.

	M		
N	0	1	2
50	0.005894	0.005894	0.003951
100	0.005913	0.005913	0.003968
150	0.005918	0.005918	0.003972
200	0.005920	0.005920	0.003973

Table 7.2: Convergence of $|\mathcal{A}(\pi/2)|$ $(= 0.003977)$ using BE method for scattering by a hemisphere of radius $a/h_0 = 0.5$ for $kh_0 = 1$.

	M				
N	0	1	2	3	4
50	0.005894	0.005894	0.065695	0.063754	0.063772
100	0.005913	0.065701	0.063757	0.063775	0.063775
150	0.005918	0.065702	0.063757	0.063776	0.063776
200	0.005920	0.065703	0.063758	0.063776	0.063776

Table 7.3: Convergence of $|\mathcal{A}(\pi)|$ $(= 0.063776)$ using BE method for scattering by a hemisphere of radius $a/h_0 = 0.5$ for $kh_0 = 1$.

We turn first to the BE method and investigate convergence for a wave where $kh_0 = 1$ incident on a seamount where $a/h_0 = 0.5$. The results which are presented

in tables 7.1 to 7.3 are to be compared against exact value determined by the multipole method which is indicated in the caption. The first point to note is that convergence in M is rapid with no improvement in the first 6 d.p. for $M = 4$ at a fixed value of N. With a modest $N = 100$ we see that we generally achieve 5 d.p. accuracy, but further improvement is extremely slow. We also observe subjectively that, as N increases the computation time increases rapidly, this is mainly due to our using a ten point Gauss-Legendre quadrature for the integral quantities. Speed might be improved by using a less sophisticated quadrature scheme for larger numbers of panels but at a potential loss in accuracy which would need to be investigated.

	M				
N	0	1	2	3	4
0	0.005592	0.076452	0.078326	0.078343	0.078343
2	0.005923	0.077438	0.079371	0.079389	0.079389
4	0.005923	0.077504	0.079445	0.079463	0.079463
6	0.005923	0.077523	0.079466	0.079485	0.079485
8	0.005923	0.077532	0.079476	0.079494	0.079494
10	0.005923	0.077536	0.079480	0.079499	0.079499
⋮	⋮	⋮	⋮	⋮	⋮
32	0.005923	0.077544	0.079489	0.079507	0.079508

Table 7.4: Convergence of $|\mathcal{A}(0)|$ $(= 0.079509)$ using Rayleigh-Ritz method for scattering by a hemisphere of radius $a/h_0 = 0.5$ for $kh_0 = 1$.

	M			
N	0	1	2	3
0	0.005592	0.005592	0.003717	0.003717
2	0.005923	0.005923	0.003989	0.003989
4	0.005923	0.005923	0.003982	0.003982
6	0.005923	0.005923	0.003979	0.003979
8	0.005923	0.005923	0.003978	0.003978
10	0.005923	0.005923	0.003978	0.003978
11	0.005923	0.005923	0.003977	0.003977

Table 7.5: Convergence of $|\mathcal{A}(\pi/2)|$ $(= 0.003977)$ using Rayleigh-Ritz method for scattering by a hemisphere of radius $a/h_0 = 0.5$ for $kh_0 = 1$.

In tables 7.4 to 7.6 we turn to the results for the same problem as in tables 7.1 to 7.3 but solved by the Rayleigh-Ritz method. The first point to note is that

	M			
N	0	1	2	3
0	0.005592	0.065273	0.063400	0.063417
2	0.005923	0.065598	0.063665	0.063683
4	0.005923	0.065663	0.063723	0.063741
6	0.005923	0.065682	0.063740	0.063758
8	0.005923	0.065691	0.063747	0.063765
10	0.005923	0.065695	0.063751	0.063769
⋮	⋮	⋮	⋮	⋮
32	0.005923	0.065703	0.063757	0.063776

Table 7.6: Convergence of $|\mathcal{A}(\pi)|$ $(= 0.063776)$ using Rayleigh-Ritz method for scattering by a hemisphere of radius $a/h_0 = 0.5$ for $kh_0 = 1$.

convergence in M is the same in this approach with no improvement in the first 6 d.p. achieved with $M > 4$ for a fixed value of N. We see from the tables that convergence in N is also achieved in $N = 7 - 10$ resulting in a significantly smaller matrix system than the BE method. Further improvement for this problem is also slow, primarily due to the end effects near the join. However, tables 7.1 to 7.6 also serve to confirm the validity of our general method, and its implementation in our two different formulations.

	M					
N	1	2	3	4	5	6
25	1.397025	1.787216	1.839638	1.843196	1.843346	1.843350
50	1.397603	1.787824	1.840248	1.843807	1.843957	1.843961
75	1.397729	1.787957	1.840382	1.843941	1.844090	1.844095
100	1.397781	1.788011	1.840437	1.843996	1.844145	1.844150
125	1.397804	1.788035	1.840462	1.844020	1.844170	1.844174
150	1.397814	1.788047	1.840473	1.844032	1.844181	1.844186
175	1.397821	1.788054	1.840480	1.844039	1.844188	1.844193
200	1.397826	1.788059	1.840485	1.844044	1.844194	1.844198

Table 7.7: Convergence of $|\mathcal{A}(0)|$ using BIE method for scattering by seamount where $\hat{h}(x) = 1$ for $0 < x < b$ and $\hat{h}(x) = 0.5(1+\cos(\pi(x-b/a)/(1-b/a)))$ for $b < x < a$. $a/h_0 = 4$, $b/h_0 = 3$, and $kh_0 = 0.5$.

We now investigate the convergence properties for a topography considered by Chamberlain & Porter [12] where they solved the axisymmetric problem by approx-

	M						
N	0	1	2	3	4	5	6
0	0.618909	1.260156	1.653392	1.704279	1.707620	1.707757	1.707760
2	0.644213	1.385082	1.775686	1.828136	1.831688	1.831837	1.831842
4	0.648517	1.396603	1.786776	1.839195	1.842753	1.842902	1.842906
6	0.648774	1.397103	1.787348	1.839766	1.843323	1.843472	1.843477
8	0.649265	1.397558	1.787771	1.840182	1.843739	1.843889	1.843893
10	0.649456	1.397724	1.787949	1.840367	1.843925	1.844075	1.844079
12	0.649480	1.397771	1.788005	1.840428	1.843986	1.844135	1.844139
14	0.649497	1.397803	1.788035	1.840458	1.844016	1.844166	1.844170
16	0.649507	1.397815	1.788046	1.840469	1.844027	1.844177	1.844181
18	0.649519	1.397827	1.788059	1.840483	1.844041	1.844191	1.844195
20	0.649520	1.397832	1.788065	1.840490	1.844049	1.844198	1.844203
⋮	⋮	⋮	⋮	⋮	⋮	⋮	⋮
30	0.649542	1.397859	1.788091	1.840516	1.844075	1.844225	1.844229

Table 7.8: Convergence of $|\mathcal{A}(0)|$ using Rayleigh-Ritz method for scattering by seamount where $\hat{h}(x) = 1$ for $0 < x < b$ and $\hat{h}(x) = 0.5(1+\cos(\pi(x-b/a)/(1-b/a)))$ for $b < x < a$. $a/h_0 = 4$, $b/h_0 = 3$, and $kh_0 = 0.5$.

imating with the Mild-Slope equation. The geometry considered in tables 7.7 and 7.8 is a seamount with a constant depth plateau of radius $b < a$ and a smoothly joining cosine shoal for $b < r < a$. We observe that, although obviously this problem is amenable to solution by the approach in this chapter, it has more similarity with the arbitrary step problem of Chapter 6 rather than the ridge of Chapter 5 for which this chapter provides the axisymmetric equivalent. The 'step' approach is followed by Chamberlain & Porter who solve the problems over the constant depth domains by a constant depth solution and match these with a MMSE solution for the shoal. We remark that, although Chamberlain & Porter discuss scattering over this topography, they concentrate on the local field over the plateau rather than the far field variation which our formulation is principally set up to find. Of course this local field may be recovered from (7.3.26) once the system has been solved.

Again, the results from the BE and RR methods appear to converge to the same values thus confirming their accuracy. In each case a choice of $M = 6$ is sufficient to seek 6 d.p. accuracy. The BE approach gives 4 d.p. and 5 s.f. accuracy for

$N \approx 125$ however, further improvement is very slow to achieve. The RR method can achieve comparable accuracy for $N = 13$ and $M = 5$ giving a much smaller system to solve. We remark that this geometry is likely to need a larger amount of terms in the approximation to solve by RR as most of the change in the geometry occurs in a small region. To see this, in tables 7.9 and 7.10 we present the results for the same plateau, but where the shoal extends for much more of the seamount's domain. It is clear that for each method convergence is more rapid with $M = 3$ being sufficient and $N \approx 75$ for the BE method or even more impressively $N \approx 5$ for the RR method to achieve 5 d.p. accuracy.

	M		
N	1	2	3
25	0.078344	0.079869	0.079880
50	0.078359	0.079884	0.079895
75	0.078361	0.079887	0.079898
100	0.078362	0.079888	0.079899

Table 7.9: Convergence of $|\mathcal{A}(0)|$ using BE method for scattering by seamount where $\hat{h}(x) = 1$ for $0 < x < b$ and $\hat{h}(x) = 0.5(1+\cos(\pi(x-b/a)/(1-b/a)))$ for $b < x < a$. $a/h_0 = 0.5$, $b/h_0 = 1$, and $kh_0 = 0.5$.

	M			
N	0	1	2	3
0	0.003065	0.076605	0.078088	0.078099
2	0.003385	0.078239	0.079763	0.079774
4	0.003424	0.078340	0.079865	0.079876
6	0.003433	0.078360	0.079886	0.079896
8	0.003433	0.078361	0.079887	0.079898
10	0.003433	0.078363	0.079889	0.079899
12	0.003433	0.078363	0.079889	0.079899

Table 7.10: Convergence of $|\mathcal{A}(0)|$ using Rayleigh-Ritz method for scattering by seamount where $\hat{h}(x) = 1$ for $0 < x < b$ and $\hat{h}(x) = 0.5(1+\cos(\pi(x-b/a)/(1-b/a)))$ for $b < x < a$. $a/h_0 = 0.5$, $b/h_0 = 1$, and $kh_0 = 0.5$.

Finally we note that, in the testing process for this particular geometry, we also considered Longuet-Higgins [52] approach where he considered long waves over a circular sill. We observe that as $b/a \to 1$ in this problem the seamount approaches

a circular sill. The limit is naturally difficult to take numerically so we used this approach simply to confirm that our scattering coefficients were of the correct orders of magnitude.

We have laboured the point for convergence over this particular topography to establish definitively that our results are correct. This is mainly because our main point of comparison with Chamberlain and Porter [12] is the scattering coefficients and in a range of numerical data kindly provided by P. Chamberlain we find our method gives markedly different values of the A_m which correspond directly with the B_m in Chamberlain & Porter [12]. We present in figure 7.2 results corresponding to their figure 2, namely contour plots of $|\Phi|$ for the cosine shoal where $a/h_0 = 5$ and $b/h_0 = 4$ and $h_1/h_0 = 15/16$ for frequencies $Kh_0 = 0.25, 0.5, 0.75$ and 1.0. We plot the wave field directly over the seamount as this is the most interesting region. In fact, our plots are remarkably similar to those in Chamberlain & Porter [12] with figure 7.2 (a) and (b) bearing the most striking similarity. In particular we observe the excitation of the fifth mode at a frequency of $Kh_0 = 0.5$. Thus we observe that although this particular geometry is itself quite a severe test for the MMSE as the slope is $O(1)$ and certainly not mild, nevertheless a visual inspection of the plots appears to indicate that the MMSE is performing well.

For further comparison we also present in figure 7.3 results corresponding to Chamberlain & Porter's [12] figure 3, namely contour plots of $|\Phi|$ for the cosine shoal where $a/h_0 = 10$ and $b/h_0 = 6$ and $h_1/h_0 = 9/10$ for frequencies $Kh_0 = 0.0715$ and 0.466. Once again the results are strikingly similar to those in Chamberlain & Porter [12] with clear excitation of the $m = 3$ mode in 7.3(a) and the $m = 8$ mode in 7.3(b). We ran experiments to see how sensitive our results for figure 7.3(a) were to perturbations of the frequency. In this respect we confirmed Chamberlain & Porter's finding that near-resonances were hard to excite, furthermore we found that our results suggested a maximum excitation at $Kh_0 = 0.0719$, however the maximum amplitude attained was only 1% greater than that at $Kh_0 = 0.0715$. Of course since we did not have access to Chamberlain & Porter's underlying data a more detailed investigation of

the MMSE's accuracy was not possible.

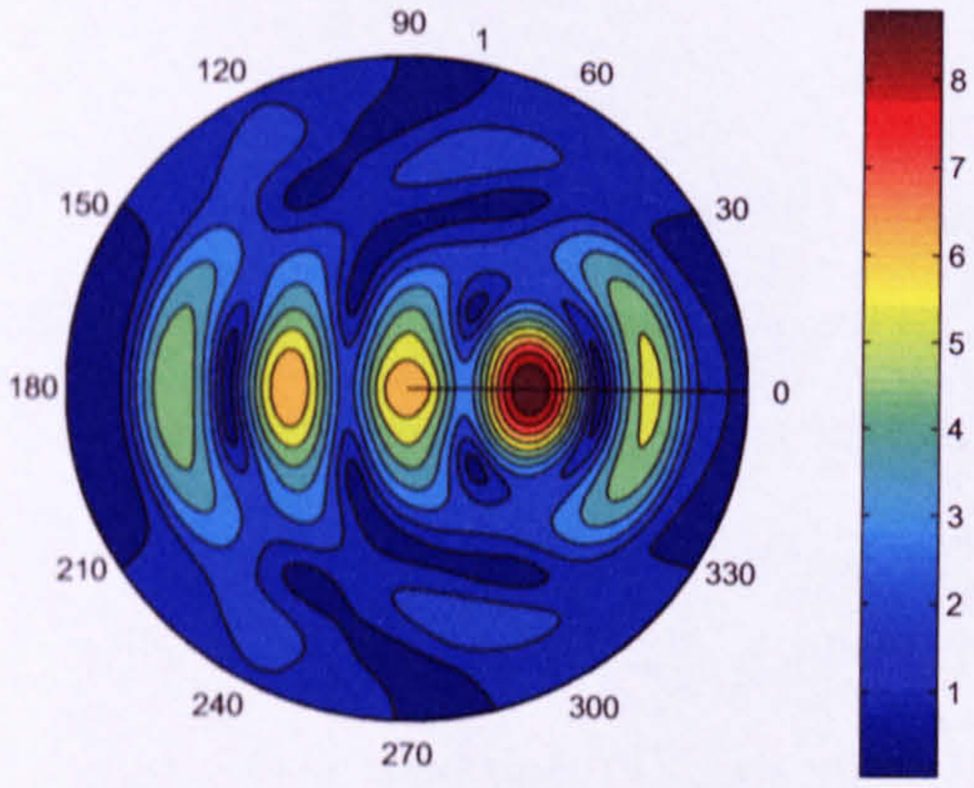

(a) $Kh_0 = 0.25$,

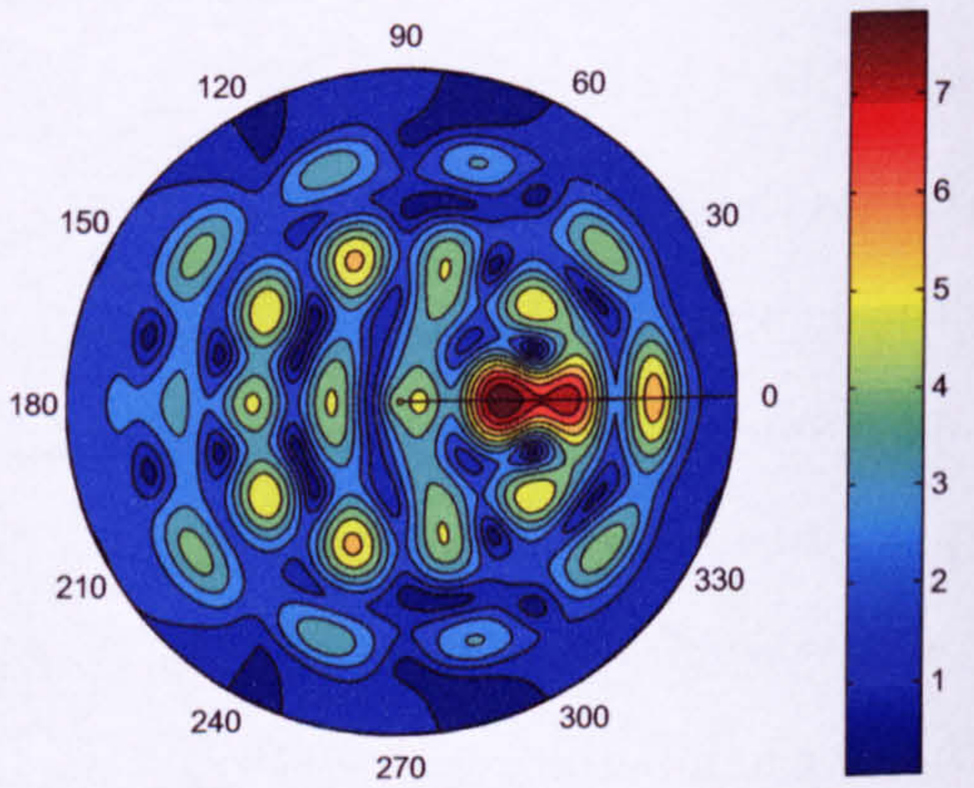

(b) $Kh_0 = 0.50$,

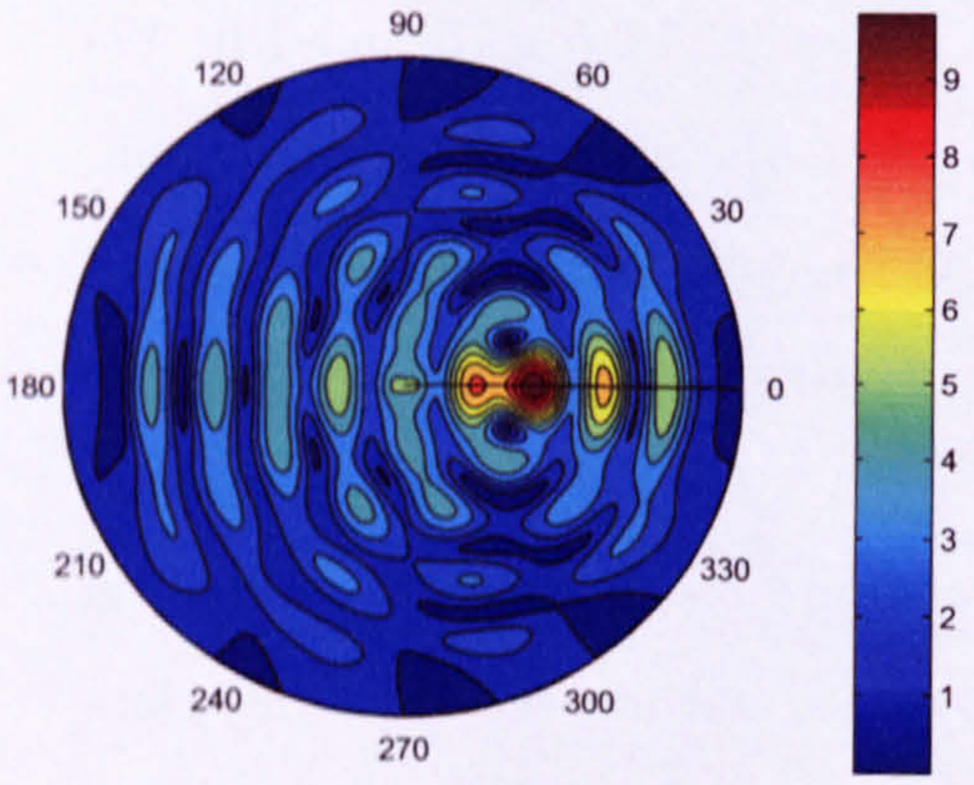

(c) $Kh_0 = 0.75$,

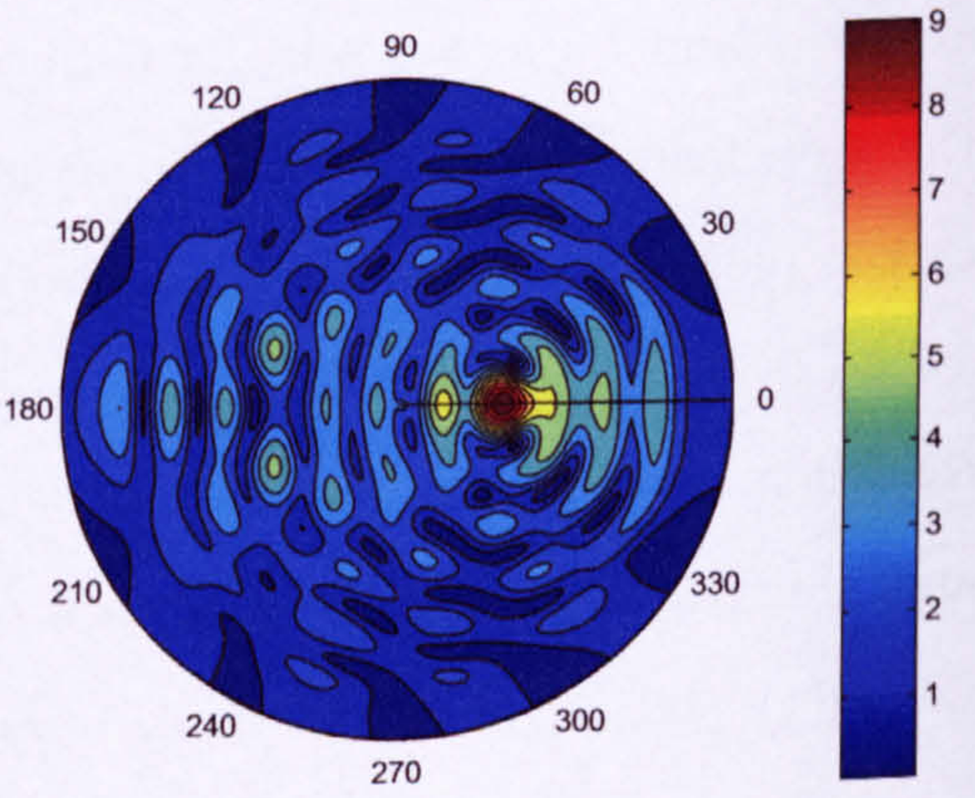

(d) $Kh_0 = 1.00$,

Figure 7.2: Contour plots of $|\Phi|$ over a seamount where $\hat{h}(x) = 1$ for $0 < x < b$ and $\hat{h}(x) = 0.5(1 + \cos(\pi(x - b/a)/(1 - b/a)))$ for $b < x < a$. $a/h_0 = 5$, $b/h_0 = 4$ and $h_1/h_0 = 15/16$.

We also present results for the following topography

$$\hat{h}(r) = \begin{cases} 0.5((1 + h_2/h_1) - (1 - h_2/h_1)\cos(ar\pi/b)), & 0 < r < b/a; \\ 0.5(1 + \cos(\pi(r - b/a)/(1 - b/a))), & b/a < r < 1. \end{cases} \tag{7.5.1}$$

where $h_2 = h_0 - h(0)$ and $h_1 = h_0 - h(b)$ and which we shall call a submerged atoll. Figure 7.4 shows the profile of $\hat{h}(r)$ for an atoll where $a/h_0 = 4$, $b/h_0 = 2$, $h_1/h_0 = 0.95$ and $h_2/h_1 = 0.5$ results for which are presented at figures 7.5 to 7.7. In figure 7.5 we see a clear excitation of the $m = 3$ mode, whereas in 7.6 there is a

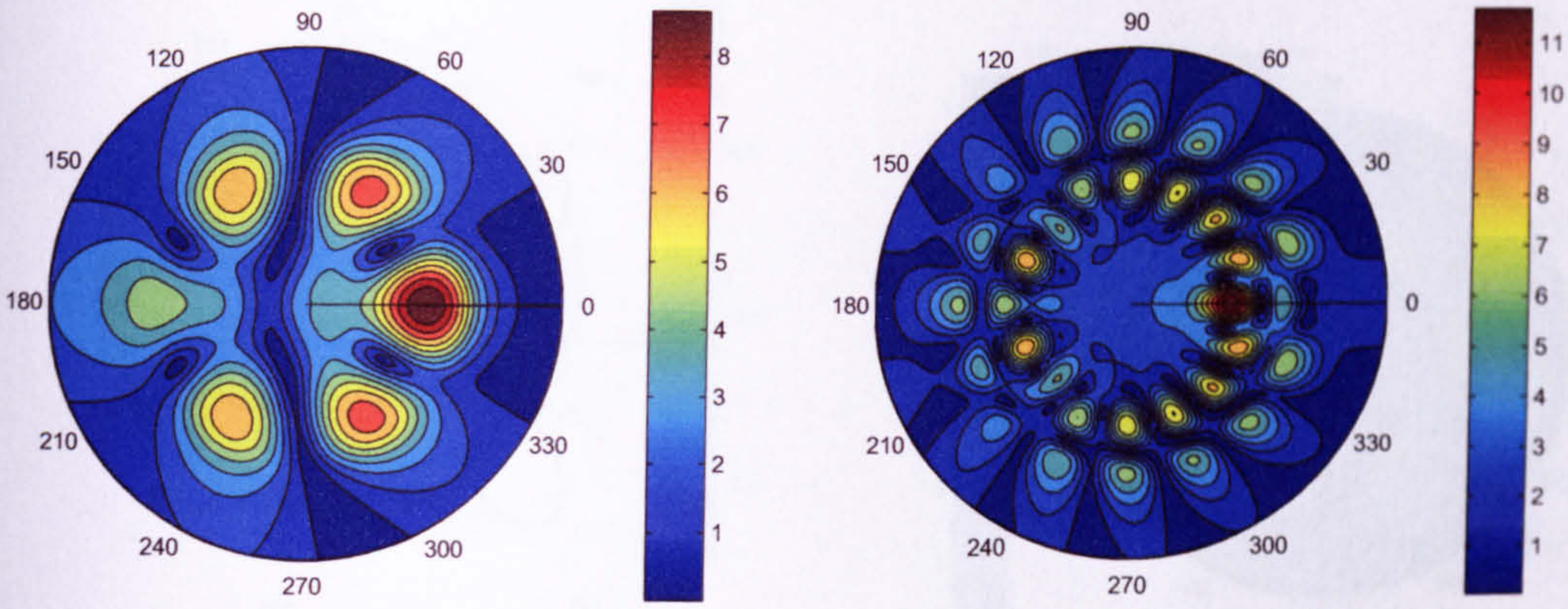

(a) $Kh_0 = 0.0715$, (b) $Kh_0 = 0.466$,

Figure 7.3: Contour plots of $|\Phi|$ over a seamount where $\hat{h}(x) = 1$ for $0 < x < b$ and $\hat{h}(x) = 0.5(1 + \cos(\pi(x - b/a)/(1 - b/a)))$ for $b < x < a$. $a/h_0 = 10$, $b/h_0 = 6$ and $h_1/h_0 = 9/10$.

clear excitation of the $m = 4$ mode. From the plots it is clear that the maximum amplitudes occurred over the rim of the atoll. It did not prove possible to excite higher order "sloshing type" modes in the interior "lagoon". In figure 7.7 we present results to demonstrate that the solution technique can handle larger frequencies. The plot is unremarkable in terms of amplitude, however it shows an interesting circular structure to the free surface. Also for this diagram we plot the Real and Imaginary parts of Φ which correspond to snapshots of the free surface at different points of time.

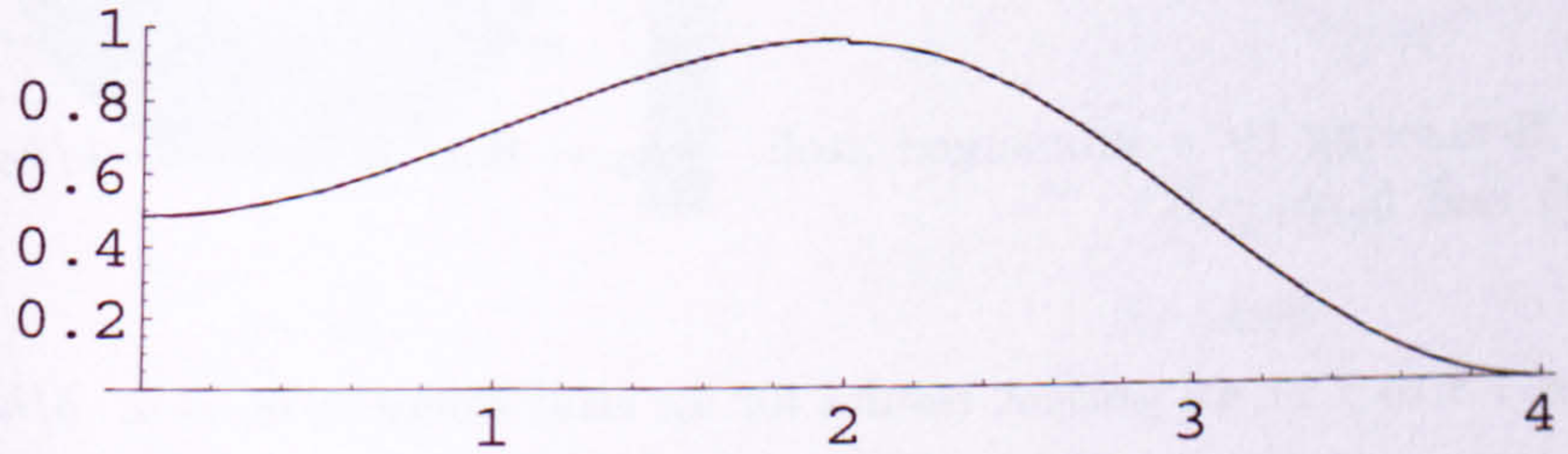

Figure 7.4: Profile of $\hat{h}(r)$ for a submerged atoll where $\hat{h}(r) = 0.5((1 + h_2/h_1) - (1 - h_2/h_1)\cos(ar\pi/b))$ for $0 < r < b/a$ and $\hat{h}(r) = 0.5(1 + \cos(\pi(r - b/a)/(1 - b/a)))$ for $b/a < r < 1$.

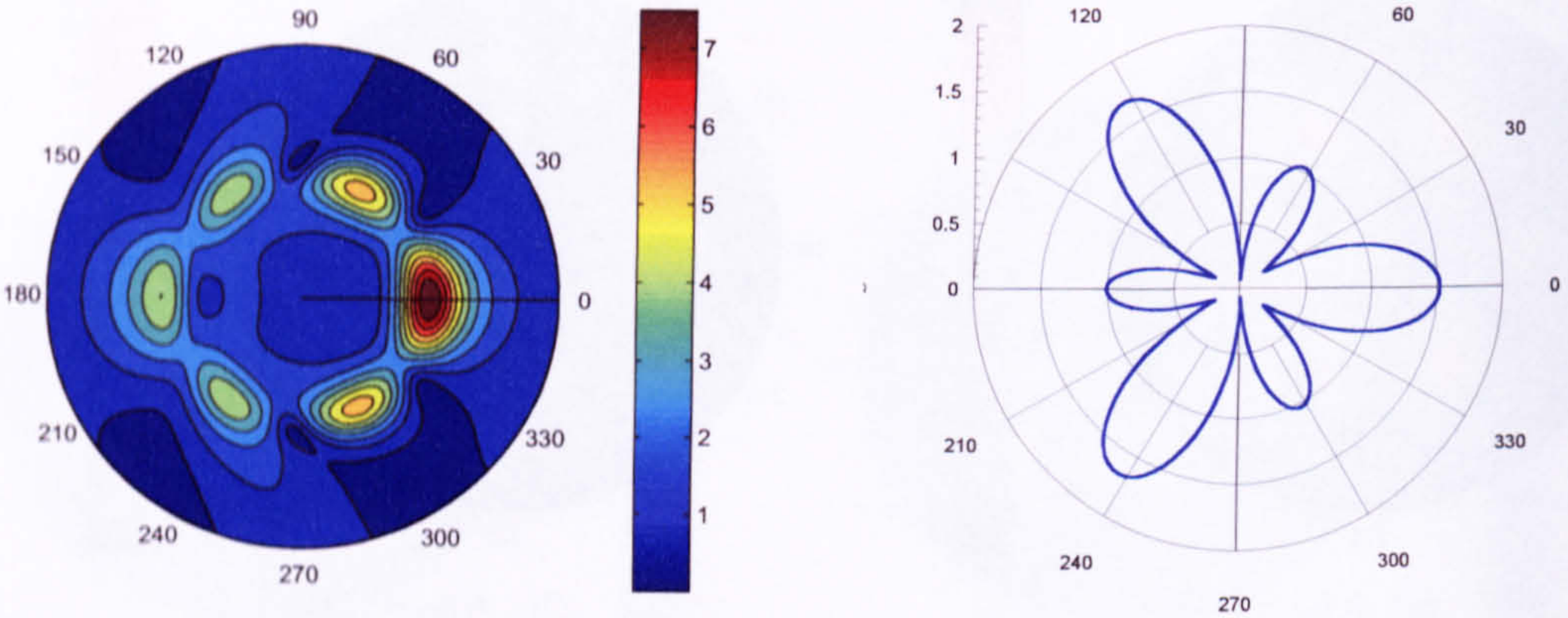

(a) $|\Phi|$ (b) $|\mathcal{A}(\theta)|$

Figure 7.5: Scattering by a submerged atoll. $kh_0 = 0.8$, $a/h_0 = 4$, $b/h_0 = 2$, $h_1/h_0 = 0.95$ and $h_2/h_1 = 0.5$.

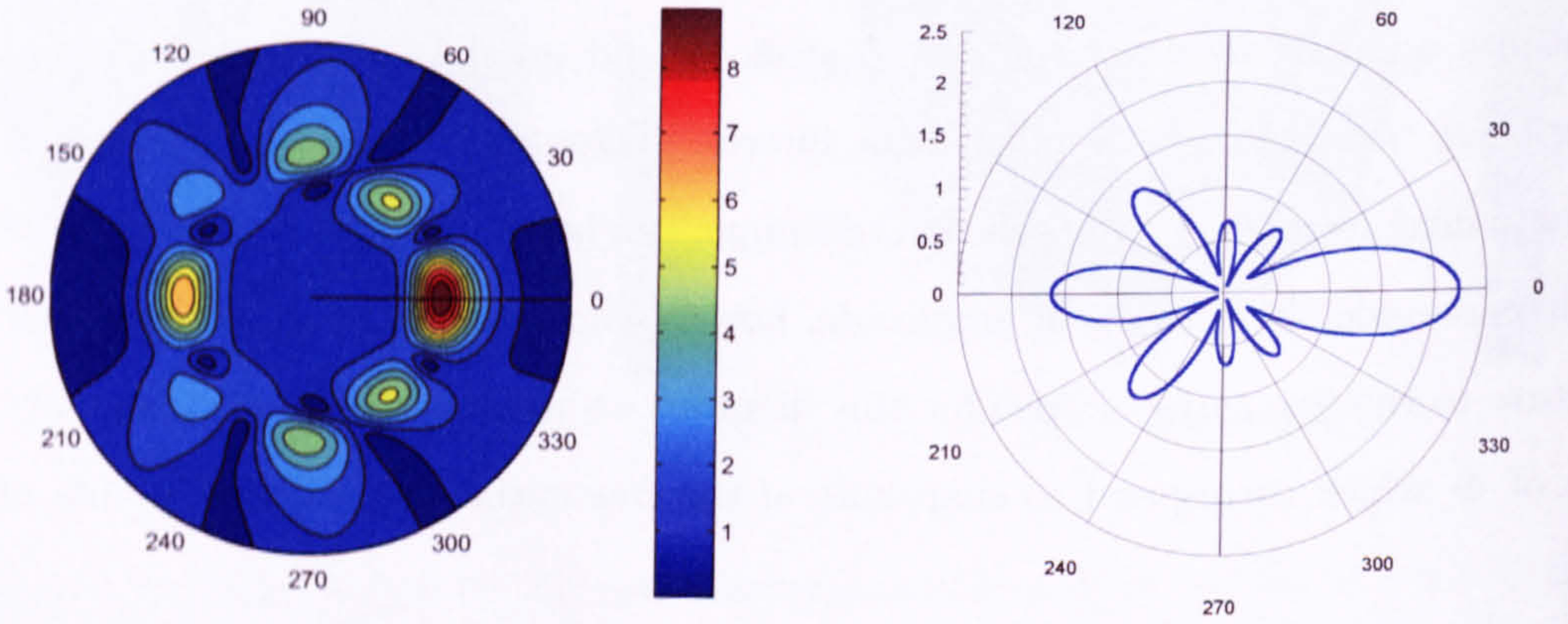

(a) $|\Phi|$ (b) $|\mathcal{A}(\theta)|$

Figure 7.6: Scattering by a submerged atoll. $kh_0 = 0.9$, $a/h_0 = 4$, $b/h_0 = 2$, $h_1/h_0 = 0.95$ and $h_2/h_1 = 0.5$.

In figures 7.8 to 7.11 we present results for an atoll where $a/h_0 = 4$, $b/h_0 = 2$, $h_1/h_0 = 0.95$ and $h_2/h_1 = 0.85$ so that the profile of the outer shoal is the same as for figures 7.5 to 7.7. However, in this case the interior "lagoon" is much shallower. We see that a low frequency wave in figure 7.8 excites the $m = 0$ mode in the interior of the lagoon. In contrast for $kh_0 = 0.6$ in figure 7.9 we observe an excitation of the

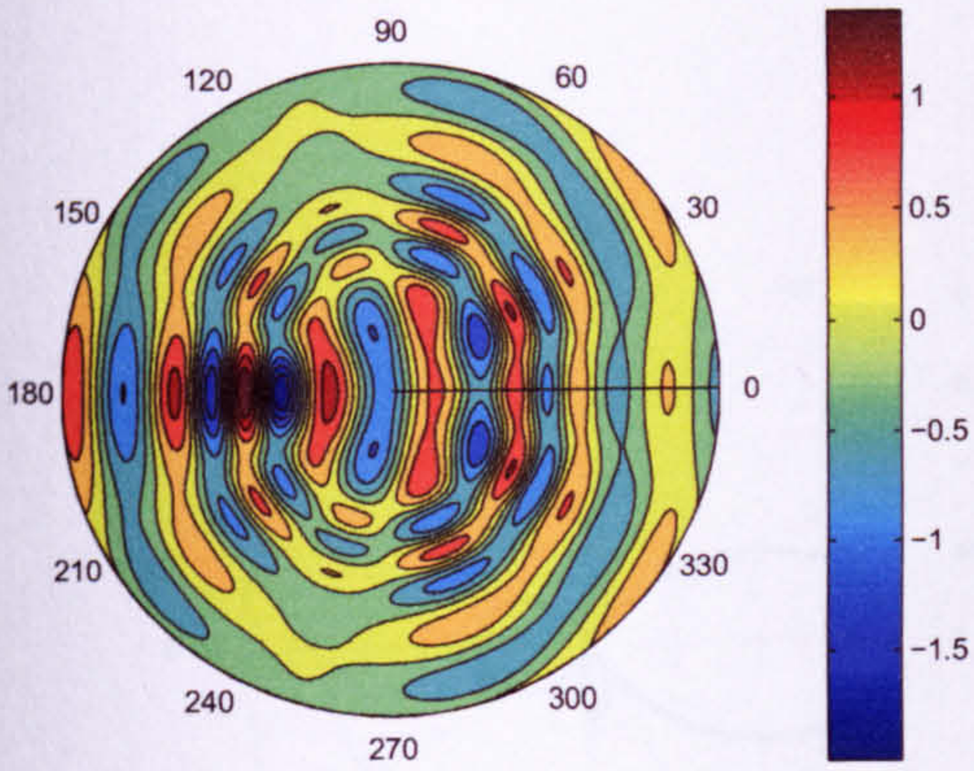

(a) ReΦ

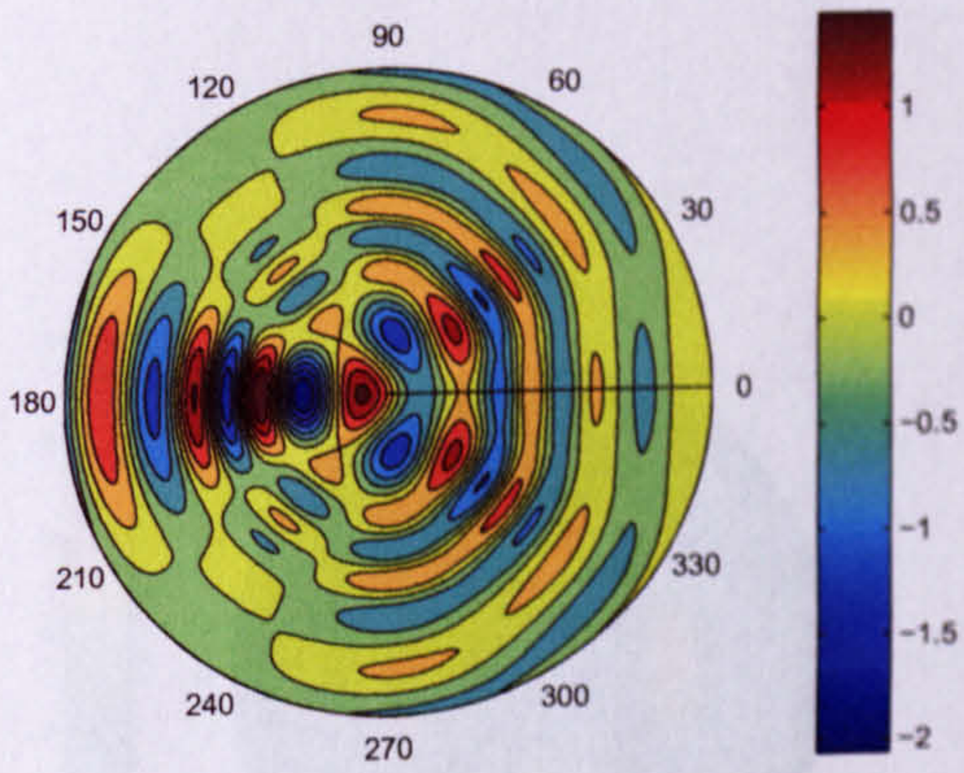

(b) ImΦ

Figure 7.7: Scattering by a submerged atoll. $kh_0 = 5.0$, $a/h_0 = 4$, $b/h_0 = 2$, $h_1/h_0 = 0.95$ and $h_2/h_1 = 0.5$.

$m = 2$ mode over the rim of the atoll and in figure 7.10, for $kh_0 = 0.7$ we see an excitation of the $m = 3$ mode. At figure 7.11, for $kh_0 = 1.0$ we see an excitation of the $m = 5$ mode, and in order to observe some of the structure we have presented it as a three-dimensional surface plot viewed from above.

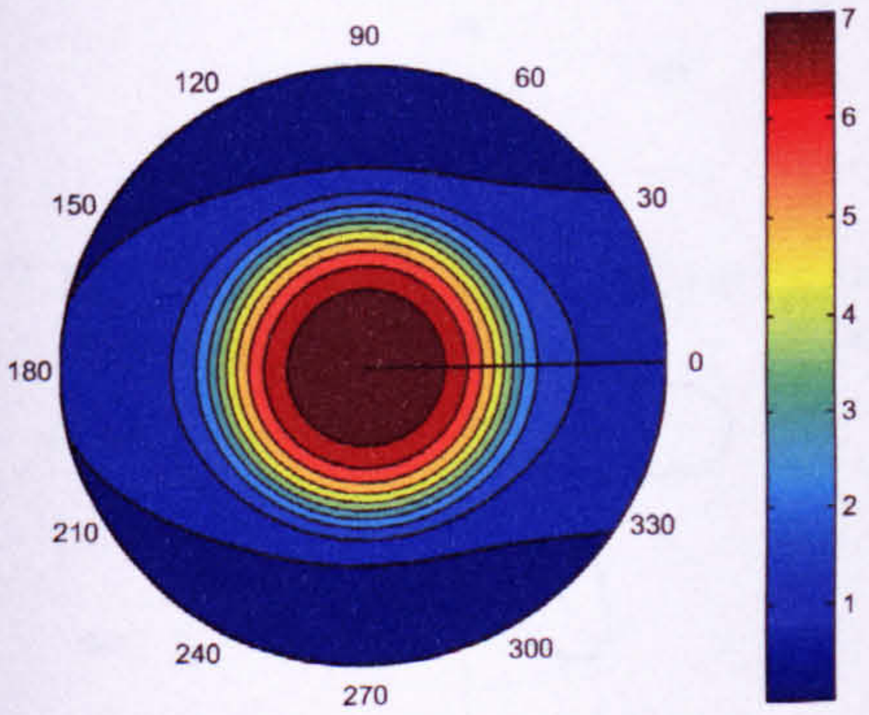

(a) $|\Phi|$

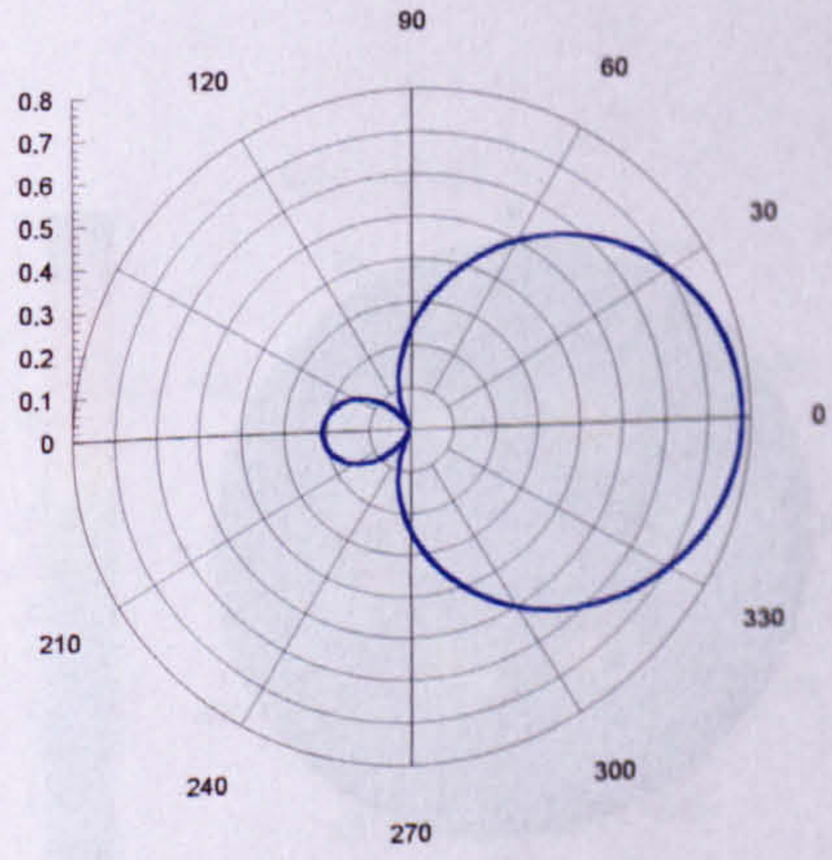

(b) $|\mathcal{A}(\theta)|$

Figure 7.8: Scattering by a submerged atoll. $kh_0 = 0.2$, $a/h_0 = 4$, $b/h_0 = 2$, $h_1/h_0 = 0.95$ and $h_2/h_1 = 0.85$.

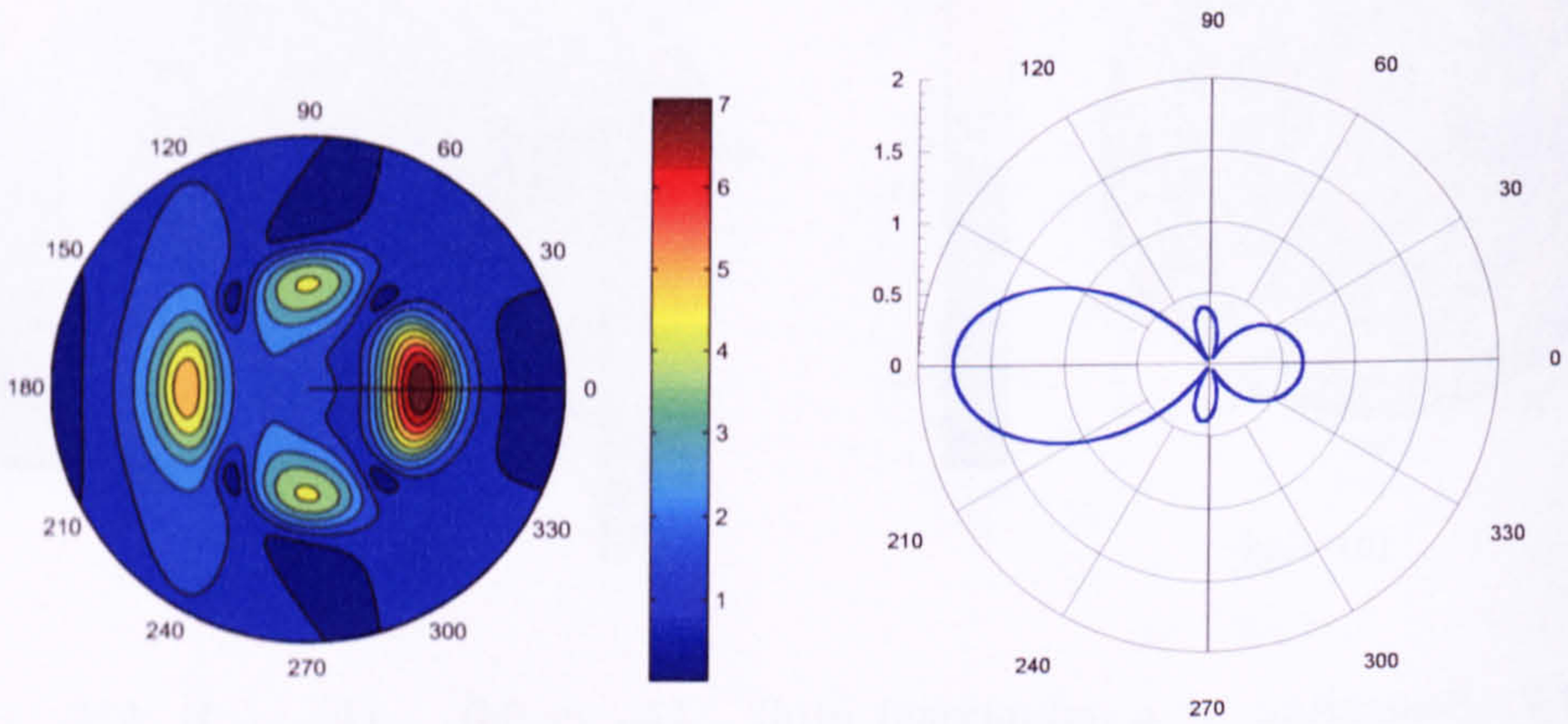

(a) $|\Phi|$ (b) $|\mathcal{A}(\theta)|$

Figure 7.9: Scattering by a submerged atoll. $kh_0 = 0.6$, $a/h_0 = 4$, $b/h_0 = 2$, $h_1/h_0 = 0.95$ and $h_2/h_1 = 0.85$.

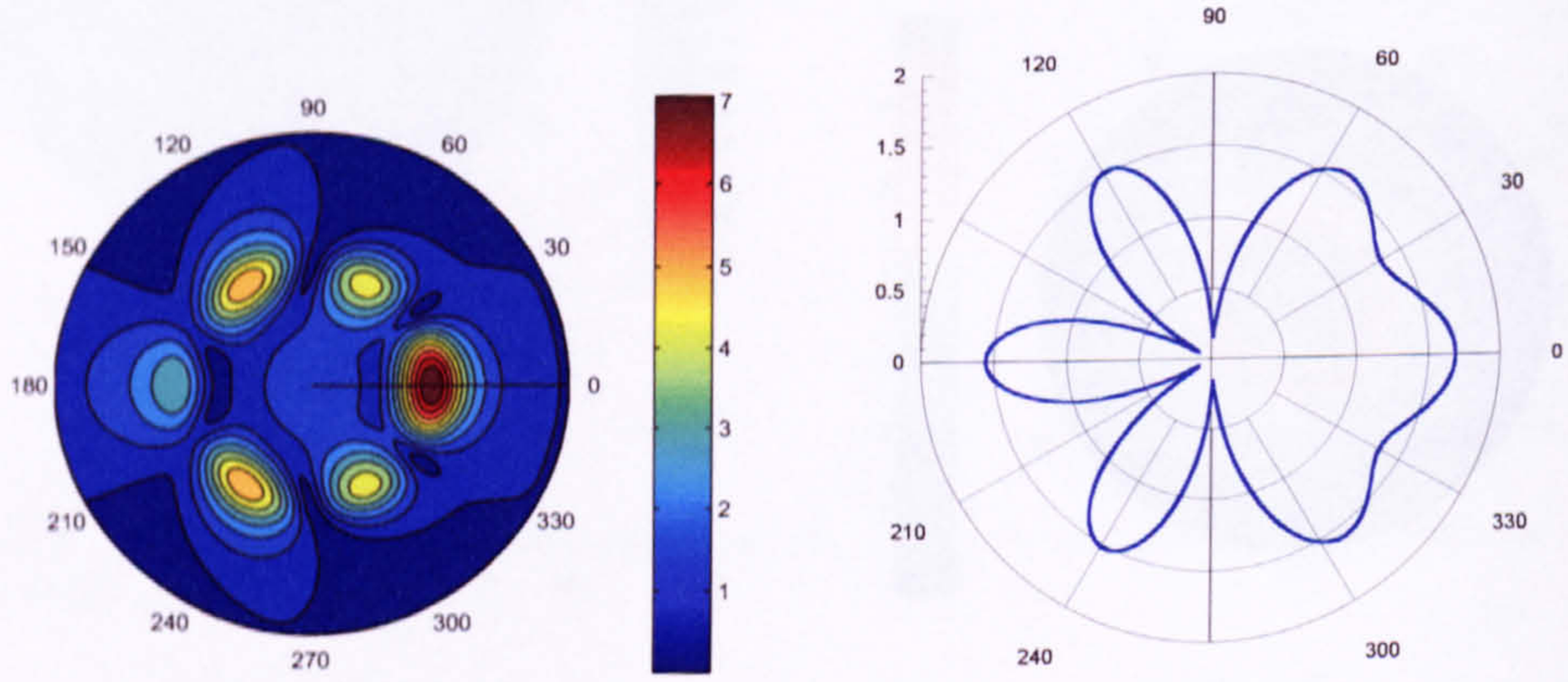

(a) $|\Phi|$ (b) $|\mathcal{A}(\theta)|$

Figure 7.10: Scattering by a submerged atoll. $kh_0 = 0.7$, $a/h_0 = 4$, $b/h_0 = 2$, $h_1/h_0 = 0.95$ and $h_2/h_1 = 0.85$.

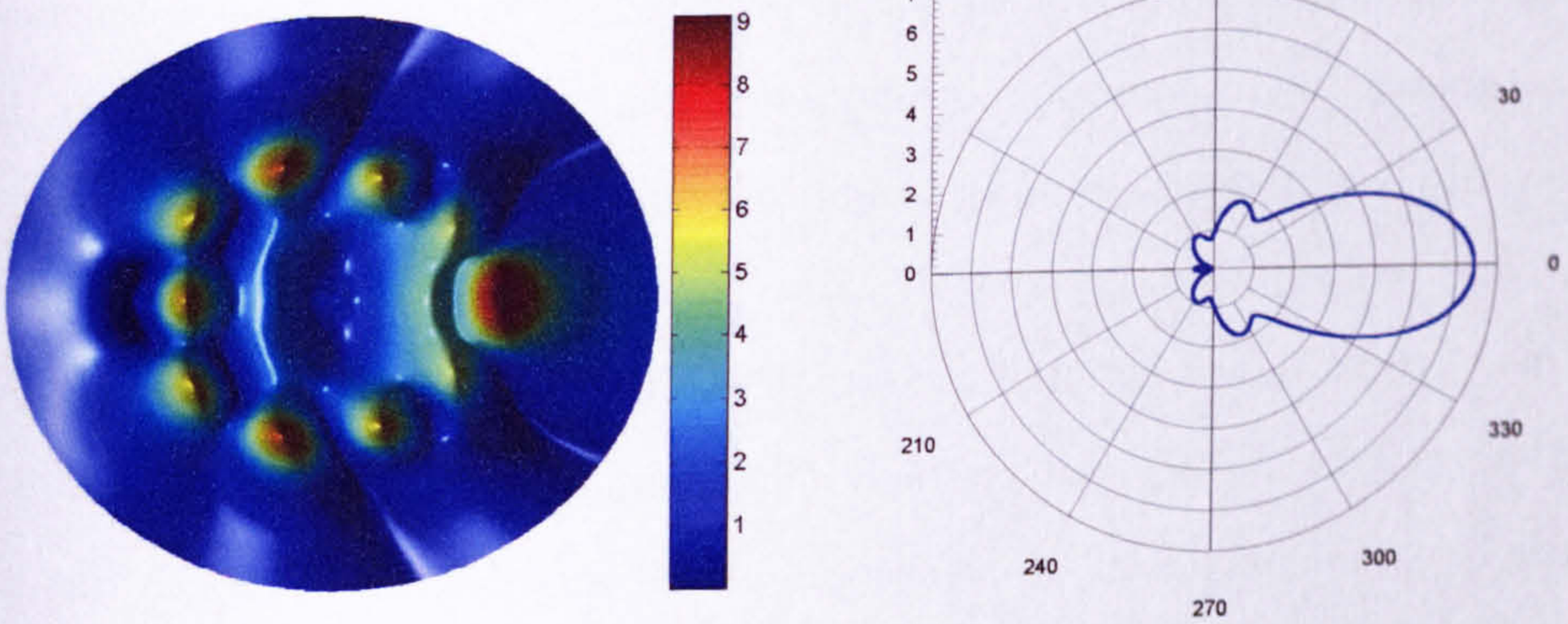

(a) $|\Phi|$ (b) $|\mathcal{A}(\theta)|$

Figure 7.11: Scattering by a submerged atoll. $kh_0 = 1.0$, $a/h_0 = 4$, $b/h_0 = 2$, $h_1/h_0 = 0.95$ and $h_2/h_1 = 0.85$.

7.6 Remarks

In this chapter we have shown how the fully linear theory may be applied to axisymmetric problems. We have shown how the principles developed in Chapters 5 and 6 may be applied to problems with a different (cylindrical) natural coordinate system. Furthermore we have also solved this problem retaining its three-dimensional nature to indicate some of the principles we develop further in the next chapter.

We compared our results with Chamberlain & Porter's [11] MMSE approach which is arguably the most sophisticated recent approximate solution. We observe that when Renardy [81] applied the full linear theory to Longuet-Higgin's [52] sill problem he found that the approximate solution predicted different resonant frequencies and overestimated the resonant amplitudes when compared with the fully linear theory. Interestingly our results appear to indicate that the MMSE predicts both the frequency and the amplitude accurately. This in itself is an important observation as, until now, there have been no exact results to compare the MMSE against (see Chamberlain & Porter [12]). Interestingly Chamberlain [13] found that for the axisymmetric problem, inclusion of evanescent modes in a MMSE approach did not introduce any new frequencies, although it did improve the approximations to their values. There has been insufficient time to test the accuracy of the MMSE for this problem extensively and it remains an area which would certainly merit further investigation.

Chapter 8

Wave scattering by an arbitrary patch of topography

8.1 Introduction

In the three previous chapters we have concentrated on developing techniques for solving scattering and related problems involving arbitrary topographies which have possessed some form of symmetry. Thus, in Chapters 5 and 6 we considered infinitely long bed protrusions or escarpments having arbitrary profile, whilst in Chapter 7 we considered axisymmetric seamounts. In each case we were able to take advantage of the symmetry in the geometry to ultimately reduce the three-dimensional problem to one involving just two coordinates, the third coordinate manifesting itself in the transformation of the field equation (often referred to as quasi-2D). In each problem we have seen that although they can be reduced to two-dimensional problems, consideration of the three-dimensional nature of the problem is still crucial to its solution.

The technique used throughout this thesis has been to derive weakly singular integral equations for wave scattering over some class of arbitrary bed topography. We have achieved this from converting from normal to tangential derivatives and have shown how, unlike the traditional approach, this produces a representation of the potential which is continuous as the field point moves from the fluid domain to the boundary. We have then shown how this alternative form can yield a simple

boundary element approach, or by a second application of the derivative switching we can derive an alternative integral equation which is set up perfectly for solution by the Rayleigh-Ritz method.

In this final chapter we take advantage of the experience gained from considering specific examples to develop a general theory applicable to a genuinely three-dimensional protrusion of bed topography from an otherwise flat bed. Having reached this point, we observe that we could have developed this theory from the outset, in which case each of the specific cases in Chapters 5, 6 and 7 would have been shown to be particular reductions of the general theory.

8.2 A general theory

We consider a bed protrusion with, for simplicity, some kind of "Cartesian" support. The bed S_b is defined by the single valued function $z = h(x, y)$ for $(x, y) \in S_p$, where S_p is the projection of the bed onto the two-dimensional plane and where, for simplicity, we assume $S_p = \{(x, y) : \ x \in (0, a), \ y \in (0, b)\}$. The bed is of constant depth $h = h_0$ for $(x, y) \notin S_p$ and we do not exclude the possibility that $h = h_0$ for points or regions of $(x, y) \in S_p$. We define a set of vectors

$$\left.\begin{aligned} \mathbf{n} &= (-h_x, -h_y, 1)/\sigma & \sigma &= \sqrt{1 + h_x^2 + h_y^2}, \\ \mathbf{s} &= (-h_x, 0, 1)/\sigma_s & \sigma_s &= \sqrt{1 + h_x^2}, \\ \mathbf{t} &= (0, -h_y, 1)/\sigma_t & \sigma_t &= \sqrt{1 + h_y^2}, \end{aligned}\right\} \tag{8.2.1}$$

so that $\mathbf{n}$ is the unit normal to S_b, oriented so that it points out of the fluid. The unit vectors $\mathbf{s}$ and $\mathbf{t}$, both of which are orthogonal to $\mathbf{n}$, are tangent to S_b and their projections onto S_p are oriented in the x and y directions respectively. It follows that

$$\mathbf{n} = \tau\, \mathbf{s} \times \mathbf{t}, \tag{8.2.2}$$

where

$$\tau = \frac{\sigma_s \sigma_t}{\sigma} = \frac{1}{\sqrt{1 - \mathbf{s}.\mathbf{t}}}. \tag{8.2.3}$$

As usual we let $\Phi(\mathbf{r})$ be the time-harmonic potential, at a position vector $\mathbf{r} = (x, y, z)$ and operating at frequency $\omega/2\pi$. A wave is incident from infinity and is described

by a potential Φ_{inc}, there is also a scattered wave field given by Φ^S so that the total potential $\Phi = \Phi_{inc} + \Phi^S$. Then Green's identity applied to the fluid domain gives

$$\mu\Phi(\mathbf{r}_0) = \Phi_{inc}(\mathbf{r}_0) - \iint_{S_b} \Phi(\mathbf{r})\mathbf{n}.\nabla G(\mathbf{r};\mathbf{r}_0)\,\mathrm{d}S \tag{8.2.4}$$

where $\mathbf{r}_0 = (x_0, y_0, z_0)$ is the "field point" and D is the fluid domain which is bounded by the surface ∂D where, of course $S_b \subset \partial D$. Here $\mu = 1$ for $\mathbf{r}_0 \in D$, $\mu = 1/2$ for $\mathbf{r}_0 \in \partial D$, and $\mu = 0$ for $\mathbf{r}_0 \notin D \cup \partial D$. Here $G(\mathbf{r};\mathbf{r}_0)$ is a point source Green's function chosen to satisfy the no-flow condition on $z = h_0$, the free-surface boundary condition on $z = 0$, and

$$\nabla^2 G(\mathbf{r};\mathbf{r}_0) = -\delta(\mathbf{r} - \mathbf{r}_0) \tag{8.2.5}$$

as well as satisfying a Sommerfeld radiation condition.

Now, as in earlier chapters, we define a vector Green's function $\mathbf{L}$ related to the Green's function G by

$$\nabla G = \nabla \times \mathbf{L} - \delta(x - x_0)\delta(y - y_0)\delta^z(z - z_0)\mathbf{k} \tag{8.2.6}$$

where $\mathbf{L} = (G^z_y, -G^z_x, 0)$ and we use the notation defined in (5.3.4). This may be verified by substitution so that

$$\nabla G = (G_x, G_y, G_z) = \begin{vmatrix} \mathbf{i} & \mathbf{j} & \mathbf{k} \\ \partial_x & \partial_y & \partial_z \\ G^z_y & -G^z_x & 0 \end{vmatrix} - \delta(x - x_0)\delta(y - y_0)\delta^z(z - z_0)\mathbf{k}. \tag{8.2.7}$$

The first two elements of ∇G work out trivially whereas the third uses

$$G^z_{zz} = -G^z_{xx} - G^z_{yy} - \delta(x - x_0)\delta(y - y_0)\delta^z(z - z_0) \tag{8.2.8}$$

which follows from integrating (8.2.5) with respect to z. Also using (5.3.6) in (8.2.4) we find that

$$\mu\Phi(\mathbf{r}_0) = \Phi_{inc}(\mathbf{r}_0) - \iint_{S_b} \Phi(\mathbf{r})\mathbf{n}.\nabla \times \mathbf{L}\,\mathrm{d}S - \iint_{S_b} \Phi(\mathbf{r})\delta(x - x_0)\delta(y - y_0)\mathrm{H}(z_0 - z)\frac{\mathrm{d}S}{\sigma} \tag{8.2.9}$$

since $\mathbf{n}.\mathbf{k} = 1/\sigma$, here $H(x)$ is the Heaviside step function. Now, careful consideration of the surface element $\mathrm{d}S$ and its projection onto the (x, y) plane shows that

$$\begin{aligned}\mathrm{d}S &= \mathbf{n}.(\sigma_s \mathbf{s} \times \sigma_t \mathbf{t})\,\mathrm{d}x\,\mathrm{d}y \\ &= \sigma_s \sigma_t \mathbf{n}.\left(\frac{\mathbf{n}}{\tau}\right)\,\mathrm{d}x\,\mathrm{d}y \\ &= \sigma\,\mathrm{d}x\,\mathrm{d}y, \end{aligned} \tag{8.2.10}$$

so that

$$\begin{aligned}-\iint_{S_b} \Phi(\mathbf{r})\delta(x - x_0)\delta(y - y_0)\mathrm{H}(z_0 - z)\frac{\mathrm{d}S}{\sigma} \\ &= -\iint_{S_p} \Phi(x, y, h(x, y))\delta(x - x_0)\delta(y - y_0)\mathrm{H}(z_0 - h(x, y))\,\mathrm{d}x\,\mathrm{d}y \\ &= -\Phi(x, y, h(x, y))\mathrm{H}(z_0 - h(x_0, y_0)) \end{aligned} \tag{8.2.11}$$

which evaluates to zero for points $\mathbf{r}_0 \in D$, $-\frac{1}{2}\Phi(x_0, y_0, h(x_0, y_0))$ for points $\mathbf{r}_0 \in S_b$ and $-\Phi(x_0, y_0, h(x_0, y_0))$ for points $\mathbf{r}_0 \notin D \cup S_b$. Thus combining this result with (8.2.9)

$$\Phi(\mathbf{r}_0) = \Phi_{inc}(\mathbf{r}_0) - \iint_{S_b} \Phi(\mathbf{r})\mathbf{n}.\nabla \times \mathbf{L}\,\mathrm{d}S \qquad \text{for } \mathbf{r}_0 \in D \cup \partial D \tag{8.2.12}$$

which establishes that, unlike the traditional form (8.2.4), the formulation in (8.2.12) gives a continuous definition of the fluid potential as the field point moves from the fluid domain to a point on the boundary. We could at this point approximate the integral equation in this form by a collocation/boundary integral approach. However, we have seen this several times so far and the extension to this case does not provide any further insight. Noblesse [67] too treats (8.2.9) as a second kind integral equation for the fluid potential in which the LHS of (8.2.12) is continuous as $\mathbf{r}_0 \to S_b$, and converts it to a weakly singular form by performing the three-dimensional analogue of integration by parts using the formula

$$(\nabla \times \mathbf{L})\Phi = \nabla \times (\Phi\mathbf{L}) - \nabla\Phi \times \mathbf{L}. \tag{8.2.13}$$

In his approach, though, Noblesse fails to make explicit the treatment of the term arising from the delta function in the equation satisfied by the Green's function. Following Noblesse's approach but glossing over any of these difficulties we would obtain

$$\iint_{S_b} \Phi \mathbf{n}.\nabla \times \mathbf{L}\, \mathrm{d}S = \oint_{\Gamma} \Phi \mathbf{L}.\, \mathrm{d}\mathbf{r} - \iint_{S_b} \mathbf{n}.(\nabla\Phi \times \mathbf{L})\, \mathrm{d}S. \qquad (8.2.14)$$

Here we have used Stokes' theorem to convert the surface integral to a line integral around Γ which includes ∂S_b plus any other "cuts" in S_b where there are jumps in $\mathbf{L}$. Noblesse does not consider points where Stokes' theorem does not apply, namely where the first derivatives of $\mathbf{L}$ are discontinuous. However, as we shall see, they make contributions which cannot be neglected. Now, since $\mathbf{L} = \mathbf{0}$ by construction for regions where $z = h_0$, then the only contributions from this line integral would be from discontinuities in $\mathbf{L}$.

Our earlier work in Chapters 5 to 7 has shown that it is possible to reformulate the integral equation in a way that allows a variational principle equivalent to Galerkin's method to be used. We know from our experience so far that the integral equation in the form (8.2.13) would result in a non- self-adjoint integral operator where the adjoint problem is not evident and so it is not amenable to solution by the Rayleigh-Ritz method. Therefore we apply the steps already seen in earlier chapters, anticipating that we will be able to construct a self-adjoint integral operator which will allow us to employ the Rayleigh-Ritz method.

Thus we manipulate (8.2.12) to get it into a form which we know will provide a self-adjoint integral operator. This requires a knowledge of the explicit form of the Green's function, a derivation of which is presented at the Appendix and where it is shown that

$$G(\mathbf{r};\mathbf{r}_0) = \frac{1}{2\pi} \sum_{n=0}^{\infty} K_0(k_n R) \frac{\psi_n(z)\psi_n(z_0)}{h_0} \qquad (8.2.15)$$

where

$$R = \sqrt{r^2 + r_0^2 - 2rr_0\cos(\theta_0 - \theta)}, \qquad (8.2.16)$$

or alternatively

$$= \sqrt{(x-x_0)^2+(y-y_0)^2}, \tag{8.2.17}$$

and we have written $(x,y) = r(\cos\theta, \sin\theta)$ and $(x_0,y_0) = r_0(\cos\theta_0, \sin\theta_0)$. Alternatively we may write

$$G(\mathbf{r};\mathbf{r}_0) = \frac{\mathrm{i}}{4}H_0(kR)\frac{\psi_0(z)\psi_0(z_0)}{h_0} + \frac{1}{2\pi}\sum_{n=1}^{\infty}K_0(k_nR)\frac{\psi_n(z)\psi_n(z_0)}{h_0} \tag{8.2.18}$$

where the first term represents the propagating mode and the sum contains the evanescent modes. We have already seen in Chapters 5 and 7 that the key step to construct a self-adjoint operator is to decompose the Green's function into its real and imaginary parts. Therefore we write $G = G_0 + \widehat{G}$ where

$$G_0 = \frac{\mathrm{i}}{4}J_0(kR)\frac{\psi_0(z)\psi_0(z_0)}{h_0} \tag{8.2.19}$$

and

$$\widehat{G} = -\frac{1}{4}Y_0(kR)\frac{\psi_0(z)\psi_0(z_0)}{h_0} + \frac{1}{2\pi}\sum_{n=1}^{\infty}K_0(k_nR)\frac{\psi_n(z)\psi_n(z_0)}{h_0}. \tag{8.2.20}$$

We also assume that the incident wave is a plane wave propagating at an angle θ_{inc} to the x-axis so that

$$\Phi_{inc}(\mathbf{r}) = \mathrm{e}^{\mathrm{i}kr\cos(\theta-\theta_{inc})}\psi_0(z) \tag{8.2.21}$$

or alternatively, using the Jacobi-Anger expansion,

$$\Phi_{inc}(\mathbf{r}) = \sum_{m=-\infty}^{\infty}\mathrm{i}^m J_m(kr)\mathrm{e}^{\mathrm{i}m(\theta-\theta_{inc})}\psi_0(z) \tag{8.2.22}$$

and for ease of notation later we define

$$\Phi_{0m}(\mathbf{r}) = \mathrm{i}^m J_m(kr)\mathrm{e}^{\mathrm{i}m\theta}\psi_0(z). \tag{8.2.23}$$

The argument, R, for the Green's function proves inconvenient to deal with and obscures some of the structure of the problem; therefore to proceed we need the following results all derived from Gradshteyn & Ryzhik [37] §8.530

$$J_0(kR) = \sum_{m=-\infty}^{\infty}J_m(kr_0)J_m(kr)\mathrm{e}^{\mathrm{i}m(\theta_0-\theta)} \tag{8.2.24}$$

$$Y_0(kR) = \sum_{m=-\infty}^{\infty}Y_m(kr_>)J_m(kr_<)\mathrm{e}^{\mathrm{i}m(\theta_0-\theta)} \tag{8.2.25}$$

and

$$H_0(kR) = \sum_{m=-\infty}^{\infty} H_m(kr_>)J_m(kr_<)\mathrm{e}^{\mathrm{i}m(\theta_0-\theta)} \tag{8.2.26}$$

where

$$r_> = \max\{r, r_0\} \qquad \text{and } r_< = \min\{r, r_0\}. \tag{8.2.27}$$

Using these results we see that we recover exactly the form of the three-dimensional Green's function in polar coordinates as detailed in the Appendix.

The final piece of information we require comes from the radiation condition which requires the scattered waves to be outgoing at infinity. The most general form of the far field of a wave which satisfies this requirement is

$$\Phi^S(\mathbf{r}_0) \to \sum_{m=-\infty}^{\infty} H_m(kr_0)\mathrm{i}^m A_m \mathrm{e}^{\mathrm{i}m\theta_0}\psi_0(z_0) \qquad \text{as} \qquad kr_0 \to \infty \tag{8.2.28}$$

see, for example Mei [61]. Then using the far field expansion of the Hankel function we may write

$$\Phi^S(\mathbf{r}_0) \to \sqrt{\frac{\pi}{2kr_0}}\,\mathrm{e}^{\mathrm{i}(kr_0-\pi/4)}\psi_0(z_0)\sum_{m=-\infty}^{\infty} A_m \mathrm{e}^{\mathrm{i}m\theta_0} \qquad \text{as} \qquad kr_0 \to \infty \tag{8.2.29}$$

which we observe is a scattered wave with angular variation defined by the complex coefficients $\{A_m\}$. So if we define the angular variation by

$$\mathcal{A}(\theta) = \sum_{m=-\infty}^{\infty} A_m \mathrm{e}^{\mathrm{i}m\theta} \tag{8.2.30}$$

then this quantity, often called the diffraction coefficient or directivity factor, may be viewed as the principal unknown of the problem.

We obtain the vector quantities $\mathbf{L}_0$ and $\widehat{\mathbf{L}}$ in an obvious manner from substituting the decomposed Green's function in (8.2.6) to give the relations

$$\mathbf{L}_0 = ((G_0)^z_y, -(G_0)^z_x, 0) \tag{8.2.31}$$

$$\widehat{\mathbf{L}} = (\widehat{G}_0|^z_y, -\widehat{G}^z_x, 0) \tag{8.2.32}$$

Now, from (8.2.19), (8.2.23) and (8.2.24) we see that G_0 may be decomposed into

$$G_0(\mathbf{r}) = \frac{\mathrm{i}}{4h_0} \sum_{m=-\infty}^{\infty} \Phi_{0m}(\mathbf{r}_0)\overline{\Phi_{0m}}(\mathbf{r}), \tag{8.2.33}$$

then defining a set of vector functions Ψ_{0m} by

$$\Psi_{0m} = \left((\Phi_{0m})_y^z, -(\Phi_{0m})_x^z, 0\right) \tag{8.2.34}$$

so that

$$\nabla\Phi_{0m} = \nabla \times \Psi_{0m}, \tag{8.2.35}$$

we deduce that

$$\mathbf{L}_0(\mathbf{r}) = \frac{\mathrm{i}}{4h_0} \sum_{m=-\infty}^{\infty} \Phi_{0m}(\mathbf{r}_0)\overline{\Psi_{0m}}(\mathbf{r}). \tag{8.2.36}$$

We are now in a position to substitute the decomposed Greens function into (8.2.12) to give

$$\Phi(\mathbf{r}_0) = \Phi_{inc}(\mathbf{r}_0) - \iint_{S_b} \Phi(\mathbf{r})\mathbf{n}.\nabla \times \widehat{\mathbf{L}}\,\mathrm{d}S - \iint_{S_b} \Phi(\mathbf{r})\mathbf{n}.\nabla \times \mathbf{L}_0\,\mathrm{d}S. \tag{8.2.37}$$

and then, if we define

$$F^{(m)}(\mathbf{r}) = \mathbf{n}.\nabla\Phi_{0m}(\mathbf{r}) = \mathbf{n}.\nabla \times \Psi_{0m}(\mathbf{r}) \tag{8.2.38}$$

and an inner product as

$$\langle u, v\rangle = \iint_{S_b} u(\mathbf{r})\overline{v(\mathbf{r})}\,\mathrm{d}S \tag{8.2.39}$$

then (8.2.37) may be rewritten as

$$\Phi(\mathbf{r}_0) = \Phi_{inc}(\mathbf{r}_0) - \iint_{S_b} \Phi(\mathbf{r})\mathbf{n}.\nabla \times \widehat{\mathbf{L}}\,\mathrm{d}S - \frac{\mathrm{i}}{4h_0} \sum_{m=-\infty}^{\infty} \Phi_{0m}(\mathbf{r}_0)\langle\Phi, F^{(m)}\rangle. \tag{8.2.40}$$

Simplifying, using (8.2.22) and (8.2.23) we obtain

$$\Phi(\mathbf{r}_0) = \sum_{m=-\infty}^{\infty} \Phi_{0m}(\mathbf{r}_0)(\mathrm{e}^{-\mathrm{i}m\theta_{inc}} - \frac{\mathrm{i}}{4h_0}\langle\Phi, F^{(m)}\rangle) - \iint_{S_b} \Phi(\mathbf{r})\mathbf{n}.\nabla \times \widehat{\mathbf{L}}\,\mathrm{d}S. \tag{8.2.41}$$

In previous chapters, consideration of the far-field behaviour as $kr_0 \to \infty$ in the equivalent of (8.2.12) has yielded a relation between the inner product term appearing

in (8.2.41), and the general case is no different. Therefore, from (8.2.18) we deduce that

$$G \sim \frac{\mathrm{i}}{4} H_0(kR) \frac{\psi_0(z)\psi_0(z_0)}{h_0} \tag{8.2.42}$$

which may be rewritten as

$$G \sim \frac{\mathrm{i}}{4h_0} \sum_{m=-\infty}^{\infty} \mathrm{i}^m H_m(kr_0) \mathrm{e}^{\mathrm{i}m\theta_0} \Phi_{0m}(\mathbf{r}) \tag{8.2.43}$$

using (8.2.26) so it follows that

$$\mathbf{L} \sim \frac{\mathrm{i}}{4h_0} \sum_{m=-\infty}^{\infty} \mathrm{i}^m H_m(kr_0) \mathrm{e}^{\mathrm{i}m\theta_0} \psi_0(z_0) \overline{\Psi_{0m}}(\mathbf{r}). \tag{8.2.44}$$

Then, taking the limit $kr_0 \to \infty$ in (8.2.13) and using (8.2.28), (8.2.38) and (8.2.44) we find that

$$\sum_{m=-\infty}^{\infty} H_m(kr_0) \mathrm{i}^m A_m \mathrm{e}^{\mathrm{i}m\theta_0} \psi_0(z_0) = -\frac{\mathrm{i}}{4h_0} \sum_{m=-\infty}^{\infty} \mathrm{i}^m H_m(kr_0) \mathrm{e}^{\mathrm{i}m\theta_0} \psi_0(z_0) \iint_{S_b} \Phi \overline{F^{(m)}} \, \mathrm{d}S, \tag{8.2.45}$$

from which it is clear that

$$A_m = -\frac{\mathrm{i}}{4h_0} \langle \Phi, F^{(m)} \rangle. \tag{8.2.46}$$

This result is the key to progressing with (8.2.41) which now becomes

$$\Phi(\mathbf{r}_0) = \sum_{m=-\infty}^{\infty} \Phi_{0m}(\mathbf{r}_0)(\mathrm{e}^{-\mathrm{i}m\theta_{inc}} + A_m) - \iint_{S_b} \Phi(\mathbf{r}) \mathbf{n}.\nabla \times \widehat{\mathbf{L}} \, \mathrm{d}S. \tag{8.2.47}$$

We will now proceed to form an integral equation by taking the normal derivative of (8.2.47) with respect to the field variable and then applying the bcd condition. Firstly we define the field variable analogue of (8.2.1) as

$$\left.\begin{array}{lll} \mathbf{n}_0 = (-h_{x_0}, -h_{y_0}, 1)/\sigma_0 & & \sigma_0 = \sqrt{1 + h_{x_0}^2 + h_{y_0}^2}, \\ \mathbf{s}_0 = (-h_{x_0}, 0, 1)/\sigma_{s_0} & & \sigma_{s_0} = \sqrt{1 + h_{x_0}^2}, \\ \mathbf{t}_0 = (0, -h_{y_0}, 1)/\sigma_{t_0} & & \sigma_{t_0} = \sqrt{1 + h_{y_0}^2}, \end{array}\right\} \tag{8.2.48}$$

and also ∇_0 is understood to be the gradient operator with respect to the field variables

$$\nabla_0 = \left(\frac{\partial}{\partial x_0}, \frac{\partial}{\partial y_0}, \frac{\partial}{\partial z_0} \right). \tag{8.2.49}$$

So

$$\mathbf{n}_0.\nabla_0\Phi(\mathbf{r}_0) = \mathbf{n}_0.\nabla_0 \sum_{m=-\infty}^{\infty} \Phi_{0m}(\mathbf{r}_0)(e^{-im\theta_{inc}} + A_m) - \mathbf{n}_0.\nabla_0 \iint_{S_b} \Phi(\mathbf{r})\mathbf{n}.\nabla \times \widehat{\mathbf{L}}\, dS. \tag{8.2.50}$$

As in earlier chapters, in order to be able to take the gradient operator inside the integral we need to be able to say that $\mathbf{r_0}$ is not on S_b. This is permissable as the definitions in (8.2.48) are all extensible off the curve $z_0 = h(x_0, y_0)$ for which they are defined. This point is crucial as it allows us to write

$$\nabla_0 \left[\mathbf{n}.\nabla \times \widehat{\mathbf{L}}\right] = \nabla_0 \times \mathbf{II} \tag{8.2.51}$$

where, in accordance with a similar transformation earlier

$$\begin{aligned} \mathbf{II} &= \left(\left[\mathbf{n}.\nabla \times \widehat{\mathbf{L}}\right]_{y_0}^{x_0}, -\left[\mathbf{n}.\nabla \times \widehat{\mathbf{L}}\right]_{x_0}^{z_0}, 0 \right) \\ &= (\mathbf{n}.\nabla \times \mathbf{L}_1\ ,\ -\mathbf{n}.\nabla \times \mathbf{L}_2\ ,\ 0) \end{aligned} \tag{8.2.52}$$

and

$$\mathbf{L}_1 = \widehat{\mathbf{L}}_{y_0}^{x_0} \equiv \left(\widehat{G}_{yy_0}^{zz_0}\ ,\ \widehat{G}_{xy_0}^{zz_0}\ ,\ 0 \right) \equiv (L_{11}\ ,\ -L_{12}\ ,\ 0), \tag{8.2.53}$$

$$\mathbf{L}_2 = \widehat{\mathbf{L}}_{x_0}^{z_0} \equiv \left(\widehat{G}_{yx_0}^{zz_0}\ ,\ \widehat{G}_{xx_0}^{zz_0}\ ,\ 0 \right) \equiv (L_{21}\ ,\ -L_{22}\ ,\ 0). \tag{8.2.54}$$

In confirming the relation in (8.2.51) with the associated definition of $\mathbf{H}$ in (8.2.52) use is made of

$$\nabla_0^2 G = 0 \qquad \Rightarrow \qquad \nabla_0^2 \left[\mathbf{n}.\nabla_0 \times \mathbf{L}\right]. \tag{8.2.55}$$

which holds for $\mathbf{r} \neq \mathbf{r}_0$, a fact which is ensured by the requirement that $\mathbf{r}_0 \notin S_b$ when the transformation in (8.2.51)is made. So we have, from (8.2.50)

$$\mathbf{n}_0.\nabla_0\Phi(\mathbf{r}_0) = \mathbf{n}_0.\nabla_0 \times \sum_{m=-\infty}^{\infty} \Psi_{0m}(\mathbf{r}_0)(e^{-im\theta_{inc}} + A_m) - \mathbf{n}_0.\nabla_0 \times \iint_{S_b} \Phi(\mathbf{r})\mathbf{H}(\mathbf{r};\mathbf{r}_0)\, dS \tag{8.2.56}$$

the transformation in (8.2.51) having been made for $\mathbf{r} \neq \mathbf{r}_0$, and then the curl operator $\nabla_0\times$ is taken back outside the integral operator so that the kernel is no

more than log-singular again. Then, and only then, can $\mathbf{r}_0$ be sent onto S_b so that the left hand side goes to zero and therefore

$$\mathbf{n}_0.\nabla_0 \times \iint_{S_b} \Phi(\mathbf{r})\mathbf{H}(\mathbf{r};\mathbf{r}_0)\,\mathrm{d}S = \mathbf{n}_0.\nabla_0 \times \sum_{m=-\infty}^{\infty} \Psi_{0m}(\mathbf{r}_0)(\mathrm{e}^{-im\theta_{inc}} + A_m); \qquad \mathbf{r}_0 \in S_b. \quad (8.2.57)$$

If we now define an integro-differential operator

$$(\mathcal{K}\Phi)(\mathbf{s}_0,\mathbf{t}_0) = \mathbf{n}_0.\nabla_0 \times \iint_{S_b} \Phi(\mathbf{r})\mathbf{H}(\mathbf{r};\mathbf{r}_0)\,\mathrm{d}S; \qquad \mathbf{r}_0 \in S_b, \quad (8.2.58)$$

and a set of functions $\Phi_m(\mathbf{s}_0,\mathbf{t}_0)$ such that

$$(\mathcal{K}\Phi_m) = \mathbf{n}_0.\nabla_0 \times \Psi_{0m} \quad (8.2.59)$$

then it follows that

$$\Phi = \sum_{m=-\infty}^{\infty} \Phi_m(\mathrm{e}^{-im\theta_{inc}} + A_m). \quad (8.2.60)$$

We now substitute (8.2.60) into (8.2.46) to obtain, after some rearrangement, an infinite system of equations for the scattering coefficients

$$A_n + \frac{\mathrm{i}}{4h_0}\sum_{m=-\infty}^{\infty}\langle\Phi_m, F^{(n)}\rangle A_m = -\frac{\mathrm{i}}{4h_0}\sum_{m=-\infty}^{\infty}\mathrm{e}^{-im\theta_{inc}}\langle\Phi_m, F^{(n)}\rangle \qquad n \in \mathbb{Z}. \quad (8.2.61)$$

In practice we would solve this problem by truncating the sum at a fixed value M anticipating convergence to the exact solution as $M \to \infty$. In this case we would end up with a matrix system to solve of the form

$$(\underline{\underline{\mathbf{I}}} + \underline{\underline{\mathbf{B}}}).\mathbf{A} = -\underline{\underline{\mathbf{B}}}.\mathbf{e} \quad (8.2.62)$$

where

$$\underline{\underline{\mathbf{I}}} = \delta_{nm} \qquad n,m = -M,\ldots,M$$

$$\underline{\underline{\mathbf{B}}} = B_{n,m} = \frac{\mathrm{i}}{4h_0}\langle\Phi_m F^{(n)}\rangle \qquad n,m = -M,\ldots,M$$

$$\mathbf{A} = A_m \qquad m = -M,\ldots,M$$

$$\mathbf{e} = \mathrm{e}^{-im\theta_{inc}} \qquad m = -M,\ldots,M$$

which is routine to solve.

Before proceeding any further it is worth highlighting that the new integral operator defined at (8.2.58) is the crux of this thesis. Although it looks unwieldy at this stage, it has a structure that is perfectly suited for solution by the Rayleigh-Ritz technique. In fact the other main aspect of our technique, as we shall see, is that the Rayleigh-Ritz method is fundamental in that it allows us to integrate by parts and therefore keep the kernel only weakly singular.

The prototype equation (8.2.59) is solved by the Rayleigh-Ritz method formulating a variational principle as illustrated at (2.3.22) to (2.3.30). We choose trial functions to model the fluid potential on S_b and these may be written as $p_i(s,t) \equiv p_i(x,y)$ which acknowledges that the surface tangential vectors can be parameterised by the area coordinates in the projected plane S_p. So we write

$$\Phi_m = \sum_{i=0}^{N} a_i^{(m)} p_i(s_0, t_0) \tag{8.2.63}$$

then the solution of

$$(\mathcal{K}\Phi_m) = F^{(m)} \tag{8.2.64}$$

which combines (5.3.38) and (8.2.59),is given by solving

$$\sum_{i=0}^{N} a_i^{(m)} \langle \mathcal{K}p_i, p_j \rangle = \langle F^{(m)}, p_j \rangle \qquad j = 0, \ldots, N. \tag{8.2.65}$$

So, consider the right hand side term

$$F_j^{(m)} = \iint_{S_b} \overline{p_j} \mathbf{n}_0 . \nabla_0 \times \Psi_{0m} \, \mathrm{d}S_0 \tag{8.2.66}$$

$$= \int_{\partial S_b} \overline{p_j} \Psi_{0m} . \, \mathrm{d}\mathbf{r}_0 - \iint_{S_b} \mathbf{n}_0 . (\nabla_0 \overline{p_j} \times \Psi_{0m}) \, \mathrm{d}S_0 \tag{8.2.67}$$

where we have used the result

$$\nabla \times (\lambda \mathbf{v}) = \lambda \nabla \times \mathbf{v} + \nabla \lambda \times \mathbf{v} \tag{8.2.68}$$

together with Stokes' theorem to convert one of the surface integrals to a line integral around the boundary of S_b. Now Ψ_{0m} is continuous on S_b and $\Psi_{0m} = 0$ on ∂S_b

so the line integral term vanishes. Also

$$\begin{aligned}\mathbf{n}_0.(\nabla p_i \times \Psi_{0m}) &= -\nabla_0 p_i.(\mathbf{n}_0 \times \Psi_{0m}) \\ &= -\nabla_0 p_i.((\mathbf{s}_0 \times \mathbf{t}_0) \times \Psi_{0m}))\tau_0 \\ &= -\nabla_0 p_i.\tau_0[(\mathbf{s}_0.\Psi_{0m})\mathbf{t}_0 - (\mathbf{t}_0.\Psi_{0m})\mathbf{s}_0))] \\ &= -\frac{1}{\sigma}[\sigma_{S_0}(\mathbf{s}_0.\Psi_{0m})\sigma_{t_0}\mathbf{t}_0.\nabla_0 p_i \\ &\qquad -\sigma_{t_0}(\mathbf{t}_0.\Psi_{0m})\sigma_{s_0}\mathbf{s}_0.\nabla_0 p_i] \\ &= -\frac{1}{\sigma}\left[(\mathbf{i}.\Psi_{0m})\frac{\partial p_i}{\partial y_0} - (\mathbf{j}.\Psi_{0m})\frac{\partial p_i}{\partial x_0}\right] \qquad (8.2.69)\end{aligned}$$

therefore

$$\begin{aligned}F_i^{(m)} &= \iint_{S_b}\left[(\mathbf{i}.\Psi_{0m})\frac{\partial \overline{p_i}}{\partial y_0} - (\mathbf{j}.\Psi_{0m})\frac{\partial \overline{p_i}}{\partial x_0}\right]\frac{\mathrm{d}S_0}{\sigma_0} \\ &= \iint_{S_p}\left[(\mathbf{i}.\Psi_{0m})\frac{\partial \overline{p_i}}{\partial y_0} - (\mathbf{j}.\Psi_{0m})\frac{\partial \overline{p_i}}{\partial x_0}\right]\mathrm{d}x_0\,\mathrm{d}y_0 \qquad (8.2.70)\end{aligned}$$

since $\mathrm{d}S_0 = \sigma_0\,\mathrm{d}x_0\,\mathrm{d}y_0$ as shown earlier. In a similar fashion we consider the left hand side terms of (8.2.66) which is of the form

$$\sum_{i=0}^{N} a_i^{(m)} K_{ij}^{(m)} \qquad (8.2.71)$$

where

$$K_{ij}^{(m)} = \iint_{S_b} \overline{p_j}(s_0, t_0)\mathbf{n}_0.\nabla_0 \times \mathbf{J}_i\,\mathrm{d}S_0 \qquad (8.2.72)$$

and

$$\mathbf{J}_i = \iint_{S_b} p_i(s,t)\mathbf{H}\,\mathrm{d}S. \qquad (8.2.73)$$

Now $\mathbf{H}$ may have discontinuities, but $\mathbf{J}_i$ is continuous. So, as before we get

$$K_{ij} = \iint_{S_p}\left[(\mathbf{i}.\mathbf{J}_i)\frac{\partial \overline{p_j}}{\partial y_0} - (\mathbf{j}.\mathbf{J}_i)\frac{\partial \overline{p_j}}{\partial x_0}\right]\mathrm{d}x_0\,\mathrm{d}y_0. \qquad (8.2.74)$$

Also

$$\begin{aligned}\mathbf{i}.\mathbf{J}_i &= \iint_{S_b} p_i\mathbf{n}.\nabla \times \mathbf{L}_1\,\mathrm{d}s \\ &= \int_{\Gamma} p_i\mathbf{L}_1.\,\mathrm{d}\mathbf{r} - \iint_{S_b}\mathbf{n}.(\nabla p_i \times \mathbf{L}_1)\,\mathrm{d}s \qquad (8.2.75)\end{aligned}$$

using Stokes' theorem, where Γ is ∂S_b on which $\mathbf{L}_1 = \mathbf{0}$ and any other curves on S_b on which $\mathbf{L}_1$ is discontinuous. Let us leave the line integral term for a while, so

$$\begin{aligned}\mathbf{i}.\mathbf{J}_i &= \iint_{S_b} \nabla p_i.(\mathbf{n}\times\mathbf{L}_1)\,\mathrm{d}s + \int_\Gamma p_i\mathbf{L}_1.\,\mathrm{d}\mathbf{r}\\ &= \iint_{S_p}\left[(\mathbf{i}.\mathbf{L}_1)\frac{\partial p_i}{\partial y} - (\mathbf{j}.\mathbf{L}_1)\frac{\partial p_i}{\partial x}\right]\mathrm{d}x\,\mathrm{d}y + \int_\Gamma p_i\mathbf{L}_1.\,\mathrm{d}\mathbf{r}\\ &= \iint_{S_p}\left[L_{11}\frac{\partial p_i}{\partial y} + L_{12}\frac{\partial p_i}{\partial x}\right]\mathrm{d}x\,\mathrm{d}y + \int_\Gamma p_i\mathbf{L}_1.\,\mathrm{d}\mathbf{r}, \qquad (8.2.76)\end{aligned}$$

where L_{11}, L_{12} are defined by (8.2.53). Similarly

$$-\mathbf{j}.\mathbf{J}_i = \iint_{S_p}\left[L_{21}\frac{\partial p_i}{\partial y} + L_{22}\frac{\partial p_i}{\partial x}\right]\mathrm{d}x\,\mathrm{d}y + \int_\Gamma p_i\mathbf{L}_2.\,\mathrm{d}\mathbf{r}, \qquad (8.2.77)$$

where L_{21}, L_{22} are defined by (8.2.54). We now consider the line integral terms where the only contribution is from curves along which $\mathbf{L}_1$ and $\mathbf{L}_2$ are discontinuous. Of course, whether or not the $\mathbf{L}_i$ have lines of discontinuity, depends critically on the form of the original Green's function chosen. So, if for example the form in (8.2.18) is chosen, then using the form of R in (8.2.16) it is clear that the $L_{\alpha\beta}$, $\alpha,\beta = 1,2$, possess no lines of discontinuity. In contrast if (8.2.18) is decomposed using (8.2.24), (8.2.25) etc. we would obtain the alternative form

$$\begin{aligned}\widehat{G} = \sum_{m=-\infty}^{\infty} \mathrm{e}^{\mathrm{i}m(\theta-\theta_0)}\Bigg\{&\frac{1}{4}J_m(kr_<)Y_m(kr_>)\frac{\psi_0(z)\psi_0(z_0)}{h_0} +\\ &\frac{1}{2\pi}\sum_{n=1}^{\infty} I_m(k_nr_<)K_m(k_nr_>)\frac{\psi_n(z)\psi_n(z_0)}{h_0}\Bigg\} \qquad (8.2.78)\end{aligned}$$

from which we deduce that the curve $r = r_0$ will be the source of any discontinuities. In fact making this choice for G will result in an additional term whose contribution may be calculated exactly as in (7.4.32) which in turn used (5.3.35). This may be established by converting both line integrals appearing in (8.2.75) and (8.2.76) into polar coordinates and calculating the jump in the integrand on the line $r = r_0$.

We proceed using the form of Green's function in (8.2.18) with the result that there are no additional terms introduced. However, we flag that if an alternative

form of the Green's function is chosen, care must be taken to consider any lines of discontinuity which might exist. Consequently we have

$$K_{ij} = \iint\limits_{S_p} \mathrm{d}x_0\,\mathrm{d}y_0 \iint\limits_{S_p} \mathrm{d}x\,\mathrm{d}y \left[L_{11}\frac{\partial p_i}{\partial y}\frac{\partial \overline{p_j}}{\partial y_0} + L_{12}\frac{\partial p_i}{\partial x}\frac{\partial \overline{p_j}}{\partial y_0} + L_{21}\frac{\partial p_i}{\partial y}\frac{\partial \overline{p_j}}{\partial x_0} + L_{22}\frac{\partial p_i}{\partial x}\frac{\partial \overline{p_j}}{\partial x_0}\right] \tag{8.2.79}$$

or alternatively

$$K_{ij} = \iint\limits_{S_p} \mathrm{d}x_0\,\mathrm{d}y_0 \iint\limits_{S_p} \mathrm{d}x\,\mathrm{d}y \left[\widehat{G}^{zz_0}_{yy_0}\frac{\partial p_i}{\partial y}\frac{\partial \overline{p_j}}{\partial y_0} + \widehat{G}^{zz_0}_{xy_0}\frac{\partial p_i}{\partial x}\frac{\partial \overline{p_j}}{\partial y_0} + \widehat{G}^{zz_0}_{yx_0}\frac{\partial p_i}{\partial y}\frac{\partial \overline{p_j}}{\partial x_0} + \widehat{G}^{zz_0}_{xx_0}\frac{\partial p_i}{\partial x}\frac{\partial \overline{p_j}}{\partial x_0}\right]. \tag{8.2.80}$$

Thus we have finally achieved a form of the kernel which is at worst Log-singular. This was achieved in (8.2.75) and also in (8.2.76) where the integration by parts switched the differential operator from the Green's function term onto the test functions.

8.3 Application to quasi two-dimensional problems

We have already considered two classes of axisymmetric problem. The first, in Chapters 5 and 6 was the case when the topography does not vary in one of the (Cartesian) coordinates. The second class, in Chapter 7, was where there is rotational symmetry, i.e. the topography does not vary with the θ coordinate in a cylindrical coordinate system. Both of these may be recovered from the general theory developed in Section 8.2.

We stress here that much of the analysis of the previous section is independent of coordinate system. Moreover if one chooses a particular coordinate system, a consistent application of the general theory will result in an equivalent system whatever coordinate system is chosen. For example if the general theory is developed in cylindrical coordinates, then we can recover the Cartesian version by a change of coordinates in the final system, and of course the reverse also applies. We remark that the algebra to demonstrate this is somewhat complicated and protracted though.

So for example in Chapter 5 all of the formulation up to (5.3.24) was essentially three-dimensional and mirrors the development in the general theory up to (8.2.41) (albeit given a slightly different form due to the different far-field structures). If the steps in the general theory from (8.2.42) on are applied to (5.3.24) we eventually recover the system of equations in (5.4.24) to (5.4.28) and (5.4.34). Here we do have to account for the discontinuity of the oblique Green's function along the line $x = x_0$.. In fact, if one apples the general theory as in Section 8.2, then it transpires that reduction of each step to its two-dimensional form recovers the equivalent step in Chapter 5.

Alternatively, had we chosen to develop the general theory in cylindrical coordinates, then the link with the axially symmetric problem would have been clearer. In any case the analysis in Chapter 7 up to (7.3.30) is totally general (in cylindrical coordinates) taking no advantage of the symmetry. Thus using (7.3.30) as the start point (which equates directly to (8.2.41)), and mirroring the steps in the general theory from (8.2.41) on we would recover the system developed in Section 7.4 *exactly*. We note that, as this approach employs the Green's function in the form of (8.2.77) there is a line of discontinuity on $\mathbf{r} = \mathbf{r}_0$ whose contribution must be included.

8.4 Numerical approach for arbitrary patch problems

Unfortunately time has precluded a numerical implementation of the General theory, therefore the efficient computation of (8.2.80) remains an area for further development. We stress, at this point that this is now purely a numerical issue whereby we now have a complicated quadruple integral to calculate, and therefore the computation time is likely to be increased significantly. In previous problems we have seen how convergence of the system is improved by selecting a set of test functions which model the local fluid flow in some sense. In this case it is somewhat more complicated to define a complete set over the surface of S_p which incorporates local fluid flow.

It would seem that, whatever coordinate system is chosen, the only prospect of simplifying the resultant system of equations is to choose a set of test functions which reduces the computational complexity of the system. We have already seen in Chapter 2, for example, how one particular simple choice of test function in (2.3.30) reduced the complexity of the system recovering a simpler form alternatively derived by the boundary element approach. With this in mind we suggest the following strategy for implementing a practical solution scheme. Firstly we form a grid on S_p by dividing one coordinate axis into N equal elements and the other into M elements so that we have $I = N \times M$ panels P_i, each of which is an element of area corresponding to a cartesian grid. Then we set our test function q_i, $i = 1, \ldots, I$ to take the form

$$q_i = \begin{cases} f_i, & \mathbf{r} \in P_i; \\ 0, & \mathbf{r} \notin P_i, \end{cases} \tag{8.4.1}$$

where f_i is a function of the coordinates in the projected space and is chosen to have some simplifying form on the panel. We remark that this definition obviously provides an orthogonal set with respect to the inner product defined on S_b as was required in our derivation of the Rayleigh-Ritz method.

If we now turn to the specific form of the test function on each panel, then from (8.2.80) the simplest form is to assume the potential is planar on the panel. There are obviously several different ways we might achieve this, for example we might define the function f_i by

$$f_i = x + b_i y, \tag{8.4.2}$$

where importantly the derivatives of this potential function are constants. The extra constant b_i is required to acknowledge that the relationship between the tangential derivatives varies from panel to panel. As this increases the number of unknowns in the system, we would need to introduce an auxiliary system to enable us to calculate the b_i by, for example requiring the potential to match at the mid points of the edges of adjacent panels. We observe that this approach is entirely equivalent to solving (8.5.3) by a boundary element method collocating at the mid-points of the edges of the panels and suggest this as a practical first step in implementing a numerical

solution.

Of course more sophisticated choices might be made. However, as we have seen in Chapters 5 to 7 simple choices can still achieve impressive results. Any numerical investigation would need to investigate whether increased sophistication had a marked improvement in accuracy, and particularly whether the increased computational complexity had a corresponding improvement in the results.

8.5 Remarks

In this chapter we have demonstrated how our techniques originally developed for three-dimensional problems having some form of symmetry can be extended to deal with genuinely arbitrary three-dimensional wave scattering problems. The theory introduces a new integral operator which at first sight looks unwieldy, but is in fact perfectly structured for implementation by the Rayleigh-Ritz method.

We observe that, although these techniques have been applied to wave/topography problems, they are equally applicable to three-dimensional wave/body problems. The method has promise in dealing with the problem of wave scattering by a floating body, particularly with forward speed. Our fully linear approach retaining an exact formulation and allowing solution by the Rayleigh-Ritz method offers the potential for extremely accurate solutions. Noblesse & Yang [68] highlight the waterline line-integrals as causing significant problems. However our approach has the potential to simplify this issue radically. This can be seen if we redefine the functions $\chi_r(z)$ introduced at (5.2.21) for example, as

$$\chi_r(z) = -k_r \int_0^z \psi_r(z')dz' = N_r^{-1/2} \sin k_r(h_0 - z), \qquad r = 0, 1, 2, \ldots. \tag{8.5.3}$$

With this definition we see that the test functions take a value of zero at the free surface which would eliminate any free surface line integrals. This is an interesting area of extension of our theory which has the potential to make a significant contribution to a problem of considerable practical interest.

Although inspired by an idea introduced by Noblesse [67] our approach differs significantly in many respects. Firstly we have established a consistent and sound mathematical framework for the techniques and have shown how a consideration of the singularities is crucial. We choose a specially constructed Green's function which restricts the contributions to the arbitrary patch of bed and whose structure allows for explicit treatment of any log singularity. We have shown how the surface integrals may be projected down onto a plane thus simplifying the numerical implementation greatly. We have also presented a wide range of experimental data to compare the techniques against existing approximate solutions. We have retained an *exact* formulation throughout making significant analytical progress with integral equation. Rather than make a simple panel based approximation of the integral equation, one of our approaches is based on an extremely accurate method of solution which incorporates the local behaviour of the fluid without discretising the topography. Above all we have shown how a second implementation of the derivative switching technique provides an alternative formulation which is perfectly set up for solution by the Rayleigh-Ritz method, which is itself fundamental to ensuring the system remains weakly singular.

Chapter 9

Conclusions

In this thesis we have considered a wide range of problems which, to one extent or another, have been discussed by other authors generally in a two-dimensional context and usually solved via making simplifying approximations such as the mild-slope equations or some form of collocation scheme. In contrast we have retained an exact formulation and applied the full linear theory to the three-dimensional extension of these problems.

In Chapter 3 we considered a two-dimensional problem of sloshing over an arbitrary bed showing how an extremely accurate first-order solution could be fed in to give a correspondingly accurate second-order solution. This chapter can be viewed as a vehicle for developing and presenting the two-dimensional techniques we sought to extent to a fully three-dimensional context in this thesis. In the absence of exact results against which we could compare our later results, in Chapter 4 we presented new results for two problems having specific geometries using a multipole based approach so that we could validate our later chapters.

In Chapter 5 we introduced our techniques to deal with the scattering of oblique waves by an infinitely long ridge of arbitrary profile. We also showed how such a topography can also support edge waves. Chapter 6 extends these ideas to deal with the much more complicated problem of the scattering of oblique waves by an infinite step. In Chapter 7 we show how the same techniques can be applied to axis-symmetric problems; however, we presented them in a different way to illustrate the

three-dimensional nature of the problem and to lead the reader more gently into a discussion of the fully three-dimensional problem.

Finally in Chapter 8 we show how the techniques can be applied to genuinely three-dimensional problems. In doing so we have developed a completely new theory and associated integral operator possessing a remarkable structure which allows extremely accurate solution techniques to be applied. Interestingly the solution technique itself plays a key and integral part in making sure the integral equation is only weakly-singular. The key difference from other approaches is that we make significant analytical progress with the formulation which remains *exact* and allows us to employ sophisticated solution techniques. We tend to be left solving a small matrix based system and still achieving a level of accuracy that would require much larger systems in a boundary integral approach.

This theory offers many areas for further development. Foremost must be development of an efficient numerical scheme to implement the fully three-dimensional theory. Once accomplished this will open up a wide range of problems to solution by the fully linear theory rather than the approximate approaches required at present. We have indicated how the theory may be applied to floating body problems where it has the potential to make a significant contribution.

As we have developed a fully linear theory, it will provide a valuable means of testing approximate solution techniques over more realistic geometries. In particular an area for further development would be to conduct an extensive evaluation of the accuracy of the MMSE for problems such as axis-symmetric scattering.

In summary, the techniques we have developed involve formulating the problem as an integral equation with at worst a weakly singular kernel. In developing them we have constructed a new theory for water wave scattering problems over arbitrary topography which allows the implementation of extremely accurate and efficient solution techniques.

Appendix A

Green's Functions for constant depth fluid domains

Throughout this thesis we make extensive use of Green's Second Identity and appropriate Green's functions to formulate our problems as integral equations. Whereas there is some freedom in the choice of the form of Green's functions we will choose them so that their contributions vanish on at least some of the boundary. Our main problems of interest are wave problems over a defined patch of topography in an otherwise constant depth domain or those involving a submerged body in a domain of constant depth. We therefore need to define Green's Functions satisfying the bed condition and the free surface condition for a constant depth domain. Where the fluid domain is of more complicated form we may use combinations of these basic Green's functions to construct more sophisticated Green's functions which simplify the integral formulation further. Thus these constant depth Green's Functions may be viewed as the basic building blocks of the solutions.

The Green's function $G(\mathbf{r}|\mathbf{r_0}; K)$ is defined to be the potential at any field point $\mathbf{r} = (x, y, z)$ due to an oscillating source of unit strength at $\mathbf{r_0} = (x_0, y_0, z_0)$ and having frequency parameter K. The precise form of the source is defined by the characteristics of the problem we wish to consider. We will consider three specific cases each of which will require a different fundamental Green's Function. However, before we progress to each of the three cases we may make some progress with determining the depth dependence of the Green's functions. We define the constant depth fluid

domain as $\mathcal{D}$ where

$$\mathcal{D} \equiv (x, y, z) : -\infty < x, y < +\infty, 0 \leq z \leq h_0.$$

In a domain $\mathcal{D}$ the conditions for $G(\mathbf{r}|\mathbf{r}_0; K)$ are

$$\nabla^2 G = \delta(z - z_0) f(x, y) \qquad \mathbf{r} \in \mathcal{D} \tag{A.1}$$

$$G_z + KG = 0 \qquad \omega^2 = Kg, \qquad z = 0 \tag{A.2}$$

$$G_z = 0 \qquad z = h_0 \tag{A.3}$$

where $f(x, y)$ depends upon the form of the source and will be discussed for each of the three cases in turn. We will also require the Green's function to satisfy a Sommerfeld radiation condition [88], implying that waves generated by the source in the fluid can only be outgoing.

A.1 Separation of the depth dependence

As we have a finite and constant depth domain, we are able to perform an eigenfunction expansion to derive the form of the depth dependence. We therefore perform a separation of variables on Laplace's equation seeking a solution of the form

$$G(x, y, z) = g(x, y)\psi(z)$$

If if this is substituted in Laplace's equation we obtain

$$\nabla_H^2 g(x, y)\psi(z) + g(x, y)\psi''(z) = 0$$

where ∇_H^2 is the two-dimensional Laplacian and $'$ represents differentiation with respect to the dependent variable. It is now a routine matter to recover the depth dependence in terms of the well-known complete orthonormal set of depth eigenfunctions $\{\psi_n(z)\}$ in $[0, h_0]$ introduced at (2.1.47). For clarity of exposition we summarise the properties of the eigenfunctions which are defined as

$$\psi_n(z) = N_n^{-1/2} \cos k_n(h_0 - z) \tag{A.4}$$

with

$$N_n = \frac{1}{2}\left(1 + \frac{\sin 2k_n h_0}{2k_n h_0}\right) \tag{A.5}$$

chosen so that the depth modes have a weight h_0 and satisfy the orthogonality relation

$$\frac{1}{h_0}\int_0^{h_0} \psi_n(z)\psi_m(z)\,\mathrm{d}z = \delta_{mn} \tag{A.6}$$

The eigenvalues $\{k_n\}$ defined for $n \geq 1$ and $k_n > 0$ are obtained as the ascending solutions of the well-known dispersion relation

$$K + k_n \tan k_n h_0 = 0 \tag{A.7}$$

which is deduced from the free-surface condition. This equation also has a single complex root which we define as $k_0 = -ik$ and where k is the single positive real root of the dispersion relation in the form

$$K = k \tanh kh_0 \tag{A.8}$$

We introduce a set of functions $\{\chi_n(z)\}$ related to the eigenfunctions and defined as

$$\chi_n(z) = N_n^{-1/2} \sin k_n(h_0 - z) \quad n = 0, 1, \ldots \tag{A.9}$$

which have the same normalizing factor and weight over $[0, h_0]$.

Continuing the separation of variables we deduce that for each depth mode there must be an associated horizontal mode $g_n(x, y)$ so that the solution of the homogeneous version of equation (A.1) may be expressed as

$$G = \sum_{n=0}^{\infty} A_n g_n(x, y)\psi_n(z). \tag{A.10}$$

Now substituting in (A.1) we deduce that

$$\sum_{n=0}^{\infty} A_n \psi_n(z)\{\nabla_H^2 g_n(x, y) - k_n^2 g_n(x, y)\} = \delta(z - z_0) f(x, y) \tag{A.11}$$

and upon multiplying throughout by $\psi_m(z)$ and integrating over $[0, h_0]$ we deduce that

$$A_n = \frac{\psi_n(z_0)}{h_0}$$

and the horizontal mode must satisfy

$$\nabla_H^2 g_n(x,y) - k_n^2 g_n(x,y) = f(x,y). \tag{A.12}$$

Finally we deduce that all constant depth Green's Functions satisfying the linearized free surface condition may be expressed as

$$G(\mathbf{r}|\mathbf{r}_0) = \sum_{n=0}^{\infty} g_n(x,y|x_0,y_0)\frac{\psi_n(z)\psi_n(z_0)}{h_0} \tag{A.13}$$

where the horizontal mode is derived from equation (A.12). We now proceed to deduce the precise form of the Green's function by solving (A.12) for three different situations.

A.2 Two-dimensional and quasi two-dimensional Green's functions - Normal and oblique incidence problems

A.2.1 2D Green's Function

In domains where the problem is independent of one of the horizontal coordinates, which we will set as y without loss of generality, the problem is two-dimensional. In this case the source function is a line source of constant strength along the line $(x,z) = (x_0,z_0)$ and $f(x,y)$ in equation (A.1) takes the form $\delta(x-x_0)$. We note that this problem may be solved by Fourier Transform techniques, see [61] for example, although it should be noted that his final result contains a sign error. However the final result can be obtained more directly by solving A.12 which in this case reduces to

$$g_n''(x) - k_n^2 g_n(x) = -\delta(x-x_0). \tag{A.14}$$

We see that the solution has the form

$$g_n(x|x_0) = \begin{cases} Ae^{k_n(x-x_0)} + Be^{-k_n(x-x_0)}, & x-x_0 < 0; \\ Ce^{k_n(x-x_0)} + De^{-k_n(x-x_0)}, & x-x_0 > 0. \end{cases} \tag{A.15}$$

Now radiation conditions require that modes are exponentially damped at infinity and propagating modes are outgoing therefore we must have $B = C = 0$. Furthermore

continuity of g_n at $x = x_0$ requires that $A = D$. Our final condition is obtained as a jump condition

$$[g_n']_{x=x_0} = -1 \tag{A.16}$$

where the square brackets denotes the jump in the enclosed quantity. This condition is obtained by integrating equation (A.14) between $[x_0 - \epsilon, x_0 + \epsilon]$ and then taking the limit $\epsilon \to 0$. From this we deduce the value of A and therefore we find that we may write the 2D Green's function in the compact form

$$G(x, z|x_0, z_0; K) = \sum_{n=0}^{\infty} \frac{\psi_n(z)\psi_n(z_0)}{2k_n d} e^{-k_n|x-x_0|} \qquad (x, z) \neq (x_0, z_0) \tag{A.17}$$

A.2.2 3D Oblique Green's Function

We consider problems of oblique incidence where an incoming wave makes an angle of θ with the x axis and where the wavenumber β in the y direction is regarded as given. In this case we may write

$$f(x, y) = -\delta(x - x_0)e^{i\beta(y_0 - y)} \tag{A.18}$$

and hence equation A.12 reduces to

$$\nabla_H^2 g_n(x, y) - k_n^2 g_n(x, y) = -\delta(x - x_0)e^{i\beta(y_0 - y)}. \tag{A.19}$$

If we make the substitutions

$$g_n(x, y) = X_n(x)e^{i\beta(y_0 - y)}$$

and

$$\alpha_n^2 = k_n^2 + \beta^2$$

equation A.19 simplifies to

$$X_n''(x) - \alpha_n^2 X_n(x) = -\delta(x - x_0), \tag{A.20}$$

which has exactly the same form as equation A.14. Hence we may immediately write

$$G(\mathbf{r}|\mathbf{r}_0; K) = \sum_{n=0}^{\infty} \frac{\psi_n(z)\psi_n(z_0)}{2\alpha_n d} e^{-\alpha_n|x-x_0|} e^{i\beta(y_0 - y)} \qquad \mathbf{r} \neq \mathbf{r}_0 \tag{A.21}$$

We note that

$$\alpha_0 = (\beta^2 - k^2)^{1/2}$$

which represents a propagating wave if $\beta < k$. In this case

$$\alpha_0 = -\mathrm{i}(k^2 - \beta^2)^{1/2}$$

and we may write

$$(k^2 - \beta^2)^{1/2} \equiv \alpha = k\sin\theta \qquad \text{and} \qquad \beta = k\cos\theta$$

thus showing the propagating wave represents a horizontal wave making an angle θ with the y axis, as required.

A.3 Three-dimensional Green's function - the ring source

In this section we develop a Green's function in the same form as Hulme [43]. In his work he takes advantage of the axisymmetry in his problem to reduce the equations to a quasi-two-dimensional form by developing a Green's function which is a ring source with a harmonic variation in θ around the ring. Our approach will recover the ring sources albeit with a slightly different normalisation than that chosen by Hulme.

The Green's function representing a time-harmonic source of unit strength at $\mathbf{r} = \mathbf{r_0}$ in a domain of constant depth h_0 satisfies

$$\nabla^2 G(\mathbf{r};\mathbf{r_0}) = -\delta(\mathbf{r} - \mathbf{r_0}), \qquad \text{in } 0 < z, z_0 < h_0 \tag{A.22}$$

with

$$\frac{\partial G}{\partial z} + KG = 0, \qquad \text{on } z = 0 \tag{A.23}$$

and

$$\frac{\partial G}{\partial z} = 0, \qquad \text{on } z = d \tag{A.24}$$

As we may separate the periodic behaviour in θ from our physical problem we therefore seek to express G as a sum of ring sources in the form

$$G(\mathbf{r};\mathbf{r_0}) = \sum_{m=-\infty}^{\infty} g_m(r, z; r_0, z_0)\mathrm{e}^{-\mathrm{i}m(\theta-\theta_0)} \tag{A.25}$$

where g_m represents the ring source. Rewriting equation (A.22) in cylindrical polar coordinates and substituting for G using equation (A.25) we obtain

$$\sum_{m=-\infty}^{\infty}\left(\frac{1}{r}\frac{\partial}{\partial r}\left(r\frac{\partial}{\partial r}\right)+\frac{\partial^2}{\partial z^2}-\frac{m^2}{r^2}\right)g_m e^{-im(\theta-\theta_0)}=-\frac{1}{r}\delta(r-r_0)\delta(\theta-\theta_0)\delta(z-z_0). \tag{A.26}$$

We deduce the equation satisfied by g_m by multiplying equation (A.26) by $e^{im(\theta-\theta_0)}$ and integrating around a ring of radius r to give

$$2\pi r\left(\frac{1}{r}\frac{\partial}{\partial r}\left(r\frac{\partial}{\partial r}\right)+\frac{\partial^2}{\partial z^2}-\frac{m^2}{r^2}\right)g_m=-\delta(r-r_0)\delta(z-z_0). \tag{A.27}$$

We may now separate out the depth dependence by writing

$$g_m(r,z;r_0,z_0)=\sum_{n=0}^{\infty}a_{mn}\frac{\psi_n(z)\psi_n(z_0)}{d} \tag{A.28}$$

and then multiplying throughout by $\psi_n(z)$ and integrating over the depth to give

$$\left(\frac{1}{r}\frac{\partial}{\partial r}\left(r\frac{\partial}{\partial r}\right)-(k_n^2+\frac{m^2}{r^2})\right)a_{mn}=-\frac{1}{2\pi r}\delta(r-r_0). \tag{A.29}$$

Solutions of the homogeneous equation are given by

$$\begin{array}{lll} n=0 & J_m(kr) & H_m^{(1)}(kr) \\ n\geq 1 & I_m(k_nr) & K_m(k_nr). \end{array}$$

By letting $r\rightarrow r_0$ in equation $A.29$ we deduce that the a_{mn} must be continuous at $r=r_0$. A further "jump condition" is found by integrating $A.29$ between $r=r_0-\varepsilon$ and $r=r_0+\varepsilon$ and then letting $\varepsilon\rightarrow 0$ to give

$$[a'_{m,n}]_{r_0-}^{r_0+}=-\frac{1}{2\pi r_0}$$

For the case $n=0$ we require bounded solutions as $r\rightarrow 0$ and outgoing waves as $r\rightarrow\infty$, so

$$a_{m0}=\begin{cases} A_{m0}\mathrm{J_m}(kr), & r<r_0; \\ B_{m0}\mathrm{H_m}(kr), & r>r_0. \end{cases} \tag{A.30}$$

Now continuity at $r=r_0$ gives

$$a_{m0}=\begin{cases} C\mathrm{J_m}(kr)\mathrm{H_m}(kr_0), & r<r_0; \\ C\mathrm{H_m}(kr)\mathrm{J_m}(kr_0), & r>r_0. \end{cases} \tag{A.31}$$

Applying the jump condition we obtain

$$kC[\mathrm{J_m}(kr_0)\mathrm{H'_m}(kr_0) - \mathrm{J'_m}(kr_0)\mathrm{H_m}(kr_0)] \equiv kC\frac{2\mathrm{i}}{\pi kr_0} = -\frac{1}{2\pi r_0} \tag{A.32}$$

and therefore

$$a_{m0} = \frac{\mathrm{i}}{4}\mathrm{J_m}(kr_<)\mathrm{H_m}(kr_>) \tag{A.33}$$

where

$$r_< = \min\{r, r_0\} \quad \text{and} \tag{A.34}$$

$$r_> = \max\{r, r_0\}. \tag{A.35}$$

For $n \geq 1$ we must choose bounded solutions, continuous at $r = r_0$, therefore

$$a_{mn} = C_n\mathrm{I_m}(k_nr_<)\mathrm{K_m}(k_nr_>). \tag{A.36}$$

The jump condition gives

$$k_nC_n[\mathrm{I_m}(k_nr_0)\mathrm{K'_m}(k_nr_0) - \mathrm{I'_m}(k_nr_0)\mathrm{K_m}(k_nr_0)] \equiv k_nC_n\frac{-1}{k_nr_0} = -\frac{1}{2\pi r_0} \tag{A.37}$$

from which we deduce that $C_n = 1/2\pi$ finally giving the expression for the m'th ring source as

$$g_m = \frac{\mathrm{i}}{4}\mathrm{J_m}(kr_<)\mathrm{H_m}(kr_>)\frac{\psi_0(z)\psi_0(z_0)}{d} + \frac{1}{2\pi}\sum_{n=0}^{\infty}\mathrm{I_m}(k_nr_<)\mathrm{K_m}(k_nr_>)\frac{\psi_n(z)\psi_n(z_0)}{d}. \tag{A.38}$$

We note that this agrees with the form given by Hulme, although it should be noted that he used a source of strength 4π rather than our unit strengh source. This scaling was unimportant to Hulme as his technique involved considering a surface distribution of sources rather than our Green's formula approach. Accordingly it should be noted that our representation of the ring source Green's function differs from Hulme's by a factor of $1/4\pi$.

A.4 Three-dimensional Green's function - an alternative derivation

An alternative form of three-dimensional Green's function may be developed from (A.22) by choosing cylindrical coordinates (R, θ) centered on (x_0, y_0) and with R

defined by

$$R = \{(x - x_0)^2 + (y - y_0)^2\}^{1/2}. \tag{A.39}$$

In which case the solution must be independent of θ and so equation A.22 satisfied by $g_n(R)$ becomes

$$\frac{\mathrm{d}^2 g_n}{\mathrm{d}R^2} + \frac{1}{R}\frac{\mathrm{d}g_n}{\mathrm{d}R} - k_n^2 g_n = -\frac{\delta(R)}{2\pi R}. \tag{A.40}$$

In fact if the problem for $G(\mathbf{r}|\mathbf{r_0}; K)$ is framed in cylindrical polars defined as above then the result we derive by eigenfunction expansion may be obtained by Hankel transforms, see for example [23]. We proceed by making the substitution $S = k_n R$ in which case equation (A.40) becomes

$$\frac{\mathrm{d}^2 g_n}{\mathrm{d}S^2} + \frac{1}{S}\frac{\mathrm{d}g_n}{\mathrm{d}S} - g_n = -\frac{\delta(S)}{2\pi S} \tag{A.41}$$

which we recognize as the modified Bessel equation of order zero. We seek the solution which is singular at $S = 0$ and satisfies a Sommerfeld Radiation Condition. The radiation condition requires that waves are outgoing at infinity and that the energy is finite. In a cylindrical coordinate system it is well known that this implies, and is implied by, the requirement that

$$\lim_{R\to\infty} R^{1/2}\left\{\frac{\partial g_n}{\partial R} - \mathrm{i}k_n g\right\} = 0.$$

We therefore chose the solution that is singular at the origin

$$g_n = AK_0(k_n R).$$

To find the value of A we apply the source condition

$$\lim_{R\to 0}(2\pi R\frac{\mathrm{d}g_n}{\mathrm{d}R}) = -1$$

which ensures that we have a unit strength source as required. In this case using the fact that $K_0(x) \approx \log(x)$ as $x \to 0$ we deduce that $A = 1/2\pi$. It remains to check that our solution satisfies the radiation condition. We note that,

$$K_0(k_n R) = \frac{1}{2}\pi \mathrm{i} H_0^{(1)}((\mathrm{i}k_n R))$$

and in the limit $R \to \infty$ it is well known that

$$H_0^{(1)}(k_n R) \sim \sqrt{\tfrac{2}{\pi k_n R}}\, \mathrm{e}^{\mathrm{i}(k_n R - \pi/4)} \quad \text{as } R \to \infty .$$

It is therefore obvious that, only the $n = 0$ mode propagates to ∞ and furthermore it satisfies the radiation condition, hence we may write

$$G(\mathbf{r}|\mathbf{r}_0; K) = \frac{1}{2\pi} \sum_{n=0}^{\infty} K_0(k_n R) \frac{\psi_n(z)\psi_n(z_0)}{d} \qquad \mathbf{r} \neq \mathbf{r}_0. \tag{A.42}$$

We observe, unsurprisingly given that both Green's functions were derived from the same equation, that we can recover the form of (A.38) by decomposing (A.42) using (8.2.26) etc.

Bibliography

[1] ABRAMOWITZ, M. & STEGUN, I. 1964 *Handbook of mathematical functions (9th printing).* Dover.

[2] ACTON, F. 1997 *Numerical methods that work.* The Mathematical Association of America.

[3] ATHANASSOULIS, G.A. & BELIBASSAKIS, K.A. 1999 A consistent coupled-mode theory for the propagation of small-amplitude water waves over variable bathymetry regions. *J. Fluid Mech.* **389**, 275–301.

[4] BARNARD, B.J.S. PRITCHARD, W.G. & PROVIS, D.G. 1983 Experiments on wave trapping by a submerged cylindrical island. *Geophys. Astrophys. Fluid Dynamics* **24**, 23–38.

[5] BENDER, C. J. & DEAN, R. G. 2005 Wave transformation by axisymmetric three-dimensional bathymetric anomalies with gradual transitions in depth. *Coastal Engineering.* **52**, 331–351.

[6] BERKHOFF, J.C.W. 1973 Computation of combined refraction-diffraction. *Proc. 13th Intl Conf. on Coastal Engng, July 1972, Vancouver Canada.* , 471–490.

[7] BONNET-BEN DHIA, A.S. & JOLY, P. 1993 Mathematical analysis of guided water waves. *SIAM J. Appl. Math.* **53**, 1507–1550.

[8] BOOIJ, N. 1983 A note on the accuracy of the mild-slope equation. *Coastal Engineering* **7**, 191–203.

[9] CADBY, J.R. & LINTON, C.M. 2000 Three-dimensional water-wave scattering in two-layer fluids. *J. Fluid Mech.* **423**, 155–173.

[10] CHAKRABARTI, S.K. 1987 *Hydrodynamics of offshore structures.* CMP/Springer.

[11] CHAMBERLAIN, P.G. & PORTER, D. 1995 The modified mild-slope equation. *J. Fluid Mech.* **291**, 393–407.

[12] CHAMBERLAIN, P.G. & PORTER, D. 1999 Scattering and near-trapping of water waves by axisymmetric topography. *J. Fluid Mech.* **388**, 335–354.

[13] CHAMBERLAIN, P.G. 2004 The effect of evanescent wave modes on scattering and near trapping. *IMA Journal of Applied Mathematics* **69**, 205–218.

[14] CHAPMAN, G.J.D. & PORTER, R. 2004 Free and forced oscillations to second-order for two-dimensional fluid motion in a tank with arbitrary bed profile. *Proc. 19th IWWWFB*

[15] CHAPMAN, G.J.D. & PORTER, R. 2005 Second-order sloshing over an arbitrary bed. *J. Fluid Mech.* **524**, 331–335.

[16] CHAPMAN, G.J.D. & PORTER, R. 2005 Scattering of obliquely incident waves by submerged ridges. *Proc. 20th IWWWFB*

[17] CRAGGS, J. W. & DUCK, P. W. 1978 A power series method for treating mixed boundary value problems. *J. Inst. Maths Applics.* **21**, 1–12.

[18] DAVIS, A. M. J. 1965 Two dimensional oscillations in a canal of arbitrary cross section. *Proc. Camb. Phil. Soc.* **61**(1) 827–846.

[19] DAVIS, A. M. J. 1974 Short surface waves in a canal; dependence of frequency on the curvatures and their derivatives. *Q. Jl Mech. appl. Math.* **27**(1) 523–535.

[20] DAVIES, A. G. 1982 The reflection of wave energy by undulations in the seabed. *Dynamics of Atmospheres and Oceans* 6 207–232.

[21] DETTMAN, J. W. 1965 *Applied Complex Variables.* Dover.

[22] DEVILLARD, P., DUNLOP, F. & SOUILLARD, B. 1988 Localization of gravity waves on a channel with a random bottom. *J. Fluid Mech.* **186**, 521–538.

[23] DUFFY, D. G. 2004 *Transform Methods for Solving Partial Differential Equations.* Chapman & Hall/CRC.

[24] EHRENMARK, U.T. & WILLIAMS, P.S. 2001 Wave parameter tuning for the application of the mild-slope equation on steep beaches and in shallow water. *Coastal Engineering* **42**, 17–34.

[25] EVANS, D.V. & KUZNETSOV, N. 1999 Trapped modes. In: J. N. Humt (ed.) Gravity waves in water of finite depth. Southampton: Computational Mathematics Publications pp127–168.

[26] EVANS, D. V. & LINTON, C. M. 1991 Sloshing frequencies *Q. Jl Mech. appl. Math.* 46(1) 71–87.

[27] EVANS, D. V. & LINTON, C. M. 1994 On step approximations for water-wave problems *J. Fluid Mech.* **278**, 229–249.

[28] EVANS, D.V. & MCIVER, P. 1983 Edge waves over a shelf: full linear theory. *J. Fluid Mech.* **142**, 79–95.

[29] FALTINSEN, O.M. 1974 A Nonlinear Theory of Sloshing in Rectangular Tanks. *Journal of Ship Research* **Vol 18, No 4**, 224-241.

[30] FALTINSEN, O.M. & ROGNEBAKKE, O.V. & LUKOVSKY, I.A. & TIMOKHA, A.N. 2000 Multidimensional modal analysis of nonlinear sloshing in a rectangular tank with finite water depth. *J. Fluid Mech.* **407**, 201–234.

[31] FALTINSEN, O.M. & TIMOKHA, A.N. 2001 An adaptive multimodal approach to nonlinear sloshing in a rectangular tank. *J. Fluid Mech.* **432**, 167-200.

[32] FALTINSEN, O.M. & TIMOKHA, A.N. 2002 Asymptotic modal approximation of nonlinear resonant sloshing in a rectangular tank with small fluid depth. *J. Fluid Mech.* 470, 319–357.

[33] FALTINSEN, O. M. ROGNEBAKKE, O. F. & TIMOKHA, A. N. 2002 Resonant three-dimensional nonlinear sloshing in a square base basin. *J. Fluid Mech.* 487, 1–42.

[34] FENTON, J.D. 1978 Wave forces on vertical bodies of revolution. *J. Fluid Mech.* 85, part 2, 241–255.

[35] FITZ-GERALD, G.F. 1976 The reflexion of plane gravity waves travelling in water of variable depth. *Phil. trans. R. Soc. Lond.* 34, 49–89.

[36] FOX, D. W. & KUTTLER, J. R. 1983 Sloshing frequencies *Z. angew. Math. Phys.* 34, 668–696.

[37] GRADSHTEYN, I. S. & RYZHIK I. M. 1965 *Table of Integrals, Series and Products.* Academic Press.

[38] GRAHAM, E. W. & RODRIGUEZ, A. M. 1952 The characteristics of fuel motion which affect airplane dynamics. *J. Appl. Mech.* 19, 381–388.

[39] HAVELOCK, T. H. 1929 Forced surface waves on water. *Phil. Mag. (7)* 8, 569–577.

[40] HEINS, A.E. 1948 Water waves over a channel of finite depth with a dock. *American Journal of Mathematics* 70, No. 4, 730–748.

[41] HENRICI, P. TROESCH, B. A. & WUYTACK, L. 1970 Sloshing frequencies for a half-space with circular or strip-like aperture *Z. angew. Math. Phys.* 21, 285–318.

[42] HULME, A. 1982 The wave forces acting on a floating hemisphere undergoing forced periodic oscillations. *J. Fluid Mech.* 121, 443–463.

[43] HULME, A. 1983 A ring-source/integral-equation method for the calculation of hydrodynamic forces exerted on floating bodies of revolution. *J. Fluid Mech.* **128**, 387–412.

[44] JONES, D. S. 1952 The eigenvalues of $\nabla^2 u + \lambda u = 0$ when the boundary conditions are given on semi-infinite domains. *Proc. Camb. Phil. Soc* **49** (1953), 668–684.

[45] KELLER, J. 1958 Surface waves on water of non-uniform depth. *J. Fluid Mech.* 4, 607–614.

[46] KIRBY, J. T. & DALRYMPLE, A. D. 1983 Propagation of obliquely incident water waves over a trench. *J. Fluid Mech.* **133**, 47–63.

[47] KREISEL G. 1949 Surface Waves *Q. Appl. Math.* **7**, 21-24

[48] KUZNETSOV, N. MAZ'YA, V. & VAINBERG, B. 2002 Linear water waves a mathematical approach. Cambridge University Press.

[49] LAMB, H. 1932 *Hydrodynamics (6th ed)* Cambridge University Press.

[50] LAVRENTIEV, M. & CHABAT, B. 1980 *Effets hydrodynamiques et modèles mathématiques* Mir, Moscow.

[51] LINTON, C. M. & MCIVER, P. 2001 Mathematical Techniques for Wave/Structure Interactions.. Chapman & Hall/CRC.

[52] LONGUET-HIGGINS, M. S. 1967 On the trapping of wave energy round islands. *J. Fluid Mech.* **29**, 781–821.

[53] MARUO, H. 1960 The drift of a body floating on waves in waves. *J. Ship Res.* 4, 1–10.

[54] MCIVER, M. 1994 Second-order wave diffraction in two dimensions. *Applicd Ocean Research* **16**, 19–25.

[55] McIver, M. & McIver, P. 1990 Second-order wave diffrction by a submerged circular cylinder. *Applied Ocean Research* **16**, 19–25.

[56] McIver, P. 1989 Sloshing frequencies for cylindrical and spherical containers filled to an arbitrary depth. *J. Fluid Mech.* **201**, 243–257.

[57] 1985 McIver, P. & Evans, D. V. 1985 The trapping of surface waves above a submerged horizontal cylinder. *J. Fluid Mech.* **151**, 243–255.

[58] 2002 McIver, P. & Porter, R. 2002 Trapping of waves by a submerged elliptical torus. *J. Fluid Mech.* **456**, 277–293.

[59] Mei, C.C. & Black, J. L. 1969 Scattering of surface waves by rectangular obstacles in waters of finite depth. *J. Fluid Mech.* **38**, 499–511.

[60] Mei, C.C. 1978 Numerical methods in water-wave diffraction and radiation. *Ann. Rev. Fluid Mech.* **10**, 393–416.

[61] Mei, C.C. 1983 The applied dynamics of ocean surface waves. Wiley-Interscience.

[62] Miles, J.W. 1967 Surface wave scattering matrix for a shelf. *J. Fluid Mech.* **28**, 755–767.

[63] Miles, J. W. 1972 On the eigenvalue problem for fluid sloshing in a half-space *Z. angew. Math. Phys.* **23**, 861–869.

[64] Miles, J.W. & Chamberlain, P.G. 1998 Topographical scattering of gravity-waves. *J. Fluid Mech.* **361**, 175–188.

[65] Moiseev, N. N. 1964 Introduction to the theory of oscillations of liquid-containing bodies *Advances in Appl. Mech.* **8**, 233–289.

[66] Moiseev, N. N. & Petrov, A. A. 1968 The calculation of free oscillations of a liquid in a motionless container *Advances in Appl. Mech.* **9**, 91–154.

[67] NOBLESSE, F. 2004 Generalised potential-flow representations. *Proc. 19th IWWWFB*

[68] NOBLESSE, F. & YANG, C. 2004 Weakly singular boundary-integral representations of free-surface flows about ships or offshore structures. *J. Ship Res.* **48**, No 1, 31–44.

[69] PACKHAM, B. A. 1980 Small-amplitude waves in a straight channel of uniform triangular cross-section. *Quart. J. Mech. Appl. Math.* **33**, 179–187.

[70] PORTER, D. & CHAMBERLAIN, P.G. 1997 Linear wave scattering by two-dimensional topography. In *Gravity Waves in water of finite depth.* (Ed J. N. Hunt), 13–53. Southampton, Computational Mechanics.

[71] PORTER, D. & STAZIKER, D.J. 1995 Extensions of the mild-slope equation. *J. Fluid Mech.* **300**, 367–382.

[72] PORTER, D. & STIRLING, D.S.G. 1990 Integral Equations. Cambridge Texts in Applied Mathematics.

[73] PORTER, R. 1995 Complementary methods and bounds in linear water waves. *PhD Thesis* University of Bristol, UK.

[74] PORTER, R. 2002 Scattering of surface waves by submerged cylinders of arbitrary cross-section. *Proc. R. Soc. Lond. A.* **458**, 581–606.

[75] PORTER, R. 2002 Trapping of water waves by pairs of submerged cylinders. *Proc. R. Soc. Lond. A.* **458**, 607–624.

[76] PORTER, R. & EVANS, D.V. 1998 The trapping of surface waves by multiple submerged horizontal cylinders. *J. Eng Math.* **34**, 417–433.

[77] PORTER, R. & PORTER, D. 2000 Water wave scattering by a step of arbitrary profile. *J. Fluid Mech.* **411**, 131–164.

[78] PORTER, R. & PORTER, D. 2001 Interaction of water waves with three-dimensional periodic topography. *J. Fluid Mech.* 434, 301–335.

[79] PORTER, R. & PORTER, D. 2003 Scattered and Free waves over periodic beds. *J. Fluid Mech.* 489, 129–163.

[80] PROVIS, D.G. 1977 Experimental studies of wave refraction, in Waves on Water of Variable Depth. *Lecture Notes in Physics.* 64, 39—45.

[81] RENARDY, Y. 1983 Trapping of water waves above a round sill. *J. Fluid Mech.* **132**, 105–118.

[82] RHEE, J.P. 1997 On the transmission of water waves over a shelf. *Applied Ocean Research* **23**, 299–304.

[83] RHEE, J.P. 2001 A note on the diffraction of obliquely incident water waves by a stepwise obstacle. *Applied Ocean Research* **23**, 299–304.

[84] ROSEAU, M. 1976 Asymptotic Wave Theory North-Holland

[85] SHEN, M.C., MEYER, R.E. & KELLER, J.B. 1968 Spectra of water waves in channels and around islands. *Phys. Fluids* **11**, 2289–2304.

[86] SMITH, R. & SPRINKS, T. 1975 The scattering of surface waves by a conical island. *J. Fluid Mech.* **72**, 373–384.

[87] SOLAAS, F. & FALTINSEN, O. M. 1997 Combined numerical and analytical solution for sloshing in two-dimensional tanks of a general shape. *Journal of Ship Research.* 41, 118–129.

[88] SOMMERFELD, A. 1949 Partial Differential Equations in Physics. *Academic Press Inc.. ,* $28.

[89] STAZIKER, D.J. PORTER, D. & STIRLING, D.S.G. 1996 The scattering of surface waves by local bed elevations. *Appl. Ocean Res.* 18, 283–291.

[90] STOKES, G.G. 1846 Report on recent researches in hydrodynamics. *Brit. Assn. Rep.*

[91] STOKES, G.G. 1847 On the theory of oscillatory waves. *Camb. Trans.* **1847 Vol 8**, 441–455.

[92] THORNE, R. C. 1953 Multipole expansions in the theory of surface waves. *Proc. Camb. Phil. Soc* **49** (1953), 707–716.

[93] TROESCH, B. A. & TROESCH, H. R. 1972 A remark on the sloshing frequencies for a half-space. *Z. angew. Math. Phys.* **23**, 703–711.

[94] TROESCH, B. A. 1973 Sloshing frequencies in a half-space by Kelvin inversion. *Pacific.J. Math.* **47**, 539–552.

[95] TROESCH, B. A. 1972 Proof of a conjecture on sloshing frequencies in a half-space. *Z. angew. Math. Phys.* **25**, 655–657.

[96] URSELL, F. 1950 Surface waves on deep water in the presence of a submerged circular cylinder. *Proc. Camb. Phil. Soc.* **46**, 141–152.

[97] URSELL, F. 1951 Trapping modes in the theory of surface waves. *Proc. Camb. Phil. Soc.* **47**, 347–358.

[98] URSELL, F. 1952 Edge waves on a sloping beach. *Proc. R. Soc. Lond.* A **214**, 79–97.

[99] VADA, T. 1987 A numerical solution of the second-order wave-diffraction problem for a submerged cylinder of arbitrary shape. *J. Fluid Mech.* **174**, 23–37.

[100] WATSON, G.N. 1962 *A treatise on the theory of Bessel functions. (2nd ed.)* Cambridge University Press.

[101] WEHAUSEN, J.V. & LAITONE, E.V. 1960 *Surface Waves.* Online Edition.

[102] WEIR, A.J. 1994 *Lebesgue integration & measure.* Cambridge University Press.

[103] Wu, G.X. & Eatock Taylor, R. 1994 Finite element analysis of two-dimensional non-linear transient water waves. *Applied Ocean Research* **16**, 363–372.

[104] Wu, G. X. & Eatock Taylor, R. 1998 Numerical simulation of sloshing waves in a 3D tank based on a finite element method. *Applied Ocean Research* **20**, 337–356.